LYOTROPIC MESOMORPHISM IN MICELLAR LIQUID CRYSTALS FORMED FROM AQUEOUS SOLUTIONS OF THE SALTS OF PENTADECAFLUOROOCTANOIC ACID.

Mark Hamish Smith

Department of Chemistry and Biochemistry

Massey University

New Zealand.

A thesis presented in accordance

with the requirements for the degree of Doctor of Philosophy.

November 1990.

Massey University Library. Thesis Copyright Form

Title of thesis: Lyotropic mesomorphism in micellar liquid crystals formed from aqueous solutions of the salts of Pentadecafluoro-octanoic acid.

(1) (a) I give permission for my thesis to be made available to readers in the Massey University Library under conditions determined by the Librarian.

~~(b)~~ I do not wish my thesis to be made available to readers without my written consent for _____ months.

(2) (a) I agree that my thesis, or a copy, may be sent to another institution under conditions determined by the Librarian.

~~(b)~~ I do not wish my thesis, or a copy, to be sent to another institution without my written consent for _____ months.

(3) (a) I agree that my thesis may be copied for Library use.

~~(b)~~ I do not wish my thesis to be copied for Library use for _____ months.

Signed M Smith

Date 12/11/90

The copyright of this thesis belongs to the author. Readers must sign their name in the space below to show that they recognise this. They are asked to add their permanent address.

NAME AND ADDRESS	DATE

ABSTRACT

High resolution phase diagrams for the caesium pentadecafluorooctanoate (CsPFO)/water and the ammonium pentadecafluorooctanoate(APFO)/heavy water systems have been determined, together with a partial phase diagram, in the liquid crystal phase transition regime, for the APFO/water system. In all three systems a discoidal nematic (N_D^+) phase occurs over an extensive concentration and temperature range. This phase is intermediate to an isotropic micellar solution phase (I), to higher temperatures/lower concentrations and a micellar lamellar phase (L_D) to lower temperatures/higher concentrations. The distinctions between the phase diagrams lies in the temperature and composition of the phase transitions. A variety of techniques have been used to delineate these temperatures including ^2H, ^{14}N and ^{133}Cs NMR spectroscopy, DSC and electrical conductivity. The NMR method is the main technique and ^{133}Cs NMR in particular has proved to be an excellent nucleus for the precise detection of phase transition temperatures. It is the first time ^{133}Cs NMR has been used for this purpose. The NMR measurements show a preference for counterion binding to sites of lowest surface curvature.

Isotope effects are shown by both the CsPFO and the APFO systems. The overall effect on substituting heavy water for water is to raise the phase transition temperatures, by about 3 K at a volume fraction amphiphile $\phi = 0.1$ and by about 1 K at $\phi = 0.4$. The isotope effect is caused by an increase in micelle size in heavy water as a result of an enhanced hydrophobic effect. Isotope effects are also shown in a study undertaken on the thermodynamics of micellization in the CsPFO/water system. The cmc's in heavy water at a given temperature occur at higher concentrations than those in water, a result which is opposite to the isotope effect in hydrocarbon surfactant systems. It is shown that small changes in both the fraction of bound ions and the aggregation numbers between the two systems have a profound effect on the calculated thermodynamic parameters. A full understanding of the thermodynamics of micellization would require precise determinations of these quantities.

The effect of substituting Cs^+ ions for NH_4^+ ions is to raise the temperature of the liquid crystal phase transitions by about 23 K at a given volume fraction. The reason for this is that the micelles in the APFO/water system are smaller than those in the CsPFO/water system for any given volume fraction and temperature. This is probably due to the greater ability of the Cs^+ ions to reduce the electrostatic repulsion between the anionic head groups in the micelle which leads to a reduction in micelle surface curvature and an increase in micelle size.

^2H NMR has been used to monitor magnetic-field induced order in an isotropic solution of discoidal micelles of CsPFO on approaching a transition to a nematic phase. The field induced order is revealed as a quadrupole splitting of the isotropic signal which is first observed, at the field strength of the experiment (6.34 T), at a temperature approximately 80 mK higher than the upper boundary to the transition (T_{IN}). The splitting increases rapidly with decreasing temperature and diverges as a hypothetical second-order transition to the nematic phase is approached at T^*. The divergence follows a $(T_{IN}-T^*)^{-1}$ dependence as predicted by molecular field theory. At T_{IN} the divergence is quenched and in the biphasic region the quadrupole splitting is constant. This facilitates the precise determination of T_{IN} and $(T_{IN}-T^*)$. This latter quantity, which was measured over the surfactant weight fraction w range of w = 0.15 to w= 0.35, approaches zero (i.e becomes second order) only at infinite dilution. $T_{IN}-T_{NI}$, which is more easily measured than $T_{IN}-T^*$ is shown to be an alternative measure of the strength of the isotropic to nematic transition.

TABLE OF CONTENTS

CHAPTER 1

CHAPTER 2

CHAPTER 3

CHAPTER 4

Abbreviation used in this Thesis

B	magnetic field
β_A	fraction of ammonium ions bound to the surface
β_{Cs}	fraction of Cs^+ ions bound to the surface of the micelle
χ	nuclear quadrupole coupling constant
cmc	critical micelle concentration
CsPFN	caesium heptadecafluorononanoate (perfluorononanoate)
CsPFO	caesium pentadecafluorooctanoate (perfluorooctanoate)
$\delta_{\alpha\beta}$	Kronecker delta
DACl	decylammonium chloride
$\Delta\chi$	diamagnetic susceptibility anisotropy
$\Delta\tilde{\nu}$	quadrupole splitting
$\Delta\nu_{1/2}$	linewidth at half height
DSC	differential scanning calorimetry
DSCG	disodium cromoglycate
e	electronic charge
FID	free induction decay
γ	magnetogyric ratio
g_N	nuclear g factor
η	asymmetry parameter
I	nuclear spin quantum number
$\kappa_\perp$	conductivity perpendicular to the director
$\kappa_{\|\|}$	conductivity parallel to the director
μ_N	nuclear magneton
MTAB	tetradecyltrimethylammonium (myristyltrimethylammonium) bromide
n	mesophase director
n or $\tilde{n}$	micellar aggregation number
$N(CH_3)_4PFN$	tetramethylammonium heptadecafluorononanoate
n_α	direction cosines of the nematic symmetry axis

NH_4PFN	ammonium heptadecafluorononanoate
NH_4PFO	Ammonium pentadecafluorooctanoate
P	spin angular momentum
$\langle(P_2(\cos\alpha)\rangle_s$	shape factor
Q	nuclear electric quadrupole moment
q	electric field gradient at the nucleus
q_{zz}	component of the nuclear quadrupole-electric field coupling parallel to the magr
$S_{\alpha\beta}$	lowest rank orientational ordering tensor
SDS	sodium decyl sulphate
$\sigma_{\gamma\gamma}$	components of the chemical shift tensor
σ_I	chemical shift of the isotropic phase
$S_{O\text{-}D}$	order parameter relating the average orientation of the O-^{2}H bond
T_2^*	apparent value of T_2
T_1	longitudinal or spin-lattice relaxation time
T_2	transverse or spin-spin relaxation time
x_A	mole fraction of amphiphile
x_W	mole fraction of water

ACKNOWLEDGEMENTS

I am grateful to a large number of people who have helped during me during the research and writing of this thesis. I am indebted to my supervisor Dr Ken W. Jolley for his guidance. His knowledge and patience made the production of this thesis possible. Also to our collaborators at Leeds University, principally Dr N. Boden.

I would also like to thank my colleague, friend and flatmate Dr David Parker for his assistance and encouragement. A valuable supporting role was played by the members of the NMR group, especially Mr Ashok Parbhu.

Thanks to the technical staff of the mechanical and glassblowing workshops who provided valuable (and usually rapid) first aid to broken equipment and glassware.

I must also thank my flatmates Miss Justine Williams and Miss Pattie Groves for their support and encouragement.

Finally I would like to acknowledge the support of my parents Rex and Lois Smith for their unflagging support both moral and financial without which this would not be possible.

This thesis is dedicated to the memory of my grandmother,

Nana Donald

who passed away this year before the completion of my

university career, which she followed with great interest

CHAPTER 1

INTRODUCTION

SELF-ORGANIZING FLUIDS

The term self-organizing fluids covers a wide range of systems as diverse as cell membranes and liquid crystal displays. In surfactant solutions and in micellar liquid crystals there are two levels of organization. In dilute solutions the surfactant molecules aggregate to form micelles which can undergo self-organization at higher concentrations. There is currently great interest being shown in the physico-chemical properties of these systems since the same forces that drive micelle formation and organization also control the properties of bilayer membranes, vesicles and microemulsions[1]. These structures play an important part in many aspects of cell biology. Information gained through the study of micelles and micellar interactions can be used to gain a greater knowledge of some of the processes that control life.

The subject of this thesis is phase behaviour and macroscopic ordering in micellar liquid crystals formed from solutions of perfluorinated surfactant salts in water. Micellar liquid crystals, which belong to the class of lyotropic liquid crystals, differ from thermotropic liquid crystals in the nature of their structural unit (mesogen), the size and shape of which depends on surfactant concentration and on temperature[2]. In contrast the mesogen in a thermotropic liquid crystal is a molecule the structure of which is independent of temperature (aside from possible conformational changes) and, in the case of mixed thermotropic systems, composition. The phases of both types of liquid crystals are, however, characterised by the degree of ordering present in the mesophase. In this introduction the emphasis will be placed on describing the structure, order and phase behaviour of lyotropic mesophases and a discussion of thermotropic liquid

crystals will be largely confined to a description of the degree of ordering in liquid crystal systems.

1.1 LIQUID CRYSTALS

It was found late last century[3] that for some organic substances the transition between solid crystal and isotropic liquid occurs via an intermediate phase (or mesophase). This mesomorphic phase is known to us as a liquid crystal. At first glance the term 'liquid crystal' seems to be a paradox but it is appropriate when we consider that these mesophases have both liquid properties and crystalline properties. Liquid crystals exhibit crystalline properties such as birefringence and liquid properties such as fluidity. On transition from solid crystal, liquid crystals lose their positional ordering but retain some degree of long range orientational ordering. The structural units, often referred to as mesogens, that make up these mesophases are anisotropic in nature.

Liquid crystals are categorised into two groups depending on the nature of the structural unit from which the mesophase is derived. In thermotropic liquid crystals the structural unit is a molecule and the properties of the mesophase depend on the inter-molecular interactions. In lyotropic liquid crystals the structural units are aggregates of molecules dispersed in a solvent (usually water). The properties of lyotropic liquid crystals depend not only on the molecular structure but also on solvent moderated interaggregate interactions.

1.2 THERMOTROPIC LIQUID CRYSTALS

There are thousands of organic molecules that exhibit liquid crystalline behaviour and it is the structure of these molecules that determines the properties of the thermotropic liquid crystalline phases. There are two main groups of anisotropic molecules that form liquid crystals. Calamitic phases are formed from long rigid (lath-like) molecules and discotic phases formed from disc shaped (discoidal) molecules. The types of liquid crystals formed by these molecules are summarised below.

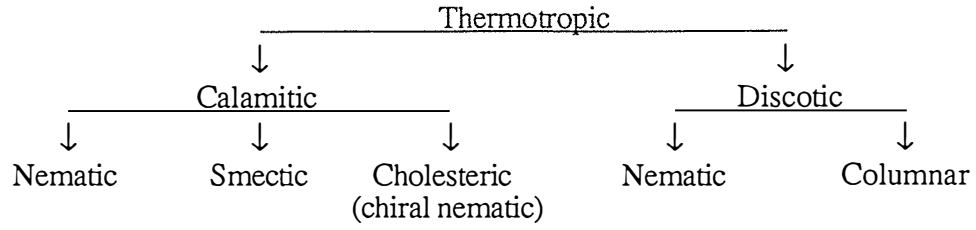

1.2.1 Calamitic Phase Structures

The majority of thermotropic liquid crystals so far discovered are of the calamitic type. The mesogens in these systems are long molecules which contain rigid regions, such as aromatic rings, in their cores (*e.g.* 4'-n-Pentyl-4-cyanobiphenyl shown in figure 1.1). These mesogens tend to align due to the mutual attraction of their aromatic cores, thus giving the liquid crystalline phases their characteristic orientational ordering. There are two basic mesophase structures, smectic and nematic, which differ in their degree of ordering.

Figure 1.1 A typical thermotropic liquid crystal 4'-n-Pentyl-4-cyanobiphenyl.

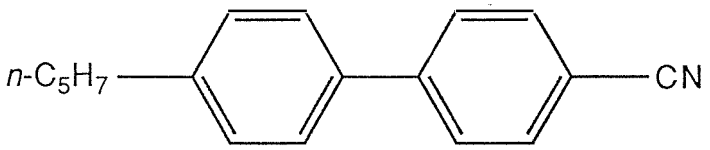

1.2.1.1 Nematic Phase

In the nematic phase, on average, the molecules are aligned with their long axes parallel to each other[4]. This gives rise to a local preferred orientation of the axes defined by the mesophase director, denoted with the vector, **n.** The nematic phase has rotational symmetry about **n**. There is no translational ordering which means that translational diffusion of the molecules readily occurs, thereby giving the nematic phase its fluidity.

The nematic ordering, in the absence of any perturbing field, extends over only a short range *i.e.* it is local. This short range ordering means that the nematic phase can be thought of as being made up of small independent nematic domains. Macroscopic alignment, to produce the equivalent of a single crystal, can be achieved by immersing the sample in a magnetic or an electric field. Extended nematic domains can also be caused by ordering induced at the interface between the liquid crystal and the containing vessel (surface alignment).

The nematic phase director has no polarity. Nematogens with nonequivalent end groups may have polarity but this property is not transferred to the bulk mesophase. This property is defined as $\mathbf{n} = -\mathbf{n}$.

The nematic liquid crystal can be studied by looking at the difference in physical properties when these are measured parallel to or perpendicular to the mesophase director. Anisotropic physical properties that can be readily measured for nematic liquid crystals include; magnetic susceptibility, conductance, refractive index (birefringence), elasticity and dielectric permittivity. These properties can be used to determine an order parameter for the mesophase where this order parameter has the value S=0 for a random distribution of the long molecular axes and the value S=1 in the case of a perfectly aligned crystal[4].

Liquid crystals are useful as models for investigating properties of liquids since their anisotropy means that interactions that can normally only be measured on the surface of an isotropic fluid can be measured in the bulk. These properties can be measured because tensoral interactions (such as quadrupole coupling) do not average to zero.

For a thermotropic nematic mesophase which is macroscopically aligned a laboratory fixed coordinate system x,y,z can be used with the mesophase director

aligned along the z axis which is also the direction of the magnetic field, **B**. The most simple type of symmetry for a nematic mesophase is $D_{\infty h}$.

In a uniaxial nematic mesophase the orientational distribution function[5] is

$$f(\Omega)=\frac{1}{8\pi^2}[1 + 5S_{\alpha\beta}n_\alpha n_\beta + ...] \qquad [1.1]$$

where n_α are the direction cosines of the nematic symmetry axis with respect to a molecule-fixed axis system, α,β = x,y,z and $S_{\alpha\beta}$ (introduced by Saupe[6]) is the lowest rank orientational ordering tensor defined by

$$S_{\alpha\beta} = <\frac{1}{2}(3n_\alpha n_\beta - \delta_{\alpha\beta})> \qquad [1.2]$$

The odd rank ordering tensors are absent in the expansion because the mesophase director has no polarity. $\delta_{\alpha\beta}$ is the Kronecker delta ($\delta_{\alpha\beta} = 1$ for $\alpha = \beta$, $\delta_{\alpha\beta} = 0$ for $\alpha \neq \beta$). In a uniaxial nematic mesophase the coordinate axes x and y are equivalent when the mesophase director is oriented along the z axis.

We need to define a molecular axis system to relate the orientation of the molecules in relation to the mesophase director[7]. A molecular fixed coordinate system is defined using the axes ξ,η,ζ with the ζ axis as the long molecular axis of the rigid molecule. The orientation of a molecule is completely determined by the three Euler angles θ, ψ and ϕ (shown in figure 1.2). θ is the angle between the z axis and the ζ axis. ψ is the angle between the ξ axis and K, the normal to the z, ζ plane and describes a rotation of the molecule around its long axis. ϕ is the angle between K and the x axis which describes the rotation of the whole molecules around the director. The third Euler angle, ϕ, can be neglected because of the uniaxial symmetry in the nematic phase.

Figure 1.2 The Euler angles defined in the molecular frame ξ, η, ζ with respect to the laboratory frame x,y,z where K is the normal to the z,ζ plane.

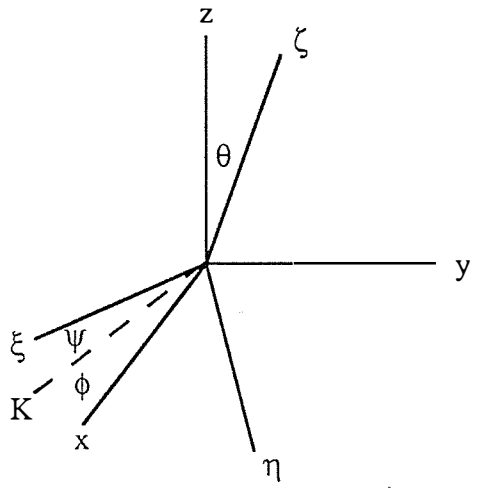

An orientational distribution function $w(\theta,\psi)$ is defined to specify the average orientation of the molecules where $w(\theta,\psi)\sin\theta d\theta d\psi$ is the fraction of molecules with Euler angles between θ and $\theta + d\theta$, and ψ and $\psi + d\psi$. The average value of any tensor property X over the orientations of all molecules is given by,

$$\langle X \rangle = \int_0^{\pi} d\theta \int_0^{2\pi} d\psi X w(\theta,\psi)\sin\theta \qquad [1.3]$$

In the nematic phase the orientational distribution function will have two maxima at $\theta = 0$ and $\theta = \pi$ and a minima at $\theta = \frac{1}{2}\pi$. The director **n** is apolar i.e. **n** = -**n** giving rise to $w(\theta,\psi) = w(\pi-\theta,\psi)$.

We need to define an order parameter in terms of the angles θ and ψ. The order parameter describes the average orientation of the long axis of the molecule with respect to the director. Thus we are looking for ζ_z, the component of a unit vector along the ζ axis projected onto the z axis. As a result of the apolarity in the director the average value of $\zeta_z = \cos\theta$ is zero. It is, therefore necessary to go to the second rank term $\zeta_z^2 = \cos^2\theta$,

$$\therefore S_{zz} = \frac{1}{2}\langle 3\zeta_z^2 - 1 \rangle \qquad [1.4]$$

$$= \frac{1}{2}\langle 3\cos^2\theta - 1\rangle \qquad [1.5]$$

For the random distribution of long molecular axes in the isotropic phase $\cos^2\theta = \frac{1}{3}$, therefore $S_{zz} = 0$. $S_{zz} = 1$ corresponds to perfect ordering when $\theta = 0$ or π. Whilst S_{zz} describes the degree of order of the long molecular axes (ζ) there is also a small contribution from projections of the ξ and η onto the z-axis. This is described by another order parameter $S_{xx} - S_{yy}$ such that

$$S_{xx} - S_{yy} = \frac{3}{2}\langle \eta_z^2 - \xi_z^2 \rangle \qquad [1.6]$$

$$= \frac{3}{2}\langle \sin^2\theta\cos 2\psi \rangle. \qquad [1.7]$$

where $\xi_z^2 = \sin^2\theta\sin^2\psi$ and $\eta_z^2 = \sin^2\theta\cos^2\psi$.

To describe a molecule in a nematic phase we use an order parameter tensor of second rank, **S**. The tensor, **S**, has nine elements collected into a 3×3 matrix to describe the orientation of solute molecules dissolved in a thermotropic liquid crystal. The tensor, **S**, is real, symmetric and traceless,

$$i.e.\ S_{\alpha\beta} = S_{\beta\alpha}$$

$$\text{and } \sum_{\alpha\alpha} = 0 \qquad \alpha,\beta = x,y,z.$$

This means that there are only five independent elements. A molecular coordinate system can be chosen (as above) to reduce the tensor to diagonal form. This simplification leaves only two independent parameters S_{zz} and $S_{xx} - S_{yy}$. For a mesophase with cylindrical symmetry about the z axis $S_{xx} - S_{yy} = 0$. This means that the order parameter S_{zz} is the only one necessary for description of the order in a uniaxial nematic mesophase of cylindrically symmetric mesogens.

1.2.1.2 Smectic Phase

Smectic phases consist of layers of thermotropic mesogenic molecules arranged in planes which have a well defined interlayer spacing[4]. Smectic liquid crystals can be grouped into one of several sub-classes depending on the orientation of the molecules within each layer. The smectic A phase consists of layers of molecules with their long axes parallel to the normal of the layers whereas in the smectic C phase the molecular axes are tilted with respect to the normal. The smectic phases occur at lower temperatures than the nematic phases and due to the presence of translational order have a higher viscosity than nematic phases.

1.3 LYOTROPIC LIQUID CRYSTALS

Lyotropic liquid crystals are formed by aggregates of amphiphillic molecules dispersed in a solvent. There are thus two levels of ordering. The amphiphillic molecules first of all undergo self assembly to form aggregates which at higher concentrations can undergo self organization to form liquid crystalline mesophases. The variety of different phases that can be formed is dependent on the size and shape of the amphiphillic aggregate. A thorough knowledge of the structure of the aggregate is therefore necessary in order to be able to interpret the macroscopic phase behaviour.

The structural units of the aggregates, the amphiphillic molecules, although diverse in their structure share one common feature, they have both hydrophillic and hydrophobic sections. Amphiphiles are of many different types including soaps, which are salts of fatty acids, detergents which are synthetic analogues of soaps (*e.g* alkyl-sulphonates and perfluorinated alkanoates) and biological surfactants such as phospho-lipids.

Early studies of surfactant solutions showed that at very low amphiphile concentrations the solution was of a molecular nature until a certain concentration

(known as the critical micelle concentration, cmc,) was reached when the surfactant molecules aggregated to form discrete micelles[8]. At high surfactant concentrations liquid crystals with an extended aggregate structure were formed[9]. Research in the area of surfactant solutions tended to treat micelles and liquid crystals as completely separate entities. The attitude that micelles are micelles and liquid crystals are liquid crystals and never the twain shall meet, hindered the understanding of both micellar solutions and liquid crystals. A joining together of these two fields of endeavour was heralded in 1967, when Lawson and Flautt[10] discovered the existence of a magnetically orientable phase, which was later determined to be a micellar nematic phase[11,12]. The characterization of the micellar nematic phase also gave rise to an obvious analogy between lyotropic and thermotropic liquid crystals.

i.e.

Thermotropic		Lyotropic
Isotropic molecular liquid	→	Isotropic micellar solution
Nematic	→	Micellar nematic
Smectic	→	Lamellar

This analogy also raises questions as to the nature of the forces which drive the phase transitions in the two types of liquid crystal. It is now known that at high concentrations of amphiphile, lyotropic phases are formed which are made up of translationally ordered small discrete micelles[13,14]. If the micelle is treated as being the basic unit of a lyotropic liquid crystal in much the same way as the molecule is the basic unit in the thermotropic liquid crystal then it can be seen that an understanding of the micelle is a prerequisite to the understanding of lyotropic liquid crystal behaviour. It is necessary to be cautious in drawing this comparison because the micelle is not an entity with a fixed size and shape such as a thermotropic nematogen but rather an aggregate whose dimensions are temperature and concentration dependent. This proviso means an integrated approach, the fusion of ideas from both the study of micelles and the study of

liquid crystals is needed to completely understand the nature of the phase behaviour in lyotropic liquid crystals.

Uniaxial nematic liquid crystals are produced from uniaxial micelles which have two basic shapes, either oblate ellipsoids (discs) or prolate ellipsoids (cylinders). If the micelle is biaxial then biaxial nematic phases will be formed. The existence of biaxial nematic phases as an intermediate in the transition between the two types of uniaxial nematic phases was predicted in several theoretical studies[15,16,17,18]. A biaxial phase was first identified in the Potassium Laurate/Decanol/^2H_2O system in 1980 by Yu and Saupe[19].

The various phases and the nature of the aggregate structural units are given in the box.

Aggregate		Phases		
spherical	→	cubic phases		
discoidal	→	discotic nematic	→	discotic lamellar / extended lamellar
cylindrical	→	calamitic nematic	→	hexagonal
biaxial	→	biaxial nematic		

In early publications[20] the nematic mesophase was classified according to the diamagnetic susceptibility anisotropy $\Delta\chi$, where in type-I mesophases the director aligned parallel to the magnetic field ($\Delta\chi > 0$) and in type-II mesophases the director aligned perpendicular to the magnetic field ($\Delta\chi < 0$). These types were identified with calamitic cylindrical micelles and discoidal micelles respectively. It is now known that this is not always the case[21], CsPFO micelles are discoidal and have a positive diamagnetic susceptibility anisotropy. It is therefore more instructive to label the nematic phase according to both the micelle shape and the diamagnetic susceptibility anisotropy of the mesophase[22]. Some examples of this type of nomenclature are given in table 1.1.

Table 1.1 Examples of micellar nematic mesophases categorised by the shape of the micelles and the diamagnetic anisotropy of the amphiphile molecules.

Micelle shape	Diamagnetic anisotropy	Phase type	Example
cylindrical	+	N_C^+	MTABr/H_2O
cylindrical	−	N_C^-	DSCG/H_2O
discoidal	+	N_D^+	CsPFO/H_2O
discoidal	−	N_D^-	DACl/H_2O

The first reported nematic mesophase[10] was in a quaternary mixture consisting of sodium decylsulphate, sodium chloride, decanol and water. Subsequent studies[23,24,25] uncovered lyotropic nematic mesophases formed in ternary systems consisting of a mixture of surfactant and water with either a long chain alcohol or an inorganic salt added. Ternary systems are difficult to study because the nematic range occurs over a very narrow composition range[26]. An important breakthrough in the study of lyotropic liquid crystals was made when it was discovered that stable nematic mesophases with wide composition ranges could be obtained from binary mixtures of perfluorinated surfactants[22]. This reduces the number of degrees of freedom in the system making it easier to determine the factors that contribute to the micelle structure and therefore to the mesophase behaviour.

Uniaxial nematic mesophases of calamitic micelles (N_C) or discoidal micelles (N_D) can be formed from either ionic or non-ionic amphiphiles[27] without the need for adding either alcohol or salt. A small nematic region has been located in the binary decylammonium chloride (DACl)/water system[28] extending from weight fraction amphiphile, w = 0.42 to 0.49. This small nematic range can be greatly increased by the addition of small amount of ammonium chloride, typically about 10% of the weight of DACl in the solution. A w = 0.36 solution of tetradecyltrimethylammonium bromide

(myristyltrimethylammonium bromide or MTAB) and water[29] also produces a binary nematic phase as does disodium cromoglycate (DSCG) and water[30]. A binary nematic phase is, however, unusual in hydrocarbon surfactants and occurs over limited concentration and temperature ranges whereas such phases are more common and more extensive in fluorocarbon surfactants. Lyotropic nematic phases have been reported for the following binary solutions of perfluorinated carboxylic acid salts and water; caesium pentadecafluorooctanoate (CsPFO)[13,21,31], caesium heptadecafluorononanoate (CsPFN)[32], NH_4PFN[33] and $N(CH_3)_4PFN$[34,35].

These systems are attractive for a number of reasons. They form nematic mesophases over large composition and temperature ranges and the temperatures at which the all important nematic mesophase occurs in these systems make experimental measurements convenient. Fluorocarbon amphiphiles are also considerably more chemically and thermally stable than their hydrocarbon analogues. A particularly useful property is that the nematic phase has a positive diamagnetic susceptibility anisotropy. This means that since it aligns in a magnetic field we can form the equivalent of single domain crystals and on cooling into the lamellar phase the single domain nature is retained. Having a single domain allows us to measure tensor properties parallel and perpendicular to the director and not just the trace of the tensor. In addition, the perfluorinated surfactant systems thus far reported show a simple phase behaviour in which the discoidal nematic and lamellar phases dominate. Lyotropic liquid crystals formed from hydrocarbon surfactants, on the other hand, display a wide range of aggregate structures and therefore a multiplicity of mesophases.

Several phase diagrams for perfluorinated surfactants have been published but they are of limited usefulness. The NH_4PFN phase diagram by Hoffmann[33] shows that there is a large nematic region stretching from 20 to 70°C and from w = 0.12 to >0.40 but it gives no indication on the phase diagram that the isotropic to nematic transition is first-order in nature although the accompanying text indicates that it is. The nematic

phase for the $N(CH_3)_4PFN$[34,35] system is also extensive, stretching from 25 to >70°C and from 0.25 to >0.45 weight fraction and a mixed nematic-isotropic biphasic region is indicated. Fontell and Lindman[32] have presented a series of approximate phase diagrams for several more of the heptadecafluorononanoate salts. These diagrams omit most of the critical points and with the exception of CsPFN do not show a nematic phase. A rudimentary phase diagram for the NH_4PFO system was published by Tiddy[36] in 1972 but this made no reference to a nematic phase at all.

All of the above phase diagrams lack the precision to be of anything more than useful background material. The most important ingredient for any study of lyotropic liquid crystals is an accurate and precise phase diagram. The researcher must know what state the system is in for structural studies, for example, to have any meaning. It is also important to know the nature of the phase transitions, *i.e.* whether they are first or second-order, and to obtain accurate locations for the various fixed points. The only phase diagram to date which contains all these features is that for the $CsPFO/^2H_2O$ system published by Boden[13] *et. al.* in 1987. The phase diagram for the $CsPFO/^2H_2O$ system is shown in figure 1.3.

In this system there are three homogeneous phase regions as well the two pure components. These are; the isotropic phase, I, which is a simple molecular solution at concentrations lower than the cmc and a micellar solution at concentrations higher than the cmc, the nematic phase, N_D^+, and the lamellar phase, L_D. The remainder of the phase diagram is made up of two-phase coexistence regions, where the composition of each component can be determined using the lever rule. The solubility curve, T_c, marks the upper temperature limit for crystalline amphiphile in solution. Pure liquid crystalline phases can, however, be detected below the solubility curve because of the large amount of supercooling in this transition. The Krafft point is the point where the cmc

Figure 1.3 The phase diagram for the CsPFO/^2H_2O system as determined by Boden *et al.*[13].

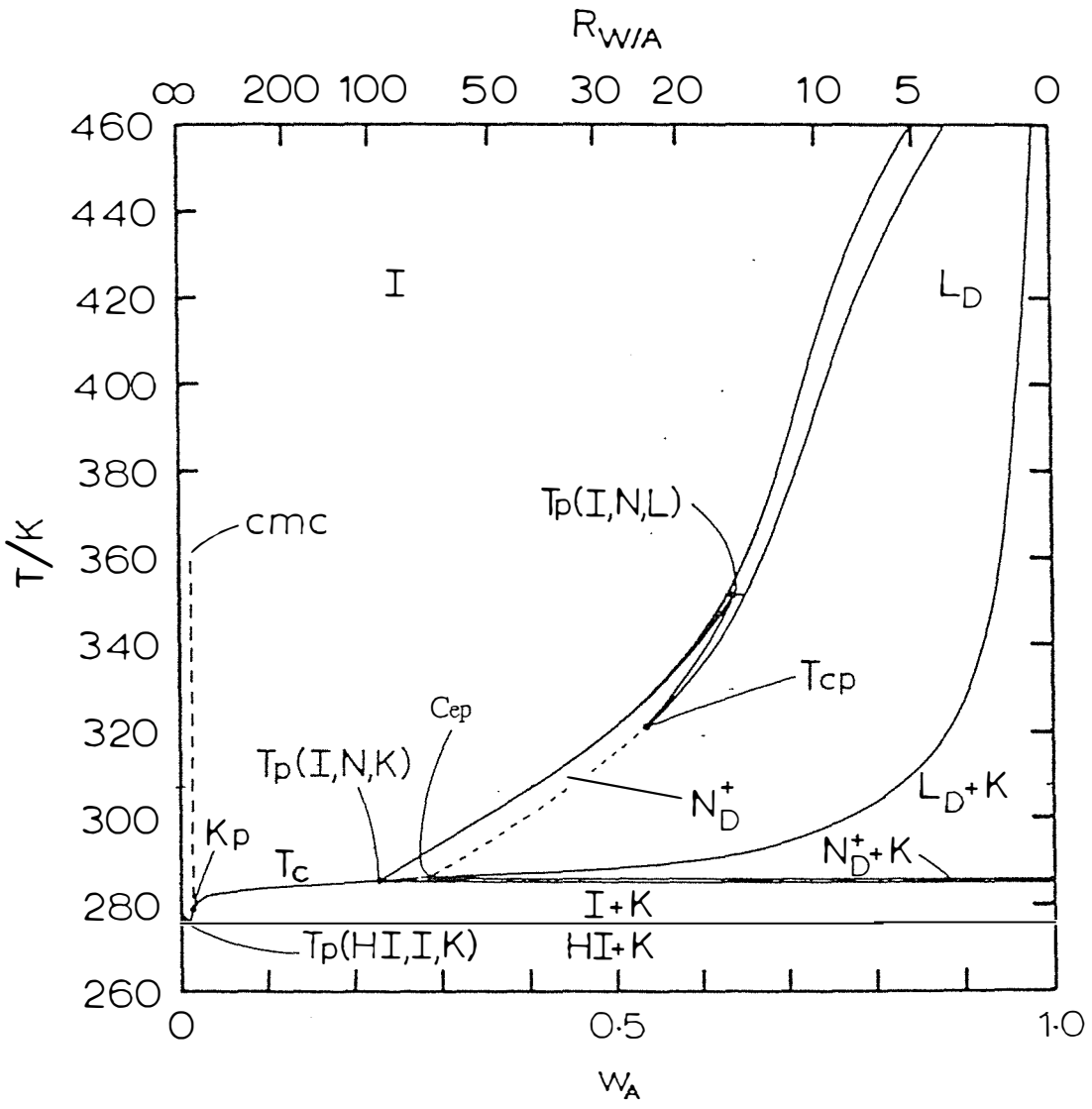

line intersects the solubility curve. This point corresponds with a rapid increase in the solubility of the amphiphile. The intersection of the solubility curve with the freezing point of the ^2H_2O in solution delineates the triple point Tp(HI,I,K), the eutectic point. Above the solubility curve the following phase transitions occur, with decreasing temperature or increasing CsPFO concentration,

$$\text{Isotropic (I)} \rightarrow \text{Nematic } (N_D^+) \rightarrow \text{Lamellar } (L_D).$$

The lamellar phase is unusually large for a simple ionic amphiphile whilst the nematic phase is the most extensive yet discovered for any lyotropic liquid crystal system stretching from w = 0.225 to 0.632. Nematic phases with weight fractions < 0.225 can be observed as the result of supercooling below T_c.

The width of the nematic/isotropic biphasic region decreases on dilution (from 350 mK for w = 0.50 to 60 mK for w = 0.15)[13,31]. This transition remains first-order to the limit of infinite dilution whereas the transition from nematic to lamellar becomes second-order at a tricritical point, T_{cp}. The tricritical point has been determined recently[31] to be located at w = 0.43.

There is strong evidence that the lamellar mesophase of this system consists of a two-dimensional array of micelles with a layer of water separating the planes of micelles[13,14]. This interpretation of lamellar structure is at odds with the classical lamellar structure of infinite bilayer aggregates separated by water. There are several series of experiments that together provide compelling evidence that the lamellar phase is discotic.

Conductivity experiments[14] on samples that have undergone alignment by passing through the nematic state have shown that there is diffusion of Cs^+ ions in the z direction, perpendicular to the lamellar planes. Figure 1.4 shows the conductivity parallel and perpendicular to the director as a function of temperature for a 0.55 weight

Figure 1.4 Electrical conductivities, κ, as a function of temperature. $\kappa_{\parallel}$ and $\kappa_{\perp}$ are conductivities measured parallel and perpendicular to the mesophase director. Data for the plot was supplied by Dr D. Parker[14], Leeds University.

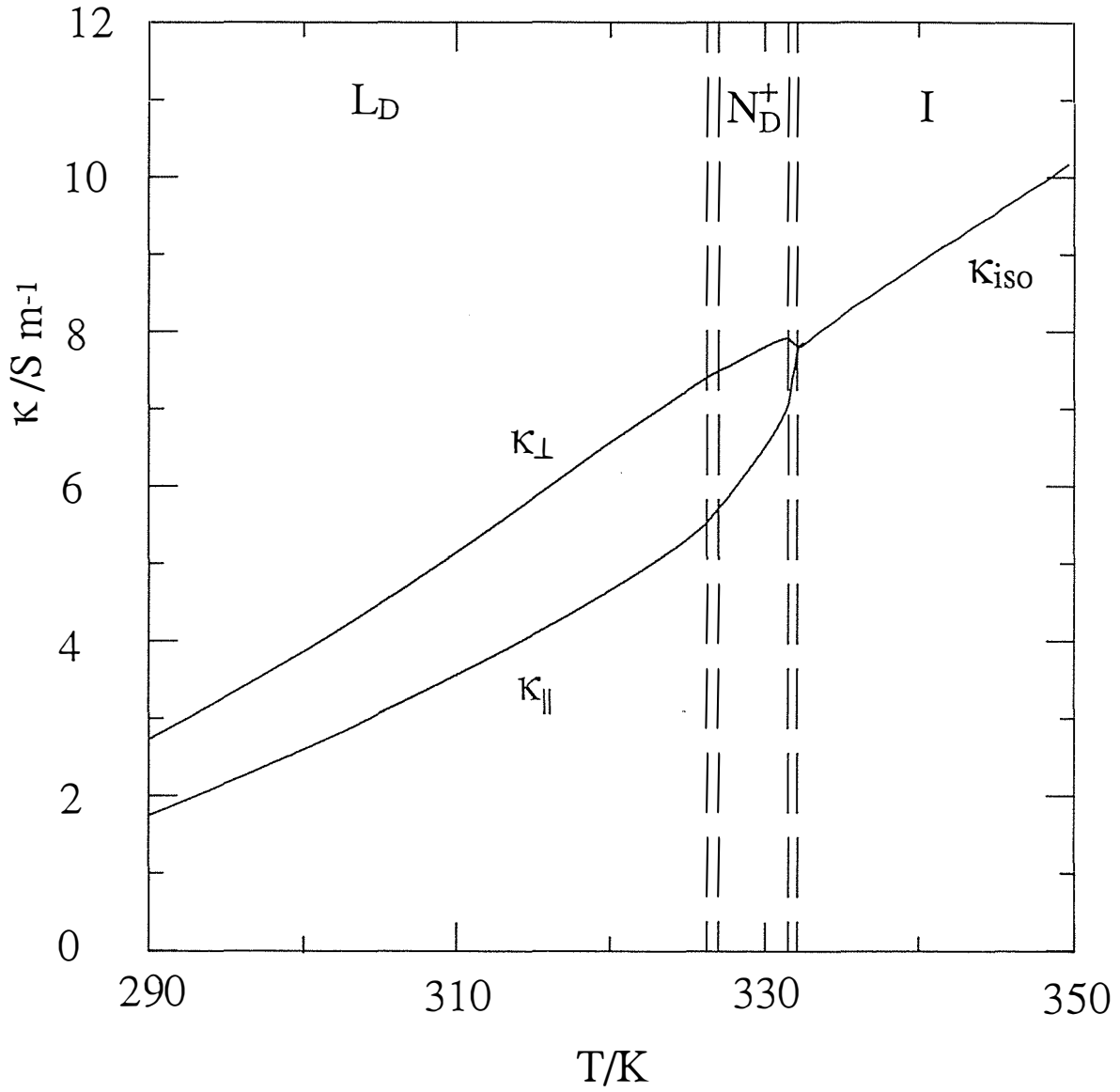

fraction sample. It can be seen that there is no discontinuity in either $\kappa_{\parallel}$ or $\kappa_{\perp}$ as the nematic to lamellar transition is traversed, indicating that the explosive growth required for the micelles to become infinite bilayers does not occur. This is not consistent with the notion that lamellar phase contains planes of infinite bilayers. There are two possibilities that explain the conductivity parallel to the lamellar planes. It is possible to conceive a lamellar phase made up of imperfect lamellae with holes to allow the passage of ions as proposed in a study of the ternary mixture DACl/H_2O/NH_4Cl[37] and the CsPFO/water system[38] although freeze-fracture transmission electron microscopy[39] and a recent X-ray scattering study[40] concludes that the lamellar structure consists of planes of small discrete micelles in the DACl/H_2O/NH_4Cl system at least. A small angle neutron scattering study on the $N(CH_3)_4PFN$/water system by Herbst[35] *et al.* also concludes that its lamellar phase is made up of small discrete micelles.

The conclusions made from the conductivity experiments are further supported by X-ray diffraction studies. The diffraction patterns in reference 14 show no real difference in the pattern on either side of the nematic to lamellar transition. This qualitative observation is backed up by a plot of $d_{\parallel}$ and $d_{\perp}$ (the separation of the centres of mass of the micelles parallel and perpendicular to the director) versus temperature as shown in figure 1.5. Again we see no discontinuity across the transition.

The presence of the tricritical point, T_{cp}, along the nematic to lamellar transition line, as revealed by ^{2}H[13] and ^{133}Cs[31] NMR, is also an indication of a simple order-disorder transition. For thermotropic liquid crystals the tricritical point was predicted by McMillan[41] and De Gennes[42] for the smectic A to nematic transition and subsequently observed in binary mixtures[43,44,45,46]. The existence of the tricritical point suggests that the sequence of transitions in thermotropics is mirrored in this system implying that the transition from N_D^+ to L is a simple order-disorder one involving micelles condensing onto points in a plane. Therefore the discoidal lamellar mesophase (L_D) is analogous to the thermotropic smectic A phase.

Figure 1.5 d-spacings for a CsPFO/^2H_2O w=0.55 sample, calculated from the maxima in the intensity of the X-ray scattering curves using Bragg's law. Data for the plot was supplied by Dr D. Parker[14], Leeds University. $d_{\|}$ (•) is the face-to-face separation measured along the meridian and $d_{\perp}$ (o) is the side-to-side separation measured along the equator.

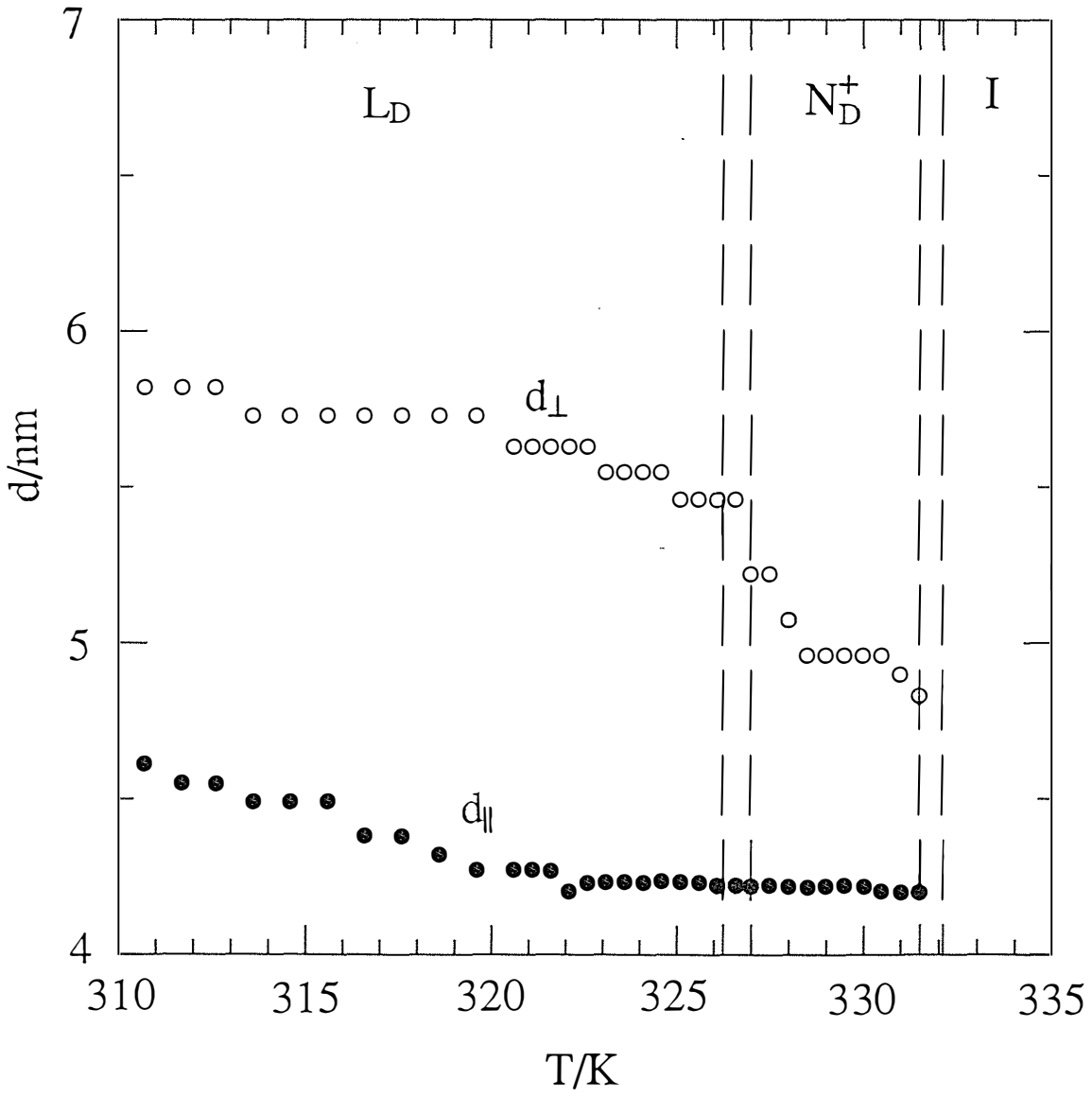

The aim of the present study was to produce high resolution phase diagrams for the CsPFO/H_2O, $NH_4PFO/^2H_2O$ and NH_4PFO/H_2O systems of the precision and accuracy of the $CsPFO/^2H_2O$ phase diagram. It was hoped to understand the role of the counter-ion and the solvent in the phase behaviour by comparing the phase diagrams of the different systems. The CsPFO/H_2O study was undertaken to provide a comparison with the $CsPFO/^2H_2O$ system and thereby establish the role of the solvent in determining the aggregate structure. The isotope effects are quite small between the two systems and a high resolution phase diagram is required for a valid comparison. A high resolution phase diagram for the CsPFO/H_2O system is also needed because of the current interest in phase transitions in aqueous CsPFO solutions[47,48,49,50] and the fact that some researchers[48-50] prefer to study the H_2O system.

There is more internal structure in ^2H_2O than in H_2O[51], due to the increased strength of the hydrogen bonding, therefore the hydrophobic effect is expected to be larger in the $CsPFO/^2H_2O$ system. Since substitution of water for heavy water could affect the micellar aggregation process a study on the thermodynamics of micellization was conducted on the $CsPFO/^2H_2O$ and CsPFO/H_2O systems. It was hoped that this study would give some insight into how the solvent affects the size and shape of the micelle in the liquid crystal regions and thus the phase behaviour.

A comparison of the NH_4PFO/water and CsPFO/water phase diagrams should provide new insight into the role of the counter-ion in determining the phase behaviour and therefore the micelle structure. It is well-known that altering the counter-ion produces marked results in fluorocarbon systems[32-34]. This is in contrast to the behaviour associated with single chain hydrocarbon surfactants where the phase behaviour tends not to be strongly dependent on the head-group or the counter-ion. The LiPFO system[52,53] exhibits a hexagonal and a lamellar phase but no nematic phase. No nematic phases have been discovered for the KPFO, NaPFO or $N(CH_3)_2H_2PFO$ systems although no high resolution phase diagrams are as yet available. Preliminary

investigations indicate that RbPFO behaves similarly to CsPFO except that it is less soluble and therefore the nematic phase is limited in its range by the onset of crystallization. The interaction of the counter-ion with the surface will dictate the size and shape of the aggregate and thus dominates the phase behaviour of the system.

The major part of this thesis is concerned with the presentation of the above phase diagrams and a discussion of the isotope effect and the effect of changing the counter-ion. During the course of this study however, the phenomenon of pretransitional field induced ordering close to the isotropic to nematic transition was detected through the observation of ^{133}Cs quadrupole splittings in the isotropic phase of the CsPFO/H_2O system. This effect was also revealed by ^{2}H quadrupole splittings in the isotropic phase of the CsPFO/$^{2}H_2O$ system. In a previous ^{2}H NMR study[13] of the latter system carried out at 2.11 T no evidence for field induced ordering had been seen. At the field strength used in the present study (6.3 T) the effect was quite marked in both the ^{2}H and ^{133}Cs spectra especially at low weight fractions of CsPFO. Accordingly a full study of the concentration and temperature dependence of the field induced quadrupole splittings was undertaken on the CsPFO/$^{2}H_2O$ system and is described in this thesis.

A variety of techniques have been used to gain information on the nature of, the structure of and the ordering in lyotropic liquid crystalline phases. The major techniques used in this study was nuclear magnetic resonance. A full discussion of the use of ^{133}Cs NMR to detect phase transitions is given and the model used to interpret ^{133}Cs and ^{2}H quadrupole splittings is tested. In order to do this information on the structure and size of the micelles and the orientational order of the mesophase is needed. The information was kindly provided by our collaborators at Leeds University.

REFERENCES

[1]Evans D. F.; Ninham B. W., *J. Phys. Chem.* **1986**, *90* , 226.

[2]Bartolino R.; Meuti M.; Chidichimo G.; Ranieri G. A., In *Proceedings of the International School of Physics, Course XC; Physics of Amphiphiles : Micelles, Vesicles and Microemulsions.* Ed. Degiorgio V. and Corti M. **1985**, p 524 (North-Holland Physics Publishing, Amsterdam).

[3]Reinitzer F., *Montash Chem.* **1888**, *9*, 421.

Lehmann O., *Z. Krist.* **1890**, *18* , 464.

[4]For example see, de Gennes P. G., *Physics of Liquid Crystals* **1974**, (Oxford University Press, London) and Chandrasekhar S., Liquid Crystals , **1977**, (Cambridge University Press, Cambridge).

[5]Buckingham A. D.; MacLauchlan K. A., in *Progress in NMR Spectroscopy* , 2, **1967**, eds Emsley J. W.; Feeny J.; Sutcliffe H. L. p63.

[6]Saupe A., *Z. Naturforsch.* **1964**, *19a* , 161.

[7]De Jeu W. H., *Physical Properties of Liquid Crystalline Materials* (Gordon & Breach, New York) **1980**.

[8]Lindman B.; Wennerström H., *Topics in Current Chemistry*, Vol 87 (Springer-Verlag) pp. 1-84 **1980**.

[9]Tiddy G. J. T., *Phys. Rep.* **1980**, *57* , 1.

[10]Lawson K. D. and Flautt T.J. *J. Phys. Chem.* **1967**, *89* , 5489.

[11]Rosevear F., *J. Soc. Cosmet. Chem.* **1968**, *19* , 581.

[12]Charvolin J.; Levelut A. M.; Samulski E. T., *J. Physique Lett.* **1979**, *40* , L587.

[13]Boden N.; Corne S. A.; Jolley K. W., *J. Phys. Chem.* **1987**, *91* , 4092.

[14]Boden N.; Corne S A.; Holmes M. C.; Jackson P. H.; Parker D.; Jolley K. W., *J. Physique* **1986**, *47* , 2135.

[15]Freiser M. J., *Phys. Rev. Lett.* **1970**, *24* , 1041.

[16]Shih C. S.; Alben R., *J. Chem. Phys.* **1972**, *57* , 3055.

[17]Alben R., *J. Chem. Phys.* **1973**, *59* , 4299; *Phys. Rev. Lett.* **1973**, *30* , 778.

[18]Straley J. P., *Phys. Rev. A* **1974**, *10* , 1881.

[19]Yu L. J.; Saupe A., *Phys. Rev. Lett.* **1980**, *45* , 1000.

[20]Radley K.; Reeves L. W.; Tracey A. S., *J. Phys. Chem.* **1976**, *80* , 174.

[21]Boden N.; Jackson P. H.; McMullen K.; Holmes M. C.,*Chem. Phys. Lett.* **1979**, *65* , 479.

[22]Boden N.; Radley K.; Holmes M. C., *Mol. Phys.* **1981**, *42* , 493.

[23]Fujiwara F. Y.; Reeves L. W., *Mol. Phys.* **1978**, *36*, 1897.

[24]Chen D M.; Fujiwara F. Y.; Reeves L. W., *Can. J. Chem.* **1977**, *55* , 2396.

[25]Yu L. J.; Saupe A., *J. Am. Chem. Soc.* **1980**, *102* , 4879.

[26]Boden N. in press

[27]Boden N; Bushby R.; Ferris L.; Hardy C.; Sixl F., *Liq. Cryst.* **1986**, *1* , 109.

[28]Rizzatti M. R.; Gault J. D., *J. Colloid Interface Sci.* **1986**,*110* , 285.

[29]Boden N.; Radley K.; Holmes M. C., *Mol. Phys.* **1981**, *42* , 493.

[30]Lee H.; Labes M. M., *Mol. Cryst. Liq. Cryst.* **1982**, *84* , 137.

[31]Boden N.; Jolley K. W.; Smith M. H., *Liq. Cryst.* **1989**, *6* , 481.

[32]Fontell K.; Lindman B., *J. Phys. Chem.* **1983**, *87* , 3289.

[33]Hoffmann H., *Ber. Bunsenges. Phys. Chem.* **1984**, *88* , 1078.

[34]Reizlein K.; Hoffmann H., *Prog. Colloid & Polymer Sci.* **1984**, *69* , 83.

[35]Herbst L.; Hoffmann H.; Kalus J.; Reizlein K.; Schmelzer U.; Ibel K., *Ber. Bunsenges. Phys. Chem.* **1985**, *89* , 1050.

[36]Tiddy G. J. T., *J. Chem. Soc., Faraday Trans. 1* **1972**, *68* , 608.

[37]Holmes M. C.; Charvolin J., *J. Phys. Chem.* **1984**, *88* , 810.

[38]Photinos P. J.; Saupe A., *Phys. Rev. A* **1990**, *41* , 954.

[39]Sammon M. J.; Zasadzinski J. A. N.; Kuzma M. R., *Phys. Rev. Lett.* **1986**, *57* , 2834.

[40]Holmes M. C.; Charvolin J.; Reynolds D.J., *Liq. Cryst.* **1988**, *3*, 1147.

[41]McMillan W. L., *Phys. Rev. A* **1971**, *4* , 1238; **1972**, *6* , 936.

[42]De Gennes P. G., *Solid St. Commun.* **1972**, *10* , 753.

[43]D Brisbin, R. Dehoff, T. E. Lockhart, and D. L. Johnson, *Phys. Rev. Lett.* **1979**, *43* , 1171.

[44]H. Marynissen, J. Thoen, and W. van Dael, *Mol. Cryst. Liq. Cryst.* **1985**, *124* , 195.

[45]S. B. Rananavare, V. G. K. M. Pisipati, and J. H. Freed, *Chem. Phys. Lett.* **1987**, *140* , 255.

[46]M. A. Anisimov, V. P. Voronov, A. O. Kulkov, V. N. Petukhov, and F. Kholmurodov, *Mol. Cryst. Liq. Cryst.* **1987**, *150b* , 399.

[47]Boden N.; Holmes M. C.,*Chem. Phys. Lett.* **1984**, *109* , 76.

[48]Rosenblatt C.*Phys. Rev. A* **1985**, *32* , 1115.

[49]Rosenblatt C., *Phys. Rev. A* **1985**, *32* , 1924.

[50]Rosenblatt C.; Kumar S.; Litster J. D., *Phys. Rev. A* **1984**, *29* , 1010.

[51]Némethy G.; Scherga H., *J. Phys. Chem.* **1964**, *41* , 680.

[52]Everiss E.; Tiddy G. J. T.; Wheeler B. A., *J. Chem. Soc. Faraday Trans. I* **1976**,*72* , 1747.

[53]Kekicheff P.; Tiddy G. J. T., *J. Phys. Chem.* **1989**, *93* , 2520.

CHAPTER 2

MATERIALS AND METHODS

2.1 MATERIALS

2.1.1 Chemicals

Deuterium oxide, 99.9 atom % deuterium, was obtained from Aldrich Chemical Company, Inc and Sigma Chemical Company USA. Pentadecafluorooctanoic acid was obtained from Aldrich and Riedel-de Haen and used without further purification. All water used in the preparation of samples was deionised and doubly distilled.

Ammonium pentadecafluorooctanoate (NH_4PFO) was produced by two different methods, both of which produced liquid crystalline samples with identical phase transition temperatures. The first method used was to bubble ammonia gas through a solution of pentadecafluorooctanoic acid in di-ethyl ether[1]. This would have been an excellent method if the resulting ammonium salt had been less soluble in the ether when it would have dropped out of solution leaving impurities and unreacted acid in solution. This did not occur in spite of using ether which had been dried using sodium wire. To recover the NH_4PFO, the ether was evaporated on a rotary evaporator and the salt was purified by recrystallization from a 12:1 (v:v) mixture of n-hexane and butanol. The second (and favoured) method[2] was to add crystalline pentadecafluorooctanoic acid to a saturated aqueous ammonia solution (Ajax Chemicals, specific gravity = 0.880). When the pH of the ammonia solution had reached 7, as measured by indicator paper (BDH). (*i.e.* there will be an excess of NH_4OH since the pK_a for the ammonium ion is less than 7), the resulting amphiphile solution was freeze dried to remove the water and excess unreacted ammonia. The ammonium pentadecafluorooctanoate was then recrystallized from a 12:1 (v:v) n-hexane butanol mixture.

Caesium pentadecafluorooctanoate (CsPFO) was prepared by neutralizing a solution of pentadecafluorooctanoic acid in water with an aqueous solution of caesium carbonate. A simple acid-base reaction occurs with the evolution of carbon dioxide. Although pentadecafluorooctanoic acid is only sparingly soluble in water, all the acid is solubilized as the reaction proceeds and the water soluble Cs salt is formed. Caesium carbonate was added until all of the acid was dissolved and the evolution of carbon dioxide had ceased. The resulting solution was then freeze dried and purified by recrystallization from a n-hexane/butanol mixture.

The recrystallized salt was dried in a vacuum for at least two days to ensure the removal of any traces of the organic solvent used in the recrystallization. This was essential as tiny amounts of solvent (or salt) can markedly affect the phase transition temperatures. There have been studies published on the effect of adding a third component to CsPFO solutions[3,4]. In these studies the effect of added cosurfactant or electrolyte is to increase the nematic to isotropic transition temperature. In contrast, traces of butanol in the samples reduced the expected transition temperatures. Both CsPFO and APFO were stored in a desiccator to keep them moisture free until needed. Prior to the preparation of a sample the amphiphile was again put on the vacuum line to ensure complete dryness. This is important because any additional water would make a difference in the calculation of the weight fraction of the sample. Caution must be taken when heating any of these salts because they tend to decompose at higher temperatures (for CsPFO ≈ 230°C and for NH_4PFO ≈ 130°C).

2.1.2 NMR Sample Preparation

Samples for use in the NMR spectrometer were produced by weighing solvent and amphiphile directly into a 5 mm o.d NMR tube which had been shortened to a length of 100 mm. The solvent was added through a long hypodermic syringe needle whilst the amphiphile was introduced by means of a long funnel to avoid contact of the

salt with the upper portion of the tube which is heated during sealing. The solvent was added first so that the amphiphile was dissolved on addition and thus took up less space. If the solvent is added on top of the amphiphile a small region of very concentrated liquid crystal is formed at the interface preventing further mixing and creating a greater volume in the tube.

Once the solvent and amphiphile were added and if the top portion of the tube was free of sample the tube was flame sealed. Once the sample was sealed in the NMR tube a section of 5 mm glass tubing was added to bring the total length up to 655 mm. This length is necessary for alignment of the sample in the sample coils of the superconducting magnet of the JEOL NMR spectrometer. Once sealed the samples were heated to a temperature at least fifteen degrees above the expected isotropic to liquid crystal transition and mixed by inverting at least fifty times. A thorough mixing is very important as newly prepared samples contain a large number of concentration gradients caused by a degree of immiscibility between the different mesophases. It has been found that for this type of liquid crystal, samples are not stable to storage at elevated temperatures (>100 °C) but if stored at room temperature they give consistent results over a period of months.

2.1.3 DSC Sample Preparation

Samples for use in the differential scanning calorimeter were prepared by weighing the appropriate solvent and amphiphile into a glass vial which was then flame sealed. Samples with a high weight fraction of amphiphile proved difficult to mix evenly even at higher temperatures. For samples with a weight fraction w >0.75, the solvent and amphiphile were weighed into a glass vial which consists of two compartments separated by a small aperture. When sealed the sample was thoroughly mixed by centrifuging from one compartment to the other a few times until the sample appeared homogeneous when viewed through cross polarisers. Samples with a lower weight fraction could be easily mixed by inverting a few times in the isotropic phase in

the same way as the NMR samples. When ready for use the DSC sample vials were broken and the sample weighed into an aluminium pan which was sealed by crimping in a press.

2.1.4 Conductivity Sample Preparation

These samples were prepared as needed by weighing amphiphile and solvent into 10 cm^3 volumetric flasks. There are no difficulties in mixing these samples as they are all in the low amphiphile concentration range with a weight fraction of less than 0.30.

2.2 INSTRUMENTATION

2.2.1 Temperature Control

Modern NMR spectrometers are equipped with temperature control systems which use a stream of hot air for heating the sample and gas from liquid nitrogen for cooling. This method is adequate for most applications in NMR spectroscopy where the temperature dependence on the measured quantity is not large. The temperature control system for the JEOL GX-270 NMR machine gives a quoted stability[5] of ±1 K. Improved systems have been reported[6] but the temperature stability of even these systems (±0.1 K) is poor compared to that needed in studies of micellar liquid crystals. In addition temperature gradients are always a problem in air control systems. The greater the measuring temperature from ambient temperature, the greater the temperature gradients.

In systems which show a strong temperature dependence of an NMR parameter it is vital to minimize temperature gradients and to achieve precise temperature control. This is illustrated by considering the w=0.502 CsPFO/^2H_2O sample where, close to the nematic to isotropic transition temperature, the temperature dependence of the quadrupole splitting is very large (1.45 kHz K^{-1} at 320.6 K). If even a small temperature gradient is present in the sample then the spectrum will be broadened due to

the presence of the consequent range of quadrupole splittings along the sample length. With an air controlled temperature system at non-ambient temperatures large temperature gradients exist. For a temperature gradient of even 100 mK over the sample length, broadening of about a 150 Hz will result. This is large when compared to the natural linewidth of 18 Hz for the $m=+\frac{3}{2}$ to $+\frac{1}{2}$ and $-\frac{1}{2}$ to $-\frac{3}{2}$ peaks for the w=0.502 CsPFO/^2H_2O sample. In the production of the CsPFO/H_2O high resolution phase diagram it was often necessary to distinguish ^{133}Cs lines separated by a few hertz and a broadening of 150 Hz cannot be tolerated. Clearly with a temperature dependence as large as 1.45 kHz K^{-1} even small temperature gradients or fluctuations will result in a reduction in the resolving power of the NMR measurements. Another problem generated by the presence of temperature gradients is the consequent concentration gradients caused by distillation of the solvent. The presence of temperature and/or concentration gradients in samples is evidenced in the appearance of the spectrum. There are several examples of such inhomogeneous samples in the literature. In a study[1] to determine the phase behaviour in heptadecafluorononanoate salt solutions the ^2H spectra of heavy water used to demonstrate the characteristic pattern of the nematic phase contains at least five lines rather than the expected doublet. The sample was at a temperature near the Tp(I,N,L,) triple point. Concentration gradients allow portions of the sample to be in different phase regimes *i.e.* simultaneously in the nematic, nematic/lamellar biphasic and nematic/isotropic biphasic regions hence the spectrum contained peaks from isotropic, nematic and lamellar signals.

The precision of air flow temperature control systems can be improved by increasing the rate of air flow or by using insulation to reduce the rate of heat loss from the sample. This would however impose restraints on the probe design. The basic problem associated with all air flow systems is the use of a disperse phase as the heat exchange medium. In the temperature control system used in this study we used water as the heat exchange medium. There are several reasons for this aside from it being readily available and cheap. Firstly we are not interested in the NMR spectrum of the ^1H

nucleus and therefore the protons circulating in the thermostatted water are of no consequence. Secondly a water flow temperature control system which uses a condensed phase with a high density means that the mass of coolant that can be circulated is far greater than those that rely on disperse phases such as air. An air flow system which passes 25 dm^3 min^{-1} over the sample requires the loss of only 27 J of heat in a minute to change the temperature by a degree. The Colora Wk 3 pumps 1.3 dm^3 min^{-1} around the sample cell. For a one degree temperature drop 5.5 kJ min^{-1} must be lost to the surroundings.

The temperature control device for the NMR and conductivity measurements was based on a double-pass waterflow system. The sample cells constructed to accommodate the NMR and conductivity samples are shown in figures 2.1 and 2.2 respectively. The temperature of the water was controlled to ± 5 mK by a Colora WK3 circulating cryostat. This system can keep the temperature stable to within a few millikelvin for several hours.

To demonstrate the capabilities of the temperature control system used in this study the time dependence of the ^{133}Cs quadrupole splitting was studied on changing the temperature setting by 1 K. Figure 2.3 is a plot of the ^{133}Cs quadrupole splitting vs time for a CsPFO/^2H_2O sample (w=0.502) following a change in the set temperature from 319.60 K to 320.60 K. The sample attained the new temperature within five minutes. Over an hour the quadrupole splittings fell in the range of 2088±7 Hz which corresponds to a temperature stability of ±0.004 K ($\frac{\partial(\Delta\tilde{\nu})}{\partial T}$ = 1.45 kHz K^{-1} at 320.60 K).

Figure 2.1 Double-pass water flow sample cell used to control the sample temperature during NMR experiments, using a JEOL GX270 spectrometer. The water is pumped to the cell by a Colora WK3 cryostat.

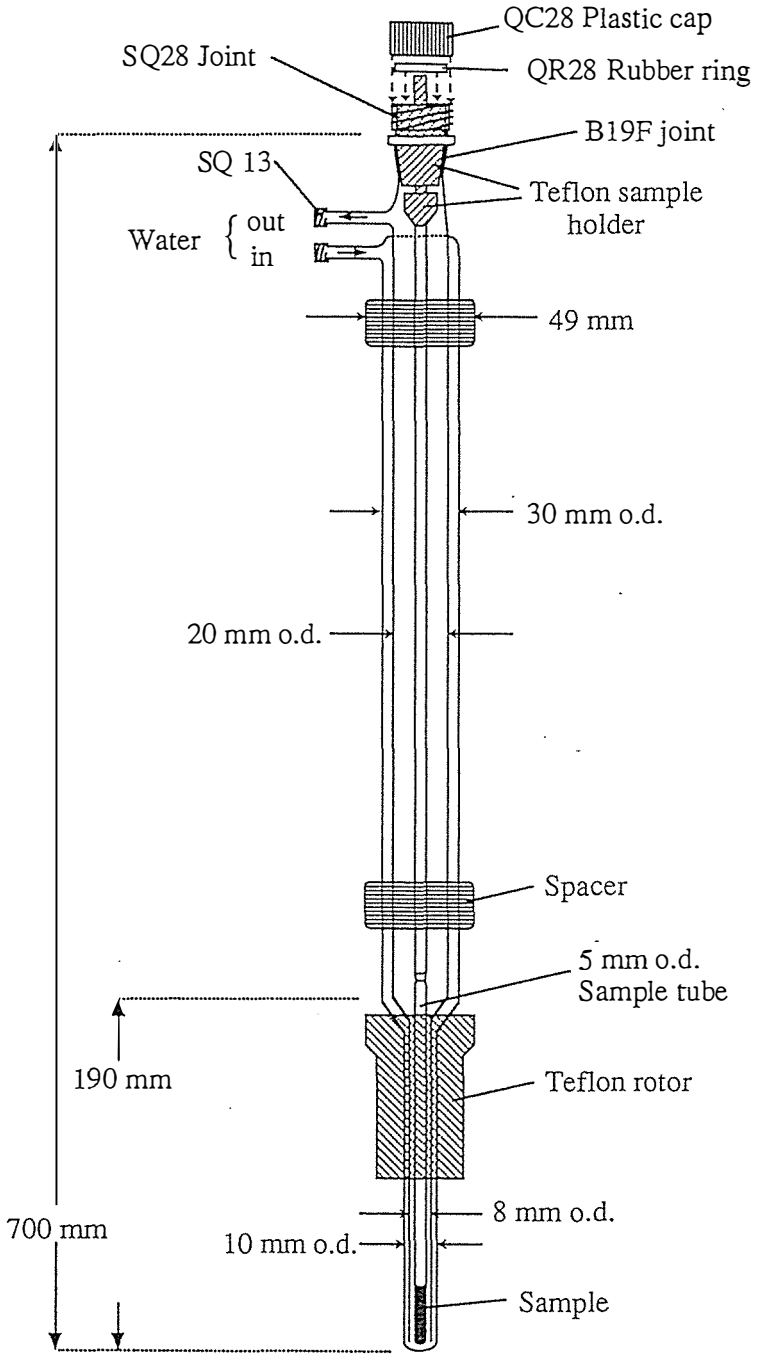

Figure 2.2 Double-pass water flow sample cell used to control the sample temperature during conductivity experiments. The water is pumped to the cell by a Colora WK3 cryostat.

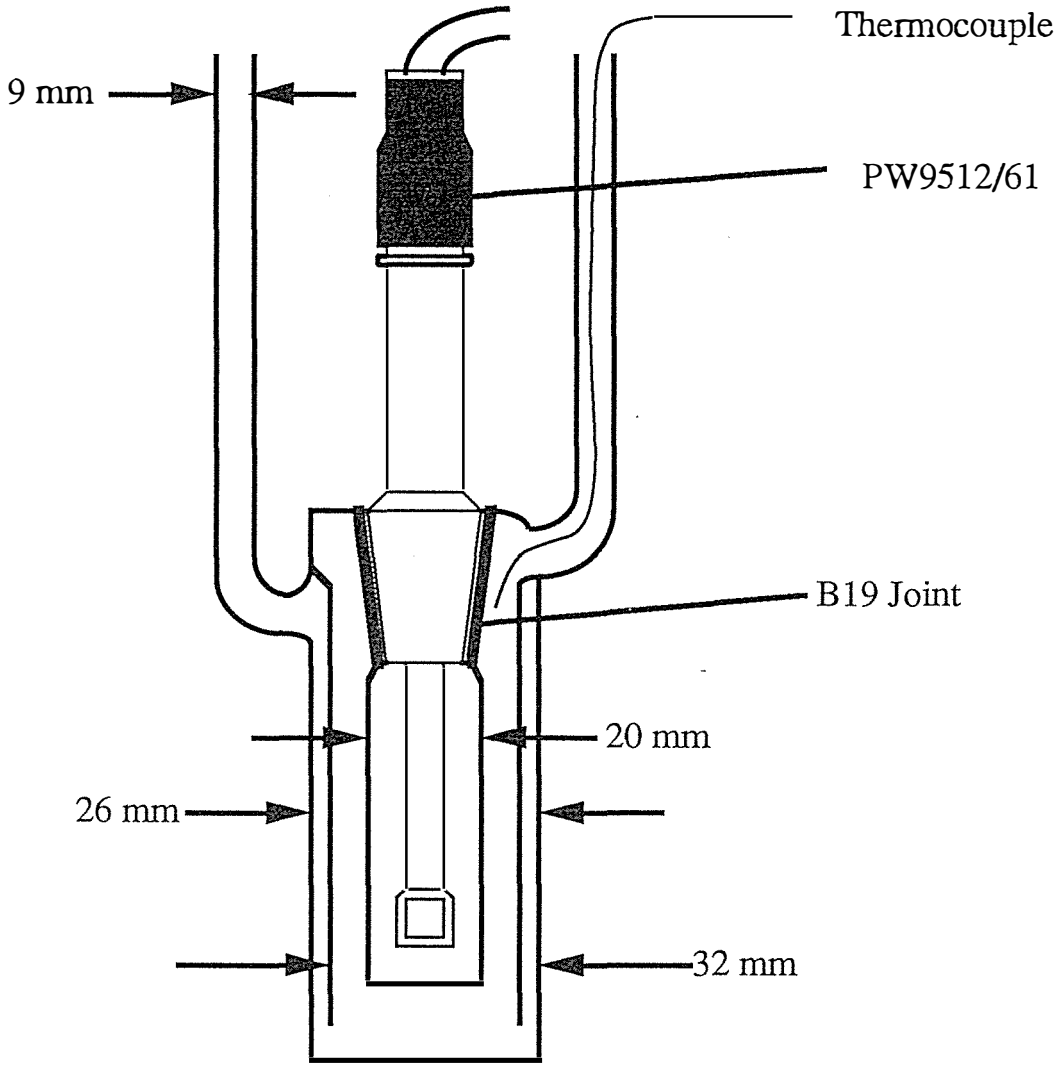

Figure 2.3 Plot of the ^{133}Cs quadrupole splitting ($\Delta\tilde{\nu}$) versus time for a CsPFO/$^{2}H_2O$ w=0.502 sample on changing the set temperature from 319.6 K to 320.6 K. $\partial\Delta\tilde{\nu}/\partial T$ at 320.6 K is 1.45 kHZ K^{-1}. The variation in $\Delta\tilde{\nu}$ from 5 min to 60 min represents a temperature stability of ± 0.004 K.

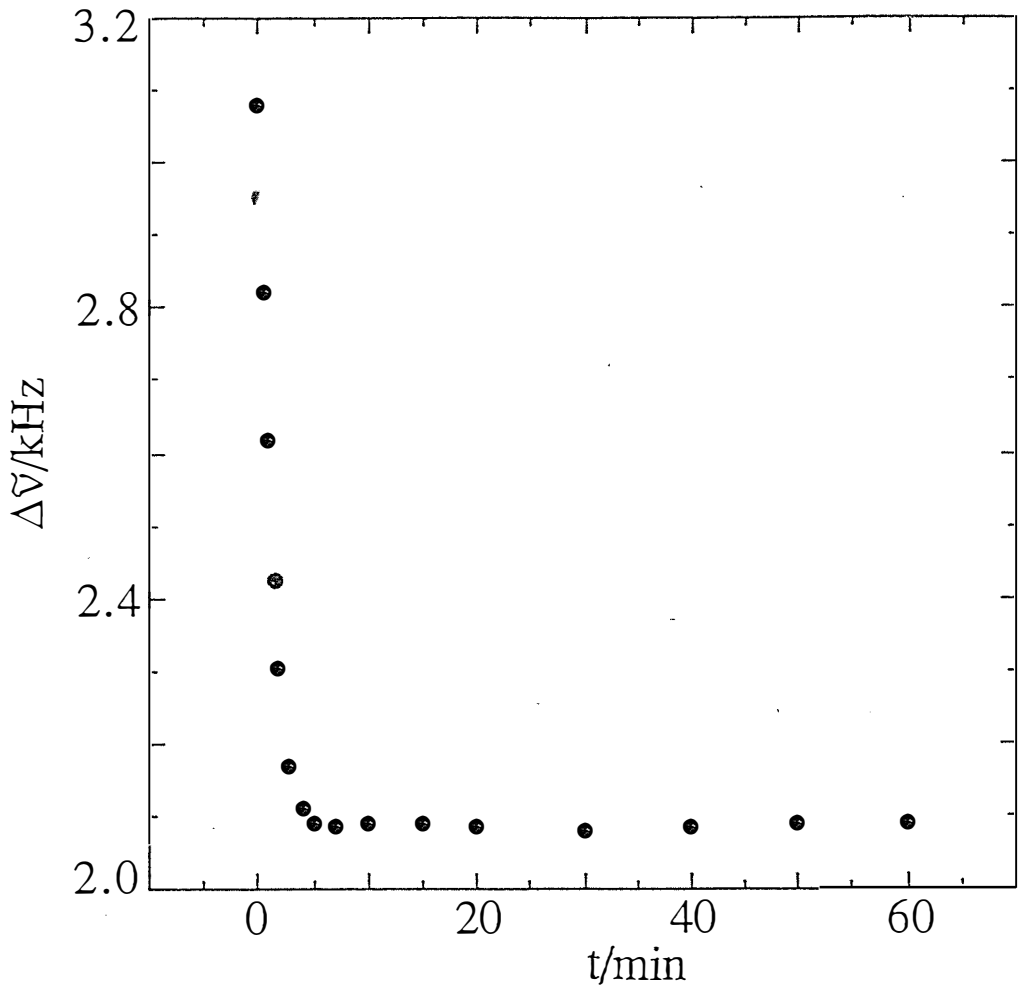

Figure 2.4 Comparison of the ^{133}Cs spectra of a CsPFO/$^{2}H_2O$ w=0.502 sample at 315.50 K with (a) the water temperature control system and (b) the air controlled system.

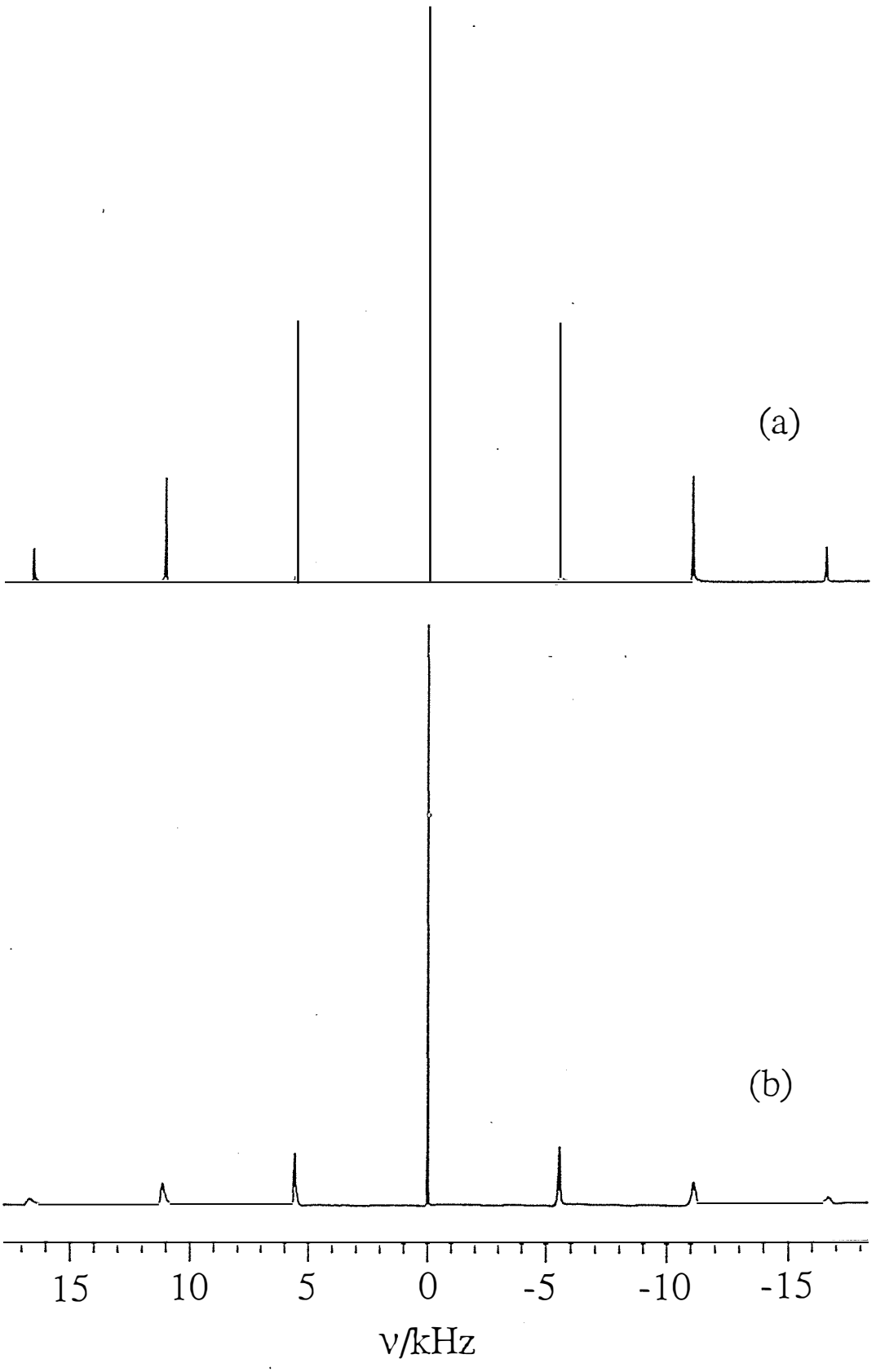

The influence of temperature gradients is clearly illustrated in figure 2.4 which shows a comparison of the ^{133}Cs spectra of the w=0.502 sample at 315.50 K using (a) the water temperature control system and (b), the air temperature control system. The line-widths at half maximum amplitude for the inner satellite peaks (|m|= 1/2 to |m|=3/2) are 18 Hz and 100 Hz for (a) and (b) respectively. At 315.5 K $\frac{\partial(\Delta\tilde{\nu})}{\partial T}$ is 1.20 kHz K^{-1} and the extra linewidth indicates that in the air flow spectra a temperature gradient of ≈ 70 mK is present along the length of the sample.

2.2.2 Temperature Measurement

Temperature measurement was carried out using a copper-constantan thermocouple which had been calibrated from 0 to 100°C at 2°C intervals against a Hewlett Packard 2801A quartz thermometer with a 2850A probe. The potential difference between the reference junction and the measurement junction of the thermocouple was measured using a Keithley 181 nanovoltmeter operating in the 2 mV range. This type of digital voltmeter gives voltages accurate to 10^{-9} V. The damping and filter options were used when making measurements to ensure that small fluctuations caused by interference from various electronic devices in the vicinity were minimized. The thermocouple leads were also insulated with earthed copper sheathing to prevent them acting as aerials. The reference junction was keep at 0 °C by immersion in an ice/distilled water slurry. The temperature of the slurry was constant over the period of a day as long as care was taken to ensure the mixture remained homogeneous. The temperature was determined from the voltage reading by interpolation between the relevant points in the calibration data using an HP85 desktop computer.

2.2.3 Nuclear Magnetic Resonance

The NMR spectra were obtained using a JEOL JNM-GX270 spectrometer with an Oxford Instruments 6.34 T wide bore superconducting magnet. The ^{133}Cs and ^{2}H

spectra were collected using a 10 mm tuneable probe, NM-G27T10 and the ^{14}N spectra were collected using a 10 mm low frequency tuneable probe, NM-G27T10L.

Typical measurement parameters are set out in the following table with explanations in the ensuing text.

Table 2.1 NMR parameters used in this thesis.

Nucleus	^{2}H	^{133}Cs	^{14}N
I	1	$\frac{7}{2}$	1
Experimental Mode	SGNON	SGNON	SGLBCM
Observation frequency	41.47 MHz	35.44 MHz	19.52 MHz
Sweep width	2 kHz	10-60 kHz	10-40 kHz
Data points	8192	32768	8192
Broadening factor	0.1 Hz	1 Hz	10-50 Hz
Accumulations	2	10	500
$\frac{\pi}{2}$ Pulse width	20 or 200 μs	20 μs	47 μs
Pulse delay	2 s	0.5 s	0.01 s

The above parameters are typical values and were altered as necessary to meet the requirements of specific experiments. For example, if the central Zeeman peak for ^{133}Cs is being closely monitored through a phase transition a sweep width of about 1 kHz is sufficient with a corresponding reduction in data points. There are two pulse widths quoted for ^{2}H, the short pulse width corresponds to the situation where the probe is tuned to ^{2}H and the long pulse for when it is tuned to ^{133}Cs (detuned from ^{2}H). When the probe is detuned a longer pulse width is required to rotate the magnetization through 90° but the quality of the ^{2}H spectra is not affected. Detuning allows the collection of both ^{2}H and ^{133}Cs spectra in a very short space of time. This is achieved by using both of the terminals on the GX-270 machine, one with parameters

set for ^{2}H observation and one set for ^{133}Cs observation. As soon as the ^{133}Cs accumulation is completed the ^{2}H accumulation can be started. This procedure enabled ^{2}H and ^{133}Cs spectra to be obtained at exactly the same temperatures.

The sweep widths used are selected to cover the expected range of frequencies. In pulse Fourier transform NMR a square pulse (a pulse of apparently monochromatic radiation of frequency, ν_c, and of duration τ_p) in the time domain has a frequency domain equivalent in which the distribution of frequencies is given by the sinc function[7] $\frac{\sin(\pi(\nu-\nu_c)\tau_p)}{\pi(\nu-\nu_c)\tau_p}$.

To provide an adequate distribution of frequencies over the range we wish to observe the condition $\Delta < \tau_p^{-1}$ must be met, where Δ is the sweep width in hertz. Using a 20 μs pulse in ^{133}Cs experiments gives an effective frequency range of 50 kHz (*cf.* a typical experimental range of 32 kHz). In the case of ^{2}H the 200 μs pulse width gives a good spectral distribution over a frequency range of 5 kHz which is much larger than the range needed for deuterium spectra (≈ 2 kHz). Thus when the probe is tuned to the ^{133}Cs resonance frequency, spectra with true intensity distributions are obtained for both ^{2}H and ^{133}Cs nuclei. Tuning to the ^{2}H resonance frequency and using a long ^{133}Cs pulse would lead to ^{133}Cs spectra with attenuated outer satellite intensities. The effective frequency range for the ^{14}N nucleus is 22 kHz.

The broadening factor is an exponential weighting function applied to the free induction decay (FID) before Fourier transformation. It is important to choose a broadening factor that gives a sufficient signal to noise ratio without loosing out on resolution. A compromise is reached by selecting a broadening factor which is roughly half the natural line-width of the spectral peaks. The signal to noise ratio can also be increased by increasing the number of accumulations. Signal to noise is increased because coherent signals add whilst random noise tends to cancel. The enhancement of signal to noise increases with the square root of the number of accumulations.

When choosing the number of data points two factors must be taken into consideration. Firstly there must be sufficient points to define the peak and secondly the number of points must be kept at a minimum so as to save time on the Fourier transform and to save space when storing the information on the storage device attached to the spectrometer. The line-width at half height for the central peak of a ^{133}Cs spectrum may vary from approximately 4 Hz in the isotropic phase to between 12 and 20 Hz in liquid crystalline mesophases. This means points at 1 Hz intervals are more than adequate to define the peaks. For deuterium spectra the line-widths can be of the order of 1 Hz so a data point is needed approximately every 0.2 Hz.

The delay between the pulses is dictated by the ability of the sample to recover to the equilibrium magnetization along the field direction before the next pulse. The faster the recovery time the less the time required between pulses. This recovery time is known as the longitudinal relaxation time, T_1. Corresponding to T_1 is the transverse relaxation time, T_2, which describes the loss of phase coherence of the magnetization in the xy plane; in liquids $T_1 \geq T_2$. It is T_2 which determines the linewidth at half height ($\Delta\nu_{1/2}$). More precisely this is given by

$$\Delta\nu_{1/2} = \frac{1}{\pi T_2^*} \qquad [2.1]$$

where T_2^* is the apparent value of T_2, given by $T_2^{*-1} = T_2^{-1} + \gamma\Delta B/2$ where ΔB is a measure of the magnetic field inhomogeneity and there is the magnetic field spread over the sample volume. There are several mechanisms for relaxation processes but the dominant one when observing quadrupole nuclei is quadrupolar relaxation[8]. In the extreme narrowing limit[9,10] $T_q=T_1\approx T_2$. The quadrupolar relaxation time is inversely proportional to χ^2 where χ is the nuclear quadrupole coupling constant $\left(=\frac{e^2qQ}{h}\right)$. Here e is the charge on the electron, Q the nuclear electric quadrupole moment and q the electric field gradient at the nucleus. In micellar liquid crystals the observed relaxation time is an average of the contribution of the relaxation times of the bound and unbound species

and the relaxation times of the unbound species are longer than the bound species. The contributions of each species to the measured relaxation time is described by $\frac{1}{T_{obs}} = x_b\frac{1}{T_b} + x_f\frac{1}{T_f}$ where the subscripts b and f refer to the bound and free species respectively and x is the mole fraction. The value of Q for ^{133}Cs is similar to that of $^{2}H^{11}$ but the bound fraction is much greater therefore the observed relaxation time is shorter which results in broader lines and allows the use of shorter pulse delays. Q is an order of magnitude larger for $^{14}N^{11}$ than for both ^{2}H and ^{133}Cs whilst the bound fraction is similar to that of the caesium ions. This results in rapid relaxation and ^{14}N line-widths which are more than an order of magnitude greater than those for ^{133}Cs spectra.

^{14}N is not an ideal nucleus to use in the determination of phase transitions. It is less sensitive than ^{133}Cs (by a factor of 50) and although it is more sensitive than ^{2}H there are many more ^{2}H nuclei in our samples than ^{14}N nuclei (for a w = 0.5 sample of $NH_4PFO/^{2}H_2O$ the ratio of ^{2}H to ^{14}N is approximately 43:1). Also, as discussed above, the very short relaxation time for ^{14}N in liquid crystalline mesophases means that the resulting quadrupole peaks are very broad with a consequent poor signal to noise ratio. The short relaxation time and low sensitivity combine to give an FID that has a significant contribution from acoustic ringing. A broad signal resulting from acoustic ringing occurs because of rf frequency vibrations in the metal of the probe caused by the pulse. The ring down typically last 100 μs which corresponds to a 10 kHz wide signal and causes undulation of the baseline. This acoustic ringing is present for other nuclei but its effect is insignificant when a strong signal is being measured. It is possible to eliminate the effects of acoustic ringing by increasing the delay time (the time between the pulse and the accumulation) to ≈100 μs. This method causes loss of some of the signal if the relaxation time is short and also leads to phase distortions. In the anisotropic mesophases the fast relaxation rate allows us to use a very short pulse delay (≈0.005 s) and therefore many accumulations can be completed in a short time. The large number of accumulation is necessary because of the diffuse nature of the

quadrupole peaks. The broad quadrupole peaks mean that a large broadening factor can be used to improve the signal to noise without any adverse effect on the resolution.The experiment mode used for the acquisition of the ^{14}N FID is SGLBCM, single pulse with bilevel decoupling. This mode was initially used to avoid any complications caused by coupling of the proton spins to the ^{14}N nucleus. The inherent broadness of the ^{14}N quadrupole peaks made this unnecessary although this practise continued throughout the whole study. The experiment mode used for the acquisition of the FID for ^{133}Cs and ^{2}H is SGNON, single pulse with no decoupling.

2.2.4 Differential Scanning Calorimetry

Differential scanning calorimetry (DSC) thermograms were recorded using a Perkin-Elmer DSC-2 instrument interfaced with a model 3600 thermal analysis data station situated at the New Zealand Dairy Research Institute, Palmerston North.

Before use the instrument was calibrated using an indium standard sample. The thermograms were obtained using a scanning rate of 5 K/min. Typical samples used ranged in weight from ten to twenty milligrams

2.2.5 Conductivity

The apparatus used in these experiments was a Phillips PW9509 digital conductivity meter attached to a Phillips PW9512/61 conductivity cell. The conductivity measurements were performed at a operating frequency of 2000 Hz.

REFERENCES

[1]Fontell K.; Lindman B., *J. Phys. Chem.* **1983**, *87* , 3289.

[2]Tiddy G. J. T., *J. Chem. Soc., Faraday Trans. I* **1972**, *68* , 608.

[3]Rosenblatt C.; Zolty N.,*J. Physique Lett.* **1985**, *46* , L-1191.

[4]Rosenblatt C.*J. Phys. Chem.* **1987**, *91* , 3830.

[5]JEOL GX-270 Instruction Manual.

[6]Vanni H.; Earl W. L.; Merbach A. E., *J. Magn. Reson.* **1978**, *29* , 11.

[7]Shaw D., in *NMR and the Periodic Table* , ed. Harris R. K.; Mann B. E. (Academic Press, London) **1978** p21.

[8]Harris R. K., in *NMR and the Periodic Table* , ed. Harris R. K.; Mann B. E. (Academic Press, London) **1978** p1.

[9]Abragam A., *The Principles of Nuclear Magnetism* **1967**, (Oxford University Press, Oxford).

[10]Lindman B.; Danielsson I., *J. Colloid Interface Sci.* **1972**, *39*, 349.

[11]Brevard C.; Granger P., *Handbook of High Resolution Multinuclear NMR*, (John Wiley & Sons, New York), **1981**.

CHAPTER 3

NMR THEORY

Nuclear magnetic resonance of quadrupole nuclei is an excellent technique for mapping the phase diagrams and studying the nature and mechanisms of phase transitions in lyotropic liquid crystals. This is because the quadrupole splitting is a characteristic signature of each type of phase and is also a function of temperature and composition. It is a particularly useful method when traversing phase coexistence regions in that the signal from both components is observable and that the relative amounts of the phases can be monitored. The ^{133}Cs nucleus has been found to be particularly useful. The ^{133}Cs quadrupole splittings are large (of the order of kHz), are concentration and temperature dependent, and the line-widths are small (of the order of Hz). When compared with ^{2}H NMR of heavy water[1] this combination offers an order of magnitude improvement in the resolution of coexisting phases in the CsPFO/$^{2}H_2O$ system[2]. In addition, the $m=+\frac{1}{2}$ to $m=-\frac{1}{2}$ Zeeman transition, to first order, contains no contribution from quadrupole interactions. In the isotropic solution phase the chemical shifts are determined by the trace of the chemical shift shielding tensor, whilst in ordered liquid crystal phases the shift depends on the parallel component of the shielding tensor. ^{133}Cs chemical shift anisotropy is large in the CsPFO/water system and observation of the Zeeman transition provides a useful method for detecting phase transitions.

In the following sections the basic theory of the NMR of quadrupole nuclei and the dependence of the quadrupole splittings and chemical shift anisotropies on the size and shape of the aggregate, the fraction of bound counter-ion and the solvent mole fraction will be developed. Examples of typical spectra will also be presented.

3.1 QUADRUPOLE SPLITTING IN ANISOTROPIC MEDIA

One of the fundamental postulates of modern chemical physics is that the total angular momentum of an isolated particle cannot have any arbitrary magnitude but must take certain discrete values.

For a nucleus the magnitude of the spin angular momentum vector, **P**, is defined by the nuclear spin quantum number, I, such that

$$\mathbf{P} = \frac{h}{2\pi}\sqrt{I(I+1)} \qquad [3.1]$$

The direction of **P** is described by a further quantum number, m_I, which represents the component of the spin angular momentum along the z-direction.

$$P_z = \frac{h}{2\pi}m_I \qquad (m_I = I, I-1, I-2 \ldots -I) \quad [3.2]$$

Since all nuclei are charged, those that possess a spin angular momentum will generate a magnetic moment, μ,

$$\mu = \frac{2\pi g_N \mu_N \mathbf{P}}{h} \qquad [3.3]$$

where g_N is the nuclear g factor and μ_N is the nuclear magneton ($= \frac{eh}{4\pi m_p} = 5.05095 \times 10^{-27}$ J T^{-1}).

This is commonly written in the form,

$$\mu = \gamma \mathbf{P} \qquad [3.4]$$

where γ is the magnetogyric ratio $\left(\gamma \equiv \frac{2\pi g_N \mu_N}{h}\right)$ *i.e.* The magnitude of μ is given by

$$\mu = \frac{\gamma h}{2\pi}\sqrt{I(I+1)}$$

with components along the reference direction, μ_z of

$$\mu_z = \frac{\gamma h}{2\pi} m_I \qquad [3.5]$$

In the absence of a magnetic field the energy of an isolated nucleus is independent of direction and therefore independent of m_I. In the presence of a magnetic field, **B**, a magnetic moment has energy,

$$E = -\mu.\mathbf{B} \qquad [3.6]$$

with the component in the field direction (along the z-axis)

$$= -\mu_z B_0 \qquad [3.7]$$

$$= \frac{-\gamma h}{2\pi} m_I B_0 \qquad [3.8]$$

i.e. there are 2I+1 energy levels each separated by $\left|\frac{\gamma h}{2\pi} B_0\right|$

Transitions can be made to occur between energy levels by using electromagnetic radiation of the appropriate frequency.

$$E = h\nu = \frac{\gamma h}{2\pi} B_0 \Delta m_I \qquad [3.9]$$

(the selection rule for NMR is $\Delta m_I = \pm 1$)

$$\therefore h\nu = \frac{\gamma h}{2\pi} B_0$$

$$\nu = \frac{\gamma}{2\pi} B_0 \qquad [3.10]$$

This gives rise to a single magnetic resonance line at a frequency, ν, comprised of 2I superposed components. The intensity of the component $m \leftrightarrow m\text{-}1$ is proportional to I(I+1)-m(m-1), to first order[3].

For a nucleus with $I > \frac{1}{2}$ the nuclear charge distribution is not spherically symmetric *i.e.* it has a nuclear quadrupole. This nuclear quadrupole moment will interact with a electric field gradient to produce a perturbation of the Zeeman energy

levels. A quadrupole interaction will split the single Zeeman resonance line into its 2I components.

Figure 3.1 shows the energy level diagram for a ^{133}Cs nucleus in the presence of an electric field gradient where to first order, the energy levels in the presence of an electric field gradient are given by[4],

$$E_m = -\frac{\gamma\hbar}{2\pi} B_0 m_I + \frac{3m_I^2 - I(I+1)}{4I(2I-1)} h q_{zz} \qquad [3.11]$$

Only the component of the nuclear quadrupole-electric field coupling parallel to the direction of the magnetic field, q_{zz}, is measured in an NMR experiment therefore the frame of reference has to be changed so that the components in the principle axes of the nuclear quadrupole-electric field gradient interaction tensor (q_{aa},q_{bb},q_{cc}) are projected onto q_{zz}.

$$q_{zz} = \frac{2}{3}\sum_{ij}^{abc} S_{ij} q_{ij} P_2(\cos\phi) \qquad [3.12]$$

$$= q_{cc}\left\{S_{cc} + \frac{q_{aa}-q_{bb}}{3q_{cc}}(S_{aa}-S_{bb})\right\}$$

$$= \frac{e^2qQ}{h}\left\{ S_{cc} + \frac{1}{3}\eta(S_{aa}-S_{bb}) \right\} \qquad [3.13]$$

where $\eta \equiv \frac{q_{aa}-q_{bb}}{q_{cc}}$ is the asymmetry parameter and where S_{ij} are elements of the Saupe[5] ordering matrix for the principle axes (a,b,c) of the nuclear quadrupole interaction tensor. In the case of a uniaxial liquid crystal the asymmetry parameter is zero.

Figure 3.1 The energy level diagram for an $I=\frac{7}{2}$ nucleus (^{133}Cs) showing the effect of a first order quadrupolar interaction on the Zeeman energies.

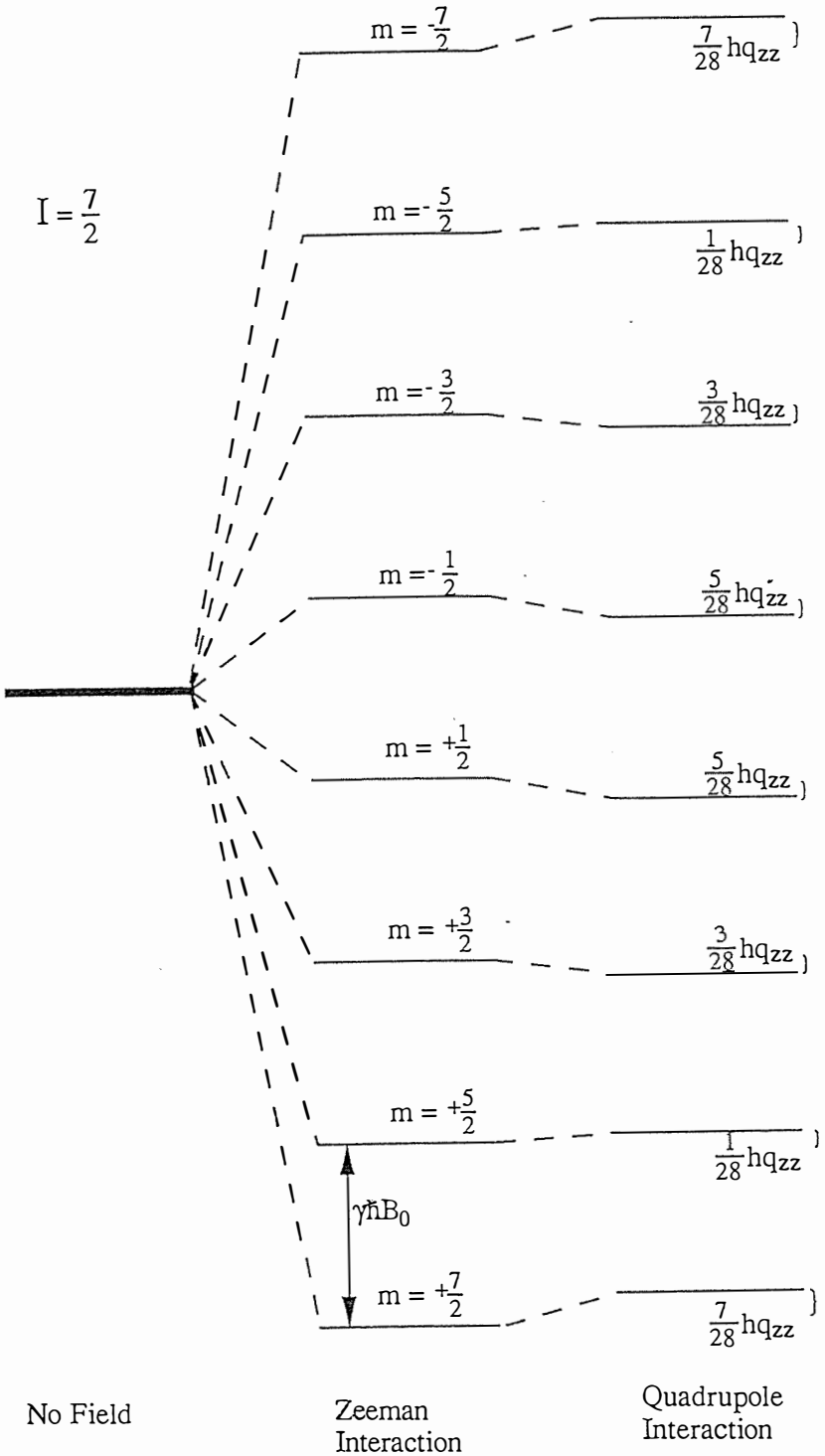

The nematic phases of CsPFO/water and NH_4PFO/water are diamagnetically positive and the mesophase director, **n**, undergoes spontaneous alignment along the direction of the field, **B**, to give a macroscopically aligned sample. Such a sample will give a first order spectrum for any spin $I>\frac{1}{2}$ consisting of 2I equally spaced lines with separation, referred to as the quadrupole splitting, $\Delta\tilde{\nu}$, given by[6,7]

$$\Delta\tilde{\nu}(\phi) = \frac{3}{2I(2I-1)}\tilde{q}_{zz}P_2(\cos\phi) \qquad [3.14]$$

The upper tilde denotes partially averaged quantities. The averaging arises as the result of reorientations that take place at a faster rate than the time-scale of the experiment, including local reorientation of the bound species and diffusion over the micelle surface. $P_2(\cos\phi)$ is a second rank Legendre polynomial which describes the orientation of the mesophase director, **n**, with respect to the magnetic field, **B**. $\tilde{q}_{zz}$ is the partially averaged component of the nuclear quadrupole-electric field gradient interaction tensor measured parallel to **n** in a perfectly ordered mesophase and is given by

$$\tilde{q}_{zz} = \sum_n p_n\chi_n[S_{cc} + \tfrac{1}{3}\eta_n(S_{aa}-S_{bb})] \qquad [3.15]$$

where S_{ij} are elements of the Saupe ordering matrix at the nth site which has a statistical weight p_n and $\chi_n = \left(\frac{e^2qQ}{h}\right)_n$ is the corresponding quadrupole coupling constant. The values of χ_n and η_n are dependent on the nucleus and vary from site to site, therefore they are determined by micellar structure.

In micellar liquid crystal systems it is useful to be able to separate the contributions to the quadrupole splitting that arise from micellar and order parameter fluctuations. This is done[2] by redefining $\tilde{q}_{zz}$ such that

$$\tilde{q}_{zz} = |\tilde{q}_{zz}|_s S \qquad [3.16]$$

where $|\tilde{q}_{zz}|_s$ now contains terms which depend only on the detailed structure of the aggregate and on the solution concentration (*i.e.* it is the value of $\tilde{q}_{zz}$ in a perfectly

ordered crystal) and S is an order parameter which represents an average of the orientations of the micellar axes with respect to **n**.

S can be further reduced to

$$S = \overline{< P_2(\cos\theta) >} < P_2(\cos\beta) > \qquad [3.17]$$

$$= \bar{P}_{2,m}\bar{P}_{2,n}$$

where θ is the angle between the micelle and the local director, *i.e.* $\bar{P}_{2,m}$ describes the average orientation of the micelle with respect to a local director, and β is the angle between the local director and the mesophase director, *i.e.* $\bar{P}_{2,n}$ describes local director fluctuations.

From equation [3.14] and [3.16] we can write[6]

$$\boxed{\Delta\tilde{\nu}(\phi) = \frac{3}{2I(2I-1)} |\tilde{q}_{zz}|_s S P_2(\cos\phi)} \qquad [3.18]$$

3.1.1 Deuterium Quadrupole Splitting

For a molecule of heavy water in the solvent there are two distinct cases; water molecules in the solvent bulk where the quadrupole interactions average to zero ($|\tilde{q}_{zz}|_s=0$) and water molecules associated with the micellar surface which result in a quadrupolar coupling ($|\tilde{q}_{zz}|_s\neq0$). From equation 3.18, the quadrupole splitting for a ^2H nucleus (I=1) in heavy water becomes

$$\Delta\tilde{\nu}(\phi) = \frac{3}{2}|\tilde{q}_{zz}|_s S P_2(\cos\phi) \qquad [3.19]$$

where
$$|\tilde{q}_{zz}|_s = <P_2(\cos\alpha)>_s \chi_D \left(\frac{x_A}{x_W}\right) n_b S_{O\text{-}D} \qquad [3.20]$$

χ_D is the quadrupole coupling constant for ^2H in heavy water, x_A and x_W are the mole fractions of amphiphile and heavy water respectively, $S_{O\text{-}D}$ is an order parameter relating the average orientation of the O-^2H bond of a water molecule with respect to

the micelle surface and n_b is the number of bound water molecules per amphiphile. $\langle P_2(\cos\alpha)\rangle_s = \frac{1}{2}\langle 3\cos^2\alpha\text{-}1\rangle_s$, where α is the angle between the normal to the micelle surface and the micelle symmetry axis, with the angular brackets denoting an average of all positions over the micelle surface. This term averages the contributions from all of the sites around the micelle surface.

Exchange between bound and unbound water molecules occurs rapidly with respect to the time scale of the NMR experiment to give a single sharp doublet the splitting of which corresponds to a weighted average of heavy water molecules in all possible sites.

The ^2H quadrupole splitting of the deuterated ammonium peak is given by equation 3.19

where $$|\tilde{q}_{zz}|_s = \langle P_2(\cos\alpha)\rangle_s \overset{A}{\chi}_D \beta_A S_{ND}. \qquad [3.21]$$

where β_A is the fraction of ammonium ions bound to the surface of the micelle, $\overset{A}{\chi}_D$ is the quadrupole coupling constant for the ND_4^+ ion and S_{ND} is an 'order parameter'.

3.1.2 Caesium Quadrupole Splitting

For ^{133}Cs ($I = \frac{7}{2}$) the spectrum is made up of seven evenly spaced lines with relative intensities of 7:12:15:16:15:12:7 and a separation of

$$\Delta\tilde{\nu}(\phi) = \frac{1}{14}|\tilde{q}_{zz}|_s S P_2(\cos\phi) \qquad [3.22]$$

where

$$|\tilde{q}_{zz}|_s = \langle P_2(\cos\alpha)\rangle_s \chi_{Cs} \beta_{Cs} \qquad [3.23]$$

β_{Cs} is the fraction of Cs^+ ions bound to the surface of the micelle and χ_{Cs} is the quadrupole coupling constant of the ^{133}Cs nucleus. In the caesium spectra only one set of lines is observed for any given phase indicating that the exchange between bound and

unbound caesium ions and exchange between bound Cs^+ ion sites is fast on the time scale of the experiment. The field gradient at the nucleus of the $^{133}Cs^+$ ion probably arises from a distortion of the hydration shell[8].

3.1.3 Nitrogen Quadrupole Splitting

For ^{14}N (I=1) the spectrum is in the form of a doublet where the spacing between the lines is

$$\Delta\tilde{\nu}(\phi) = \frac{3}{2}|\tilde{q}_{zz}|_s S P_2(\cos\phi) \qquad [3.24]$$

where

$$|\tilde{q}_{zz}|_s = \langle P_2(\cos\alpha)\rangle_s \chi_N \beta_A. \qquad [3.25]$$

χ_N is the ^{14}N quadrupole coupling constant and β_A is the fraction of ammonium ions bound to the surface.

3.3 CHEMICAL SHIFT ANISOTROPIES

The chemical shift of a nucleus in an anisotropic liquid is composed of an isotropic and an anisotropic component. The ^{133}Cs nucleus has a large chemical shift range and it is possible to observe the anisotropic component. In a micellar liquid crystalline environment with uniaxial symmetry, the measured effective anisotropic shielding tensor $(\sigma_\parallel - \sigma_\perp)_{eff}$ is given by[9]

$$\Delta\sigma = (\sigma_\parallel - \sigma_\perp)_{eff} = (\sigma_\parallel^b - \sigma_\perp^b) S \langle P_2(\cos\alpha)\rangle_s \beta_{Cs} \qquad [3.26]$$

where $\sigma_\parallel^b - \sigma_\perp^b$ are the components of the chemical shift shielding tensor for bound counter-ions parallel and perpendicular to the micelle symmetry axis respectively.

The measured chemical shift σ_o $(= (\sigma_\parallel + 2\sigma_\perp)/3)$ depends on the ratio of free and bound ions and is given by[9]

$$\sigma_o = \frac{\nu_{sample} - \nu_o}{\nu_o} = (1-\beta)\sigma_o^f + \beta\sigma_o^b \qquad [3.27]$$

where ν_{sample} and ν_0 are the resonance frequencies for the sample in question and an infinitely dilute solution of caesium chloride, and $\sigma_o^b = \frac{1}{3}Tr\sigma = \frac{1}{3}(2\sigma_\perp^b + \sigma_{||}^b)$. For a polycrystalline sample, $\Delta\sigma$ can be determined directly from the powder spectrum[10] but in a macroscopically aligned sample with positive diamagnetic susceptibility anisotropy only the parallel component is observed. The chemical shift anisotropy for such a sample can still be determined, however, as the difference between the chemical shift of the isotropic phase and that of the ordered sample, providing σ_0 is either temperature independent or the temperature dependence is known, when

$$\sigma_{||} - \sigma_0 = \frac{2}{3}\Delta\sigma \qquad [3.28]$$

3.4 APPEARANCE OF NMR SPECTRA

3.4.1 Appearance of ^{133}Cs Spectra

Figure 3.2 shows the appearance of the ^{133}Cs spectrum for a w=0.55 sample in the I phase (S=0), the macroscopically aligned N_D^+ phase (S>0), and the polycrystalline L_D phase. In the superconducting solenoid magnet used in this study, the long axis of the NMR tube is aligned along the field direction. The spectra always, therefore, correspond to the ϕ=0 orientation giving a quadrupole splitting, $\Delta\tilde{\nu} = \frac{1}{14}|\tilde{q}_{zz}|_s S$. The nematic phase spectrum is symmetric about the m = $+\frac{1}{2}$ to $-\frac{1}{2}$ transition and the intensity distribution is as expected for a first order spectrum. The separation of the peaks of the powder spectrum is half that of an ordered sample at the same temperature[8].

The appearance of the m= $+\frac{1}{2}$ to $-\frac{1}{2}$ transition on cooling from the I through to the L_D phase is shown in Figure 3.3. The chemical shift of the isotropic peak is determined by the trace of the chemical shift shielding tensor whereas that of the nematic phase is dependent only on the parallel component. In the mixed I/N_D^+ mixed phase region two peaks are observed (Figure 3.3b). The frequency separation of these peaks is $\frac{2}{3}\Delta\sigma$ (equation 3.28) and the nematic peak is to high frequency of the isotropic peak because

Figure 3.2 ^{133}Cs spectra for a CsPFO/H_2O w=0.55 sample in

(a) the isotropic phase (S=0),

(b) the macroscopically aligned nematic phase (S≠0), and

(c) the lamellar phase with a random distribution of directors (polycrystalline).

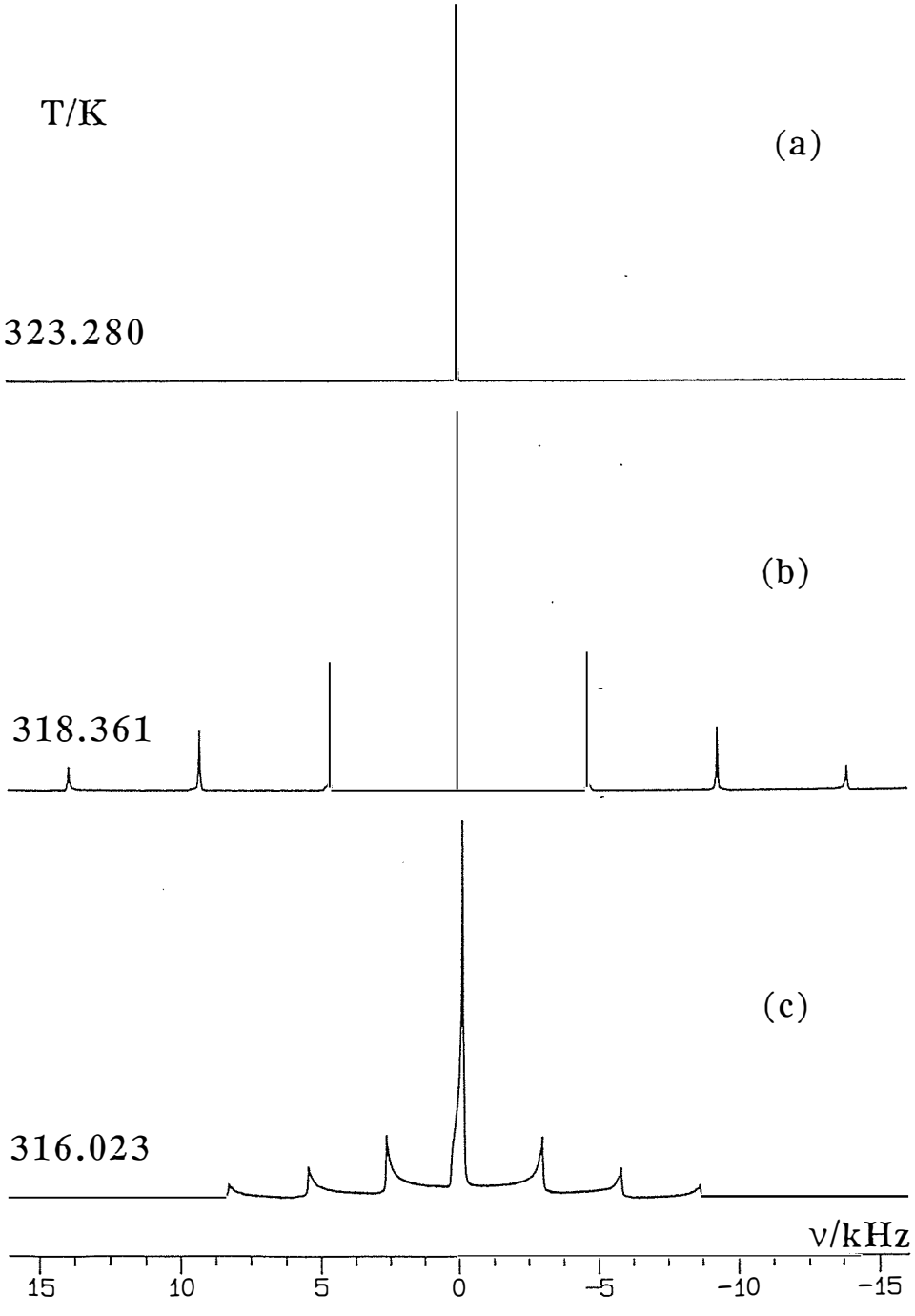

Figure 3.3 (a) to (c) ^{133}Cs NMR spectra for a macroscopically aligned w=0.55 CsPFO/ H_2O sample showing changes in the m = $+\frac{1}{2}$ to $-\frac{1}{2}$ transition peak as the sample is cooled from the isotropic (a) into the nematic/isotropic biphasic region (b) and then into the nematic/lamellar mixed phase region (c).

The spectrum labelled (d) is for a polycrystalline sample in the lamellar phase. The appearance of this spectrum is consistent with an isotropic distribution of directors.

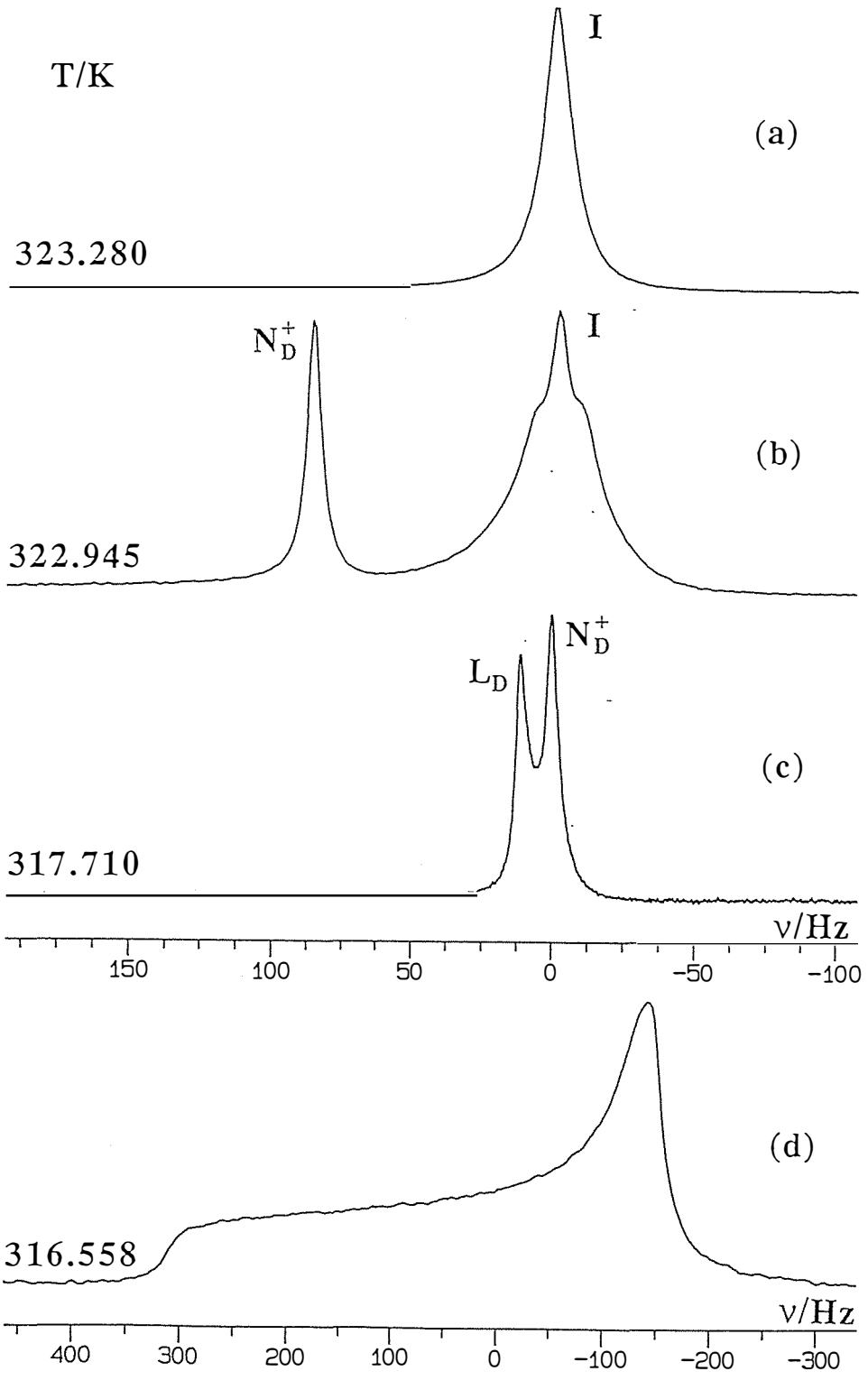

the nematic phase has positive diamagnetic susceptibility anisotropy. The structure in the isotropic signal is the result of magnetic field induced order in the I phase and will be discussed more fully in a later section. In the L_D/N_D^+ mixed phase region (Figure 3.3c), the chemical shift difference between the two peaks reflects the quantity $\sigma_{\parallel}(L_D)$-$\sigma_{\parallel}(N_D^+)$ and is small as a result of the small discontinuities in S, $\langle P_2(\cos\alpha)\rangle_s$ and β_{Cs} across the weak first order transition (see equation 3.26). The spectrum of the polycrystalline L_D phase shown in Figure 3.3d is typical for a powder pattern of a chemical shift anisotropy ($\sigma_{\parallel}>\sigma_{\perp}$) with an effectively cylindrically symmetric chemical shift shielding tensor[10].

Thus both ^{133}Cs quadrupole coupling and chemical shift anisotropy can be used for phase identification purposes. In addition the temperature dependence of these quantities can be used to precisely locate phase transition temperatures[1,2]. The best method for detecting phase transition temperatures depends on the nature of the particular transition. These are discussed in the appropriate section of the phase diagram chapter.

3.4.2 Appearance of I=1 Spectra

Figure 3.4 shows the appearance of the ^2H spectrum of heavy water for a w=0.55 CsPFO/^2H_2O sample in the I phase (S=0), in the macroscopically aligned N_D^+ phase (S>0) and in a polycrystalline lamellar state (isotropic distribution of mesophase directors). The ^2H quadrupole splitting in the nematic phase is given by $\Delta\tilde{\nu} = \frac{3}{2}|\tilde{q}_{zz}|_s S$, and thepolycrystalline spectrum shows the characteristic Pake structure with singularities at $\phi = 0°$ and $\phi = 90°$.

^{14}N spectra are identical in appearance to the ^2H spectra of heavy water but have greater quadrupole splittings and line-widths.

Figure 3.4 (a) and (b) ^2H NMR spectra for a macroscopically aligned w=0.55 CsPFO/^2H_2O sample showing changes in the spectrum as the sample is cooled from the isotropic (a) into the nematic phase region (b).

The spectrum labelled (c) is for a polycrystalline sample in the lamellar phase. The appearance of this spectrum is consistent with an isotropic distribution of directors.

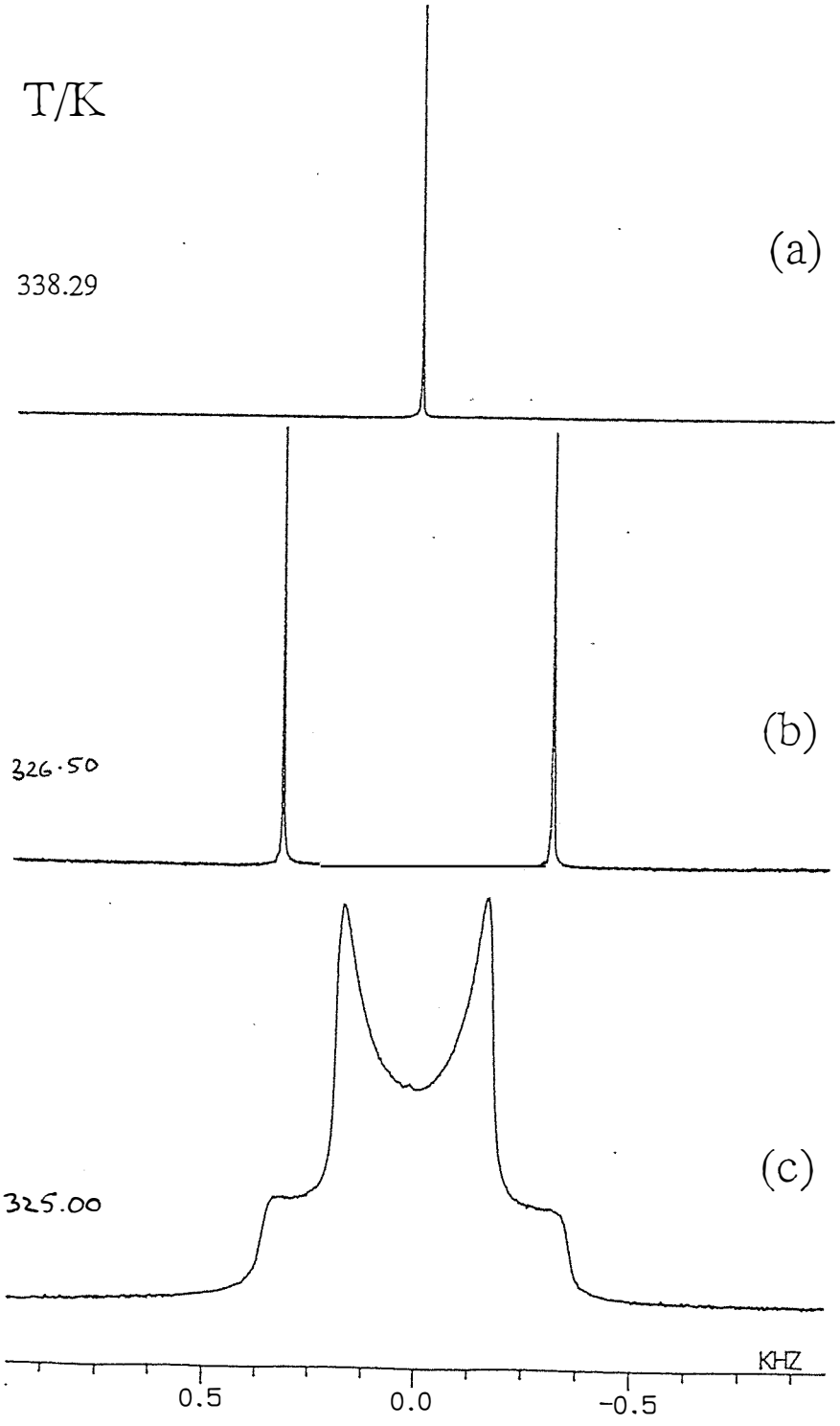

REFERENCES

[1]Boden, N.; Jolley, K. W.; Smith, M. H. *Liq. Crystals* **1989**, 6, 481.

[2]Boden N.; Corne S. A.; Jolley K. W., *J. Phys. Chem.* **1987**, *91* , 4092.

[3]Pake G. E., *Solid State Phys.* **1956**, *2* , 1.

[4]Abragam A., *The Principles of Nuclear Magnetism* **1967**, (Oxford University Press, Oxford).

[5]Saupe A., *Z. Naturforsch.* **1964**, *19a* , 161.

[6]Boden N.; Jones S. A., *N. A. T. O. ASI. Sci. C. Maths. Phys. Sci.* **1985**, *141* , 437.

[7]Cohen M. H.; Reif F., *Solid State Physics* **1957**, *5* , 321.

[8]Wennerström H.; Lindblom G.; Lindman B.,*Chem. Scr.* **1974**, *6* , 97.

[9]Persson, N-O; Lindblom, G., *J. Phys. Chem* . **1979**, 83, 3015.

[10]Dietrich, R.; Trahms, L., *J. Magn. Reson.* **1987**, 71, 337.

CHAPTER 4

PHASE DIAGRAM FOR THE SYSTEM CsPFO/WATER

A complete and accurate phase diagram is essential to any researcher conducting studies of phase behaviour in lyotropic liquid crystal systems. In these systems the composition and the temperature determines the state of the system and the nature of the phase transitions. In this chapter the phase diagram for the system caesium pentadecafluorooctanoate and water is presented along with a description of the physical techniques used to determine the transition temperatures.

Strictly the phase behaviour is dependent on three variables; temperature, composition and pressure. All measurements are assumed to have been made at a pressure of one atmosphere thus reducing the phase diagram to a two dimensional representation. The phase diagram is presented in figure 4.1, the fixed points in table 4.1, and the polynomials for the phase transition temperatures in table 4.2. In the phase diagrams the ordinate gives the temperature in degrees Kelvin and the abscissa gives the composition in terms of weight fraction of amphiphile.

Figure 4.1 The phase diagram for the CsPFO/H_2O system. There are three pure phase regions; isotropic micellar solution (I), discotic nematic micellar solution phase (N_D^+) and discotic lamellar solution phase (L_D). All other regions are mixed phase regions where K:- crystalline amphiphile. The fixed points are described in the text and schematically illustrated in chemical potential/temperature space in figure 4.2.

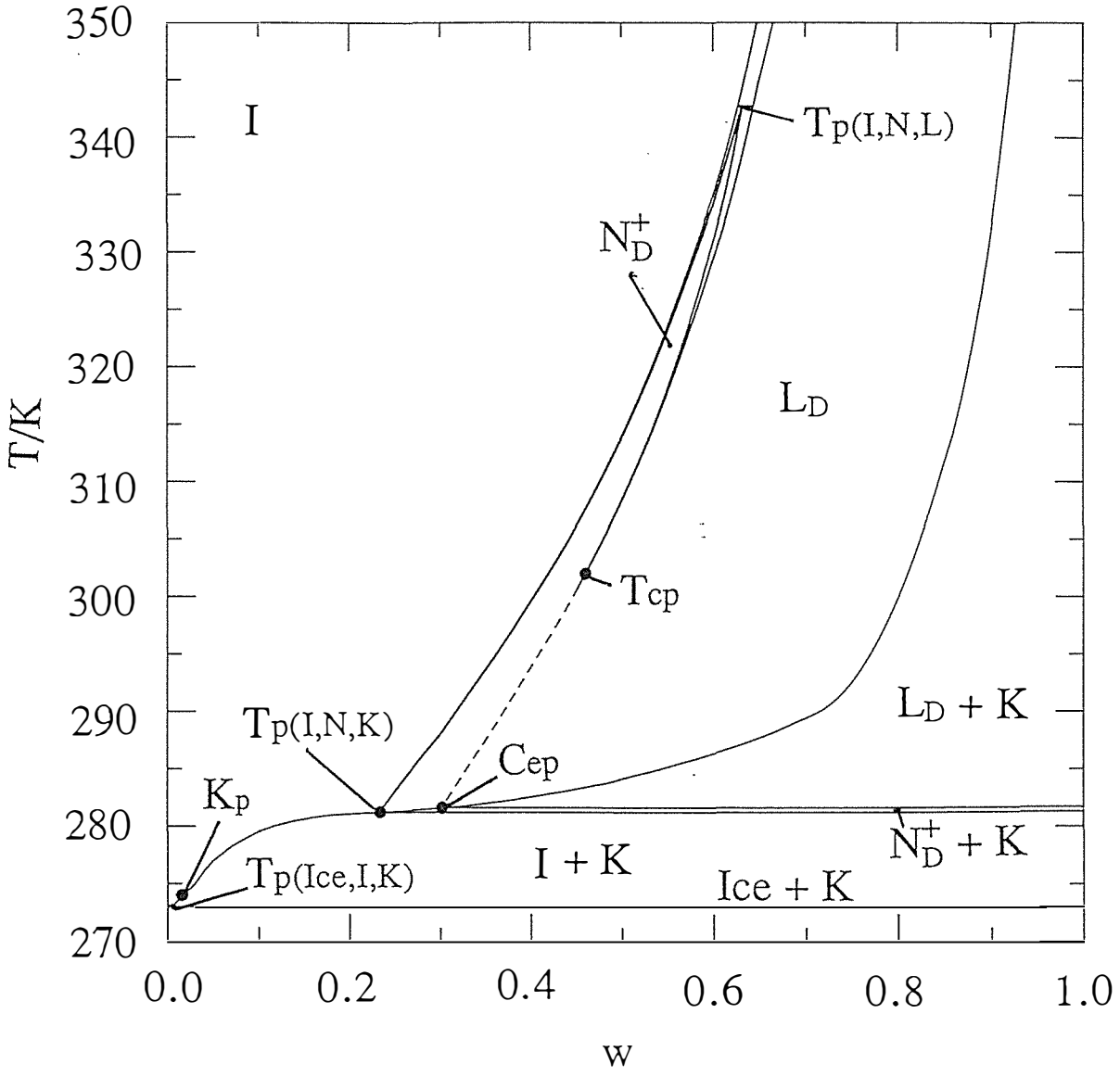

Table 4.1 The fixed points for the CsPFO/H_2O system.

CsPFO/H_2O

		T/K	w	ϕ	c/mol dm^{-3}	x
$T_{p(I,N,L)}$	isotropic	342.72	0.628	0.398	1.821	0.0527
	nematic		0.632	0.402	1.840	0.0536
	lamellar		0.644	0.414	1.897	0.0563
$T_{p(I,N,K)}$	isotropic	281.31	0.233	0.108	0.496	0.00992
	nematic		0.235	0.109	0.501	0.0100
$T_{p(Ice,I,K)}$	isotropic	272.0	0.009	0.0036	0.016	0.0003
C_{ep}	nematic =	281.7				
	lamellar		0.302	0.148	0.675	0.0141
K_p		274.0	0.016	0.0066	0.030	0.00054
T_f	ice	273.15				
T_{cp}		302.05	0.46	0.25	1.16	0.027

Table 4.2 The transition temperatures for the CsPFO/H_2O system have been fitted to polynomials for ease of generating transition temperatures for any sample. The polynomial takes the form $a+bw+cw^2+dw^3$ with the valid concentration range falling within w_{max} and w_{min}.

Transition	a	b	c	d	w_{min}	w_{max}
T_{IN}	229.96	333.04	-664.56	669.45	0.238	0.650
T_{NI}	238.52	263.08	-482.11	514.99	0.238	0.6325
T_{NL}	-101.89	2246.1	-4393.7	3087.7	0.450	0.6325
T_{LN}	202.13	465.40	-925.85	839.76	0.300	0.650
T_c	271.71	133.09	-648.22	1087.8	0.030	0.250
T_c	247.94	234.91	-524.63	395.84	0.250	0.875

4.1 FEATURES OF THE PHASE DIAGRAM

The phase diagram shows three regions in which the system exists in a homogeneous one phase state. The remainder of the phase diagram is made up of two phase coexistence regions.

The single phase regions are the isotropic, nematic and lamellar mesophases. The feature that distinguishes this phase diagram from the phase diagrams of hydrocarbon surfactant water mixtures is the large range of the nematic mesophase. The nematic mesophase has a concentration range from 0.233 to 0.632 weight fraction and a temperature range from 281.31 K to 342.72 K. The lamellar phase is found at lower temperatures or higher concentrations whilst the isotropic phase is found at higher temperatures or lower concentrations. The area of the phase diagram above the solubility curve is dominated by these homogeneous single phase regions and in particular by the isotropic phase. The isotropic phase is made up of two separate entities; single amphiphile molecules and aggregates of amphiphile molecules. Below a certain concentration (c.m.c) the isotropic phase is a molecular solution and above the c.m.c. the isotropic phase consists of amphiphile aggregates in equilibrium with amphiphile molecules. In the area above the solubility curve there are small biphasic regions along most of the boundaries of the single phase regions. The transition between isotropic and nematic and between isotropic and lamellar is first-order over the complete range and therefore the pure phases are separated by biphasic coexistence regions whereas the nematic to lamellar transition changes from first-order to second-order at a tricritical point. Below this tricritical point the second-order nature of the transition means that there is no mixed phase region.

Below the solubility curve, T_C, the three mesophases are in equilibrium with solid crystalline amphiphile and at an even lower temperature, $T_{P(Ice,I,K)}$, the solution freezes to a mixture of ice and crystalline amphiphile.

There are several points of special interest on this phase diagram including triple points (T_p), a critical end point (C_{ep}) and a tricritical point (T_{cp}). A tricritical point is defined as the point at which a line of second-order transitions meets a line of first-order transitions and a critical end point is the point at which a line of second-order transitions ends on a line of first-order transitions[1]. The triple point $T_{p(I,N,L)}$ is actually a line which denotes the upper temperature stability limit of the nematic mesophase and is a line along which the three mesophases are in equilibrium. $T_{p(I,N,K)}$ is a series of triple points where isotropic mesophase, nematic mesophase and crystalline amphiphile are in equilibrium. $T_{p(I,N,K)}$ is where the nematic/isotropic biphasic region intersects the solubility curve and thus is a line of constant temperatures from the intersection of T_{IN} with T_C to the intersection of T_{NI} with T_C. C_{ep} is the critical end point situated at the intersection of T_{LN} with T_C. This point is not a triple point since the nematic and lamellar mesophases do not coexist (because the phase transition, T_{LN}, is of a second-order nature) and therefore the three components are not in equilibrium. At the C_{ep} the composition of the liquid crystal mesophases are identical and differ only in symmetry. The sometimes subtle differences between the types of fixed points is best illustrated in chemical potential/temperature space as shown schematically in figure 4.2.

The compositions of the constituent phases in a biphasic region are given by the intersection of horizontal lines, known as tie-lines, with the phase boundaries. The relative proportions of the two components is given by the 'lever rule'.

Figure 4.2 Schematic phase diagram in surfactant chemical potential/temperature space illustrating the nature of the various fixed points in the CsPFO/H_2O system. Continuous lines represent first order transitions and the dotted line represents a second order transition.

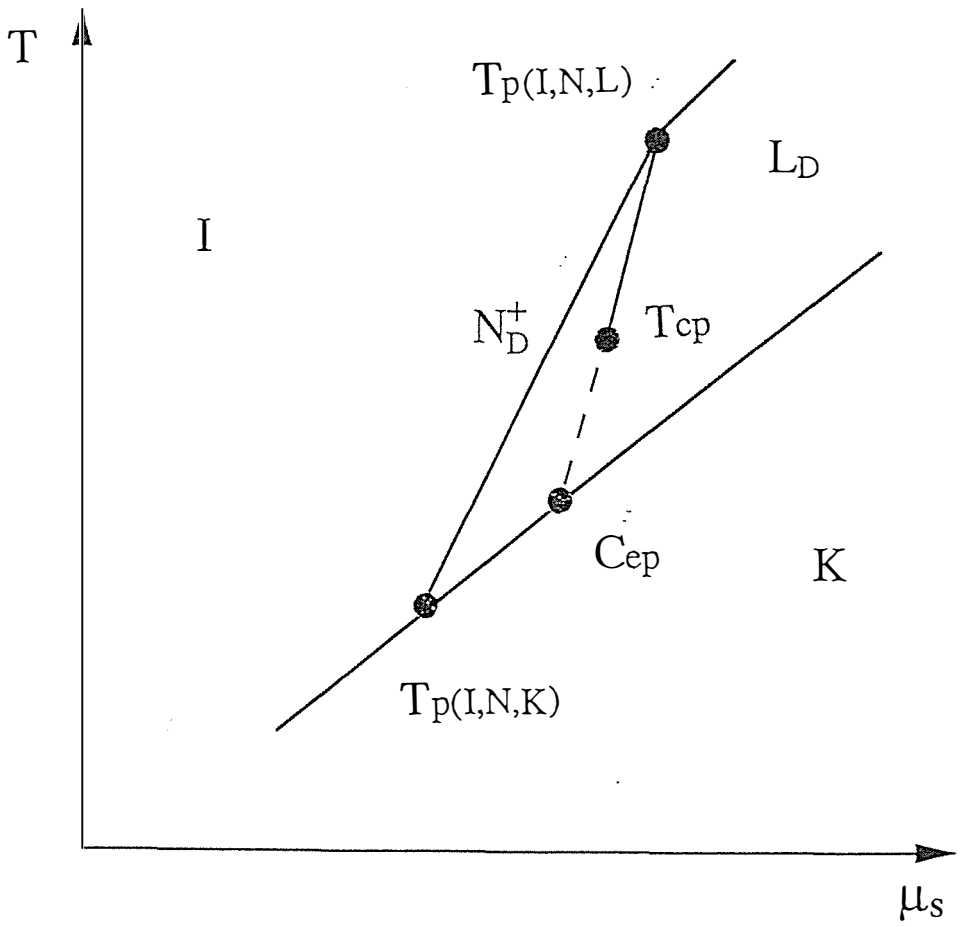

4.2 DETERMINATION OF LIQUID CRYSTAL PHASE BOUNDARIES

The phase boundaries in this phase diagram were determined using a combination of three methods. Transitions involving the isotropic, nematic and lamellar mesophases were mapped using ^{133}Cs NMR whilst transitions involving phases in equilibrium with crystalline amphiphile were determined using a combination of conductivity and differential scanning calorimetry.

In determining the phase transition temperatures it is important to approach the transition from a pure phase region. Thus, for example, the upper boundary of the isotropic to nematic transition is obtained by cooling from the isotropic phase whereas the lower boundary to the transition is approached from the nematic phase. The importance of the procedure cannot be over-emphasized if precise values of the phase transition temperatures are to be obtained. In mixed phase regions phase separation occurs at a rate which depends directly on the density difference between the two immiscible phases. For small density differences (*e.g.* between isotropic and nematic phases in low w samples) a few hours are needed before separate phases are actually revealed by the presence of a phase boundary interface whilst for a large density difference (*e.g.* between isotropic and lamellar phases in high w samples) this process will occur in a matter of minutes.

The presence of separate immiscible phases is clearly demonstrated in figure 4.3 which shows a w = 0.408 CsPFO/^2H_2O sample viewed through cross polarizers after the sample had been left for 24 hours in the middle of the isotropic/nematic mixed phase region (T= 307.15 K). Following phase separation, in order to obtain a sample which is homogeneous in concentration, it is necessary to heat to above the T_{IN} of the lower (more concentrated) phase before carrying out a thorough mixing. Fortunately this is easily carried out in an NMR tube. ^{133}Cs quadrupole splittings are particularly sensitive

Figure 4.3 These photographs demonstrate the effect of phase separation in the nematic/isotropic mixed phase region of a CsPFO/^2H_2O w=0.408 sample at 307.15 K.

The sample is viewed through cross-polarizers and in photograph (a) immediately after cooling into the biphasic region it appears homogeneous. After being left overnight in the biphasic region phase separation is seen (b). The lower portion contains the more dense nematic phase whilst the top half of the sample is in the isotropic phase.

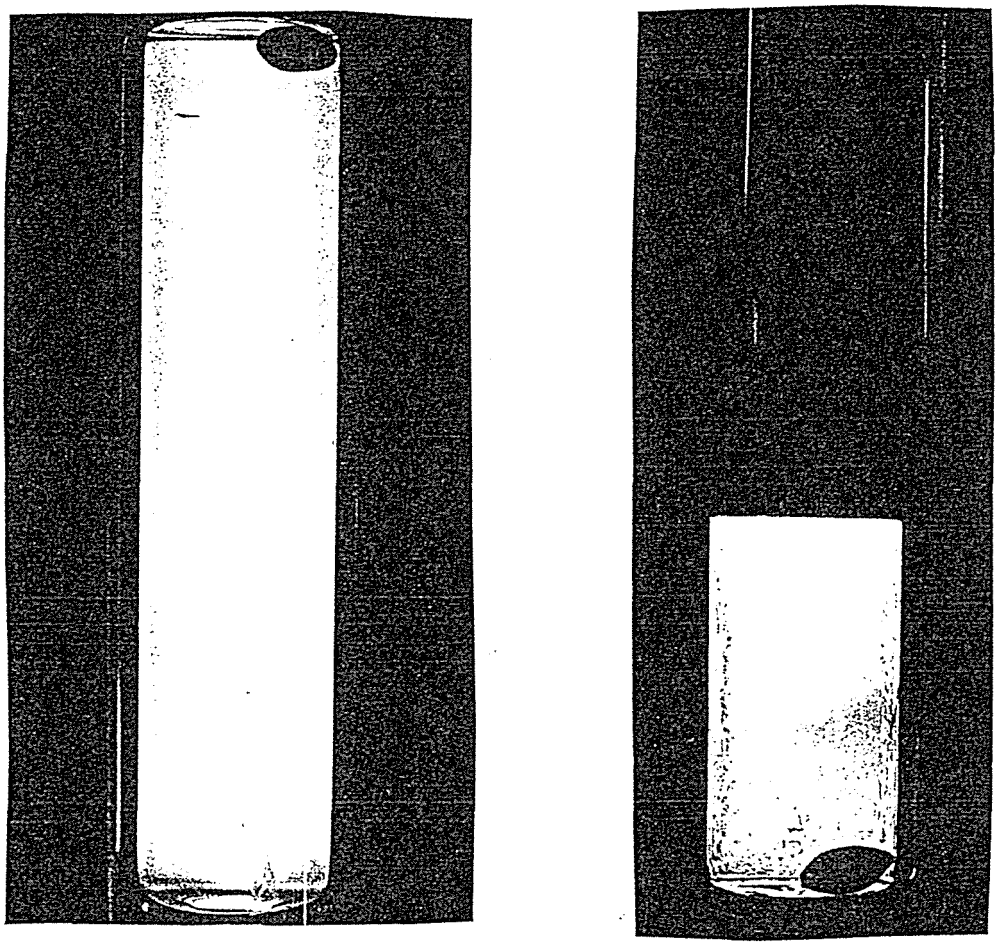

(a) (b)

to both concentration and temperature gradients which will lead to a 'smearing out' of the phase transition temperatures. Mixed phase regions are therefore best avoided and if that is not possible they should be traversed as quickly as possible.

The various techniques for the determination of the phase transition temperatures, which will be discussed in detail in the following sections evolved with this object primarily in mind. It is the first time that ^{133}Cs NMR has been used for the purpose of obtaining a high resolution phase diagram although ^{133}Cs quadrupole splittings[2,3], chemical shifts[2,4,5] and chemical shift anisotropies[2,6,7] have previously been used to provide information on ion binding, structure, and order in liquid crystalline mesophases.

4.2.1 Isotropic to Nematic-Isotropic Biphasic Region

The technique for the determination of T_{IN} depends on the concentration of the sample. A very precise measurement of a transition temperature can be made when there is a property that can be studied on both sides of the transition. For samples with $w < 0.45$ the phenomenon of field induced ordering was exploited to give T_{IN} to a high precision since the quadrupole splitting of the isotropic signal was evident on both sides of the transition and there is a discontinuity in temperature dependence at T_{IN}. When $w > 0.45$ the magnitude of the pretransitional splitting was too small to monitor above T_{IN} and therefore an alternative method had to be employed.

To illustrate the determination of T_{IN} using the field induced ordering method consider a CsPFO/H_2O sample with a weight fraction w=0.35. ^{133}Cs spectra for this sample at various temperatures in the vicinity of the transition from isotropic to nematic/isotropic biphasic region are shown in figure 4.4. At high temperatures the spectrum consists of a single line with a half width of approximately 2 Hz determined by natural relaxation processes. As the temperature is lowered the line broadens (a) due to the onset of quadrupole splitting induced by pretransitional ordering in the isotropic

Figure 4.4 ^{133}Cs NMR spectra showing the onset of field induced ordering on cooling a CsPFO/H_2O w=0.35 sample from the isotropic phase into the isotropic/nematic biphasic region.

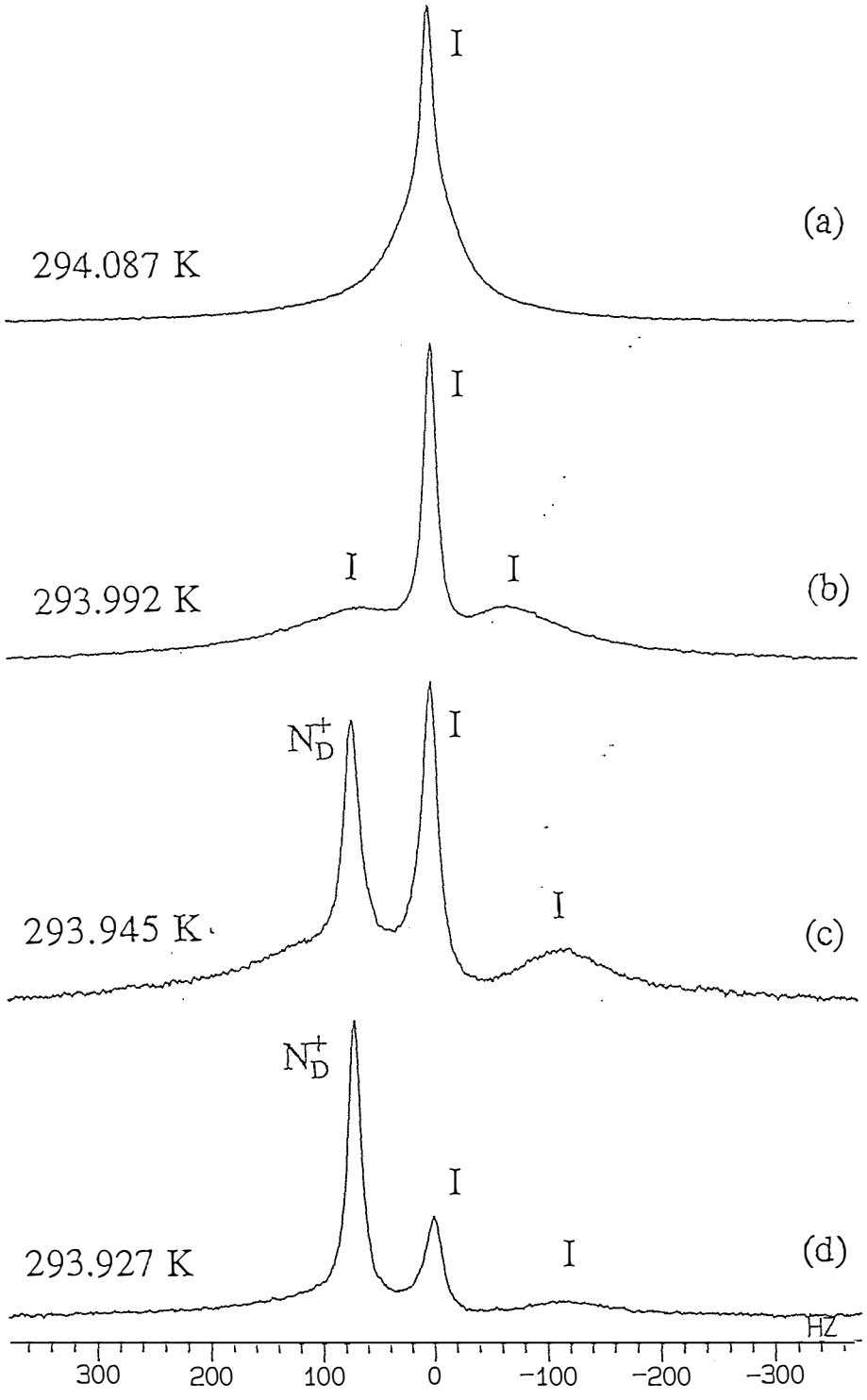

phase. As the magnitude of this splitting increases (b) the broad quadrupole peaks associated with the $-\frac{1}{2}$ to $-\frac{3}{2}$ and $+\frac{3}{2}$ to $+\frac{1}{2}$ transitions are resolved from the isotropic signal peak. The magnitude of the splitting continues to increase until the biphasic region is entered (c,d) and then remain fairly constant. In these spectra the nematic peak corresponding to the $+\frac{1}{2}$ to $-\frac{1}{2}$ transition appears coincident with the isotropic quadrupole peak to high frequency of the isotropic Zeeman peak. The transition temperature, T_{IN}, is determined from a plot of the inverse of the quadrupole splitting versus temperature. The plot is linear (see section 5.2.3) on both sides of T_{IN} and the transition temperature is determined from the intercept of the two best fit lines. Figure 4.5 shows the plots of both the quadrupole splitting and the inverse quadrupole splitting versus temperature and illustrates the precision (± 0.002 K) to which the transition temperature can be determined. The phenomenon of field induced ordering will be discussed in detail in chapter 5.

For samples where the magnitude of the field induced quadrupole splitting is too small to monitor an alternative method is required. The onset of pretransitional ordering is an excellent indicator of the proximity of T_{IN}. The first appearance of the nematic peak corresponding to the $+\frac{1}{2}$ to $-\frac{1}{2}$ transition then indicates that the transition has occurred. It is much better to monitor the $+\frac{1}{2}$ to $-\frac{1}{2}$ transition for this purpose than the quadrupole nematic peaks which are much broader and harder to detect. The nematic signal is only present on the biphasic region side of the transition and obviously can not be studied crossing T_{IN} whereas the isotropic singlet is present on both sides of T_{IN}. The nematic peak first resolves at a temperature just below T_{IN} and therefore this method of identification of the transition is not as precise as the field induced order method since we only see the nematic peak when we are already in the biphasic regime. The maximum error in T_{IN} as a result of this depends on the sensitivity of detection of the N_D^+ phase peak and the temperature range of the mixed phase region. The linewidth of the m = $+\frac{1}{2}$ to $-\frac{1}{2}$ transition is only about 4 Hz and it is easy to detect the N_D^+ peak at a I

Figure 4.5 The temperature dependence of (a) the field induced quadrupole splitting ($\Delta\tilde{\nu}$) and (b) $(\Delta\tilde{\nu})^{-1}$, in the isotropic phase and in the isotropic/nematic biphasic region of a CsPFO/ H_2O w=0.35 sample. The discontinuity in $\Delta\tilde{\nu}$ and $\Delta\tilde{\nu}^{-1}$ clearly identifies T_{IN} and T^* is obtained by extrapolating to $\Delta\tilde{\nu}^{-1} = 0$.

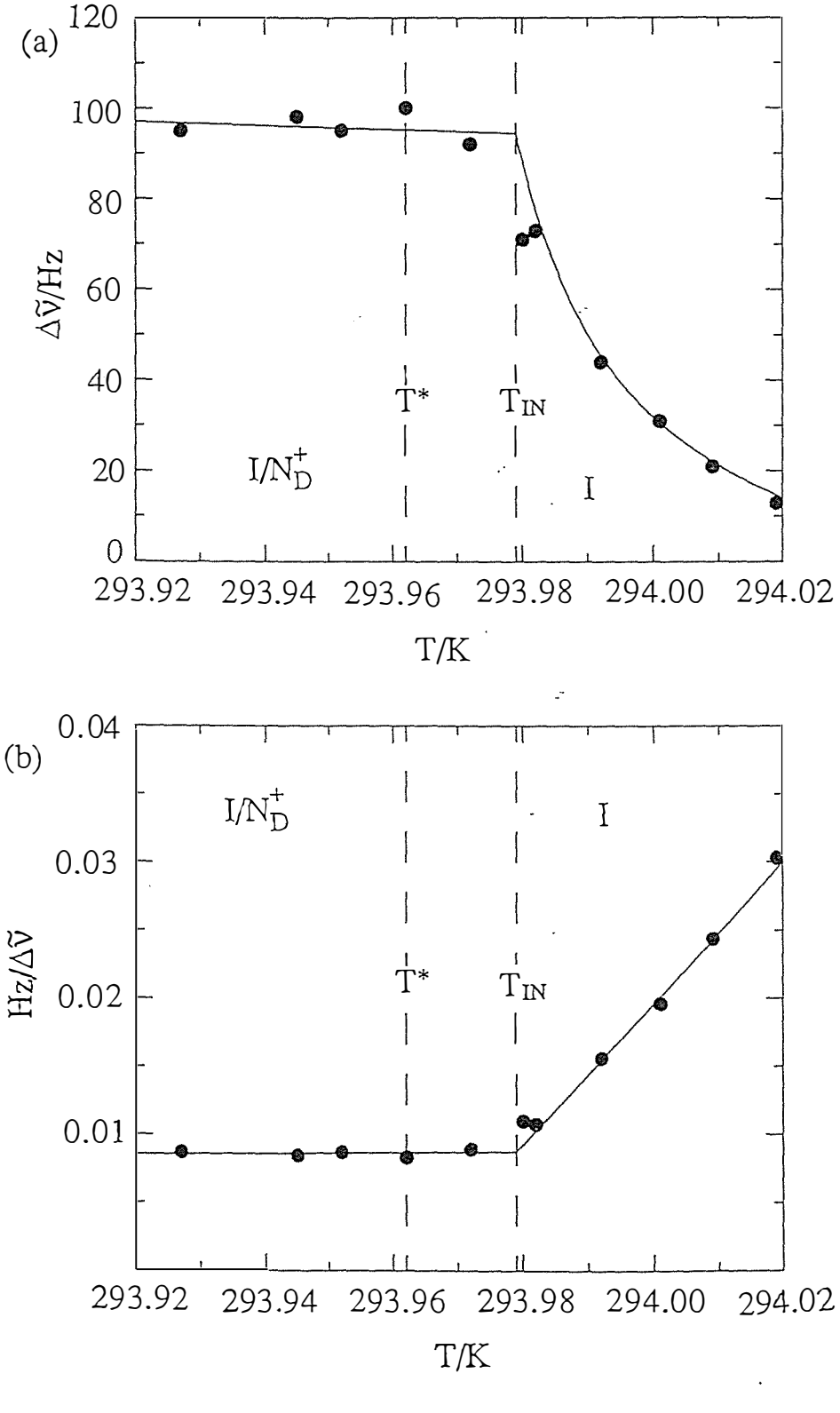

to N_D^+ peak ratio of ≈50:1. For the w = 0.55 sample the temperature range of the I/N_D^+ coexistence regime is 0.400 K, so the N_D^+ peak should be readily observable at ≈T_{IN} - 0.008 K. For samples with concentrations of less than 0.55 the corresponding systematic error will be even smaller since T_{IN} - T_{NI} decreases with decreasing w.

The disappearance of the nematic signal when reheating from the biphasic region does not necessarily coincide with T_{IN}. If phase separation has occurred the transition is non-reversible and the nematic peak does not disappear until a temperature higher than the T_{IN} of the homogeneous sample.

4.2.2 Nematic-Isotropic to Nematic

This transition, T_{NI}, is the lower temperature limit of the isotropic micellar phase and therefore the disappearance of the isotropic signal can be used as a guide to the location of this point. This is not a particularly good technique however since phase separation which occurs when slowly crossing a mixed phase region will lead to a blurring of the transition temperature *i.e.* the nematic phase will have a composition higher than and the isotropic phase a composition lower than the nominal composition. It is much better to determine T_{NI} by monitoring the change in the temperature dependence of the quadrupole splitting of the nematic signal on heating from the nematic phase. This method is superior to looking for the first appearance of the isotropic signal because we measure quadrupole splittings on either side of the transition. To determine T_{NI} the sample is rapidly cooled into the nematic phase and left until the sample has time to become well ordered as indicated by the sharpness of the nematic peaks. The temperature dependence of the quadrupole splittings is then determined (figure 4.6 for w = 0.35) and T_{NI} obtained from the discontinuity in $\Delta\tilde{\nu}$. The rapid fall in $\Delta\tilde{\nu}$ on approaching T_{NI} is due to the rapid change in S (equation 3.22) close to T_{NI}[8]. The constant value of the quadrupole splitting of the nematic signal in the temperature range of the biphasic region is due to a balancing of factors. From equations 3.22 and 3.23 it

Figure 4.6 The temperature dependence of quadrupole splittings ($\Delta\tilde{\nu}$) for a CsPFO/ H_2O w=0.350 sample. T_{NI} is clearly identified from the discontinuity in $\Delta\tilde{\nu}$.

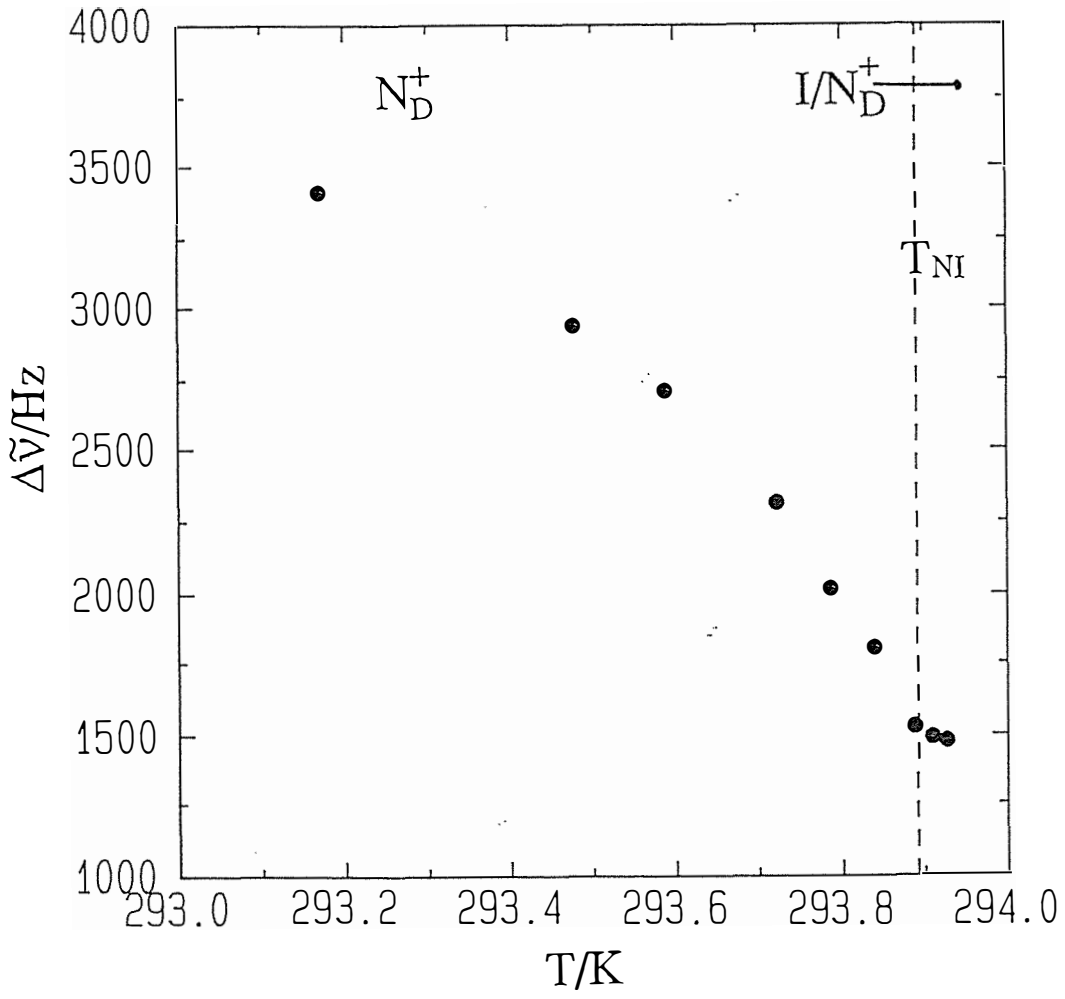

Figure 4.7 Illustration of the change in concentration of the components of a mixed phase region with temperature. As the temperature is increased along line (c) the isotropic concentration changes along line (a) from x to y and the nematic concentration changes along line (b) from z to v. The increase in the nematic concentration on heating counters the decrease in order parameter (see text). The relative amounts of the two phases are given by the lever rule.

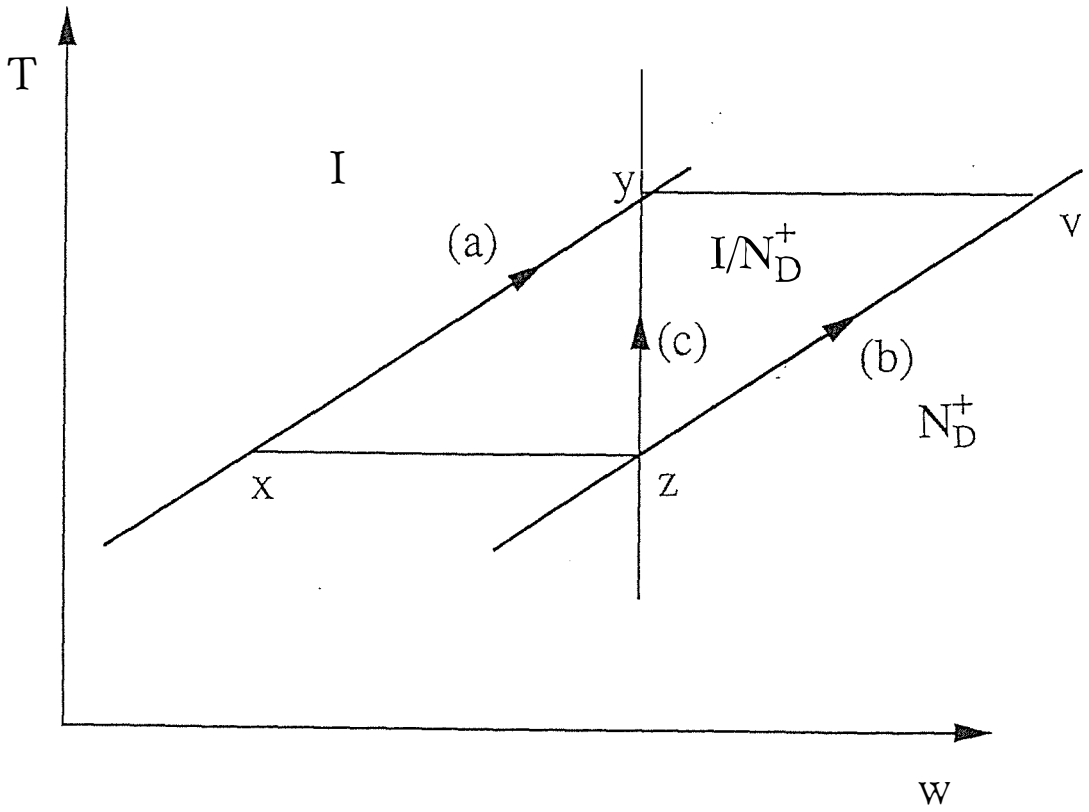

is clear that the magnitude of $\langle P_2(\cos\alpha)\rangle_s S\beta_{Cs}$ for the nematic phase component must be a constant in the mixed phase regime. This must mean that the decrease in the value of S due to an increase in temperature is offset by an increase in β_{Cs} as the concentration of the nematic component increases. The value of $\langle P_2(\cos\alpha)\rangle_s$ will also decrease slightly with increasing temperature as the transition is crossed[8,9]. The changes in the concentrations of the isotropic and nematic components of the biphasic region on heating are illustrated in figure 4.7.

4.2.3 Nematic to Lamellar

The technique used to identify the phase transition between the nematic and lamellar mesophases also depends on the sample concentration.

For high weight fraction samples, at concentrations well above T_{cp}, the width of the nematic/lamellar biphasic region is large and therefore the composition difference between the nematic and lamellar phases is large and there is a correspondingly large difference in the magnitude of the quadrupole splittings $\Delta\tilde{\nu}_N$ and $\Delta\tilde{\nu}_L$ (*i.e.* $S\langle P_2(\cos\alpha)\rangle_s\beta_{Cs}$(L phase) > $S\langle P_2(\cos\alpha)\rangle_s\beta_{Cs}$(N phase)). As the width of the biphasic region decreases so does $\Delta\tilde{\nu}_N$-$\Delta\tilde{\nu}_L$. At the tricritical point $\Delta\tilde{\nu}_N$-$\Delta\tilde{\nu}_L$= 0 and the transition is second-order.

When the difference in quadrupole splitting becomes of the same order as the line-widths (≈20 Hz) the quadrupole peaks of the two components in a mixed phase merge. This is a difficulty associated with NMR spectroscopy and makes the identification of a mixed phase region difficult when the samples are of a composition close to the tricritical point. In a mixed phase region the size of the domains of each components dictates the type of spectrum seen. If τ is the mean lifetime in each phase then $\tau = p_N\tau_L = p_L\tau_N$, where τ_N and τ_L refer to the mean lifetimes in the two components and p_N and p_L the population of each phase. If exchange of $^{133}Cs^+$ ions between the two phases is fast *i.e.* $\frac{1}{\tau} >> \pi|\Delta\tilde{\nu}_L-\Delta\tilde{\nu}_N|$ then the nucleus samples a weighted average of the nematic

and lamellar components and a single sharp septet is observed. The other extreme is when the domains are large therefore the nucleus is contained in one domain for the duration of the NMR experiment and a separate signal is seen for each component, *i.e.* for slow exchange $\frac{1}{\tau} << \pi\left|\Delta\tilde{\nu}_L - \Delta\tilde{\nu}_N\right|$. Another possible case is intermediate exchange where $\frac{1}{\tau} \approx \pi\left|\Delta\tilde{\nu}_L - \Delta\tilde{\nu}_N\right|$. Under this condition, the resultant spectrum consists of a single septet in which the peaks are exchange broadened. Thus as $\left|\Delta\tilde{\nu}_L - \Delta\tilde{\nu}_N\right|$ decreases τ needs to get bigger for the slow exchange condition to apply, *i.e.* the size of the phase domains needs to be large. It takes time for the domains to grow on entering a mixed phase region and it is therefore possible to miss a narrow mixed phase region. Chemical exchange can be a particular problem in ^2H NMR of these systems[8] because the magnitude of $\left|\Delta\tilde{\nu}_L - \Delta\tilde{\nu}_N\right|$ for the ^2H nuclei of heavy water close to T_{cp} is smaller than that for the ^{133}Cs nuclei by about an order of magnitude. ^{133}Cs is a much better nucleus for the detection of T_{cp}. The quadrupole splittings of ^2H nuclei of heavy water decrease with decreasing w whereas those of ^{133}Cs increase. The ratio of the ^{133}Cs to the ^2H quadrupole splittings actually increases with decreasing w.

4.2.3.1 Transitions for samples with w > T_{cp}

For transitions with $T_{NL} > T_{cp}$ there is a lamellar-nematic coexistence region. This region varies in width from three Kelvin at $T_{p(I,N,L)}$ to zero at T_{cp}. Spectra for a w=0.55 sample as the sample is cooled from the nematic to lamellar phases via a nematic/lamellar biphasic region are presented as figure 4.8. The phase transitions are determined from the intercept of the $\Delta\tilde{\nu}$ vs T curve in the mixed phase region with the curves for the pure mesophases, this is shown for the w=0.55 in figure 4.9. There is a sharp pretransitional increase in $\Delta\tilde{\nu}$ vs T on cooling just before T_{NL} whilst after T_{NL} the quadrupole splitting of the nematic component remains constant. The discontinuity in $\Delta\tilde{\nu}$ of the nematic phase clearly identifies T_{NL}, the upper temperature limit to the nematic/lamellar coexistence regime. T_{LN} is determined from the intercept of the $\Delta\tilde{\nu}$ vs T curve of the lamellar phase in the mixed phase region with that in the pure lamellar

Figure 4.8 ^{133}Cs NMR spectra for a CsPFO/H_2O w=0.55 sample as the sample is cooled from the nematic phase (a) through the nematic/lamellar biphasic region (b)-(d) and into the pure lamellar phase (e).

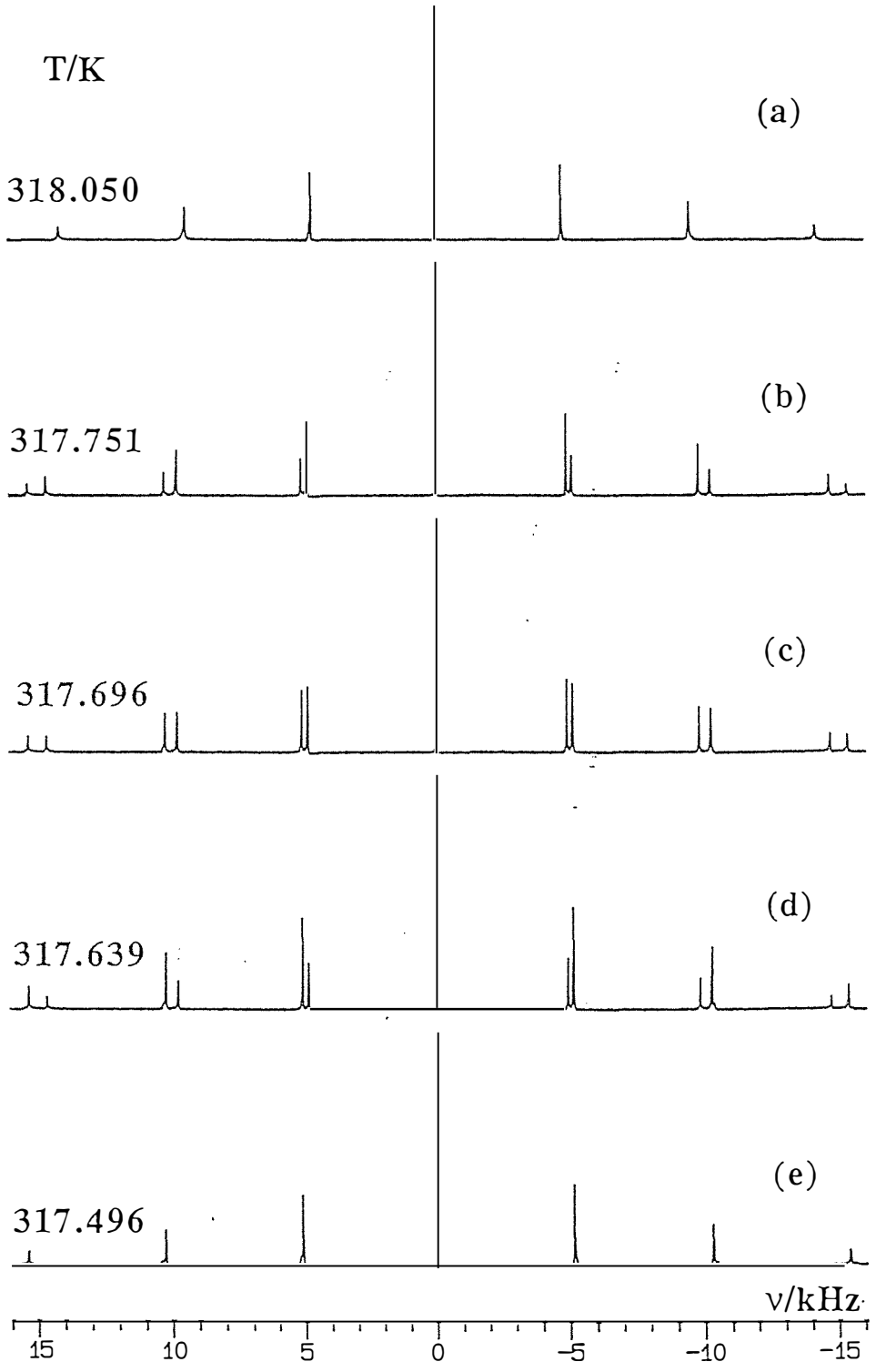

Figure 4.9 Temperature dependence of the ^{133}Cs quadrupole splittings across the nematic to lamellar transition for a CsPFO/H_2O w=0.55 ($w > T_{cp}$). The discontinuities in the quadrupole splittings clearly identify the upper (T_{NL}) and lower (T_{LN}) boundaries to the transition.

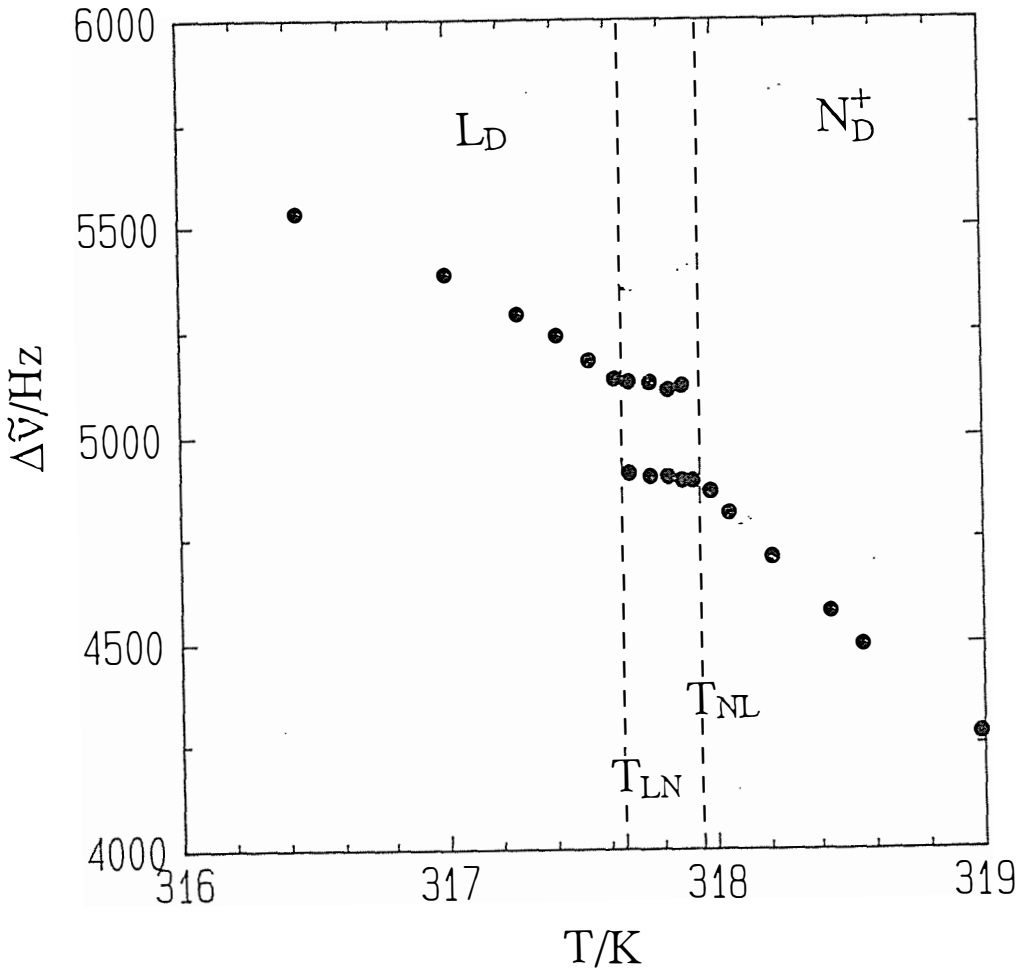

mesophase. The value of the quadrupole splittings close to T_{LN} changes rapidly with temperature due to pretransitional fluctuations.

When the transition occurs only slightly above T_{cp}, separate nematic and lamellar signals are not immediately observed because the quadrupole peaks of the nematic and lamellar signals are so close together that in an intermediate exchange regime the two are broadened into one peak. As slow exchange takes over the broad peak slowly resolves into separate nematic and lamellar signals. Care must be taken to ensure that the peaks have fully resolved because if they have not the value of the quadrupole splittings obtained for the lamellar and nematic components will be too low and too high respectively.

4.2.3.2 Transitions for samples with $w < T_{cp}$

When the sample has a concentration below the tricritical point, the transition between the nematic and lamellar mesophases is second-order. This means that at the transition there is no discontinuity in order parameter and therefore no discontinuity in the plot of quadrupole splitting versus temperature (see figure 4.10). A second-order transition is identified by a discontinuity in the first derivative of the temperature dependence of the quadrupole splitting. There is an increased rate of change in the quadrupole splitting in pure phase samples on either side of the biphasic region for first-order nematic to lamellar transitions. Just below T_{NL} this is due to an increase in the order parameter due to the presence of a small number of lamellar-like clusters whilst just above T_{LN} it is due to a decrease in the order parameter of the lamellar phase due to fluctuations giving rise to transient nematic-like domains. This behaviour also occurs at a second-order transition and the resulting point of inflection is taken to be T_{LN}. When the concentration is less than the tricritical point the transitions T_{LN} and T_{NL} are coincident.

Figure 4.10 Temperature dependence of the ^{133}Cs quadrupole splittings across the nematic to lamellar transition for a w=0.352 ($w < T_{cp}$). The discontinuity in the temperature dependence of the quadrupole splittings identifies T_{LN}.

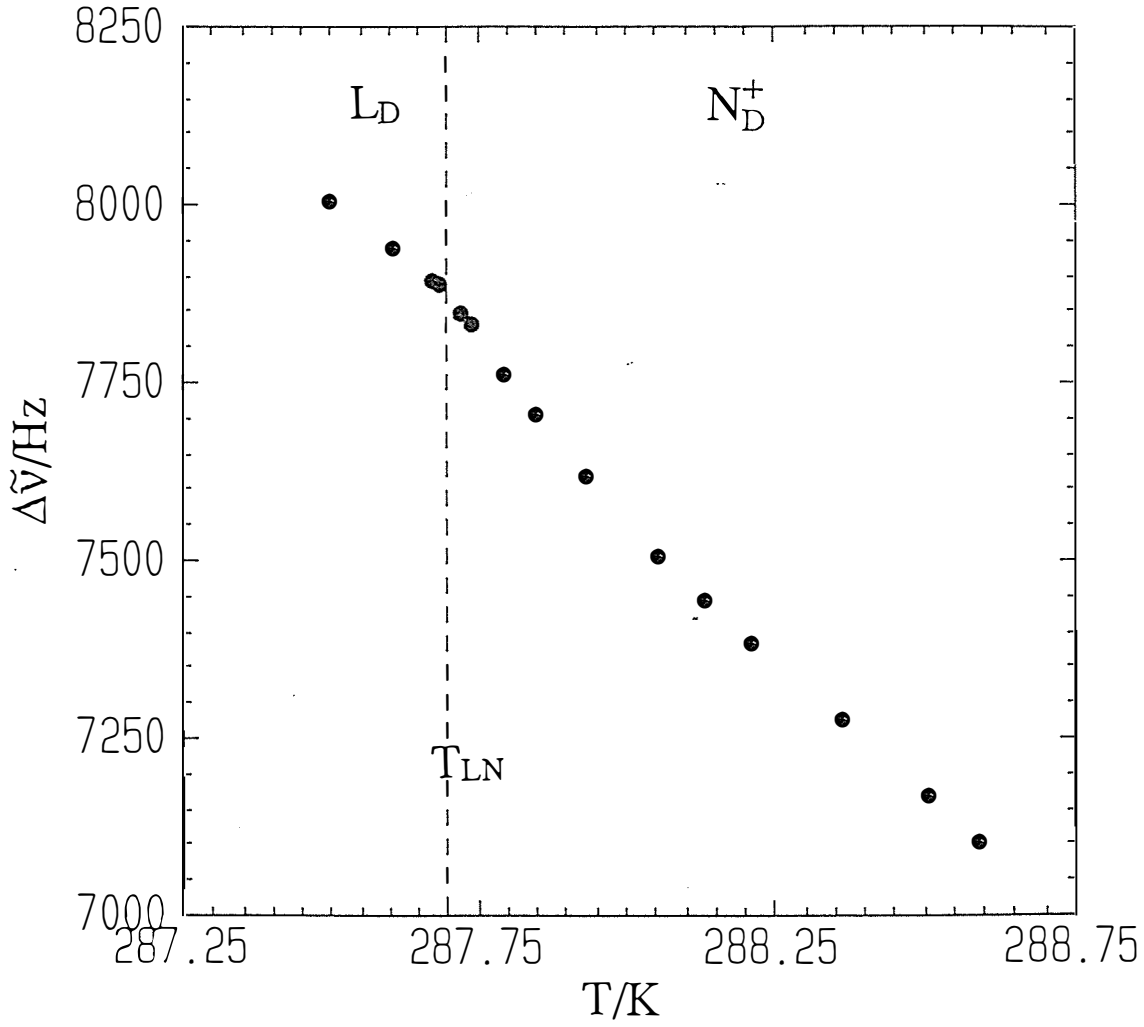

The appearance of the spectra of ordered nematic and lamellar mesophases is the same *i.e.* a septet, the only difference is in the magnitude of the quadrupole splitting. One property that differentiates the two mesophases is the infinite value of the twist viscosity in the lamellar mesophase. This property means that an isotropic sample cooled into the lamellar phase in the absence of an ordering field retains an isotropic distribution of local directors 'set in' the sample, resulting in a characteristic powder spectrum (see figure 3.2c).

When the quadrupole splitting is measured in an NMR spectrometer with an iron core magnet it is possible to test which phase the sample is in by rotation of the sample about the x-axis. The lamellar mesophase has an infinite twist viscosity and thus does not readily reorient in a magnetic field whereas the nematic mesophase has a finite twist viscosity and will therefore reorientate. This simple test is not possible in a superconducting magnet in which the field is along the long axis of the tube (z axis). Rotation about the z axis has no effect on the appearance of ordered samples. It might be thought that T_{LN} could be obtained from the temperature at which reorientation of a polycrystalline sample occurs on heating. This is not possible since in the higher field of the superconducting magnet, 6.3 T, we observe reorientation of the powder spectrum on the approach to T_{LN} at $\approx T_{LN}$ - 0.5 K. This is not due to a decrease in the twist viscosity of the lamellar phase *per se* but rather it is a pretransitional effect brought about by fluctuations caused by the proximity of the nematic mesophase. These fluctuations cause small fleeting domains of nematic behaviour where some reorientation can take place.

4.2.4 Location of T_{cp}

The tricritical point, T_{cp}, is a point of great interest to theoreticians as it is analogous to the $^3He/^4He$ superfluid transition. T_{cp} has proved difficult to determine experimentally due to the "weakness" of the transition. In earlier studies[9] the values

given for T_{cp} are too high. The reason for this is that the difference in ^2H quadrupole splitting for the two phases is of the same order as the resolution at a concentration greater than that of T_{cp} and thus a single averaged doublet is observed instead of two close but distinct doublets. The use of ^{133}Cs NMR gives spectra with quadrupole splittings an order of magnitude larger than ^2H NMR and therefore giving an order of magnitude improvement in resolving power. Although the use of ^{133}Cs gives better resolution of the nematic and lamellar signals the signals still merge at compositions close to the tricritical point. The composition of T_{cp} is identified by plotting the temperature width of the lamellar/nematic biphasic region against composition (figure 4.11) and extrapolating to $\Delta T_{NL}=0$ *i.e.* to T_{cp}. The corresponding temperature was calculated from the appropriate polynomial of table 4.2. The extrapolation procedure is unsatisfactory in that ΔT_{NL} is not a linear function of w but appears to become asymptotic to the w axis as w decreases. In the absence of an analytical expression for ΔT_{NL}, the visual extrapolation technique does at least provide an upper limit to T_{cp} and a starting point for attempts to determine a more precise value.

4.2.5 Isotropic to Lamellar-Isotropic Biphasic Region

The method of identification for this transition, T_{IL}, is identical to that used for T_{IN} when the pretransitional quadrupole splitting is too small to monitor. For the high concentration samples in which an isotropic to lamellar-isotropic transition occurs the amount of field induced pretransitional ordering is very small and is only manifested as a small broadening of the isotropic singlet. The sample is cooled from the isotropic phase until the first appearance of the central peak of the lamellar septet. This peak appears further downfield of the isotropic signal than the nematic signal does when crossing T_{IN}. The reason for this is a larger discontinuity in S, $\langle P_2(\cos\alpha)\rangle_s$ and β_{Cs} due to the large concentration difference between the two phases. The width of the I/L_D mixed phase region is $\approx$ 6 K and so the true value for T_{IL} could be as much as 0.12 K higher than the temperature at which the lamellar signal is first seen (see section 4.2.1).

Figure 4.11 Plot of the transition gap T_{NL} - T_{LN} as a function of the weight fraction of amphiphile. T_{NL} - T_{LN} appears to go to zero in the vicinity of w = 0.46 and this is taken to be the location of the tricritical point, T_{cp}.

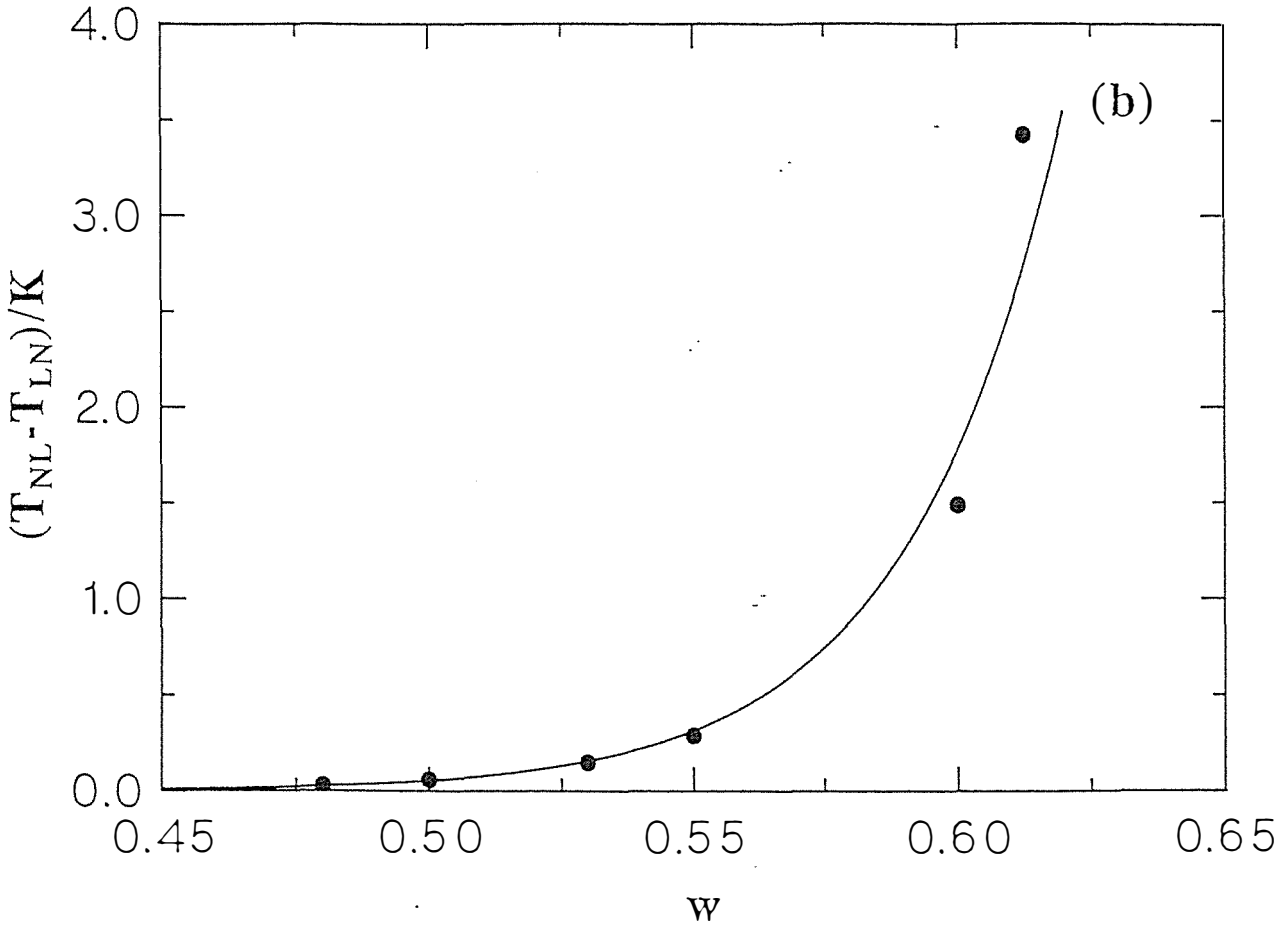

The reversibility of this transition is dependent on the amount of time spent in the biphasic region. If a lamellar-isotropic biphasic sample is left for even a short period of time phase separation occurs due to the large difference in composition, and therefore density, between the two components. When phase separation occurs the more dense lamellar phase sinks to the bottom of the sample tube and this means that the nominal concentration of the portion of the sample within the observation coils of the spectrometer is changing and therefore the transition temperature will appear to change. To illustrate consider a CsPFO/H_2O sample with a weight fraction of 0.650 which will have a T_{IL} of 350.8 K. If the sample is cooled to 347.5 K we will have a 50:50 mix of isotropic and lamellar with weight fractions (obtained by applying the lever rule) of 0.658 and 0.642 respectively. To allow mixing the sample must be totally in the isotropic phase, therefore the lamellar portion of the sample must be heated above T_{IL} which, for a 0.658 weight fraction sample, is at 354 K. This represents an increase of approximately 3 K from the T_{IL} of the original sample and demonstrates the importance of heating well into the isotropic phase to ensure sample homogeneity.

4.2.6 Lamellar to Lamellar-Isotropic Biphasic Region

As a result of the aforementioned phase separation problems it is not possible to determine T_{LI} precisely, by cooling through the lamellar-isotropic biphasic region. To determine T_{LI} the sample is first cooled rapidly from isotropic micellar solution to lamellar mesophase by immersion in a beaker of cold water. Since this is done outside the magnetic field a polycrystalline sample is produced but importantly it is homogeneous. Figure 4.12 presents a series of spectra for a w=0.65 sample which show the effect on the m = $+\frac{1}{2}$ to $-\frac{1}{2}$ transition peak of heating from a polycrystalline lamellar state into the isotropic/lamellar mixed phase region. The series of spectra begin with the polycrystalline (a), then at the temperature ≈0.5 K below T_{LI} reorientation takes place (b-e) and on heating further the isotropic phase appears (f) and eventually becomes the major component (g). The reorientation of the polycrystalline sample has

Figure 4.12 Appearance of the ^{133}Cs m = $+\frac{1}{2}$ to $-\frac{1}{2}$ transition line on approach to and passage into the isotropic/lamellar biphasic region. Spectrum (a) is for a polycrystalline sample. On heating reorientation of the lamellar phase starts to occur below T_{LI}. Spectrum (e) is taken one hour after (b) and reorientation to give a macroscopically aligned sample is complete. The presence of the isotropic peak (f) indicates that T_{LI} has been passed. On heating into the biphasic region (g) the peak intensities change as the relative amounts of the two phases change.

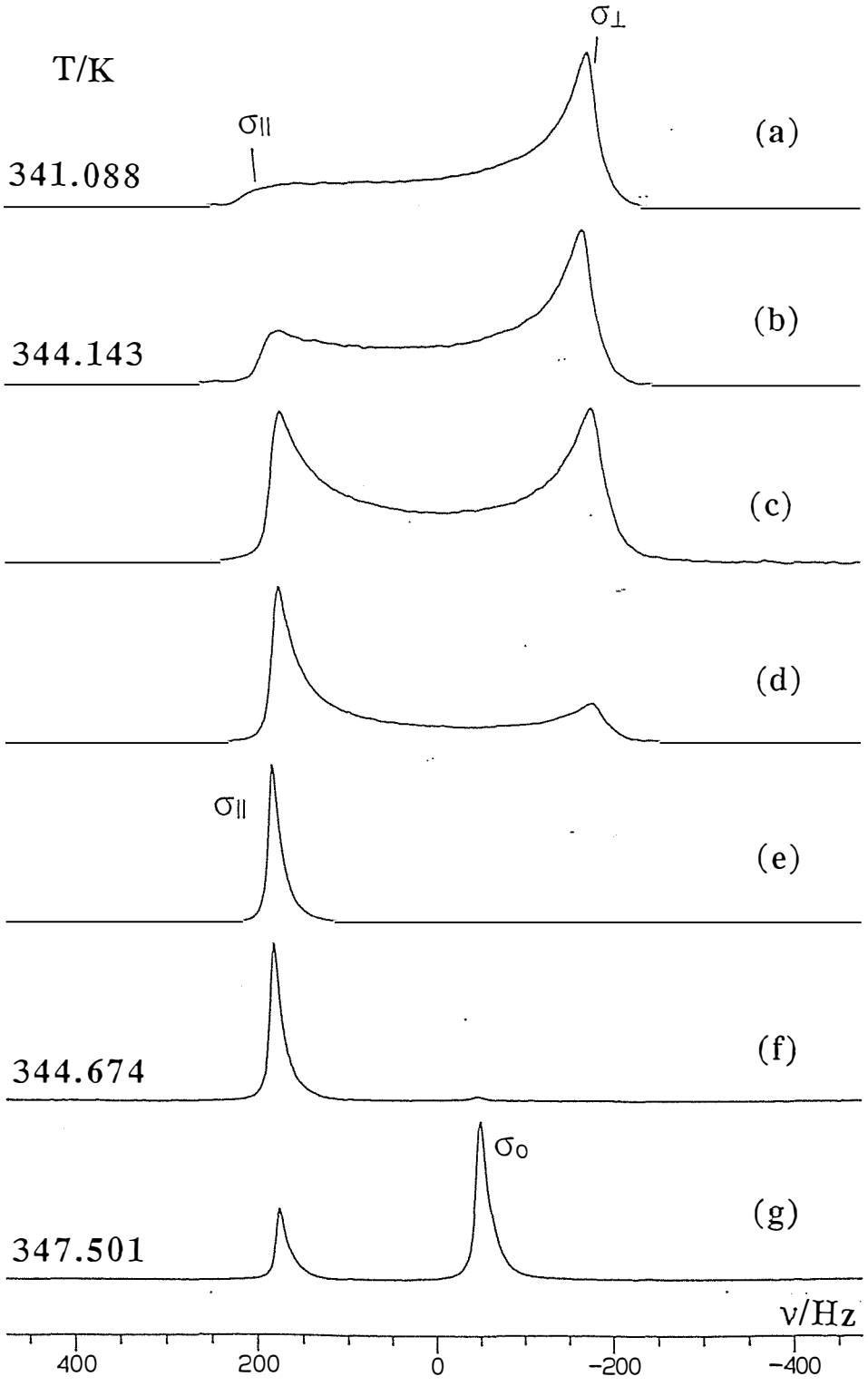

the same origins as those discussed in more detail in section 4.2.3.2. Precise values of T_{LI} are best determined from plots of the quadrupole splittings of the ordered L_D phase sample against temperature across the phase boundary. The plots so obtained show a discontinuity in $\Delta\tilde{\nu}$ at T_{LI} (see figure 4.9 for an example of this type of behaviour).

4.2.7 Determination of $T_{p(I,N,L)}$

$T_{p(I,N,L)}$ is a line of triple points at which the nematic mesophase, lamellar mesophase and isotropic micellar solution are at equilibrium. These triple points mark the upper temperature limit of the stability of the nematic mesophase. $T_{p(I,N,L)}$ was determined from observation of the $m = +\frac{1}{2}$ to $-\frac{1}{2}$ transition peak on cooling an isotropic solution $w = 0.64$ sample along the isopleth of figure 4.13a when the spectra shown in figure 4.13b were obtained. The sample is cooled from the isotropic phase into the lamellar-isotropic biphasic region where the lamellar signal appears. On further cooling, at a point just below $T_{p(I,N,L)}$, a nematic phase signal appears. The formation of the peak is accompanied by a rapid disappearance ($\approx$ 10 minutes) of the isotropic phase (figure 4.13b). Phase separation has no effect on the value of $T_{p(I,N,L)}$ because $T_{p(I,N,L)}$ occurs over a range of compositions which have in common the temperature at which the nematic phase first appears. Phase separation whilst not being a problem is manifest in the broadness of the peaks due to a range of compositions being present. As with previous determinations that relied on the appearance of a peak to signal the arrival of a mixed phase region, the measured transition is slightly lower than the actual transition. The values quoted for $T_{p(I,N,L)}$ (table 4.1) could be too low by about 0.04 K. The triple point concentrations of the isotropic, nematic and lamellar phases are given respectively by the abscissae of the isotropic, nematic and lamellar phase boundary curves (table 4.2) at the triple point temperature.

Figure 4.13b ^{133}Cs NMR spectra observed on cooling a CsPFO/H_2O (w = 0.640) sample along the isopleth in figure 4.13a.

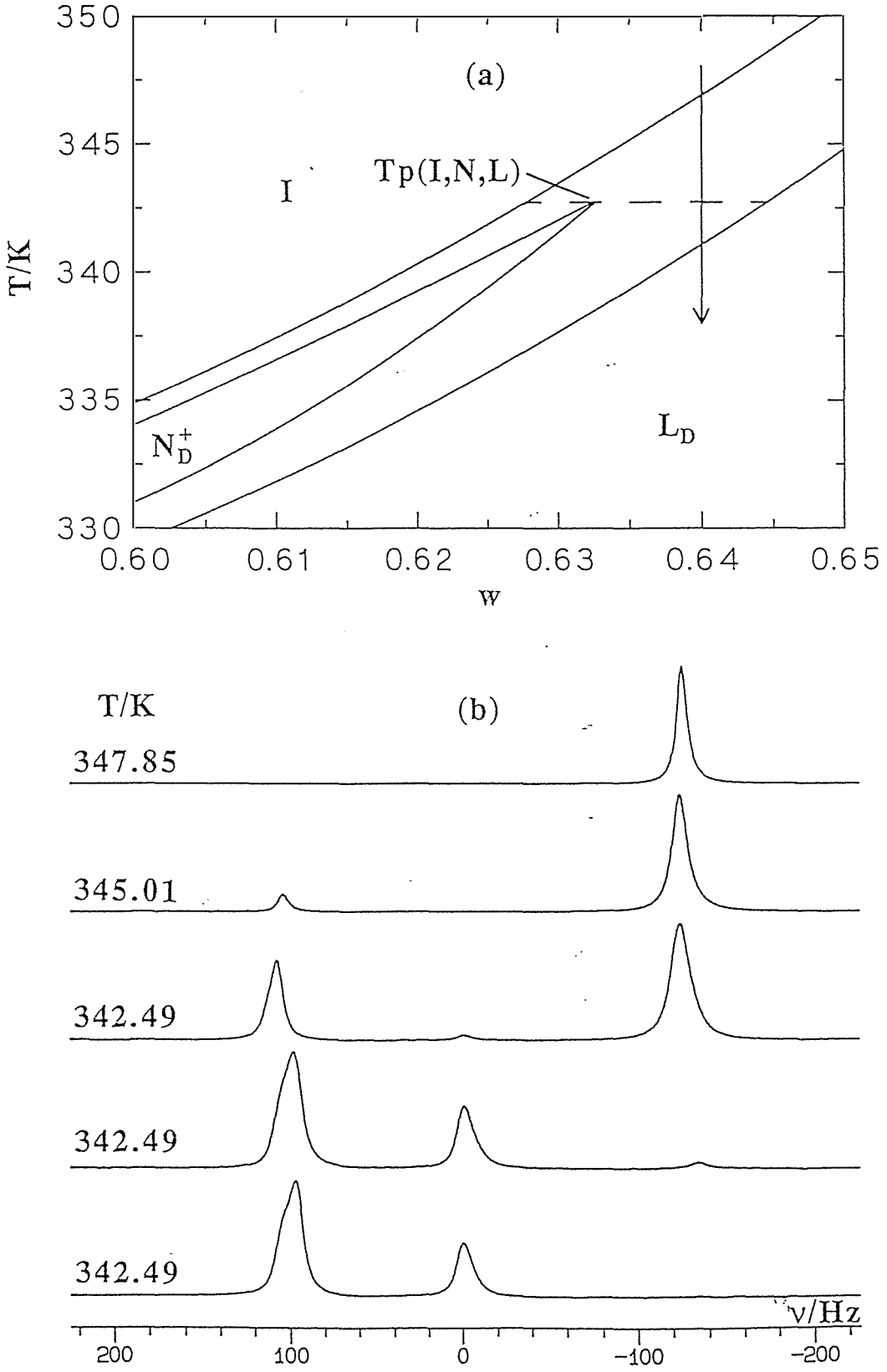

4.3 DETERMINATION OF THE SOLUBILITY CURVE

4.3.1 Dilute Region

The solubility curve, T_C, in the dilute region of the phase diagram (w<0.25) was determined using conductivity measurements. When cooling an aqueous solution of a pentadecafluorooctanoate salt supercooling occurs. The method[9,10] used to determine T_C was to measure the conductivity of the solution as it was cooled to the point where the salt precipitated and then to heat until all the salt was dissolved. On cooling the conductance initially shows a linear dependence on temperature and this continues to the point where precipitation begins and is marked by a sudden drop in the conductance of the solution. Following crystallization of the salt the conductance again shows a slow decrease as the temperature is lowered giving the cooling curve its characteristic sigmoid type shape[9,10]. The same sigmoid shaped curve is seen on reheating the sample although it is displaced to higher temperatures. On heating the conductance of the sample shows a gradual increase until a point is reached at which rapid solubilization takes place. The rapid solubilization of the bulk of the surfactant is accompanied by a rapid increase in the value of the conductance. Once the solubilization has been completed the heating curve is found to coincide with the cooling curve and this point of intersection is taken to be T_C the value of the solubility curve.

4.3.2 Concentrated Region

Measurements of the solubility curve, T_C, in the moderate to high amphiphile concentration region of the phase diagram (w>0.25) are carried out using differential scanning calorimetry. DSC measurements of the solubility curve were always made on heating because of supercooling of the precipitation of the crystalline amphiphile. The DSC thermogram is measured by cooling the sample until frozen and then heating at a constant rate. When measuring amphiphile solutions under these conditions the

thermogram shows two separate peaks. The large peak at lower temperature reflects the latent heat of fusion as the sample melts corresponding to the transition from ice+crystal (or heavy ice+crystal) to solution+crystal. This always starts at the same temperature and defines $T_{p(Ice,I,K)}$. Figure 4.14 shows a DSC thermogram for a w = 0.1 sample. The second smaller peak at higher temperatures corresponds to the heat of solubilization of the amphiphile. As a result of the melting peak being much larger than the solubilization peak the smaller peak is often partially obscured. To avoid this problem the sample is cooled below T_c to a temperature just greater than $T_{p(Ice,I,K)}$ and left until precipitation of the surfactant occurs. The desolubilization of the amphiphile can be followed by observing the cursor of the thermal analysis data station as the latent heat of solution is released by the system. Once the system has reached equilibrium the DCS thermogram is taken with only the solubilization peak being observed (see figure 4.15, w = 0.676). A comparison of the values obtained from conductivity measurements is needed to reconcile the behaviour of the DSC thermograms to the solubilization of the amphiphiles. The shape of the peak obtained is broad because the solubilization is a gradual process as can be seen by the sigmoid curves measured by conductivity. The shape of the trace is due to several different factors; the initial portion of the peak shows a slow increase as the amphiphile begins to dissolve, then a sharp jump when the isotropic+crystal to lamellar+crystal transition is crossed (corresponding to the flat part of the T_c curve) and finally a peak due to the end of the solubilization process as the transition into pure lamellar phase is made. When the composition of the sample is less than that of the triple point $T_{p(I,N,K)}$ the peak contains only two distinct portions with the first corresponding to gradual solubilization and the second to the transition from isotropic+crystal to isotropic.

4.3.3 The Krafft Point

The Krafft point, Kp, is located at the intersection of the solubility curve with the line of critical micelle concentrations.

Figure 4.14 A DSC trace for a CsPFO/H_2O (w = 0.10) sample. The peak corresponds to the latent heat of fusion of ice.

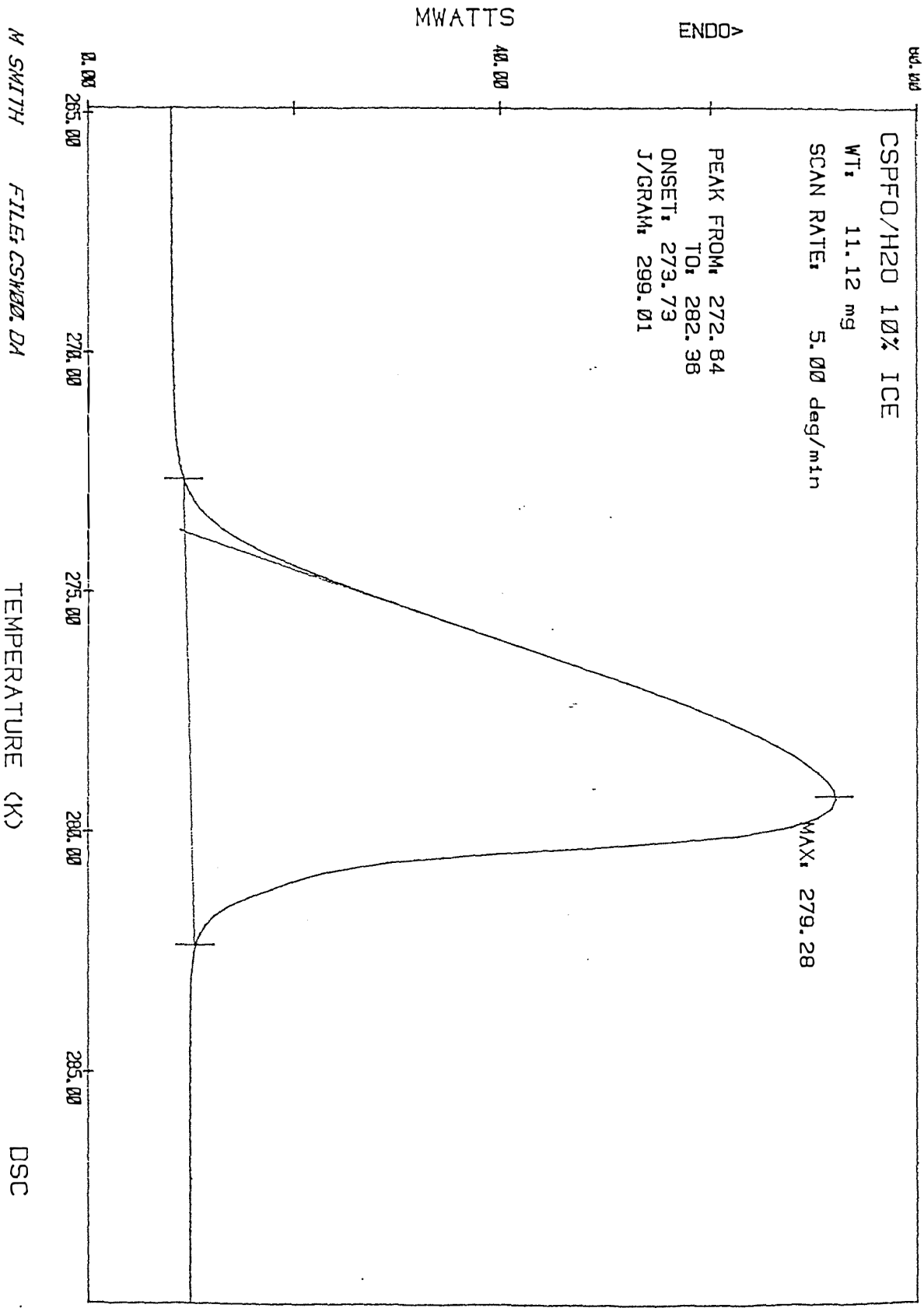

Figure 4.15 A DSC trace for a CsPFO/H_2O (w = 0.676) sample showing the latent heat of solubilization of the amphiphile.

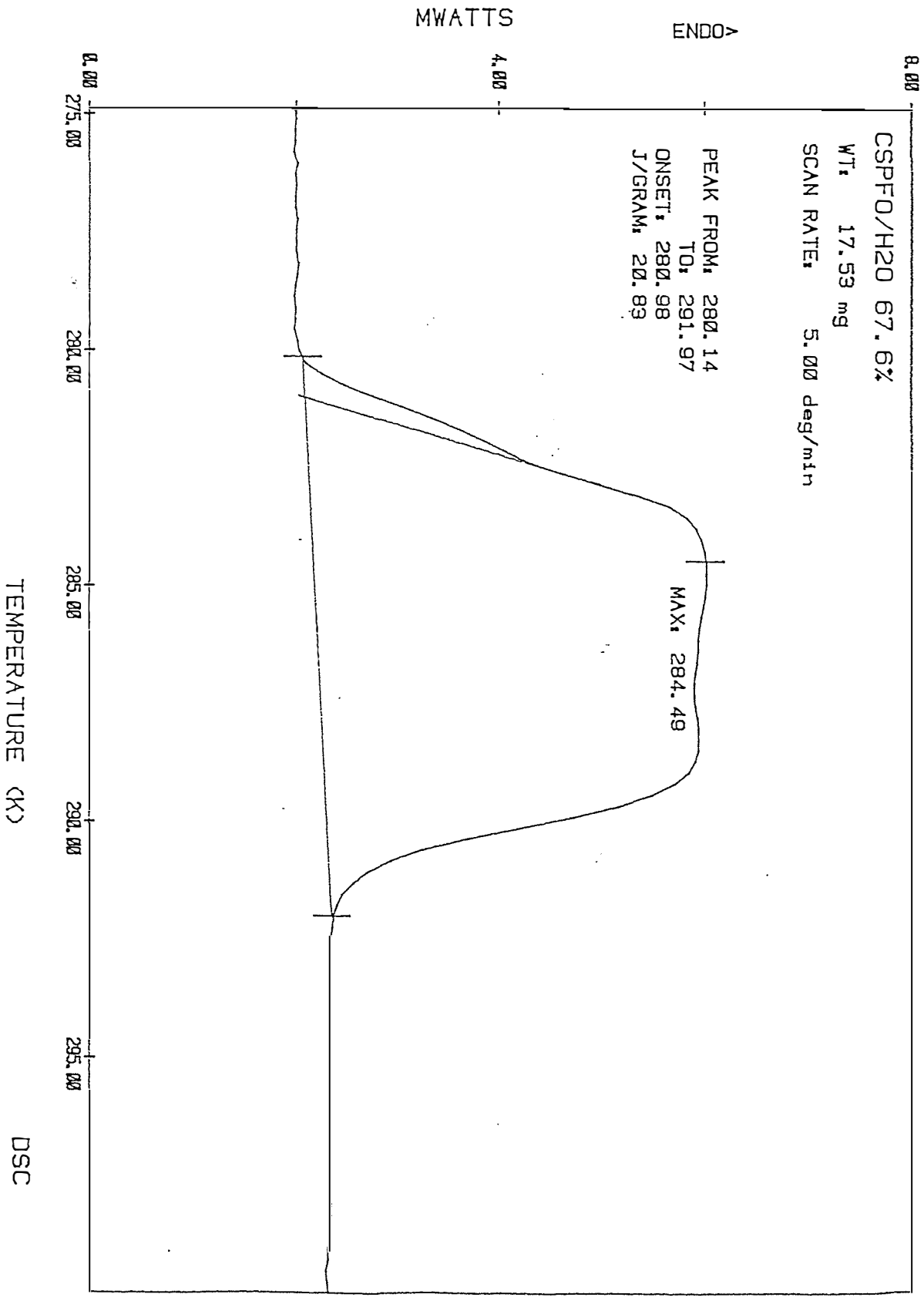

4.4 TESTING THE VALIDITY OF THE NMR MODEL

4.4.1 The Origin of the Quadrupole Splittings

In order to test the validity of the model, developed in chapter 3, it is necessary to have information on the size and shape of the aggregates and the order parameter. It is also useful to isolate the components of the quadrupole splitting that are temperature dependent from those that are not. By defining a reduced quadrupole splitting, the temperature independent terms can be eliminated. Considering first the deuterium quadrupole splittings in the CsPFO/^2H_2O system. Equation 3.20 may be used to define a reduced quadrupole splitting $(\Delta\tilde{\nu}_D)_r$,

$$(\Delta\tilde{\nu}_D)_r \equiv \frac{\Delta\tilde{\nu}_D}{\Delta\tilde{\nu}_D^{\ddagger}} = \frac{\frac{3}{2} S\langle P_2(\cos\alpha)\rangle_s \chi_D \left(\frac{x_A}{x_W}\right) n_b S_{O\text{-}D}}{\frac{3}{2} S^{\ddagger}\langle P_2(\cos\alpha)\rangle_s^{\ddagger} \chi_D \left(\frac{x_A}{x_W}\right) n_b S_{O\text{-}D}}$$

$$= \frac{S\langle P_2(\cos\alpha)\rangle_s \chi_D n_b S_{O\text{-}D}}{S^{\ddagger}\langle P_2(\cos\alpha)\rangle_s^{\ddagger} \chi_D n_b S_{O\text{-}D}} \qquad [4.1]$$

where the parameters marked with ‡ denote reference values (in this case at T_{LN}). It is reasonable to assume that n_b, $S_{O\text{-}D}$ and χ_D are independent of temperature and that $(\Delta\tilde{\nu}_D)_r$ changes as a consequence of changes in S and in $\langle P_2(\cos\alpha)\rangle_s$. It is therefore possible to compare directly the temperature dependence of the reduced quadrupole splittings with that of the reduced quantity $S\langle P_2(\cos\alpha)\rangle_s$. This latter temperature dependence has been determined from a combination of x-ray diffraction and conductivity measurements at Leeds University[8,11]. Figure 4.16 shows a plot of the reduced deuterium quadrupole splittings and reduced $S\langle P_2(\cos\alpha)\rangle_s$ values versus temperature for a w=0.55 CsPFO/^2H_2O sample. It is encouraging to note the high degree of correlation between the two sets of data. There is some divergence deep in the lamellar phase which is probably due to a breakdown in the model caused by the

Figure 4.16 Temperature dependence for a CsPFO/^2H_2O (w = 0.55) sample of the reduced ^2H quadrupole splittings (o) and reduced $S\langle P_2(\cos\alpha)\rangle_s$ values[11] (continuous line) (see equation 4.1).

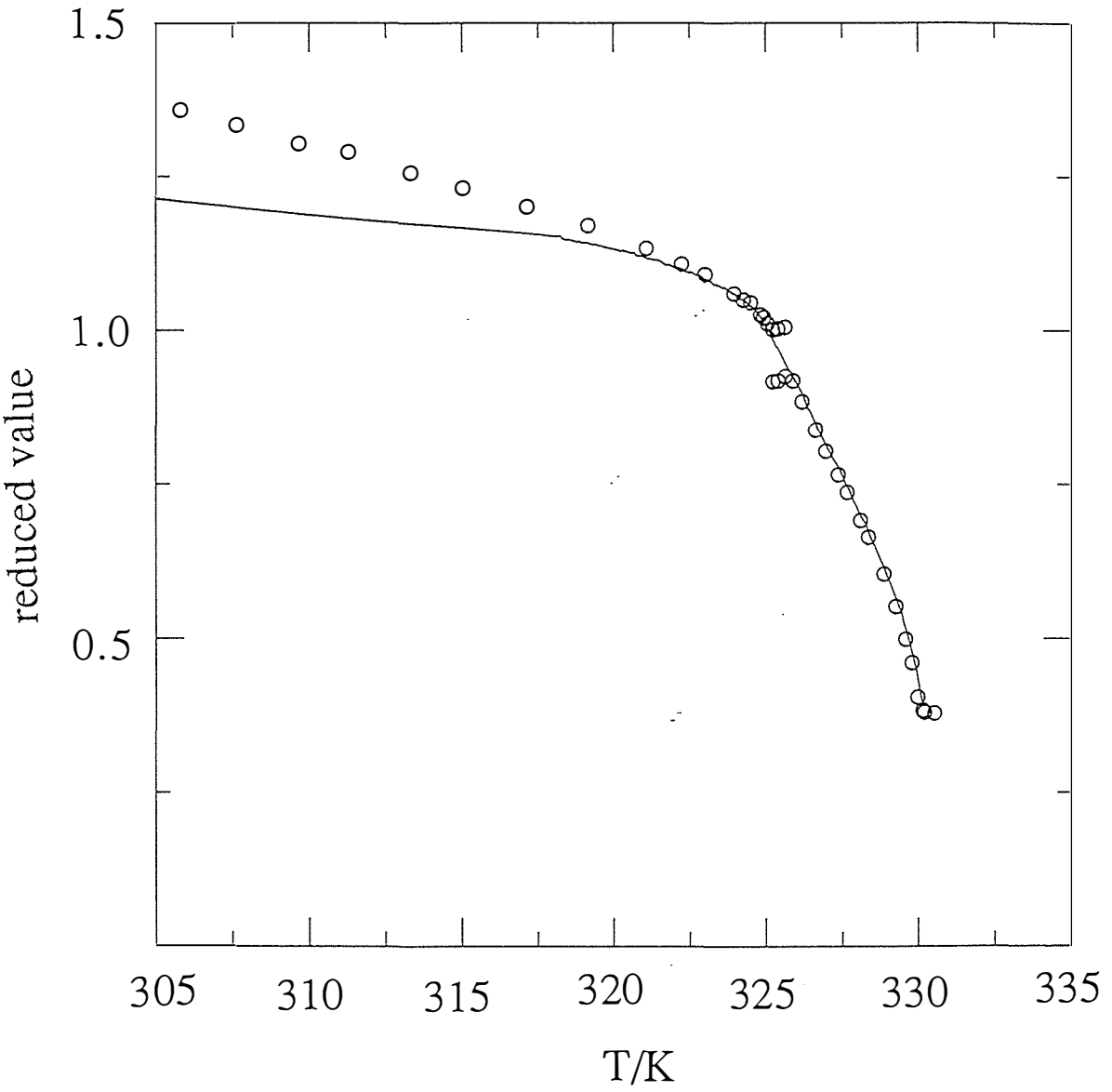

micelles running out of room for growth thereby distorting their shape *i.e.* the diameters of the micelles grow with decreasing temperature until the centre to centre separation in the planes is of the order of the micellar diameter[12]. This will force the water molecules from the 'rims' to the 'caps', which will give rise to higher values of $\Delta\tilde{\nu}$ than would be predicted from the uniform distribution model. The correlation vindicates our assumption of a constant $\chi_D n_b S_{O\text{-}D}$ and shows that for comparative purposes we can use the reduced deuterium quadrupole splitting data instead of the reduced $S<P_2(\cos\alpha)>_s$ derived from the other sources *i.e.* ^2H quadrupole splittings can monitor changes in order and in aggregate size in micellar liquid crystals, at least in the nematic phase.

Looking now at the caesium quadrupole splittings, the temperature dependence of the fraction of the total caesium ions interacting with the surface of the micelles must be considered and the reduced quadrupole splitting, $(\Delta\nu_{Cs})_r$, is therefore defined by

$$(\Delta\nu_{Cs})_r \equiv \frac{\Delta\tilde{\nu}_{Cs}}{\Delta\tilde{\nu}_{Cs}^{\ddagger}} = \frac{\frac{1}{14} S<P_2(\cos\alpha)>_s \chi_{Cs}\beta_{Cs}}{\frac{1}{14} S^{\ddagger}<P_2(\cos\alpha)>_s^{\ddagger} \chi_{Cs}\beta_{Cs}^{\ddagger}}$$

$$= \frac{S<P_2(\cos\alpha)>_s \beta_{Cs}}{S^{\ddagger}<P_2(\cos\alpha)>_s^{\ddagger} \beta_{Cs}^{\ddagger}} \qquad [4.2]$$

An indication of the degree that β_{Cs} should change with temperature is given by the relationship

$$\frac{(\Delta\nu_{Cs})_r}{(\Delta\nu_D)_r} = \frac{\dfrac{S<P_2(\cos\alpha)>_s \beta_{Cs}}{S^{\ddagger}<P_2(\cos\alpha)>_s^{\ddagger} \beta_{Cs}^{\ddagger}}}{\dfrac{S<P_2(\cos\alpha)>_s}{S^{\ddagger}<P_2(\cos\alpha)>_s^{\ddagger}}}$$

$$= \frac{\beta_{Cs}}{\beta_{Cs}^{\ddagger}} \qquad [4.3]$$

i.e. the reduced caesium splittings divided by the reduced deuterium splittings yield the reduced value for the fraction of caesium ions associated with the surface of the micelles at any given temperature. The reduced values of β_{Cs} vs temperature obtained from equation 4.3 are compared with the reduced values of β_{Cs} determined by conductivity methods[11] for a w = 0.55 CsPFO/^2H_2O sample in figure 4.17. In both cases there is a steady increase in β_{Cs} as the temperature is decreased. The reduced quadrupole splittings are considerably higher than the reduced β's, however, especially in the lamellar phase. The reason for this lies in the assumptions we have made in the model. Our model assumes in the calculation of $<P_2(\cos\alpha)>_s$ that all sites on the micelle surface have an equal probability which may be true for small micelles, where the centre to centre separation is greater than the micelle diameter, but as the micelles grow the sites on the caps of the micelles become more favoured. As the micelles grow the counter-ions will be forced out from between the rims and also since there is less curvature on the caps the negative charge density will be greater thus attracting more of the positively charged counter-ions. The cap sites are associated with the larger magnitude quadrupole splittings. To accommodate this into a model would require some knowledge of the charge distribution over non-spherical micelles. There are no reported calculations to date for ion-binding to such a micelle, the ion condensation models thus far proposed have only been developed for spherical micelles[13,14].

4.4.2 The Origin of the Chemical Shift Anisotropy

It is easily shown that the measured quadrupole splittings scale exactly as the shift anisotropies by plotting the reduced quadrupole splittings (reduced to $\Delta\tilde{\nu}(T_{NI})$) against the reduced shift anisotropies (reduced to $\Delta\sigma(T_{NI})$). This is done for a w = 0.55 CsPFO/^2H_2O sample in figure 4.18 where it is seen that there is an excellent correlation

Figure 4.17 Temperature dependence for a CsPFO/^2H_2O (w = 0.55) sample of reduced β_{Cs} values[11] (continuous line) and a reduced ratio of the ^{133}Cs and ^2H quadrupole splittings (o) $\left(\frac{\Delta\tilde{\nu}\ (^{133}Cs)}{(\Delta\tilde{\nu}\ (^2H))}\right)$ (see equation 4.3).

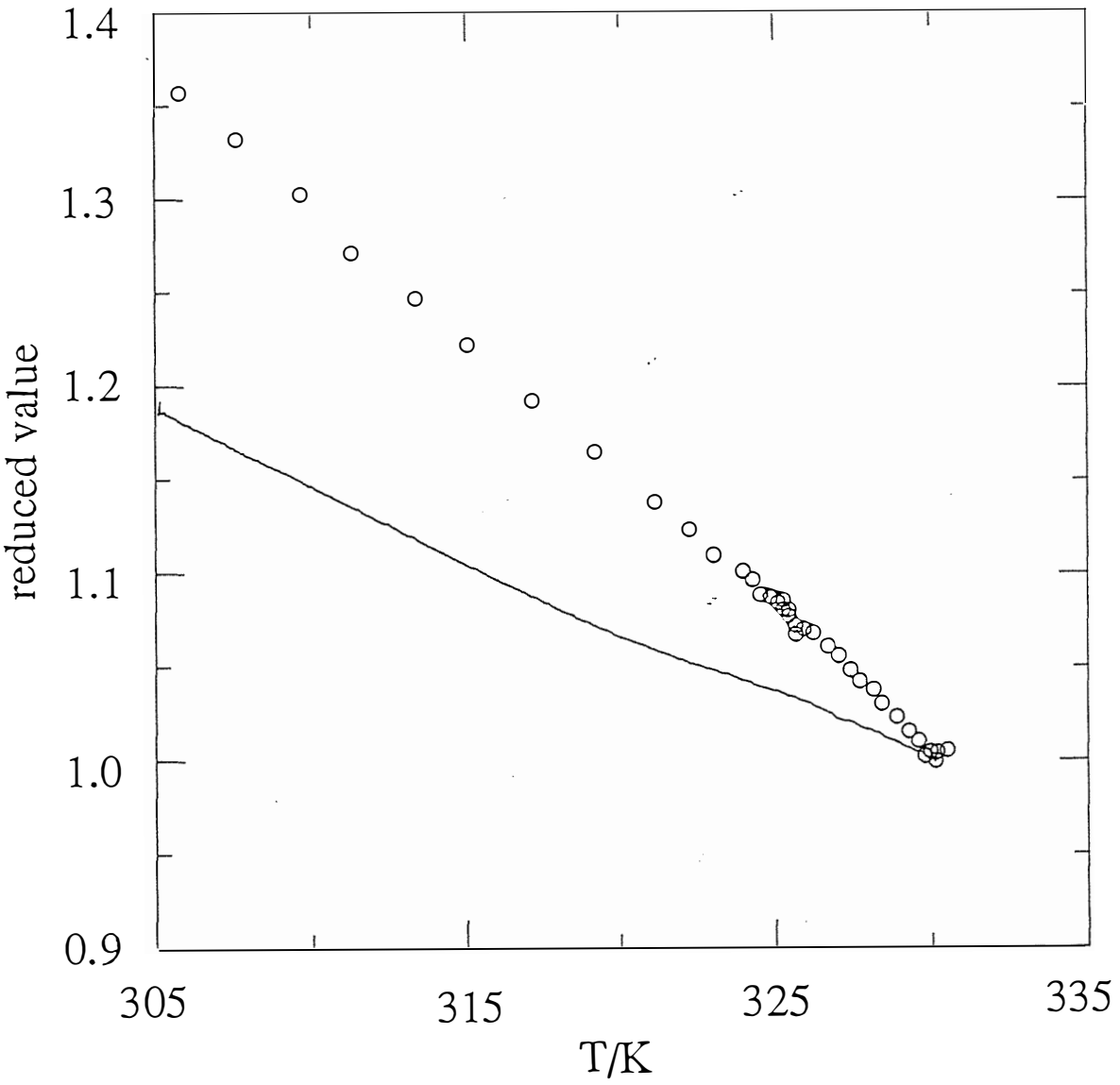

Figure 4.18 Reduced ^{133}Cs quadrupole splittings vs reduced ^{133}Cs chemical shift anisotropies. The slope is 1.00(1) with an intercept of 0.002. $\Delta\sigma$ and $\Delta\tilde{\nu}$ at T_{NI} are 142 Hz and 1.745 kHz respectively.

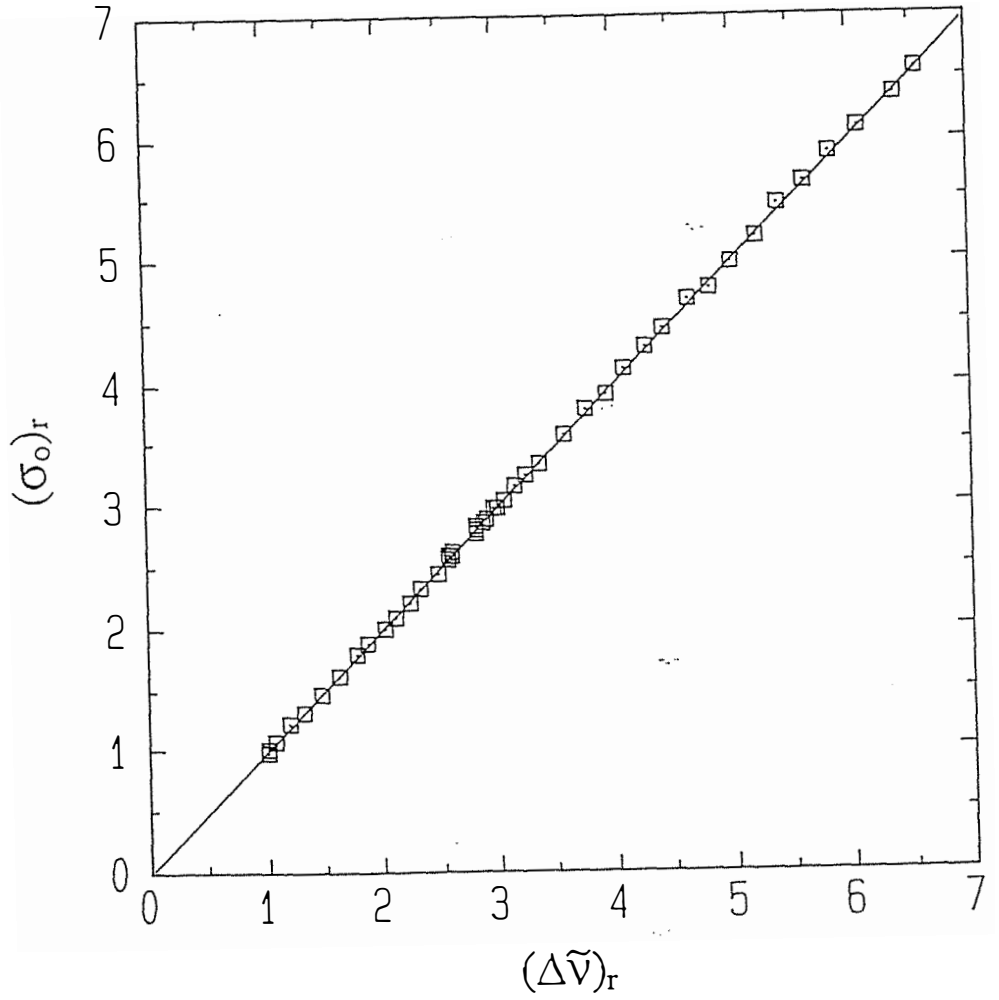

to give a straight line of slope 1 and an intercept zero. The conclusions are two-fold. Firstly it is likely that over the temperature range studied both χ_{Cs} and $\sigma^b_{||} - \sigma^b_{\perp}$ are temperature independent. The alternative explanation that they have the same temperature dependence is less likely[2]. Secondly changes in anisotropy are caused by exactly the same factors as the change in the quadrupole splittings, *i.e.* they are a consequence of molecular interactions rather than changes in the local susceptibility anisotropy.

4.4.3 The Origin of the Quadrupole Couplings

The assertion that the origin of the quadrupole couplings is a distortion of the inner hydration sphere can be tested by looking for possible isotope effects in the ^{133}Cs chemical shifts between the water and heavy water systems. In order to calculate σ_0 using equation 3.27 it is first of all necessary to obtain values for ν_0 in the two systems. This was done by determining the concentration dependence of the ^{133}Cs chemical shift for $CsCl/H_2O$ and $CsCl/^2H_2O$ systems as shown in figure 4.19a. The corresponding value of σ_0 is a function of mole fraction of surfactant are shown in figure 4.19b. There is a small isotope effect consistent with a slightly higher bound fraction of Cs^+ ions in the heavy water system (see equation 3.27) but the isotope effect is constant over the full concentration range. The implication of this is that there is no elimination of water of hydration on binding of the ion to the micelle, *i.e.* the ion retains its inner hydration sphere[4] and electric field gradients induced at the nucleus are a consequence of a distortion of this hydration sphere.

Figure 4.19 (a) Concentration dependence of the ^{133}Cs chemical shifts of $CsCl/H_2O$ (o) and $CsCl/^2H_2O$ (•) solutions. ν_o ($CsCl/H_2O$) =35435439 Hz and ν_o ($CsCl/^2H_2O$) = 35435411 Hz.

(b) ^{133}Cs chemical shifts (σ_o) of the $CsPFO/H_2O$ (o) and $CsPFO/^2H_2O$ (•) systems vs mole fraction of surfactant (x), referenced to their respective CsCl infinite dilution shifts (ν_o).

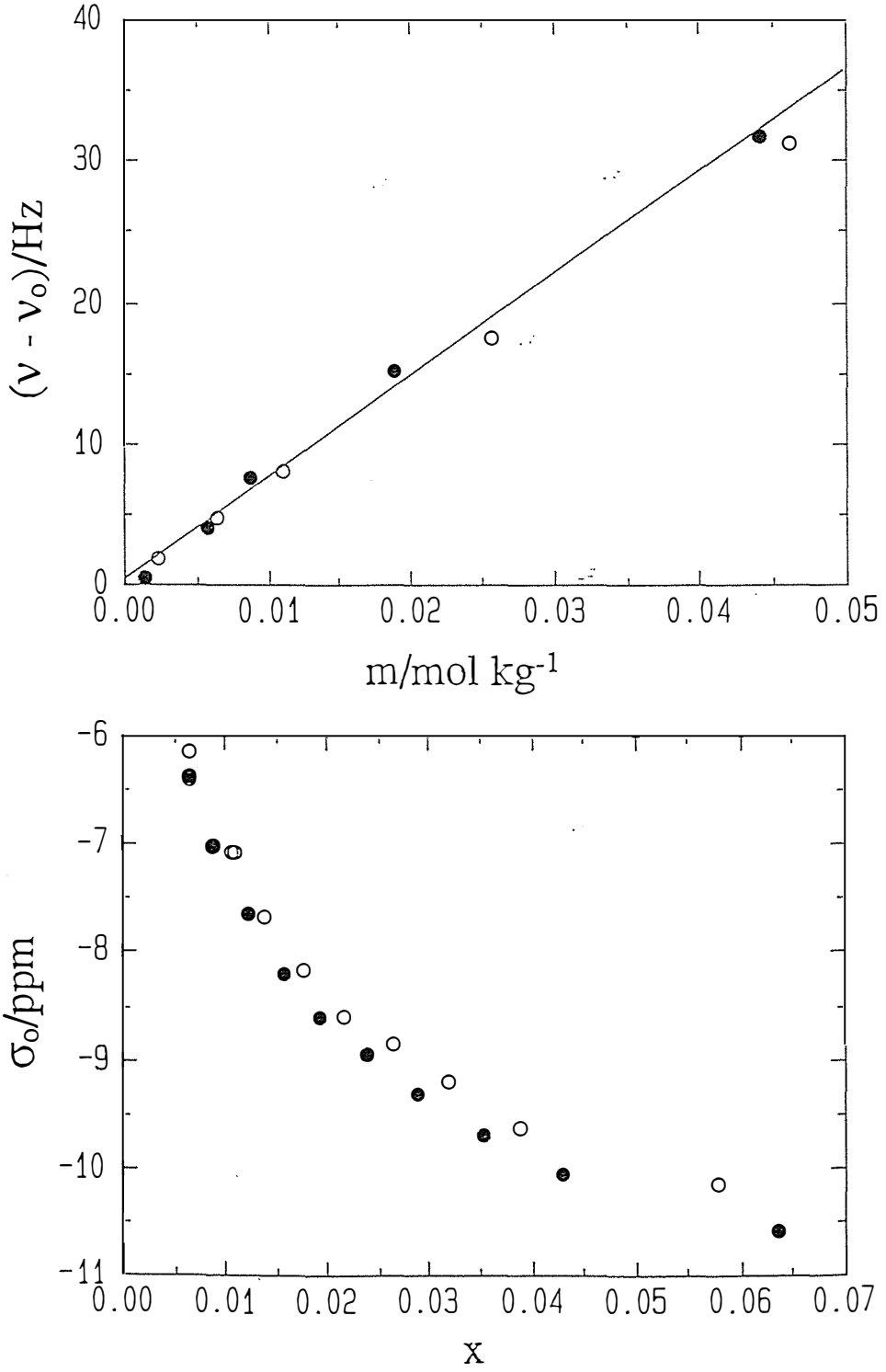

REFERENCES

[1]Chandrasekhar S., *Contemp. Phys.* ,**1988,** *29* , 527.

[2]Persson N.-O.; Lindblom G. *J. Phys. Chem* . **1979,** *83* , 3015.

[3]Boden N.; Jolley K. W.; Smith M. H., *Liq. Cryst.* **1989,** *6* , 481.

[4]Gustavson H.; Lindmann B., *J. Am. Chem. Soc.* **1978,** *100* , 4647.

[5]Lindman B.; Soderman O.; Wennerstrom H., *Annali. di Chimica* **1987,** *77* , 1.

[6]Wennerstrom H.; Personn N.-O.; Lindblom G.; Lindman B. *J. Magn. Reson.* **1978,** *30* , 133.

[7]Reeves L. W.; Fernandes M. D. P. O.; Becerra L., *Liq. Cryst* **1988,** *3* , 771.

[8]Boden N.; Corne S A.; Holmes M. C.; Jackson P. H.; Parker D.; Jolley K. W., *J. Physique* **1986,** *47* , 2135.

[9]Boden N.; Corne S. A.; Jolley K. W., *J. Phys. Chem.* **1987,** *91* , 4092.

[10]Corne S. A., Ph. D. Thesis, Leeds University, **1986.**

[11]Parker D., Ph. D. Thesis, Leeds University, **1988.**

[12]Boden N.; Clements J.; Jolley K. W.; Parker D.; Smith M. H., *J. Chem. Phys.*, in press.

[13]Engström S.; Wennerström H., *J. Phys. Chem.* **1978**, *82* , 2711.

[14]Gunnarsson G.; Jönsson B.; Wennerström H., *J. Phys. Chem.* **1980**, *84* , 3114.

CHAPTER 5

FIELD INDUCED ORDER

5.1 INTRODUCTION

In liquid crystalline systems the observation of phenomena associated with the onset of order in the isotropic phase immediately prior to the isotropic to nematic phase transition temperature yields valuable information concerning the mechanism of the transition. In many liquid crystal systems the isotropic to nematic transition is weakly first-order in nature. This means that as the transition is approached the isotropic phase develops nematic-like properties which give rise to an increase in the extent of the microscopic ordering of the isotropic phase. The nematic-like properties derive from small groups of molecules which have local ordering *i.e.* a degree of correlation between their long axes. These small groups of molecules are anisotropic domains suspended in an isotropic medium. The aim for experimentalists is to link the pretransional behaviour to the increase in size of these small anisotropic regions and therefore the increase in order of the sample as a whole. These regions, sometimes known as swarms, are more easily aligned by the external field as their size is increased. A measure of the size of these swarms is given by the quantity $\xi(T)$, the coherence length, which for thermotropics is of the order of ten times the molecular length[1]. Microscopic ordering can be converted into measurable macroscopic ordering by the application of an external field.

The Landau-De Gennes model[2], based on mean field theory, predicts that tensor properties such as birefringence which result from pretransitional ordering are proportional to $(T-T^*)^{-\gamma}$ where T^* is the temperature of the theoretical second-order transition. According to mean field theory $\gamma = 1$. As the temperature tends to T^* the size

of the anisotropic swarms tends towards infinity, $\xi(T^*) = \infty$, therefore T^* is identified as the temperature at which a second-order transition would have occurred had the first-order transition not intervened. If this theoretical second-order transition occurred there would be no discontinuity in the order parameter in going from the isotropic (paranematic) phase to the nematic phase.

There are a variety of techniques that have been employed to study pretransitional behaviour in thermotropics; these include flow birefringence[3], depolarized light scattering[4], magnetic birefringence[5,6,7,8,9] and Kerr effect[10,11] measurements and NMR[12-18].

Birefringence measurement techniques make use of an applied external field and are classified according to the type of field. Magnetic birefringence and electric birefringence are referred to as the Cotton-Mouton effect and the Kerr effect respectively. Δn, the measured birefringence can be related to the field strength by the following

$$\Delta n = n_{\parallel} - n_{\perp} = CH^2 \qquad [5.1]$$

where C is the Cotton-Mouton coefficient, $n_{\parallel}$ and $n_{\perp}$ are the refractive indices measured parallel and perpendicular to the magnetic field and H is the field strength. Similarly the Kerr constant, C' is given by

$$C' = \frac{n_{\parallel} - n_{\perp}}{E^2} \qquad [5.2]$$

where E is the electric field strength. Flow birefringence is measured when the sample is subjected to a shear force along the x-axis as the sample flows in the z direction. Pretransitional ordering can be related to an increase in I, the scattering intensity as the isotropic to nematic transition is approached.

An applied external field is an integral part of nuclear magnetic resonance spectroscopy. There have been several studies reporting the use of deuterium NMR to

monitor field induced ordering in the isotropic phase of thermotropic liquid crystal systems. It is possible to determine the degree of ordering by measuring the quadrupole splitting of deuterons substituted on to the nematogen molecules as in 4-*n*-pentyl-4'-cyanobiphenyl (5CB)[12], or of deuterons on a solute molecule such as perdeuterated anthracene and *p*-xylene dissolved in the thermotropic solvent[13,14]. Information on pretransitional effects has also been gained by spin-spin relaxation time measurements on partially deuterated nematogens[15] and from the appearance of NMR spectra obtained in the presence of an external electric field[16,17,18].

NMR has several advantages over other techniques; it provides the system with a stable magnetic field to drive the pretransitional ordering and the nematic signal is separate from the isotropic signal in the mixed phase region. This enables field induced ordering of the isotropic phase to be monitored in the isotropic/nematic biphasic region. In the case of optical birefringence measurements, the field induced ordering can only be measured at temperatures above T_{IN} because in the isotropic/nematic biphasic regime the birefringence is measured through an average response in which the nematic contribution overwhelms the field induced contribution.

5.2 PRETRANSITIONAL ORDERING IN CsPFO/^2H_2O

The sequence of transitions in the CsPFO/^2H_2O system is analogous to the isotropic to nematic to smectic A transition scheme of thermotropic calamitic liquid crystals. A major difference between thermotropics and CsPFO/^2H_2O is the low packing fraction of the micelles in the lyotropic system (from 0.11 to 0.43 along the N_D^+ to I transition). The isotropic to nematic transition is first-order, although only weakly so and weakens on dilution. $T_{IN}-T^*$ is a measure of the 'strength' of the first-order transition, therefore a weakening of the transition will be reflected in a reduction in the magnitude of $T_{IN}-T^*$.

Rosenblatt et al[19] have used magnetic birefringence to measure the quantity T_{IN} -T^* for the CsPFO/H_2O system. The weakness of the transition allows measurements in the isotropic phase close to T^* making it possible to measure the critical exponent for the transition. Their results show that the value of T_{IN} -T^* is strongly concentration dependent, decreasing with decreasing concentration (600 mK for w = 0.588, 170 mK for w = 0.516 and 15 mK for w = 0.382) . The weakening of the transition has its origin in the effect of diluting the intermicellar interactions by reducing the packing fraction of the micelles. The order parameter susceptibility χ_s was fitted to $\chi_s = \chi_o(T-T^*)^{-\gamma}$ where χ_o, T^* and γ are adjustable parameters. The best fit value for the critical exponent, γ, obtained from these experiments was 1.01±0.04, which is very close to one, the value predicted by mean field theory.

Rosenblatt and co-workers have also carried out a series of experiments in which the effects of adding a third component to the binary CsPFO/H_2O system are studied. These extra components include: electrolyte[20], co-surfactant[21], surfactant with a longer fluorocarbon chain[22] and RbPFO[23]. These experiments were conducted using a fixed weight ratio of water to surfactant with the third component being substituted for CsPFO in varying quantities except for the case of the electrolyte CsCl where the ratio of CsPFO to water is kept constant. The object of these experiments is to attempt to relate the size and shape of the aggregate to the properties of the bulk material. The results are examined in terms of the quantity Φ which is defined such that,

$$\Phi \equiv C(T-T^*) \qquad [5.3]$$

The significance of the values of Φ produced by Rosenblatt *et al.* for these experiments is apparent when the factors that contribute to Φ are examined.

$$\Phi = \frac{\Delta\varepsilon\Delta\chi}{9\bar{n}a_0} \qquad [5.4]$$

where $\Delta\varepsilon$ and $\Delta\chi$ are the volume dielectric and magnetic susceptibility anisotropies, $\bar{n} = \sqrt{\bar{\varepsilon}}$ and a_0 is the coefficient of the quadratic term of the Landau free energy expansion. Addition of CsCl as a third component in these systems causes a sharp decrease in Φ. This is due to two principle factors, the effect of altering the size and shape of the micelle and a moderation of the intermicellar forces. The addition of more Cs^+ ions into the system increases the fraction of these positive ions bound to the negatively charged micellar surface[24]. This leads to a reduction in the charge density between the polar head groups thus allowing them to come closer together therefore promoting growth of the micelle. $\Delta\varepsilon$ and $\Delta\chi$ are both proportional to the number density of the micelle times a shape factor[25]. a_0 is a function of the number density and the inverse of the aggregation number, $\tilde{n}$,. Therefore Φ is proportional to the aggregation number, the number density of the micelles and the square of the shape factor. Rosenblatt discusses his results in terms of an effective change in micelle size i.e. the way a micelle would change if the effect of the third component was only to change the micelle size and not the interaggregate interaction. In contrast to studies undertaken in this laboratory[24], he concludes that the micelle size is not significantly affected by the addition of electrolyte and that the dependence of Φ on the concentration of CsCl is more to do with a change in the pair potential. The component of the pair potential that is modified to the greatest degree is the Coulombic repulsion. The repulsion between the micelles is lowered because the negative charge on the micelles is screened by the added electrolyte.

5.2.1 NMR and Pretransitional Behaviour in CsPFO/^2H_2O

The first observation of pretransitional ordering in the isotropic phase of the CsPFO/^2H_2O system by NMR spectroscopy was made[26] on a spectrometer operating at a field strength of 6.3 T. In a previous study on the system[27] at a field strength of 2.1 T no effects due to the phenomenon were observed.

The pretransitional behaviour is much more evident in ^{133}Cs NMR than in ^{2}H NMR since the field induced quadrupole splitting is much larger. ^{2}H NMR is more useful in determining the degree of pretransitional ordering, however, because the isotropic and nematic signals do not overlap. Also the peaks in the ^{133}Cs spectra are much broader making it more difficult to resolve the field induced order peaks.

When it became apparent that the JEOL GX-270 NMR was of a sufficient field strength to enable magnetic field induced ordering effects to be observed in the isotropic phase, a systematic study was undertaken along the isotropic to nematic transition line to determine $T-T^{*}$ as a function of temperature and composition and to discover whether the observed behaviour fitted the theories established for pretransitional ordering in thermotropic liquid crystals.

To illustrate the phenomenon of field induced ordering consider the deuterium spectra for the w=0.302 sample shown in figure 5.1. At high temperatures the spectrum is a single line with a width at half height of ≈1.2 Hz which is determined by spin relaxation processes and field inhomogeneities. As the temperature is lowered (a) the single isotropic peak broadens and then splits into a doublet (b). It is at this point that the pretransitional ordering becomes obvious but it is actually the broadening of the singlet peak that heralds the onset of measurable field induced ordering. The magnitude of the quadrupole splitting increases rapidly (b-d) until T_{IN} is reached. Spectrum (c), taken at just above T_{IN}, shows good resolution of the doublet peaks and no sign of nematic phase being present. At a temperature slightly below T_{IN} (d) an outer doublet for the nematic phase can be clearly seen. As the temperature is lowered further (e) the relative amount of the nematic component increases until finally when T_{NI} is reached the sample becomes purely nematic. Taken on the whole this series of spectra shows a rapid divergence in the quadrupole splitting of the isotropic signal which is quenched on the intervention of the first-order phase transition at T_{IN}.

Figure 5.1. A sequence of ^2H NMR spectra observed on cooling a CsPFO/^2H_2O (w = 0.302) sample from the isotropic phase into the isotropic/nematic biphasic region along the isopleth shown in figure 5.2. The rapid divergence of the field induced quadrupole splitting and its quenching at T_{IN} are clearly seen.

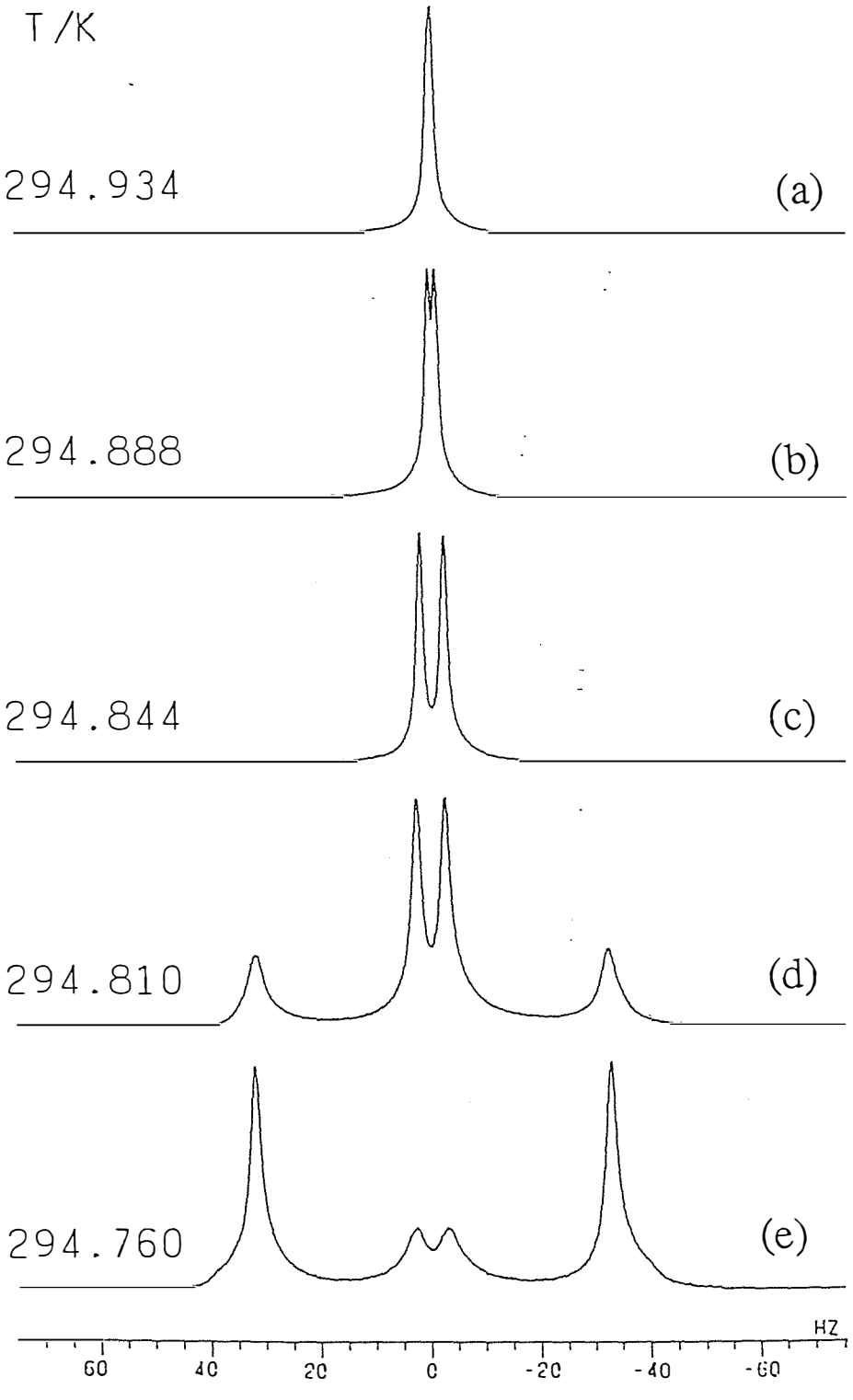

Figure 5.2 Partial phase diagram of the CsPFO/^2H_2O system showing the upper T_{IN} and lower T_{NI} boundaries to the isotropic to nematic transition. The dashed line represents the hypothetical supercooling limit T^* of the isotropic phase. The letters along the isopleth refer to spectra shown in figures 5.1 and 5.3.

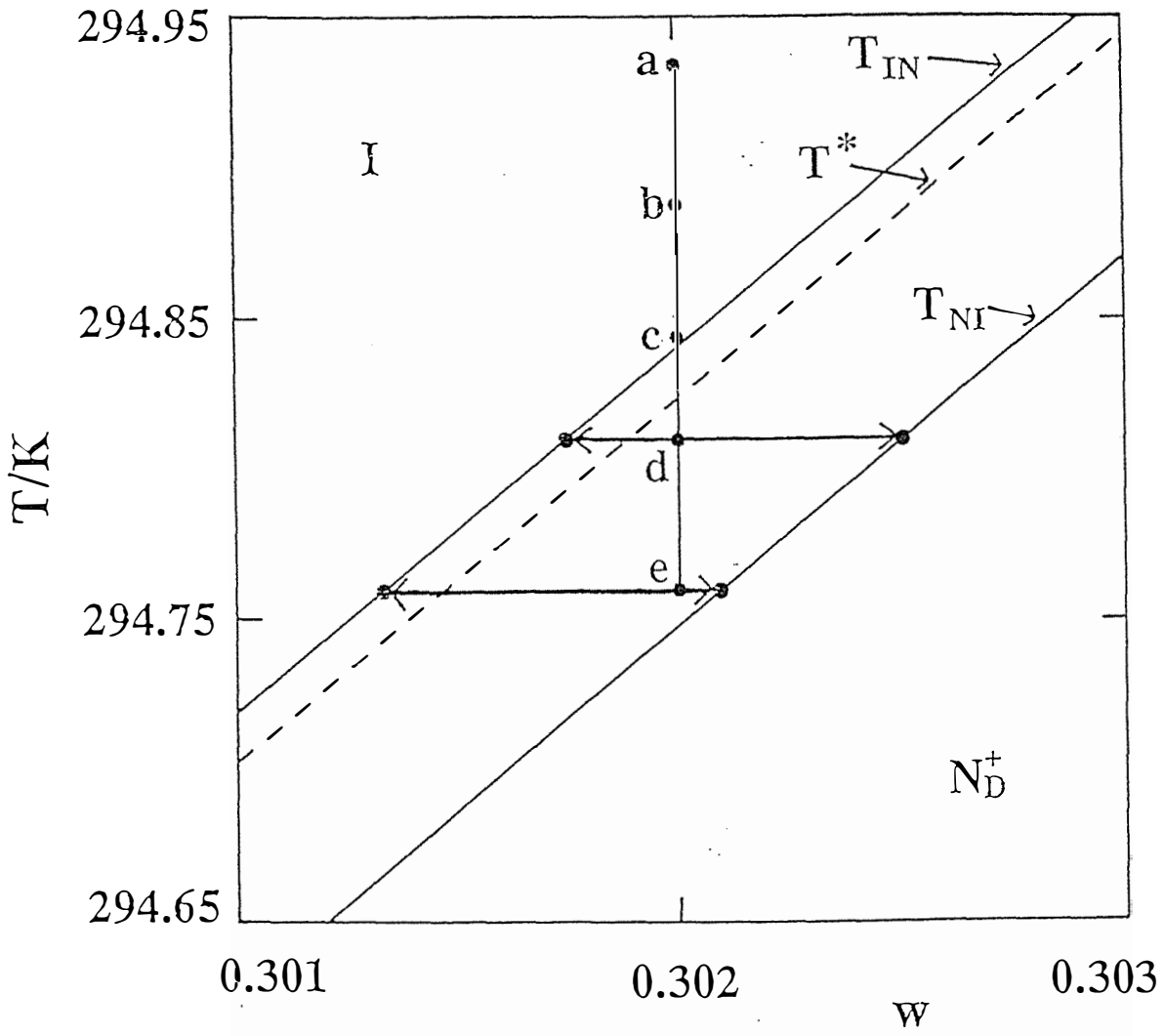

Figure 5.3 shows a series of ^{133}Cs spectra corresponding to the deuterium spectra of figure 5.1. Spectrum (a) shows a single isotropic peak which broadens as the temperature decreases (spectrum (b)). In spectrum (b) it is noted that the peak is no longer of a Lorentzian shape. The shape of this peak is due to the onset of field induced ordering causing quadrupole splitting. At a temperature just above T_{IN} (c) the quadrupole splitting has increased to such an extent that the quadrupole peaks can clearly be seen as satellites on the Zeeman peak. In the biphasic region (d) the spectral peaks are (from low to high frequency), the isotropic quadrupole peak ($+\frac{3}{2}$ to $+\frac{1}{2}$), the isotropic phase Zeeman peak ($+\frac{1}{2}$ to $-\frac{1}{2}$) and the nematic Zeeman peak. (The isotropic quadrupole peak corresponding to the $-\frac{1}{2}$ to $-\frac{3}{2}$ transition is obscured by the nematic Zeeman peak.) The chemical shift difference between the two phases can be clearly seen. The origin of this difference in the chemical shift has been discussed in chapter 3. Close to T_{NI} (e) the intensity of the isotropic components has dropped away but it can be seen that the isotropic ^{133}Cs quadrupole splitting is similar to the splitting in spectrum (d). For ^{133}Cs ($I = \frac{7}{2}$) there should be seven peaks instead of the three that are visible. The peaks that cannot be observed have been broadened to such an extent that they have disappeared into the base-line. All of the quadrupole peaks associated with the isotropic phase component are broader than those associated with the nematic phase. This is because of the short lifetime of the ordered paranematic state as it fluctuates between isotropic and nematic behaviour.

This discussion will concentrate on the use of ^{2}H NMR as a means of measuring the field induced ordering although ^{133}Cs NMR can also be useful to investigate pretransitional behaviour in this system. Because of the large excess of $^{2}H_2O$ molecules in the free state the ^{2}H line-widths of $^{2}H_2O$ are small and the splittings are easily resolved. ^{133}Cs NMR is a complimentary technique in the CsPFO/$^{2}H_2O$ system and it is the only appropriate method to use in the CsPFO/H_2O system for the study of field induced order. The magnitude of the field induced quadrupole splitting is often difficult

Figure 5.3 A sequence of ^{133}Cs NMR spectra observed on cooling a CsPFO/$^{2}H_2O$ (w = 0.302) sample from the isotropic phase into the isotropic/nematic biphasic region along the isopleth shown in figure 5.2. The rapid divergence of the field induced quadrupole splitting and its quenching at T_{IN} are clearly seen.

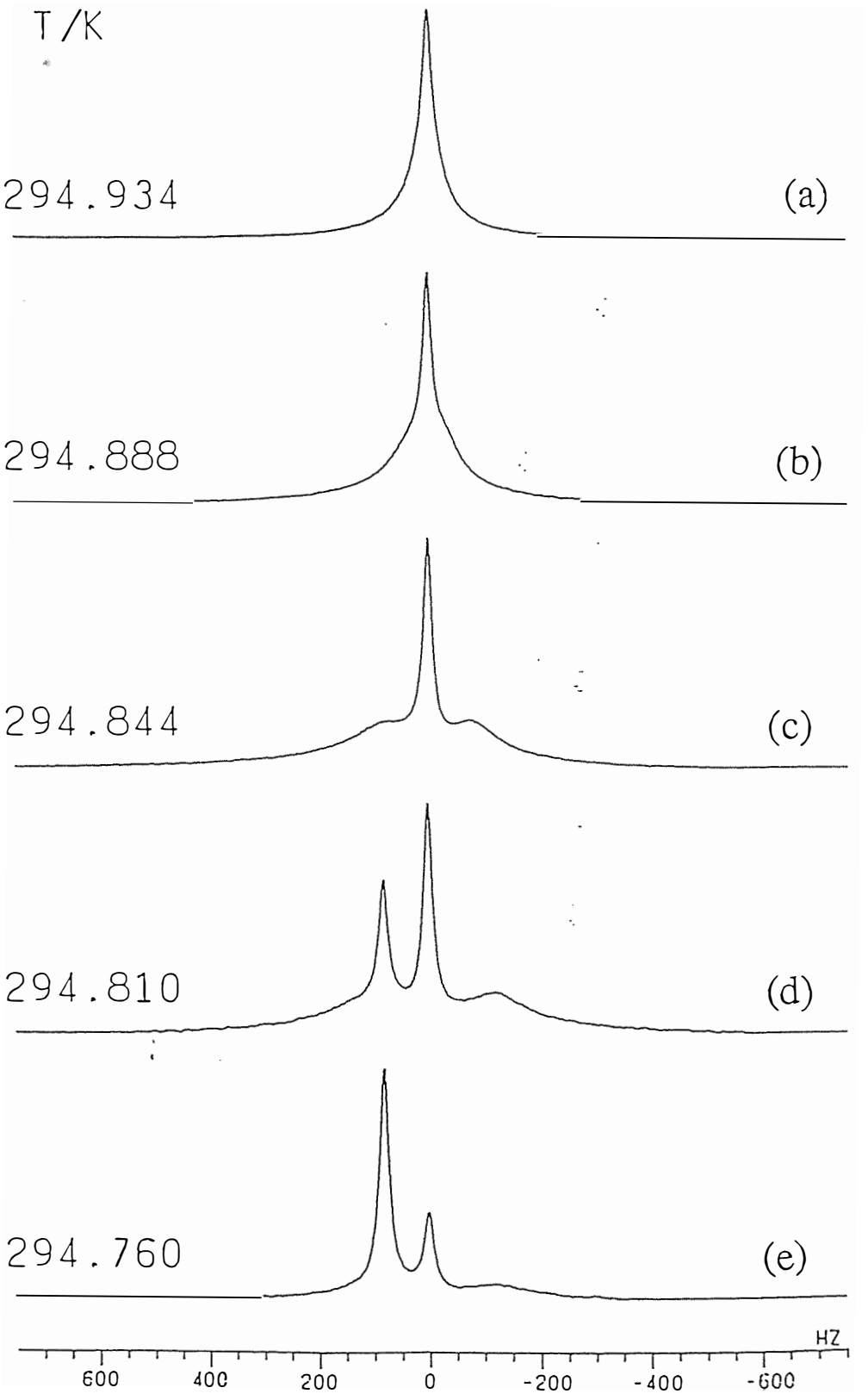

to determine in the ^{133}Cs spectra, however, because the quadrupole peaks are very broad. This is particularly so at low CsPFO weight fractions.

5.2.3 Origin of the Pretransitional Quadrupole Splitting

In the isotropic phase the CsPFO micelles are discoidal and therefore they exhibit an anisotropy in their magnetic susceptibility. In the presence of a magnetic field this anisotropy gives rise to small domains of ordered micelles, immersed in the isotropic phase, which increase in size as the temperature approaches T^*. These domains are analogous to the 'swarms' that are proposed to exist in pretransitional thermotropic liquid crystals. We cannot directly measure the increased ordering of these domains but since we measure an ensemble average their presence is indicated in an overall increase in the ordering of the sample.

The quadrupole splitting of the deuterium signal has a direct relationship with the second rank order parameter P_2,

$$P_2 \equiv \overline{P_2(\cos\gamma)} \qquad [5.5]$$

where γ is the angle between the magnetic field **B** and the micellar symmetry axis. P_2 is therefore a measure of the macroscopic ordering induced by the magnetic field. The relationship between $\Delta\nu$ and P_2, for a ^2H nucleus in heavy water, is given by

$$\Delta\nu = \frac{3}{2}|q_{zz}|_s P_2 \qquad [5.6]$$

where $|q_{zz}|_s$ is the partially averaged component of the quadrupole-electric field gradient tensor parallel to **B** in a perfectly ordered mesophase (*cf.* equation 3.19).

Using an adaptation of the molecular field theory of Luckhurst[28,29], P_2 can be related to the Maier-Saupe interaction parameter ε by

$$P_2 = \frac{\Delta\chi B^2 + 3\varepsilon}{15kT} \qquad [5.7]$$

where $\Delta\chi$ is the anisotropy in the magnetic susceptibility of the micelle. For a solution of disc shaped micelles ε is related to the aggregation number $\tilde{n}$ and the volume fraction of micelles ϕ_m by the relationship

$$\varepsilon = c\tilde{n}\phi_m P_2 \qquad [5.8]$$

where c is a constant.

Substituting eq. [5.8] into eq. [5.7] gives

$$P_2 = \frac{\Delta\chi B^2}{15k(T-T^*)} \qquad [5.9]$$

where the divergence temperature T^* is given by

$$T^* = \frac{c\tilde{n}\phi_m}{5k} \qquad [5.10]$$

When eq. [5.9] is substituted into eq. [5.6] an expression for the dependence of the quadrupolar splitting on the temperature is obtained.

$$\Delta\nu = \frac{|\tilde{q}_{zz}|_s \Delta\chi B^2}{10k(T-T^*)} \qquad [5.11]$$

Over the small temperature range for which the pretransitional quadrupole splittings can be determined the micellar aggregation number is practically constant and since the aggregation number influences other factor such as $|\tilde{q}_{zz}|_s$, $\Delta\chi$ and T^*, to a first approximation these also remain constant. It is apparent that the magnitude of the quadrupole splitting is a function of the square of the magnetic field strength and $T-T^*$. In NMR the field strength is dependent on the spectrometer and is therefore a constant for any given experiment. Thus the splitting is predicted to diverge at T^*. Figures [5.4a...5.8a] show the field induced quadrupole splitting as a function of temperature for a range of samples from w = 0.15 to 0.35. A striking feature of all of these plots is that the divergence of the quadrupole splitting at T^* is quenched at T_{IN}.

Figure 5.4 Plot of the temperature dependence of (a) the field induced quadrupole splitting $\Delta\tilde{\nu}$ and (b) $\Delta\tilde{\nu}^{-1}$ for ^2H_2O in the isotropic phase and in the nematic/isotropic biphasic region for a CsPFO/^2H_2O (w = 0.15) sample. The discontinuity in the temperature dependence, especially in the $\Delta\tilde{\nu}^{-1}$ vs T plot clearly identifies T_{IN}. T^* is given by extrapolation of $\Delta\tilde{\nu}^{-1}$ to zero. The solid lines were obtained from a least squares fit through the $\Delta\tilde{\nu}^{-1}$ vs T data.

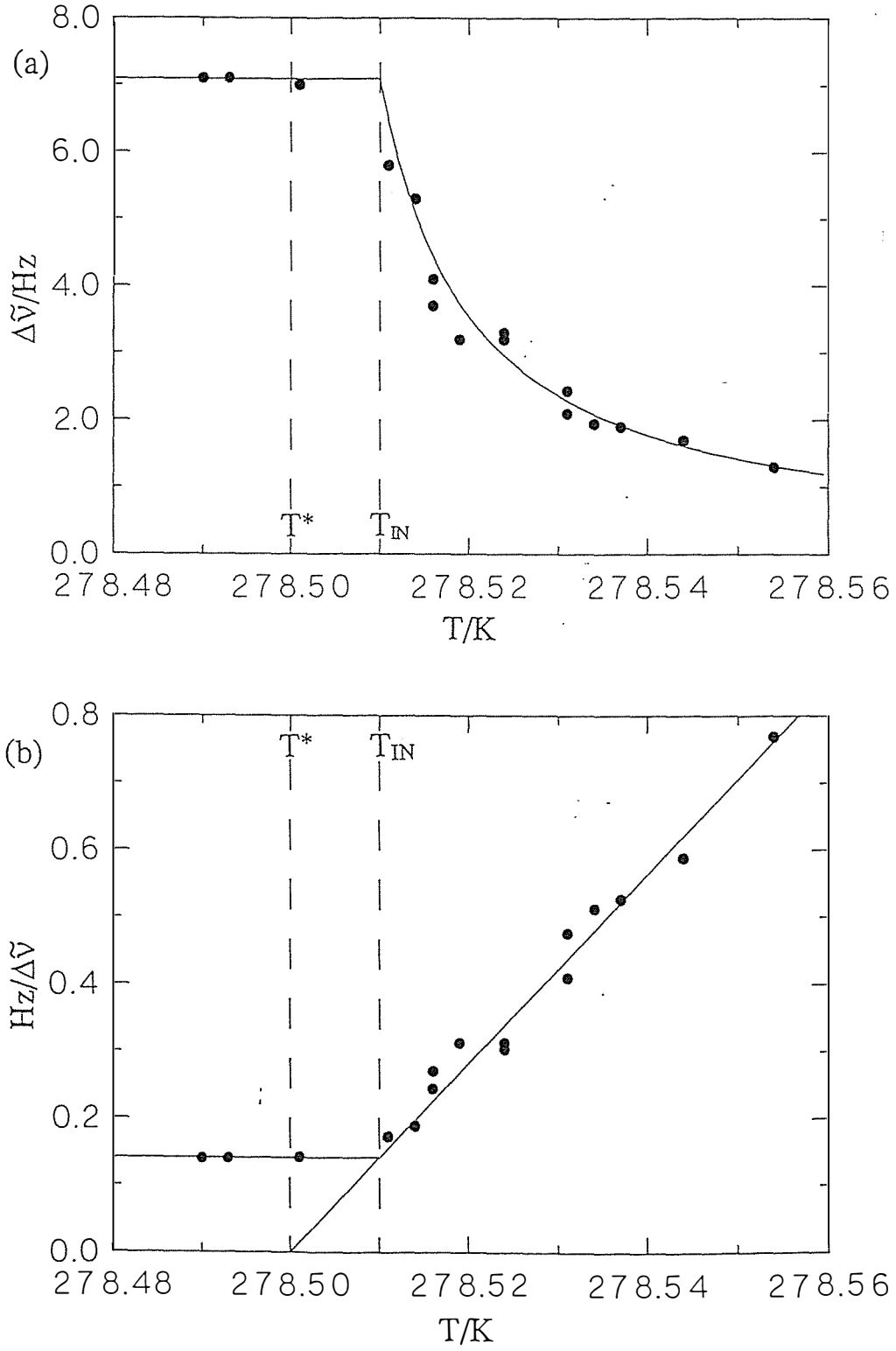

Figure 5.5 Plot of the temperature dependence of (a) the field induced quadrupole splitting $\Delta\tilde{\nu}$ and (b) $\Delta\tilde{\nu}^{-1}$ for ^2H_2O in the isotropic phase and in the nematic/isotropic biphasic region for a CsPFO/^2H_2O (w = 0.20) sample.

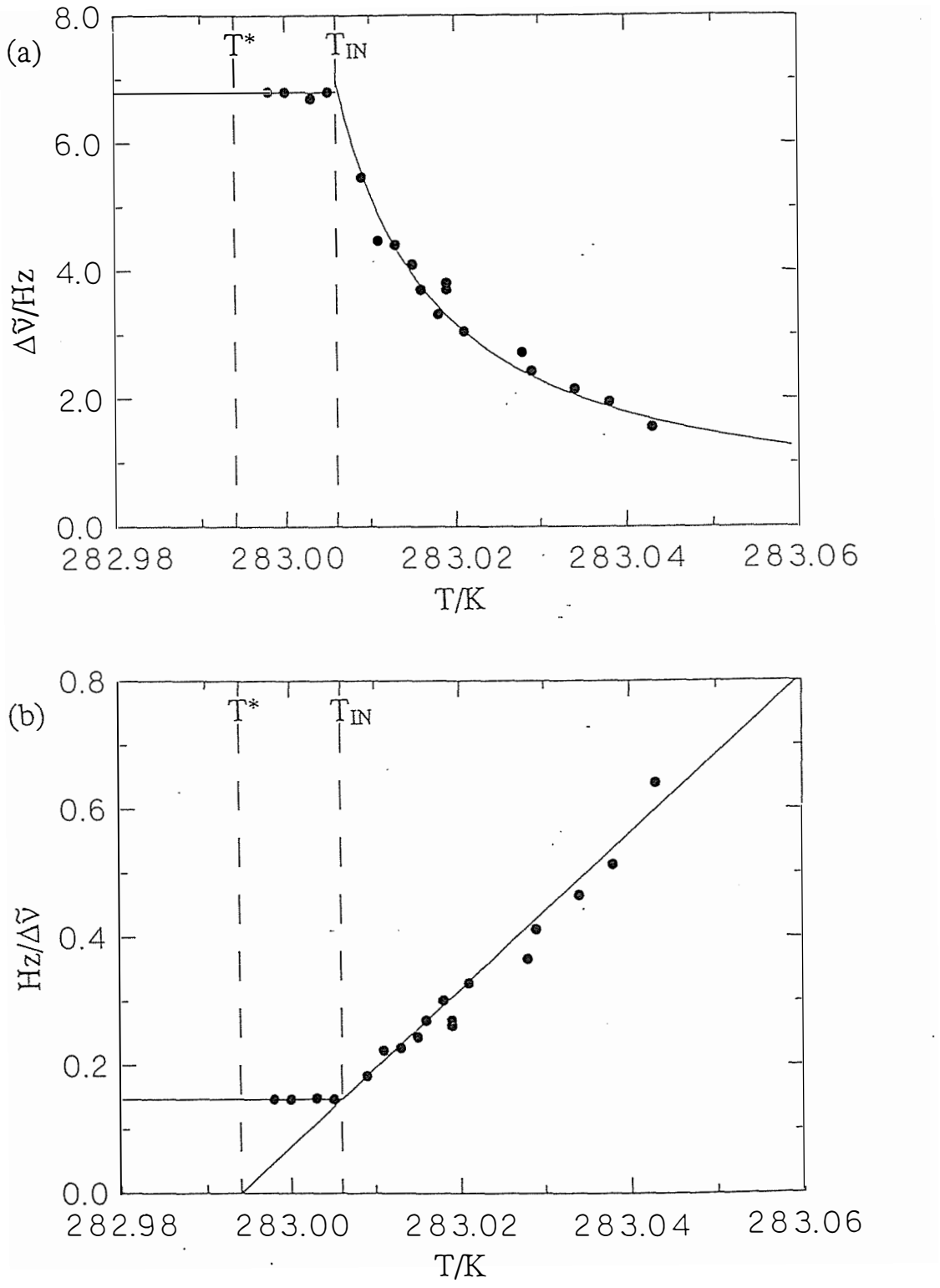

Figure 5.6 Plot of the temperature dependence of (a) the field induced quadrupole splitting $\Delta\tilde{\nu}$ and (b) $\Delta\tilde{\nu}^{-1}$ for ^2H_2O in the isotropic phase and in the nematic/isotropic biphasic region for a CsPFO/^2H_2O (w = 0.25) sample.

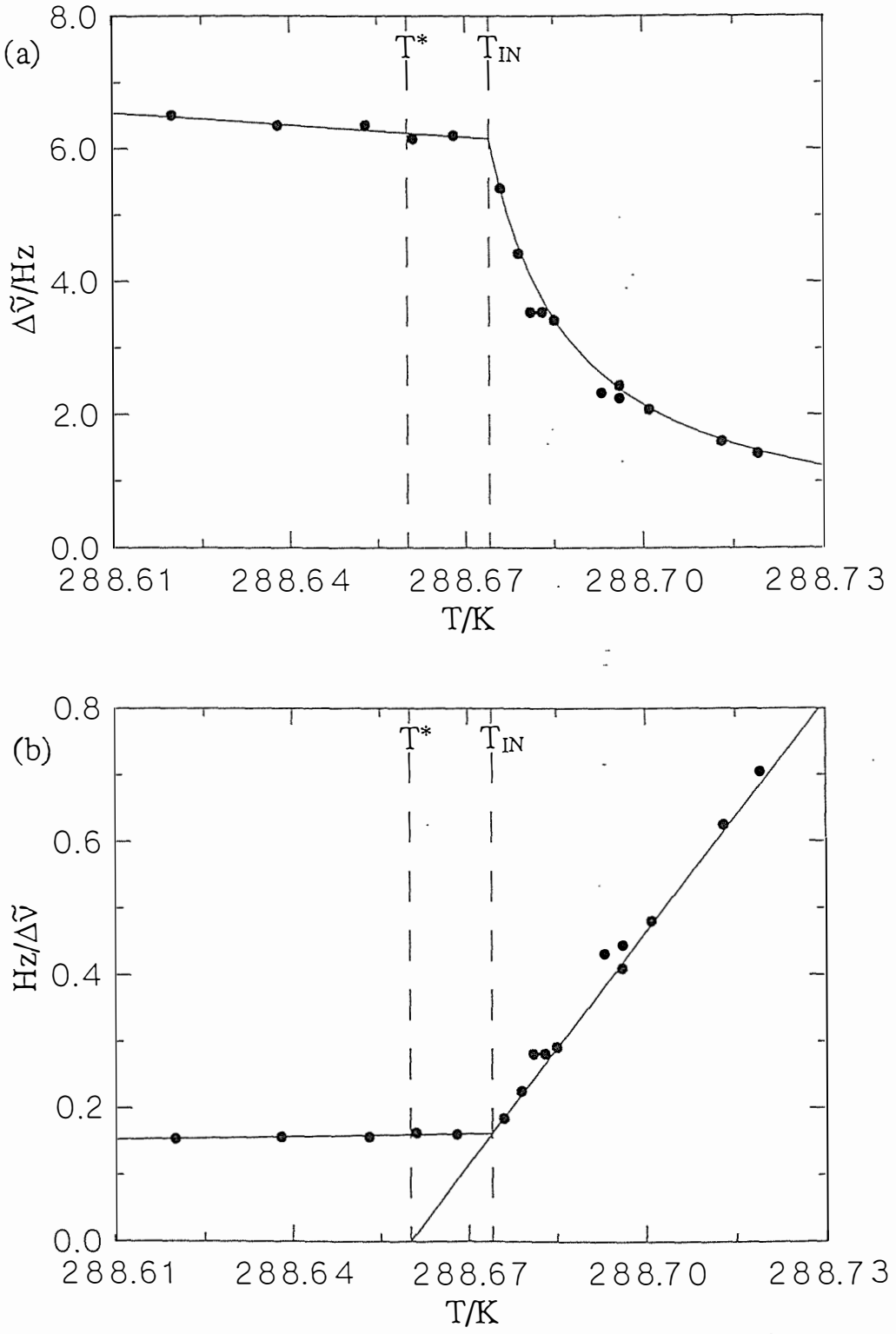

Figure 5.7 Plot of the temperature dependence of (a) the field induced quadrupole splitting $\Delta\tilde{\nu}$ and (b) $\Delta\tilde{\nu}^{-1}$ for ^2H_2O in the isotropic phase and in the nematic/isotropic biphasic region for a CsPFO/^2H_2O (w = 0.302) sample.

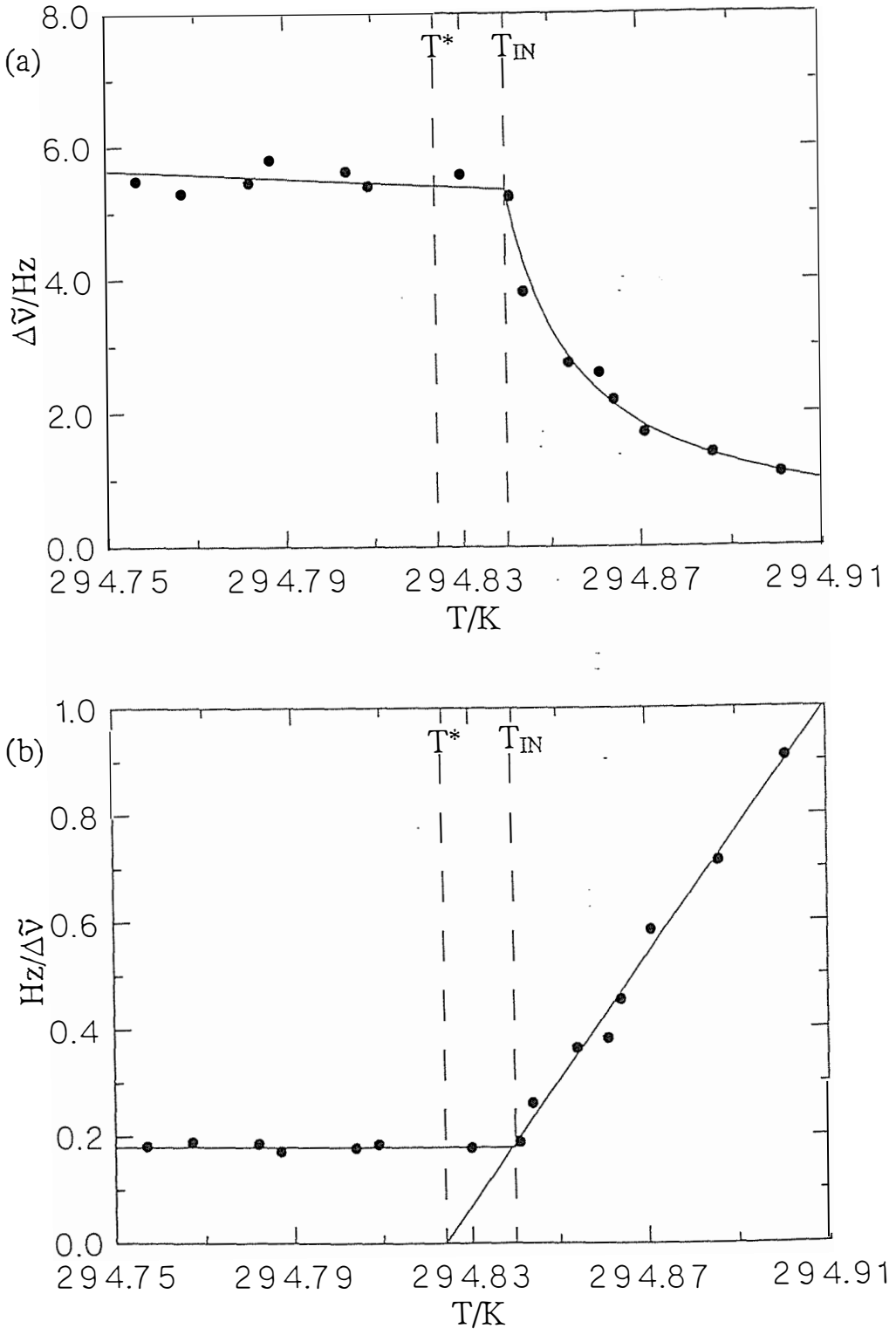

Figure 5.8 Plot of the temperature dependence of (a) the field induced quadrupole splitting $\Delta\tilde{\nu}$ and (b) $\Delta\tilde{\nu}^{-1}$ for ^2H_2O in the isotropic phase and in the nematic/isotropic biphasic region for a CsPFO/^2H_2O (w = 0.349) sample.

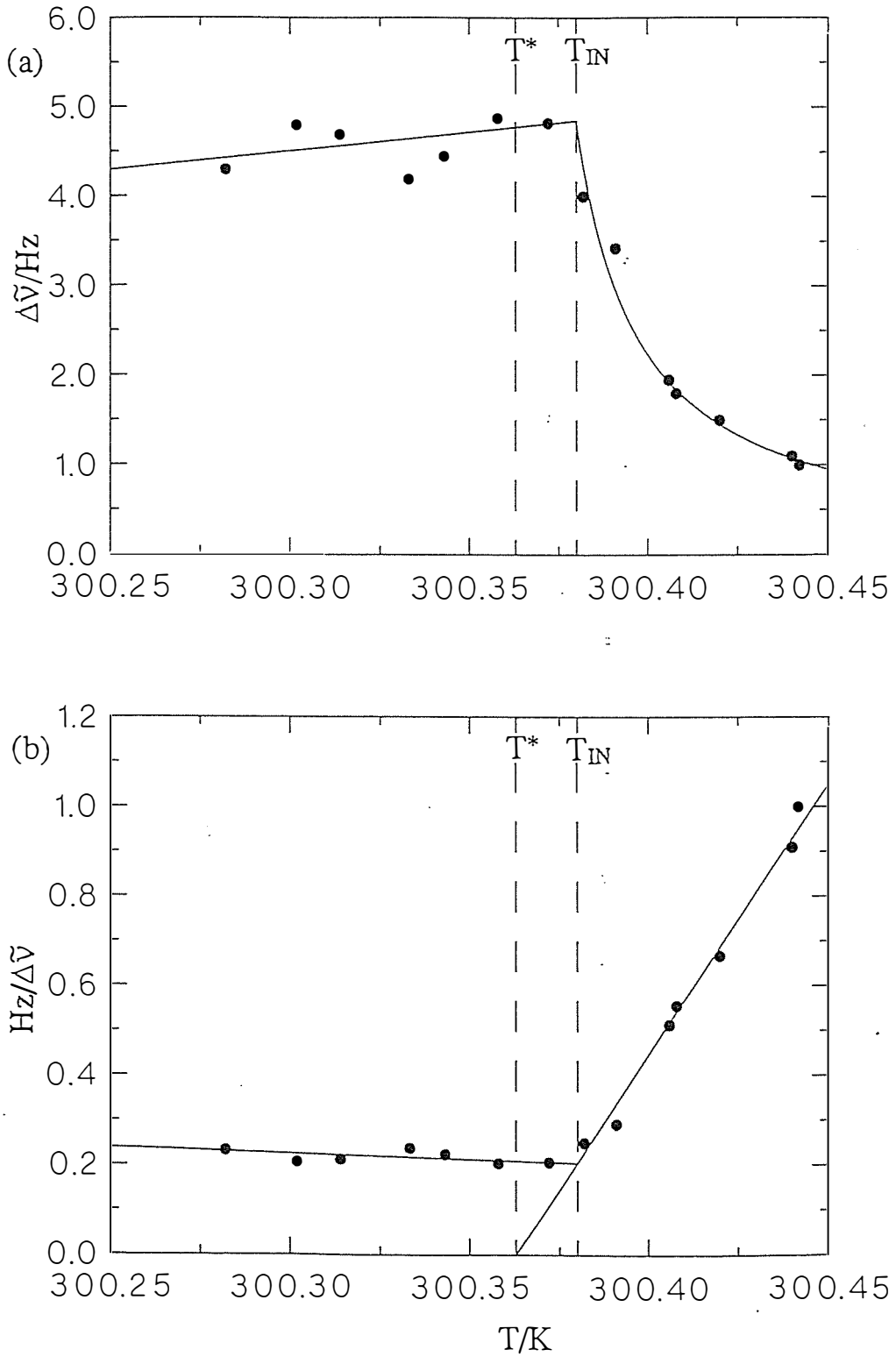

Taking the inverse of equation [5.11]

$$(\Delta\nu)^{-1} = \left(\frac{10k}{\Delta\chi B^2 |q_{zz}|_s}\right)(T-T^*) \qquad [5.12]$$

leads to the prediction that a plot of $(\Delta\tilde{\nu})^{-1}$ versus temperature will give a straight line with an intercept of zero at $T=T^*$. Figures [5.4b...5.8b] show the predicted behaviour and also the quenching of the effect at T_{IN}. Precise values of both T_{IN} and T^* and, in particular, $T_{IN} - T^*$ can be obtained from the plots in figure 5.4b to 5.8b.

The quenching of the temperature dependence of the field induced quadrupole splitting at T_{IN} and the invariance of the quadrupole splitting of the isotropic signal in the biphasic region can be explained qualitatively as follows. When the first-order transition intervenes the composition of the isotropic component of the sample becomes temperature dependent with the volume fraction of the micelles, ϕ_m, decreasing with decreasing temperature (figure 5.2). The value of T^* is directly proportional to the volume fraction of micelles (see eq. [5.10]) therefore T^* is a function of temperature in the biphasic region. Eq [5.11] must be modified to allow for the effect of change in the value of T^* and therefore an analytical expression for the variation of ϕ_m along T_{IN} is required. The variation in T^* with composition has been determined for thermotropic nematogenic mixtures within the limit of Henry's law[28,29]. We can draw a comparison between these systems if we consider the micelles to be the nematogen and the water to be equivalent to the isotropic solute although we are limited in this treatment because we cannot extrapolate the behaviour of our nematogen back to the limit of infinite dilution. Furthermore we will need an expression for the effect of temperature and composition on the aggregation number. In the biphasic region the temperature of the sample is identified with the T_{IN} of the nominal concentration of the isotropic component, as given by the upper curve in figure 5.2, therefore the denominator in eq. [5.11], becomes proportional to $T_{IN} - T^*$. The magnitude of $T_{IN} - T^*$ will not change appreciably as the temperature is lowered since both are dependent on the nominal composition of the

isotropic component. Over the small range of the biphasic region $|\tilde{q}_{zz}|_s$ will not change significantly and therefore the magnitude of the quadrupole splitting will be approximately constant.

5.3 DISCUSSION

5.3.1 The Dependence of the Field Induced Quadrupole Splitting on B

The plot of $\Delta\nu^{-1}$ versus temperature is linear for all samples. This suggests that at a magnetic flux density of 6.34 T the higher order terms of molecular field theory are not significant. This is not the case when fields of >10 T are used[30], where higher order terms (P_4) can contribute to the observed behaviour. The fourth rank term in the expansion of molecular field theory, which shows a dependence on B^4 and is therefore expected to become of relatively more importance as the field strength is increased, takes the form $\Delta\chi^2B^4/(T-T^*)^3$.

Figure 5.10 shows the concentration dependence of the quadrupole splittings of the isotropic and nematic signals in the biphasic region. We can see that the magnitude of $\Delta\tilde{\nu}_N$ decreases with decreasing w whilst the magnitude of $\Delta\tilde{\nu}_I$ increases. The availability of increasingly higher fields poses interesting questions for studying pretransitional effects by NMR spectroscopy. For each concentration the difference between the order parameter of the isotropic phase and the nematic phase is dictated by the amount of pretransitional ordering induced by the magnetic field. As the field strength increases the difference between the two phases decreases. For each concentration there will be a critical field strength above which there will be no discontinuity in order parameter as the transition is crossed transition *i.e.* a second-order transition[31]. There are therefore a series of critical points that have coordinates of T, ϕ_A and B.

In the nematic/isotropic biphasic region a 6.34 T magnet produces ^2H quadrupole splittings of the isotropic component of a w=0.15 sample of $\Delta\nu_I$ = 7.1 Hz compared with the nematic quadrupole splitting of $\Delta\nu_N$ =30 Hz. A continuous transition from

Figure 5.9 A comparison of T_{IN} - T^* for the CsPFO/^2H_2O system (•) with those from reference 25 for the CsPFO/H_2O system (o).

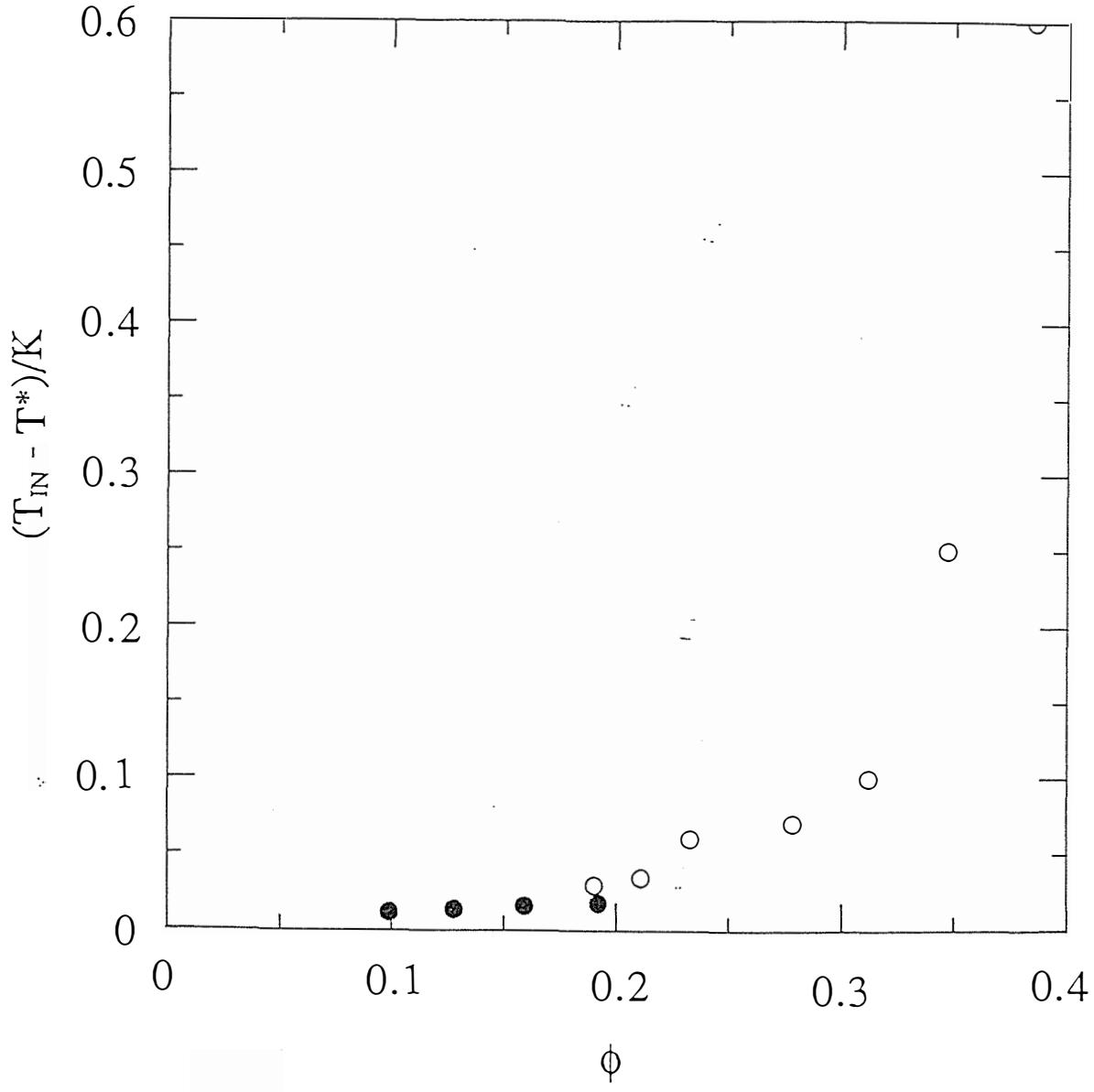

isotropic to nematic will occur when a field of sufficient strength to produce a field induced quadrupole splitting in the isotropic phase of 30 Hz. If we neglect any higher order terms then the field strength necessary to produce a second-order transition in this sample is 13 T. This field strength corresponds to a proton operating frequency of 555 MHz which is within the range of spectrometers that some researchers have access to. This is a best case scenario, for other samples the field strength needed to produce a second-order transition is beyond the means of present NMR spectrometers. The ^2H quadrupole splitting for a w=0.349 sample is 4.8 Hz for the isotropic signal in the mixed phase region whereas the ^2H quadrupole splitting of the nematic component is of the order of 80 Hz. If we neglect any higher order terms then the field strength necessary to produce a second-order transition is approximately 25.9 T.

5.3.2 The Strength of the Isotropic to Nematic Transition

The 'strength' of a first-order transition is defined in terms of the difference in entropy between the two states. The usual method for determining the strength of a transition is to make heat capacity measurements across the transition. There is no data available for the CsPFO/^2H_2O system and so other methods must be considered.

As mentioned in section 5.2 the strength of the transition is proportional to the quantity $T_{IN}-T^*$ for the transition from isotropic to nematic. The smaller the difference between T_{IN} and T^* the greater the amount of nematic-like behaviour in the isotropic immediately prior to the transition.

Theory[27] predicts

$$T_{IN} = \frac{0.2202}{k}\frac{\varepsilon\phi_m}{V_m} \qquad [5.13]$$

where V_m is the volume of the micelle. Assuming that $\varepsilon \propto \tilde{n}^2$ and $V_m \propto \tilde{n}$ then

$$T_{IN} = \frac{0.2202}{k} c\tilde{n}\phi_m \qquad [5.14]$$

Subtracting equation 5.10 from equation 5.14 gives us

$$T_{IN} - T^* = \frac{0.0202}{k} c\tilde{n}\phi_m \qquad [5.15]$$

The aggregation number varies with ϕ_m and T but at T_{IN} there is a decrease in $\tilde{n}$ as ϕ_m increases[32] whilst c is a complex function of both T and ϕ_m. Qualitatively, at least, equation 5.15 accounts for the decrease in $T_{IN} - T^*$ with decreasing ϕ_m, but the decrease is moderated to some extent by a concomitant increase in $\tilde{n}$.

The behaviour of $T_{IN} - T_{NI}$ with composition[27,33] is similar to that for $T_{IN} - T^*$ This is shown graphically in figure 5.11, where it is clear that $T_{IN} - T_{NI} \propto T_{IN} - T^*$. This provides a method for estimating the $T_{IN} - T^*$ for samples in which it is too large to measure directly. Since $T_{IN} - T_{NI}$ is ≈5 times bigger than $T_{IN} - T^*$, the former quantity provides a convenient tool for exploring the nature of the transition. Figure 5.9 shows a plot of $T_{IN} - T^*$ vs volume fraction of CsPFO in which data from this study is compared with data from studies by Rosenblatt[25] conducted in H_2O. It is clearly seen in this figure that $T_{IN} - T^*$ approaches zero only as $\phi \rightarrow 0$, *i.e.* the transition only becomes second order at infinite dilution. There is no experimental evidence of the proposed Landau point where the system crosses from uniaxial to biaxial behaviour[19].

5.3.3 The Concentration Dependence of the Magnitude of the Deuterium Quadrupole Splitting

The magnitude of the deuterium quadrupole splitting over a range of compositions is dependent on several factors (see equation 5.11) the effects of which must be considered separately. In order to compare the magnitude of the field induced ordering at various concentrations T_{IN} (the temperature at which the splittings are quenched) has been chosen as a convenient reference temperature. $T_{IN} - T^*$ can be measured and the

Figure 5.10 Concentration dependence of nematic (o) and field induced isotropic (•) quadrupole splittings in the nematic/isotropic mixed phase region of the CsPFO/^2H_2O system.

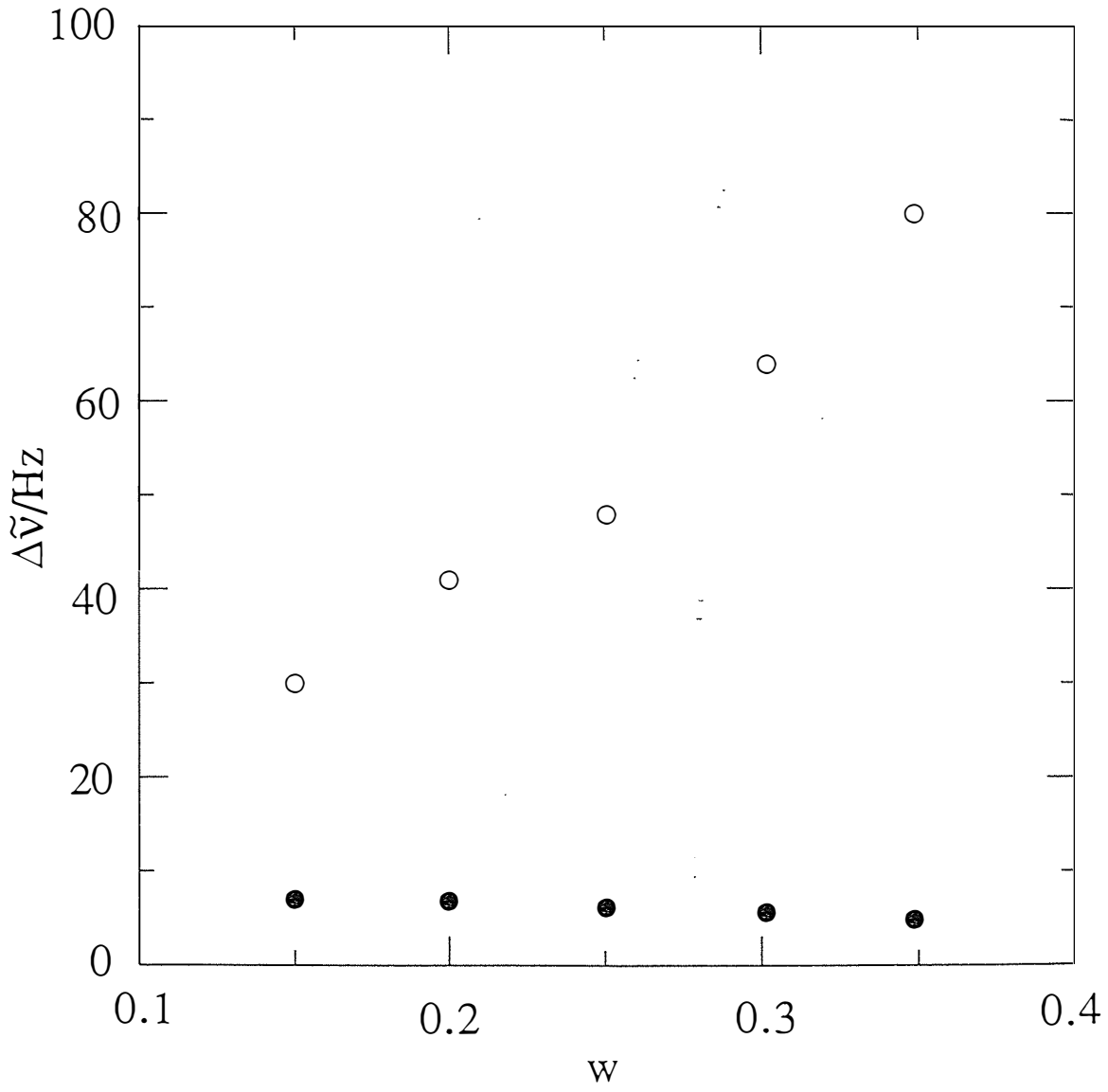

Figure 5.11 T_{IN} - T_{NI} vs T_{IN} - T^* for the CsPFO/^2H_2O system.

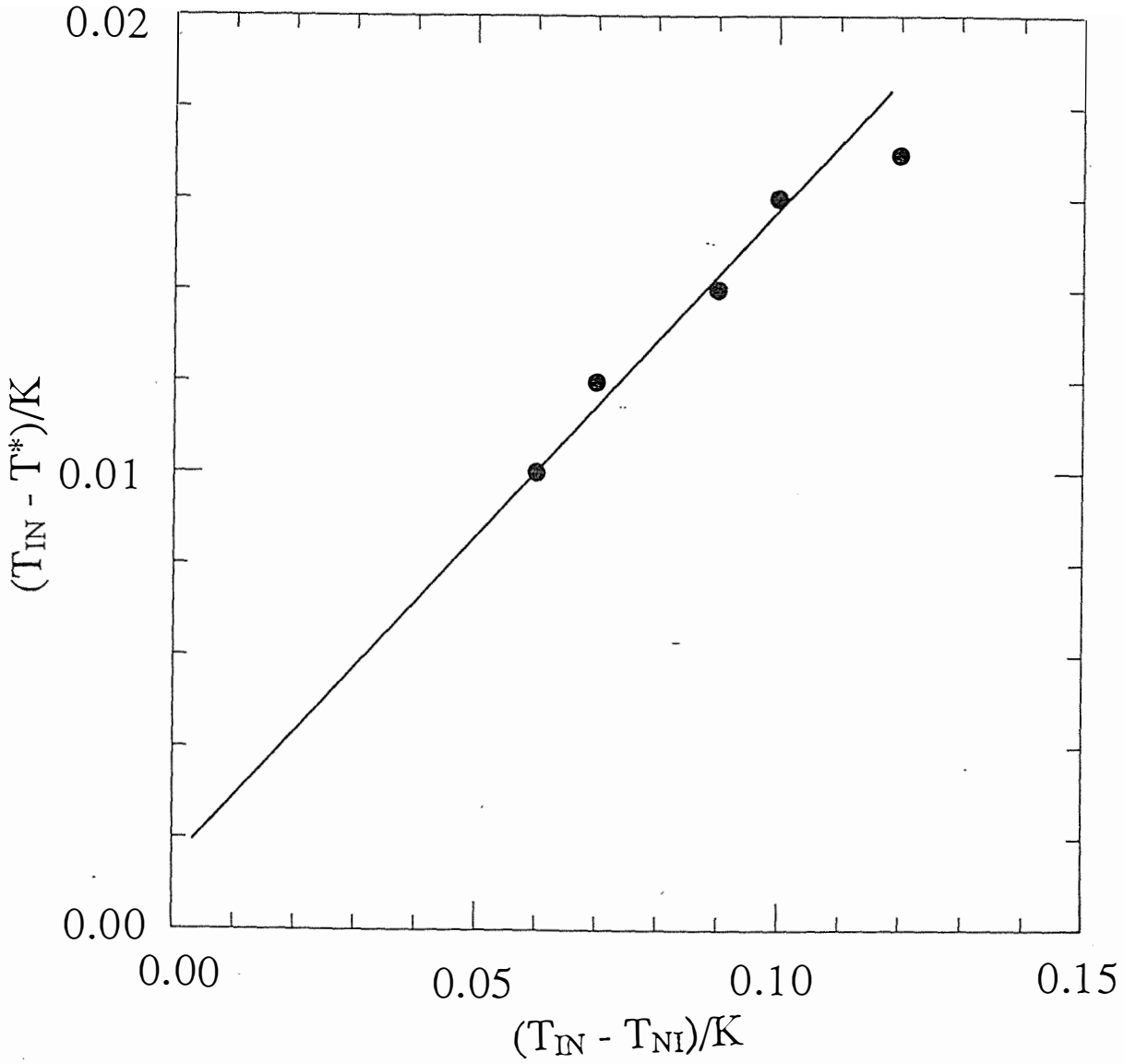

field strength B is a constant, leaving just two variables, $\Delta\chi$ and $|\tilde{q}_{zz}|_s$. In chapter 3 it was shown that for a ^2H spin in heavy water

$$|\tilde{q}_{zz}|_s = \langle P_2(\cos\alpha)\rangle_s \chi_D \left(\frac{x_A}{x_W}\right) n_b S_{O\text{-}D} \qquad [5.16]$$

From this equation it can be seen that $|\tilde{q}_{zz}|_s$ is dependent on three constants; χ_D, n_b and $S_{O\text{-}D}$ and two variable parameters: the shape factor, $\langle P_2(\cos\alpha)\rangle_s$, which which can be calculated from a knowledge of the aggregation number[27], and $\frac{x_A}{x_W}$ the ratio of amphiphile to water. As the weight fraction of amphiphile is lowered the aggregation number at T_{IN} increases[27,32] therefore the eccentricity of the micelle increases resulting in an increase in $\langle P_2(\cos\alpha)\rangle_s$. Values for $\Delta\tilde{\nu}$,T_{IN}-T^*,$\langle P_2(\cos\alpha)\rangle_s$ and the ratio of amphiphile to water at T_{IN} are given for a range of samples in Table 5.1. Substituting equation 5.16 into equation 5.11 we obtain

$$\Delta\tilde{\nu} = \frac{\Delta\chi \langle P_2(\cos\alpha)\rangle_s \frac{x_A}{x_W}}{X(T_{IN}-T^*)} \qquad [5.17]$$

where all the constants have been collected as X. We still do not know what $\Delta\chi$ is but we can see what the variation in $\Delta\chi$ needs to be if equation 5.17 holds true. Values for $\frac{\Delta\chi}{X}$ have been calculated from equation 5.17 and are given in table 5.1. $\Delta\chi$ is predicted to decrease by a factor of two from w=0.20 to 0.349.

It is reasonable to expect that the micellar anisotropy, $\Delta\chi$, is consequent upon the size and shape of the aggregate and $\Delta\chi$ can be defined in terms of the anisotropy of a single amphiphile molecule, $\Delta\chi_A$, such that

$$\Delta\chi = \tilde{n}\Delta\chi_A S_A \langle P_2(\cos\alpha)\rangle_s \qquad [5.18]$$

where S_A is an order parameter describing the order of the amphiphile molecule within the micelle. Making the reasonable assumption that $\Delta\chi_A S_A$ is temperature independent, equation 5.15 predicts that $\Delta\chi$ is proportional to $\langle P_2(\cos\alpha)\rangle_s\tilde{n}$. From table 5.1 it can

be seen that the magnitude of $\langle P_2(\cos\alpha)\rangle_s\tilde{n}$ also decreases by a factor of two between w= 0.20 and 0.359. This is encouraging and does give support to the model.

Table 5.1 This table sets out values for $\langle P_2(\cos\alpha)\rangle_s$ at T_{IN} determined from the axial ratio as measured by x-ray scattering at Leeds University[34]. The value for $\Delta\nu$ in this table is for the isotropic signal at T_{IN}. The calculated values of $\Delta\chi$ are given in the format $\frac{\Delta\chi}{X}$ since the magnitude of all of the constants is not known.

w	$\Delta\nu$ / Hz	$\langle P_2(\cos\alpha)\rangle_s$	$(T_{IN}-T^*)$/K	$\frac{x_A}{x_W}$	$\tilde{n}$	$\frac{a}{b}$	$\frac{\Delta\chi}{X}$
0.200	6.8	0.7810	0.013	0.0092	351	0.210	12.30
0.251	6.2	0.7325	0.014	0.0123	292	0.244	9.63
0.302	5.6	0.7025	0.015	0.0159	248	0.265	7.52
0.349	4.8	0.6841	0.017	0.0197	212	0.278	6.05

5.3.4 The Slope of the Inverse Quadrupole Splitting vs Temperature

The slope of the $(\Delta\tilde{\nu})^{-1}$ vs T line is (see equation 5.12)

$$\frac{d(\Delta\tilde{\nu})^{-1}}{dT} = \frac{10k}{\Delta\chi B^2|\tilde{q}_{zz}|_s} \qquad [5.19]$$

Substituting for $|\tilde{q}_{zz}|_s$ (equation 5.16) and $\Delta\chi$ (equation 5.18) gives

$$\frac{d(\Delta\tilde{\nu})^{-1}}{dT} = \frac{10k}{\tilde{n}\Delta\chi_A S_A\left(\langle P_2(\cos\alpha)\rangle_s\right)^2\chi_D\left(\frac{x_A}{x_W}\right)n_b S_{O\text{-}D}} \qquad [5.20]$$

$$i.e \quad \frac{d(\Delta\tilde{\nu})^{-1}}{dT} \propto \frac{1}{\tilde{n}\left(\langle P_2(\cos\alpha)\rangle_s\right)^2\left(\frac{x_A}{x_W}\right)} \qquad [5.21]$$

In the absence of values for $\Delta\chi_A$, S_A and $\chi_D n_b S_{O\text{-}D}$ it is only possible to compare the trends in the slopes by comparing them with the trends in the right hand side of equation 5.21. This is done in table 5.2 where it can be seen that over the concentration range w=0.20 to 0.35, within the limits of experimental uncertainty, the value of $1/\left(\tilde{n}\langle P_2(\cos\alpha)\rangle_s^2 \frac{x_A}{x_W}\right)$ is constant as are the measured slopes. It appears that the magnitude of the slope will not be greatly affected by an increase in weight fraction of amphiphile because a decrease in $\tilde{n}$ (and $\langle P_2(\cos\alpha)\rangle_s$) at the transition temperature on increasing w is offset by an increase in $\frac{x_A}{x_W}$.

Table 5.2 This table the experimental values of $\frac{d(\Delta\tilde{\nu})^{-1}}{dT}$ are compared with the inverse of the product of $\tilde{n} \times \langle P_2(\cos\alpha)\rangle_s^2 \times \frac{x_A}{x_W}$ calculated from the values given in table 5.1.

w	$\frac{1}{\tilde{n}\langle P_2(\cos\alpha)\rangle_s^2 \frac{x_A}{x_W}}$	measured $\frac{d(\Delta\tilde{\nu})^{-1}}{dT}$ / s K^{-1}
0.200	0.508	11.8(6)
0.251	0.519	11.7(4)
0.302	0.514	11.7(7)
0.349	0.512	12.4(5)

As an additional test of our model it is instructive to compare the slope of the $(\Delta\tilde{\nu})^{-1}$ vs T plot for ^2H and ^{133}Cs nuclei. Figure 4.5a shows a plot of $\Delta\tilde{\nu}$ vs T for a CsPFO/H_2O (w=0.35, ϕ=0.18) sample and figure 4.5b is the corresponding $(\Delta\tilde{\nu})^{-1}$ vs T plot. This sample has a slope of 0.50±0.02 Hz^{-1} K^{-1} and T_{IN} -T^*= 0.017 K. The magnitude of T_{IN} -T^* is identical to that obtained for the CsPFO/^2H_2O w=0.349 (ϕ=0.19) sample. It is not possible to carry out a systematic study of these slopes in the

CsPFO/H_2O system because the number of sample for which it is possible to measure the field induced ordering by ^{133}Cs NMR is limited for reasons already indicated.

For ^2H the slope is proportional to $\frac{1}{\frac{3}{2}\Delta\chi B^2|q_{zz}|_s}$ and the ^{133}Cs slope is proportional to $\frac{1}{\frac{1}{14}\Delta\chi B^2|q_{zz}|_s}$. The ratio of the slopes can therefore be written

$$\frac{\text{slope } ^2H}{\text{slope } ^{133}Cs} = \frac{\frac{1}{14}\beta_{Cs}\chi_{Cs}}{\frac{3}{2}\frac{x_A}{x_W}n_bS_{OD}\chi_D}$$

If we assume, $\chi_D \approx \chi_{Cs}$[35] and $\beta_{Cs} \approx 0.5$[34] then from the experimental slope ratio we calculate n_bS_{OD} to be 0.05 which falls in the range the values ($0.01 < n_bS_{OD} < 0.12$) for classical lamellar phases of hydrocarbon soaps[36].

5.3.5 Concluding Comments

It is a tribute to the temperature control system used in this study that pretransitional behaviour can be seen at all. The whole effect occurs within about 80 mK of T_{IN} and $\frac{\partial\Delta\tilde{\nu}_I}{\partial T}$ close to T_{IN} is very large ($\approx$ 390 Hz K^{-1}). In spite of this it was possible to show that the transition from isotropic to nematic follows the mean field prediction *i.e.* the critical exponent for the divergence is 1 as was previously shown by Rosenblatt. It is interesting to note that for the transition from nematic to isotropic the critical exponent for the order parameter variation[37], β, gives a value of 0.34 instead of the mean field value of 0.5. However, since the transition is first order there is no reason to assume the effective exponents to be the same on either side of the transition[37].

It has been possible to measure $T_{IN} - T^*$ in more dilute solutions than those measured by magnetic birefringence. We have shown that $T_{IN} - T^*$ tends to zero as ϕ tends to zero (*i.e.* the transition becomes second order only at infinite dilution) and there

is no evidence for the existence of a Landau point as has been suggested by other workers[19].

The possibility of discovering critical points for the transition at higher field strengths also poses interesting questions for future investigation.

REFERENCES

[1]De Gennes P.G. in "The Physics of Liquid Crystals", Clarendon Press, Oxford (1974).

[2]De Gennes P.G., *Mol. Cryst. Liq. Cryst.* **1971**, *12*, 193.

[3]Tolstoi N. A.; Fedotov L. N., *J. Exp. Theor. Phys. (USSR)* **1947**, *17* , 564.

[4]Gierke T.D.; Flygare W.H., *J. Chem. Phys.* **1974**, *61*, 2231.

[5]Zadoc Kahn J., *Ann. Physique* **1936**, *6* , 31.

[6]Zvetkov V., *Acta Physicochemica (USSR)* **1944**, *19* , 86.

[7]Stinson T. W.; Litster J. D., *Phys. Rev. Lett.* **1970**, *25* , 503.

[8]Fan C.-P.; Stephen M. J., *Phys. Rev. Lett.* **1970**, *25* , 500.

[9]Rosenblatt C., *Phys. Rev. A* **1983**, *27* , 1234.

[10]Beevers M.S., *Mol. Cryst. Liq. Cryst.* **1975**, *31*, 333.

[11]Coles H. J.; Jennings B. R., *Mol. Phys.* **1978**, *36* , 1661.

[12]Attard G. S.; Beckmann P. A.; Emsley J. W.; Luckhurst G. R.; Turner D. L., *Mol. Phys.* **1982**, *45* , 1125.

[13]Attard G. S.; Emsley J. W.; Luckhurst G. R., *Mol. Phys.* **1983**, *48* , 639.

[14]Attard G. S.; Emsley J. W.; Khoo S. K.; Luckhurst G. R., *Chem. Phys. Lett.* **1984**, *105* , 244.

[15]Martin J. F.; Vold R. R.; Vold R. L., *J. Chem. Phys.* **1984**, *80*, 2237.

[16]Ruessink B. H.; Barnhoorn J. B. S.; MacLean C., *Mol. Phys.* **1984**, *54* , 939.

[17]Ruessink B. H.; Barnhoorn J. B. S.; Bulthuis J.; MacLean C., *Liq. Cryst.* **1988**, *3*, 31.

[18]Emsley J. W.; Imrie C. T.; Luckhurst G. R.; Newmark R. D., *Mol. Phys.* **1988**,*63*, 317.

[19]Rosenblatt C.; Kumar S.; Litster J. D., *Phys. Rev. A* **1984**, *29* , 1010.

[20]Rosenblatt C.; Zolty N., *J. Physique Lett.* **1985**, *46* , L-1191.

[21]Rosenblatt C., *J. Phys. Chem.* **1987**, 91 , 3830.

[22]Rosenblatt C., *J. Phys. Chem.* **1988**, *92* , 5770.

[23]Rosenblatt C., *J. Colloid. Interface. Sci.* **1989**, *131*, 236.

[24]Parbhu A. N., M. Sc. Thesis, Massey University **1990**.

[25]Rosenblatt C., *Phys. Rev. A* **1985**, *32* , 1924.

[26]Jolley K. W.; Smith M. H.; Boden N., *Chem. Phys Lett.* **1989**, *162* , 152.

[27]Boden N.; Corne S. A.; Jolley K. W., *J. Phys. Chem.* **1987**, *91* , 4092.

[28]Luckhurst G. R., *J. Chem. Soc., Faraday Trans. 2,* **1988**, *84* , 961.

[29]Attard G. S.; Luckhurst G. R., *Liq. Cryst.* **1987**, *2* , 441.

[30]Kumar S.; Litster J. D.; Rosenblatt C., *Phys. Rev. A* **1983**, *28* , 1890.

[31]Gramsbergen E. F.; Longa L.; de Jeu W. H., *Phys. Rep.* **1986**, *135* , 195.

[32]Holmes M. C.; Reynolds D.J.; Boden N., *J. Phys. Chem.* **1987**, *91*, 5257.

[33]Boden N.; Jolley K. W.; Smith M. H., *Liq. Cryst.* **1989**, *6* , 481.

[34]Parker D., Ph. D. Thesis , Leeds University, **1988**.

[35]Brevard C.; Granger P., *Handbook of High Resolution Multinuclear NMR*, (John Wiley & Sons, New York), **1981**.

[36]Persson N.-O.; Lindman B., *J. Phys. Chem.* **1975**, *79* , 1410.

[37]Boden N.; Clements J.; Dawson K. A.; Jolley K. W.; Parker D., *Phys. Rev. Lett.* Submitted for Publication.

CHAPTER 6

NH_4PFO PHASE DIAGRAM

A complete phase diagram for the ammonium pentadecafluorooctanoate/heavy water system ($NH_4PFO/^2H_2O$) has been constructed along with a partial phase diagram for the NH_4PFO/H_2O system which maps only the isotropic, nematic and lamellar phases. The phase behaviour demonstrated by these systems is almost identical in form to the phase behaviour of the CsPFO systems in the temperature versus volume fraction coordinates, except that the transition temperatures are lower for the ammonium system.

The $NH_4PFO/^2H_2O$ phase diagram was determined using deuterium NMR. The identification of phase transition temperatures using this technique has been discussed in detail elsewhere[1] and will not be repeated here. Basically it involves the identification of phases from the quadrupole spectra of the ^2H nucleus (I=1) of heavy water which consist of a doublet in ordered mesophases (see figure 3.4 for typical spectra), and the identification of phase transition temperatures from the temperature dependence of the quadrupole splittings. Since the deuterium quadrupole splitting is approximately an order of magnitude smaller than that for ^{133}Cs it is more difficult to detect the very narrow mixed phase regions. At the start of this study it was expected that the ^{14}N (I=1) of the ammonium ion would prove to be a high resolution probe for the detection of coexisting nematic and lamellar phases since the quadrupole splitting was larger even than the ^{133}Cs quadrupole splitting at an equivalent volume fraction. For the w=0.451 $NH_4PFO/^2H_2O$ sample at T_{LN} (296.32 K) the ^{14}N quadrupole splitting is 34660 Hz compared with 702 Hz for the ^2H splitting. The line-widths for ^{14}N and ^2H are however 400 Hz and 5 Hz respectively, and so the larger quadrupole splittings are more than offset by the larger line-widths. The broad ^{14}N peaks coupled with the inherent lack of sensitivity of the ^{14}N nucleus made it very difficult to determine phase transition

temperatures using ^{14}N NMR. For the NH_4PFO/H_2O system ^{14}N NMR is, however, the best that is available.

The partial phase diagram for the NH_4PFO/H_2O system was mapped using the ^{14}N NMR technique. The T_{NI}, T_{NL} and T_{LN} transition temperatures for the NH_4PFO/H_2O system were determined from plots of $\Delta\tilde{\nu}$ versus temperature as for the ^{133}Cs case *i.e.* on either heating or cooling from the pure phase region across the transition into the mixed phase region. This method gives the location of the phase boundary to within ± 10 mK. Figure 6.1 shows the temperature dependence of a w = 0.55 NH_4PFO/H_2O sample in which the discontinuities in the temperature dependence of the quadrupole splitting identify the phase transitions. The location of the transition from isotropic to the nematic/isotropic coexistence region, T_{IN}, is more difficult to determine since it relies on the first observation of a very broad quadrupole peak. The observation of the quadrupole peak indicates that the sample is already in the mixed phase region and therefore the precision of the measurement of T_{IN} is low in comparison to the other transitions. The triple point of the NH_4PFO/H_2O system, $T_{p(I,N,L)}$, is extremely difficult to determine because of the effect of phase separation on the already very broad ^{14}N quadrupole peaks. $T_{p(I,N,L)}$ was estimated by cooling a w=0.661 sample from the isotropic phase into the biphasic isotropic/lamellar region. The first appearance of the nematic phase signal was taken to be $T_{p(I,N,L)}$. This point is estimated to be accurate to only ± 0.2 K.

The location of T_{cp} in both systems is also a problem. Using ^{2}H NMR of heavy water on the $NH_4PFO/^{2}H_2O$ system an estimate of T_{cp} at ϕ = 0.362 (w=0.490) was obtained.By comparison with the CsPFO/water systems[1,2] this could be far too high and the true T_{cp} is probably closer to w = 0.40. That w=0.49 is too high is demonstrated by ^{14}N NMR measurements on a w=0.502 NH_4PFO/H_2O sample where it is clearly seen (figure 6.2) that the width of the nematic/lamellar biphasic region is ≈ 80 mK. This sample represented a lower limit for the observation of separate signals for

Figure 6.1 Temperature dependence of the ^{14}N quadrupole splittings for a NH_4PFO/H_2O w=0.55 sample. The discontinuities in the quadrupole splittings clearly identify the lower boundary (T_{NI}) of the isotropic to nematic transition and the upper (T_{NL}) and lower (T_{LN}) boundaries to the nematic to lamellar transition.

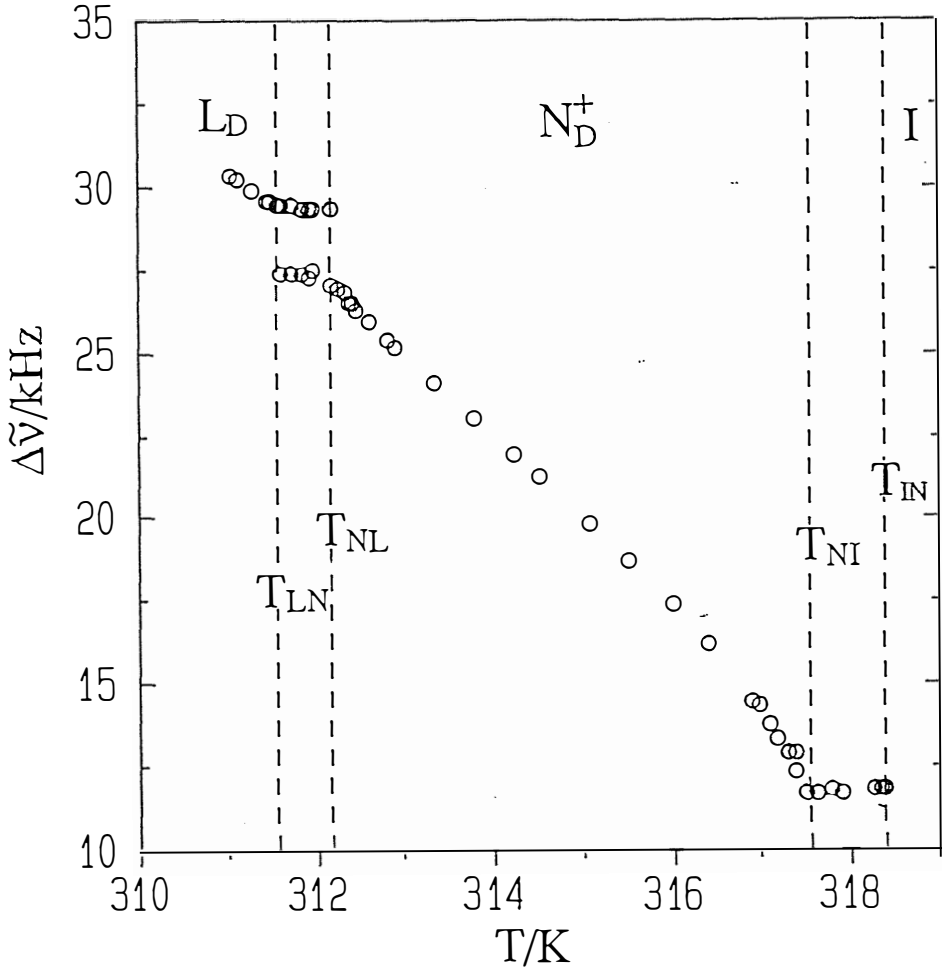

Figure 6.2 Temperature dependence of the ^{14}N quadrupole splittings across the nematic to lamellar transition for a NH_4PFO/H_2O w=0.502 sample. The discontinuities in the quadrupole splittings clearly identify the upper (T_{NL}) and lower (T_{LN}) boundaries to the transition.

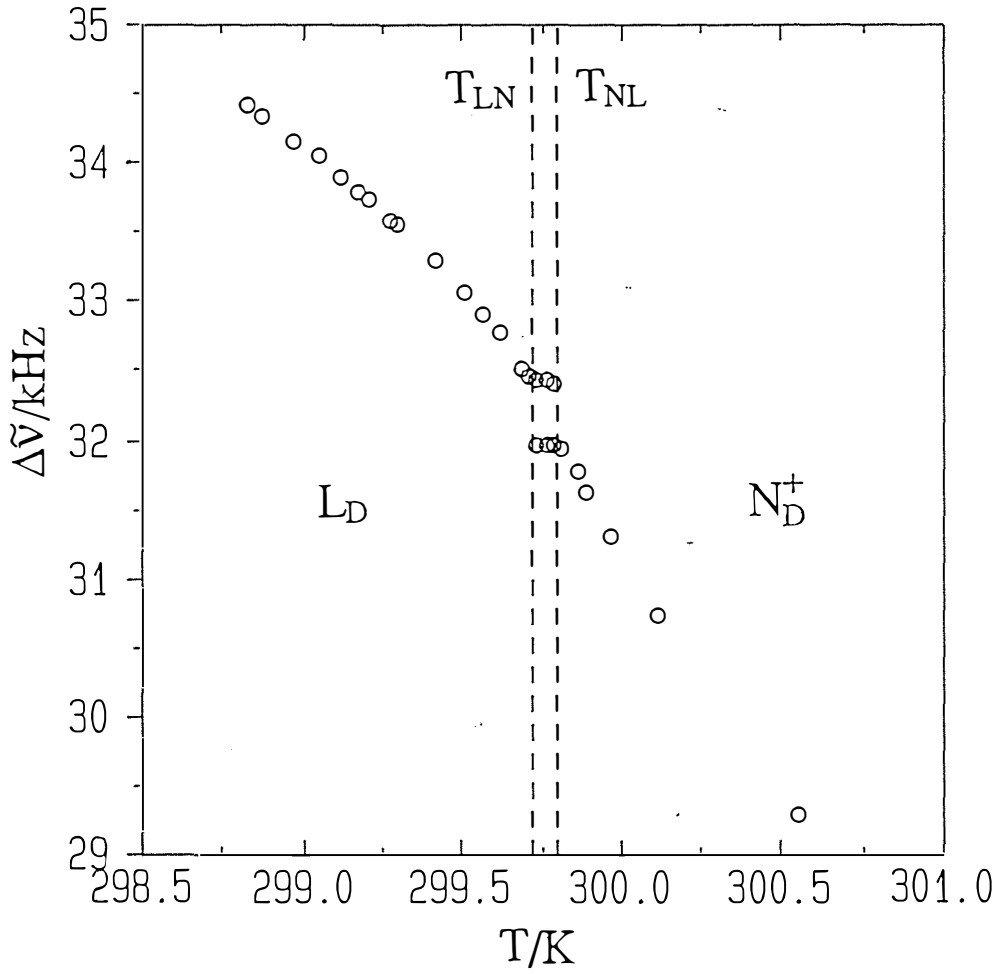

the nematic and lamellar components, but quite clearly by analogy to the CsPFO behaviour[2] (figure 4.11), a weight fraction of 0.5 is well above the tricritical point composition. The T_{cp} values given for the NH_4PFO systems represent the limit of experimental resolution and not the true T_{cp} position.

6.1 Features of the NH_4PFO/Heavy Water Phase Diagram

The full phase diagram is presented in figure 6.3. The phase behaviour is identical to that of the CsPFO/^2H_2O system and differs only in the location of the various fixed points and phase transition temperatures. There is an extensive nematic phase, N_D^+, stretching from w = 0.395 to 0.589 and between temperatures of 292.1 K and 338.1 K, although extensive supercooling allows a pure nematic phase to be observed well below the solubility curve. The tricritical point has been fixed at w = 0.490 (T = 304.0) by extrapolating the temperature width of the mixed nematic/lamellar phase region to zero as for the CsPFO systems. This should be taken as an upper limit in view of the intrinsic limitations in the resolution of deuterium NMR signals from the coexisting nematic and lamellar phases. The lamellar phase has been shown to consist of discoid micelles[3], *i.e.* it is an L_D phase. Table 6.1 lists the various fixed points of the system and the polynomials for the phase transition temperatures are given in table 6.2.

Figure 6.3 The phase diagram for the $NH_4PFO/^2H_2O$ system. There are three pure phase regions; isotropic micellar solution phase (I), discotic nematic micellar solution phase (N_D^+) and discotic lamellar solution phase (L_D). All other regions are mixed phase regions. K:- crystalline amphiphile. The fixed points are described in the text.

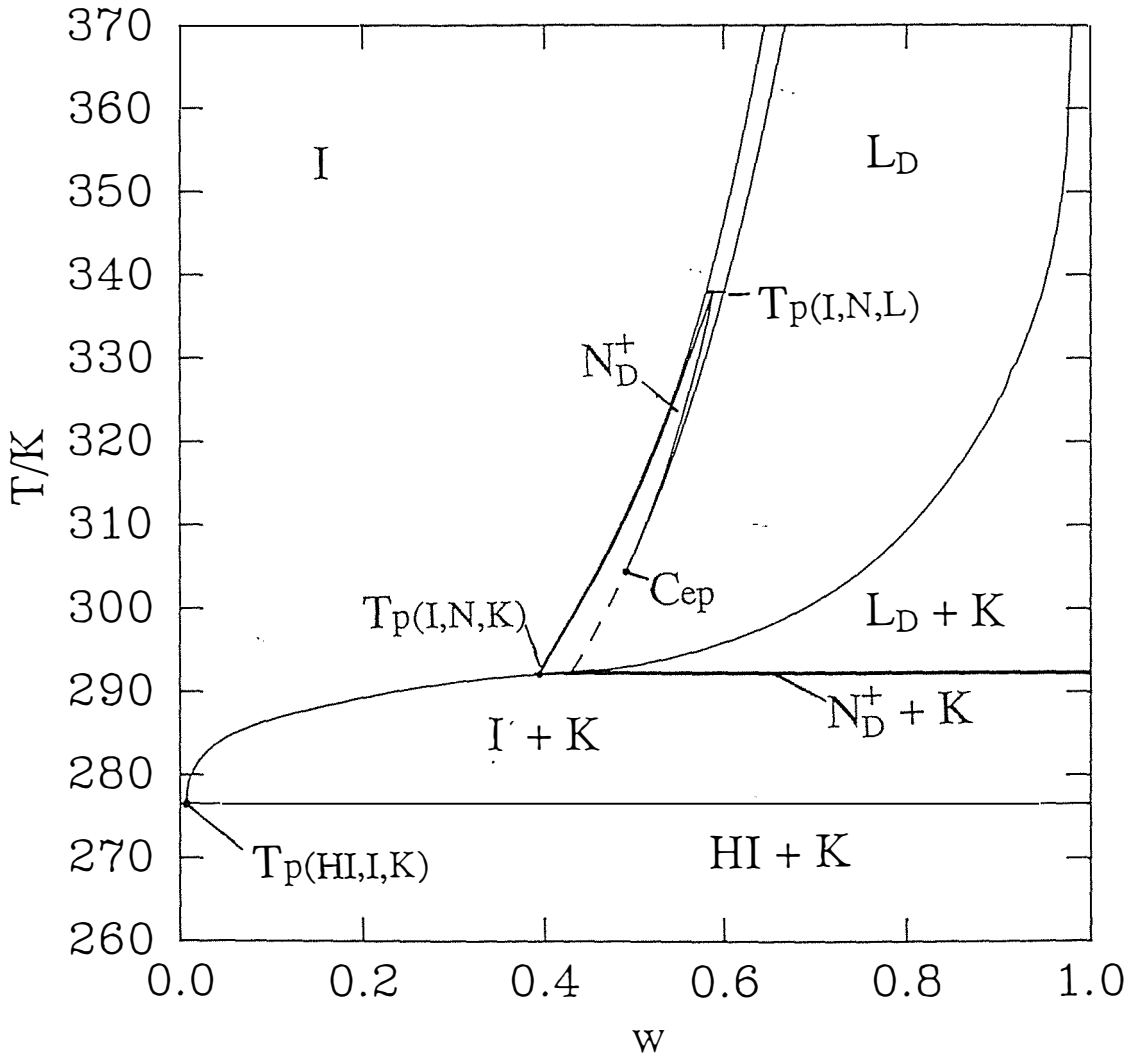

Table 6.1 Fixed points for the $NH_4PFO/^2H_2O$ system. The density of NH_4PFO was calculated from measurements of the densities of solutions in the weight fraction range of 0.228 to 0.604[3].

		T/K	w	ϕ	c/mol dm^{-3}	x
Tp(I,N,L)	isotropic	338.10	0.581	0.446	1.96	0.0605
	nematic		0.589	0.455	1.99	0.0624
	lamellar		0.604	0.470	2.06	0.0662
Tp(I,N,K)	isotropic	292.1	0.393	0.277	1.20	0.0292
	nematic		0.395	0.279	1.21	0.0294
Tp(HI,I,K)	isotropic	276.5	0.006	0.004	0.02	0.0003
Cep	nematic =					
	lamellar	292.4	0.430	0.308	1.34	0.0339
Kp		279.8	0.011	0.0065	0.028	0.00052
T_f	heavy ice	276.95				
Tcp		304.0	0.490	0.362	1.57	0.0427

Table 6.2 The transition temperatures for the $NH_4PFO/^2H_2O$ system. The polynomial takes the form $a+bw+cw^2+dw^3$ with the valid concentration range falling within w_{max} and w_{min}.

Transition	a	b	c	d	w_{min}	w_{max}
T_{IN}	-2.8111	1746.4	-3662.8	2870.2	0.393	0.645
T_{NI}	224.45	291.56	-580.21	702.78	0.395	0.589
T_{NL}	-688.43	5629.4	-11099	7639.8	0.495	0.589
T_{LN}	123.94	911.57	-1930.8	1639.8	0.430	0.665
T_c	278.51	133.62	-608.60	1029.6	0.015	0.300
T_c	232.70	355.16	-698.65	467.84	0.300	1.000

6.2 Features of the Partial NH_4PFO/Water Phase Diagram

The partial phase diagram for the system, showing just the liquid crystalline phase transitions, is given in figure 6.4. The tricritical point has been estimated, as was described above to have a weight fraction of 0.480. The line of triple points $T_{p(I,N,L)}$ has been placed at a temperature of 336.8 K and between w=0.609 and 0.623. Table 6.3 includes polynomials for the phase transition temperatures. The NH_4PFO/H_2O phase diagram shows the same features as that for the $NH_4PFO/^2H_2O$ phase diagram but there are slight displacements to lower temperatures as was the case for the CsPFO water and heavy water systems.

Table 6.3 The transition temperatures for the NH_4PFO/H_2O system. The polynomial takes the form $a+bw+cw^2+dw^3$ with the valid concentration range falling within w_{max} and w_{min}.

Transition	a	b	c	d	w_{min}	w_{max}
T_{IN}	280.74	-106.11	260.25	107.50	0.380	0.628
T_{NI}	312.07	-317.11	733.53	-249.72	0.380	0.618
T_{NL}	262.30	-80.393	260.30	107.47	0.480	0.618
T_{LN}	273.62	-103.95	260.25	107.50	0.380	0.628

Figure 6.4 A partial phase diagram for the NH_4PFO/H_2O system showing only three pure phase regions; isotropic micellar solution phase (I), discotic nematic micellar solution phase (N_D^+) and discotic lamellar solution phase (L_D).

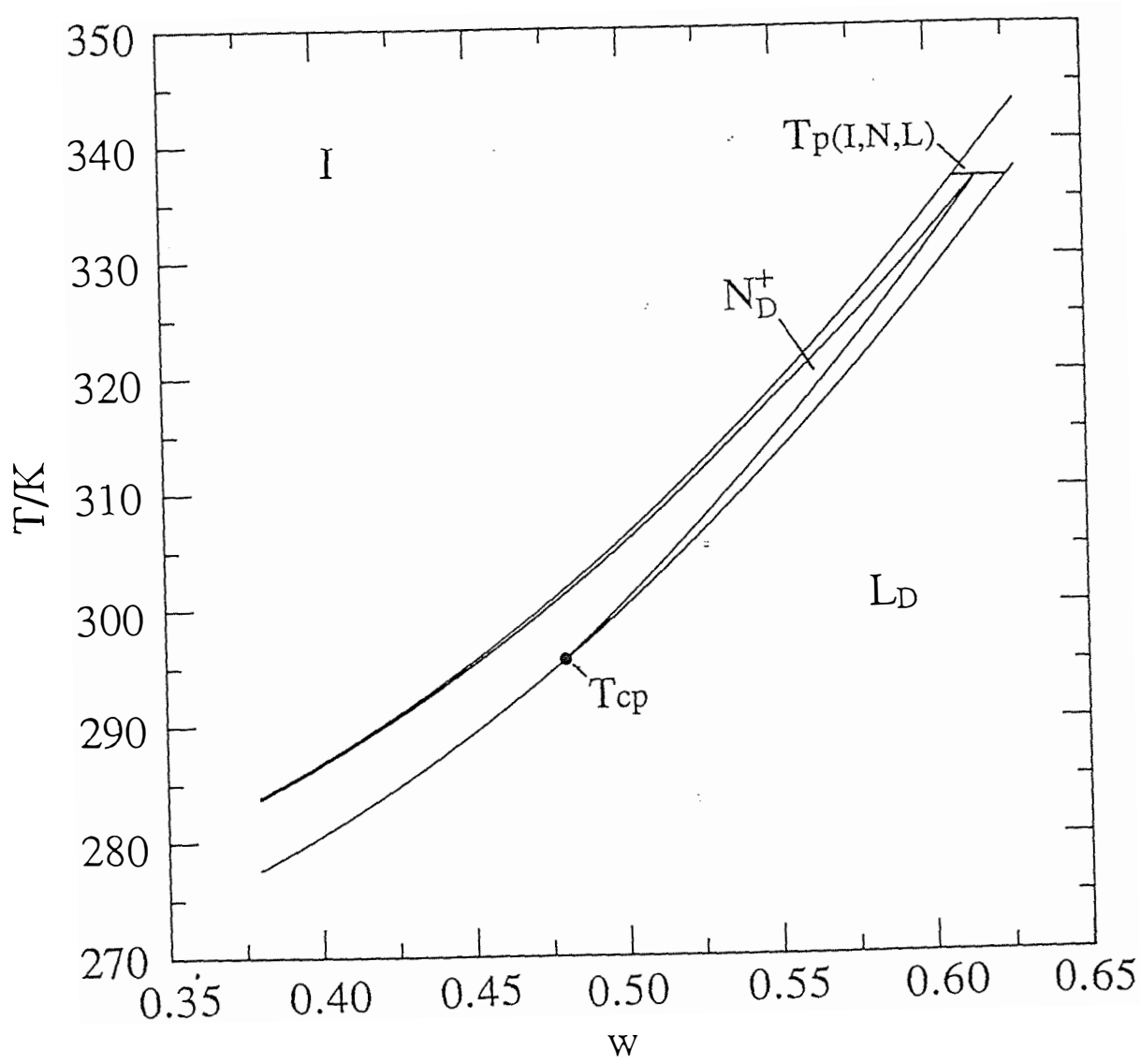

6.3 TESTING THE NMR MODEL

A comparison between ammonium phase diagrams and between the ammonium and caesium systems will be presented in chapter 8. In the remainder of this chapter, the dependence of the quadrupole splittings in the $NH_4PFO/^2H_2O$ system, on the structure and order of the liquid crystal mesophases will be considered in some detail.

6.3.1 The Origin of the Temperature Dependence of the Quadrupolar Splittings of the Deuterons of Heavy Water and of the Deuterated Ammonium Ion in the NH_4PFO/Heavy Water System.

The ^2H spectra of $NH_4PFO/^2H_2O$ samples, differs from those for $CsPFO/^2H_2O$ samples in that there are two deuterium containing species. The presence of the deuterated counter-ion is shown by a peak to high frequency of the ^2H_2O peak (figure 6.5). The ratio of the $^2H_2O:ND_4^+$ peaks in this w = 0.451 sample is 1:13. This is consistent with a statistical distribution of deuterons brought about by chemical exchange between water molecules and the ammonium ions. The ND_4^+ peak, therefore, contains contributions from all species $NH_nD_{4-n}^+$. The absence of scalar couplings $J_{^2H-^1H}$ (1.2 Hz) and $J_{^2H-^{14}N}$ (8.1 Hz) shows that the exchange of deuterons between these species must be faster than 50 s^{-1} ($2\pi J$). To observe these spin interactions requires a pH of about 1.0[4,5] as compared to the value of 5.5 for our sample. The line-widths of the ^2H NMR peaks in the isotropic phase for ^2H_2O and ND_4^+ are 5 Hz and 42 Hz respectively. (*cf.* 2 Hz for the ^2H_2O in the $CsPFO/^2H_2O$ system.) The contributions to the linewidth for the $NH_4PFO/^2H_2O$ are spin-spin relaxation, field inhomogeneities and chemical exchange of deuterons between the solvent and the counter-ion. If we take the width of the isotropic peak in the $CsPFO/^2H_2O$ as a baseline for the spin-spin and field inhomogeneities, the contributions from chemical exchange to the heavy water and ammonium ion peaks are 3 Hz and 40 Hz respectively. These contribution can be identified with $(\pi\tau_A)^{-1}$ and $(\pi\tau_W)^{-1}$ where τ_A and τ_W are the mean lifetimes of a

Figure 6.5 ^2H NMR spectra as observed on cooling the sample $NH_4PFO/^2H_2O$ (w = 0.451) from the I (top) into the N_D^+ phase (bottom). In the I phase spectrum the deuteriated ammonium ion peak is clearly seen to high frequency (84 Hz) of the ^2H_2O peak while in the N_D^+ phase both the deuterated ammonium ion and the heavy water show a quadrupole splitting. The D_2O peaks have been "cut off" for convenience of presentation but the intensities of the two signals are in the ratio of 13.4:1 which is to be compared with the expected ratio of heavy water to ammonium ion deuterons of 13.1:1.

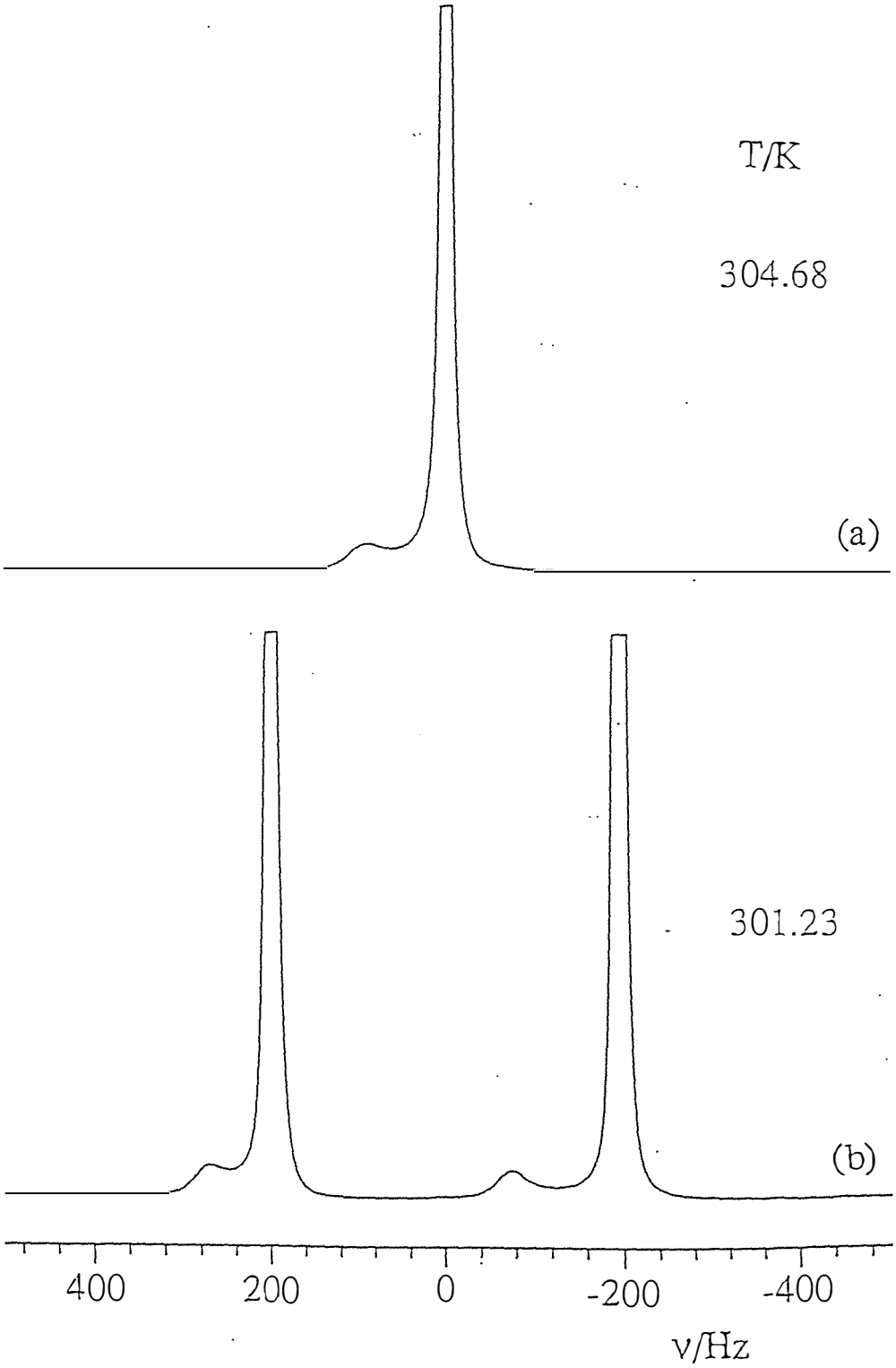

deuterium spin at the ammonium and water sites respectively. These quantities can be used to estimate the mean time interval between successive transfers of a deuterium spin from the relationship $\tau = p_W\tau_A = p_A\tau_W$, where p_W (=0.929) and p_A (=0.071) are the fractional populations of the water and ammonium sites. This gives a value of 135 s^{-1} for τ^{-1}. On cooling into the nematic, and subsequently into the lamellar phase, each resonance is split into a doublet (figure 6.5) and these quadrupole splittings are plotted as a function of temperature in figure 6.6. The variation with temperature of both splittings is seen to reflect the behaviour of the order parameter[6] (see figure 6.7), although there are clearly other contributions, especially for the ND_4^+ ion.

The observation of a quadrupole doublet for the ND_4^+ peak is at first sight, surprising, since the ion has tetrahedral symmetry. In such molecules the field gradient at the nucleus can only arise due to a loss of tetrahedral symmetry on binding. The magnitude of the quadrupole splitting is therefore reflective of the local order parameter at the bound site and the loss of symmetry. The most simple case that can be considered for ND_4^+ is the change from T_d symmetry to C_{3v} symmetry. This involves the interaction of one of the deuterons with the micellar surface, with the three remaining deuterons retaining three-fold rotational symmetry about the axis of this interaction. In this case the expression for the ND_4^+ quadrupole splitting is[4],

$$\Delta\tilde{\nu} = \tfrac{1}{4}(\tfrac{3}{2}Q_D S_C) + \tfrac{3}{4}(\tfrac{3}{2}Q_D S_C \tfrac{1}{2}(3\cos^2\gamma - 1))$$

$$= \tfrac{3}{2}Q_D S_C(\tfrac{1}{4} + \tfrac{3}{8}(3\cos^2\gamma - 1)) \qquad [6.1]$$

Figure 6.6 Temperature dependence of the ^2H quadrupole splittings of ^2H_2O (o) and ND_4^+ (□) for a $NH_4PFO/^2H_2O$ w=0.452 sample.

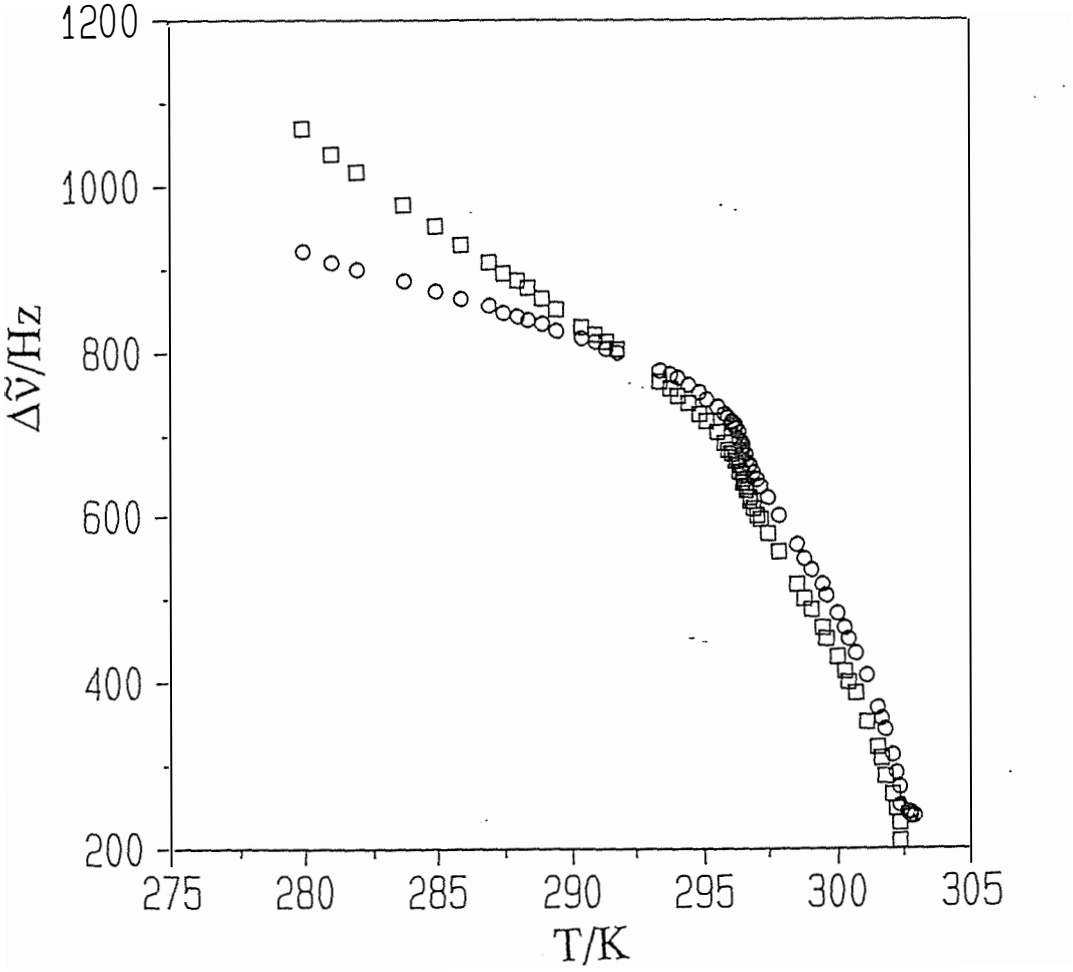

Figure 6.7 Temperature dependence of the order parameter[3,6], S, for a $NH_4PFO/^2H_2O$ (w = 0.45) sample.

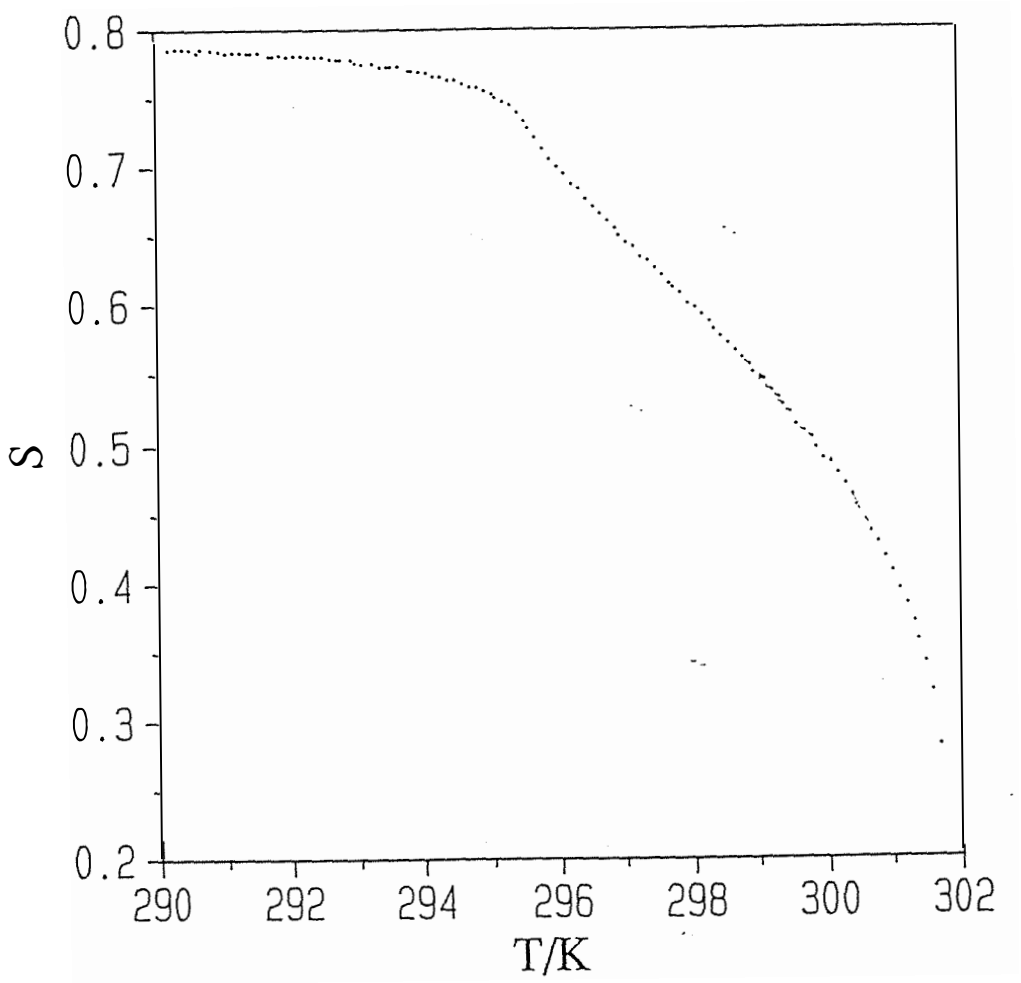

If we define two pseudo-order parameters,

$$\langle P_2(\cos\gamma)\rangle \equiv \tfrac{1}{2}(3\cos^2\gamma - 1) \qquad [6.2]$$

$$\text{and } S_{ND} \equiv \tfrac{1}{4} + \tfrac{3}{4}\langle P_2(\cos\gamma)\rangle \qquad [6.3]$$

where $\langle P_2(\cos\gamma)\rangle$ describes the contribution of the deuterons that do not lie along the C_z axis and S_{ND} describes the total contribution of the deuterons in the ND_4^+ ion, Equation 6.1 can be restated (see equations 3.19 and 3.21) as

$$\Delta\tilde{\nu} = \tfrac{3}{2}S\langle P_2(\cos\alpha)\rangle\chi_D\beta_A(\tfrac{1}{4} + \tfrac{3}{4}\langle P_2(\cos\gamma)\rangle)$$

$$= \tfrac{3}{2}S\langle P_2(\cos\alpha)\rangle\chi_D\beta_A S_{ND}. \qquad [6.4]$$

where β_A is the bound fraction of ammonium ions. Considering first the temperature dependence of the ^2H quadrupole splittings of heavy water. To a good approximation, all quantities other than S and $\langle P_2(\cos\alpha)\rangle_s$ in equation 3.20 are expected to be constant over the temperature interval of the measurement. We can therefore write

$$(\Delta\tilde{\nu}_D)_r \equiv \frac{\Delta\tilde{\nu}_D}{\Delta\tilde{\nu}_D^{\ddagger}} = \frac{S\langle P_2(\cos\alpha)\rangle_s}{S^{\ddagger}\langle P_2(\cos\alpha)\rangle_s^{\ddagger}}$$

$$= (S\langle P_2(\cos\alpha)\rangle_s)_r \qquad [6.5]$$

where the superscript, ‡, refers to the value of the quantity at some reference state (in this case T_{NI}). The subscript, r, refers to the reduced value of a quantity i.e. the value divided by the value of the quantity at T_{NI}. If our model is correct a plot of $(\Delta\tilde{\nu}_D)_r$ vs $(S\langle P_2(\cos\alpha)\rangle_s)_r$ will yield a straight line of slope 1. The values of S and $\langle P_2(\cos\alpha)\rangle_s$ for a w = 0.40 sample have been determined from electrical conductivity and X-ray measurements at Leeds University[3,6]. Over the temperature range T_{NI} to T_{LN} - 5 the plot is indeed linear (figure 6.8) with a slope of unity (1.02(2)), consistent with the model. The minor inconsistencies that appear are due to the NMR, conductivity and x-ray samples being of slightly differing concentration. In order to match the data

Figure 6.8 Plot of reduced ^2H quadrupole splittings versus reduced $S\langle P_2(\cos\alpha)\rangle_s$ values[3,6] for a $NH_4PFO/^2H_2O$ (w = 0.452) sample (see equation 6.5). The straight line has a slope of 1.0 and an intercept of 0 as predicted. The best fit values for these two quantities are 1.02(2) and -0.04(4) respectively.

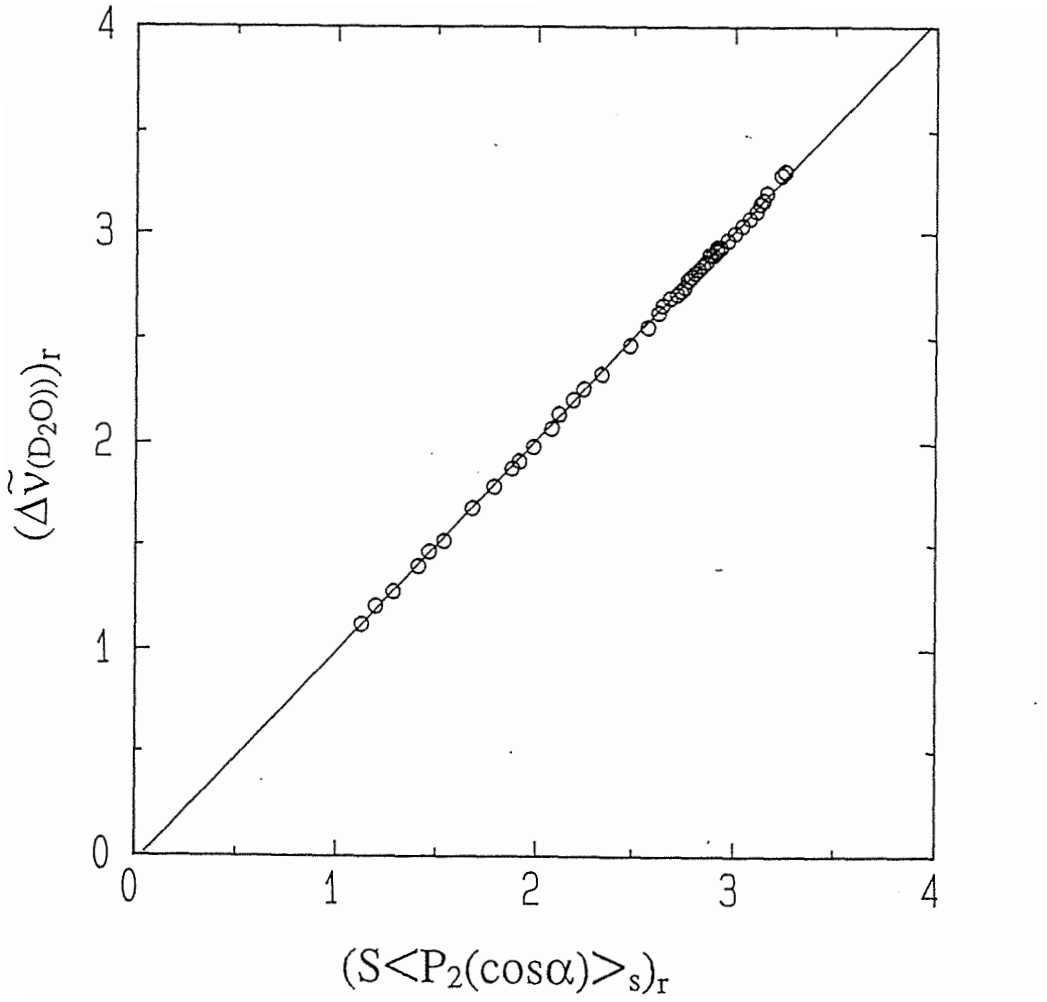

and carry out the above comparison the measured temperatures were first normalized to their respective T_{NI} values. The behaviour of the ^2H quadrupole splittings of heavy water in the nematic phase is dominated by the temperature dependence of S (figure 6.7) whilst in the lamellar phase it is the temperature dependence of the shape factor which prevails[3]. The excellent fit to the model also indicates that the interaction of the water molecules with the micelle surface is not substantially altered by changes in the fraction of bound ammonium ions.

From figure 6.6 it is clear that there is an extra contribution to the quadrupole splittings of the ammonium ion. This arises from the variation with temperature of the fraction of ammonium ions bound to the surface of the micelle (see equation 6.4). This quantity has been determined[3,6] and its temperature dependence is given in figure 6.9. Now proceeding as for the ^2H_2O quadrupole splittings, that is writing

$$(\Delta\tilde{\nu}_{ND_4^+})_r = \frac{S<P_2(\cos\alpha)>_s\beta_A}{S^{\ddagger}<P_2(\cos\alpha)>_s^{\ddagger}\beta_A^{\ddagger}}$$

$$= (S<P_2(\cos\alpha)>_s\beta_A)_r \qquad [6.6]$$

and plotting the quantity on the left hand side against the quantity on the right hand side of equation 6.6, a positive departure from the behaviour predicted assuming a uniform distribution of binding sites is revealed (figure 6.10). This is consistent with a preference for the sites with the smaller radius of curvature which are those having higher charge densities. The quadrupole-electric field gradient interaction for an ion bound parallel to the director, *i.e.* along the short axis of the micelle, is greater than the value for an ion bound perpendicular to the director. If ions bound preferentially to the 'caps' of the micelles (parallel to the director) rather than to the 'rims' then the overall contribution to the magnitude of $|\tilde{q}_{zz}|_s$ and hence $\Delta\tilde{\nu}_{ND_4^+}$ will be larger than it would be for a uniform distribution of sites. The shape factor $<P_2(\cos\alpha)>_s$ is calculated using the a/b ratio determined by x-ray measurements and is a measure of the contribution of all sites on

the micellar surface. To describe the contribution of individual ND_4^+ ions, $<P_2(\cos\alpha)>_s$ must be modified by another term to account for the preferential binding of ions to the caps as opposed to the rims of the micelles. These results could be used as a test of models for ion-condensation[7,8] on ellipsoidal micelles.

Figure 6.9 Temperature dependence of the bound ammonium ion fraction[3,6], β, for a $NH_4PFO/^2H_2O$ (w = 0.45) sample.

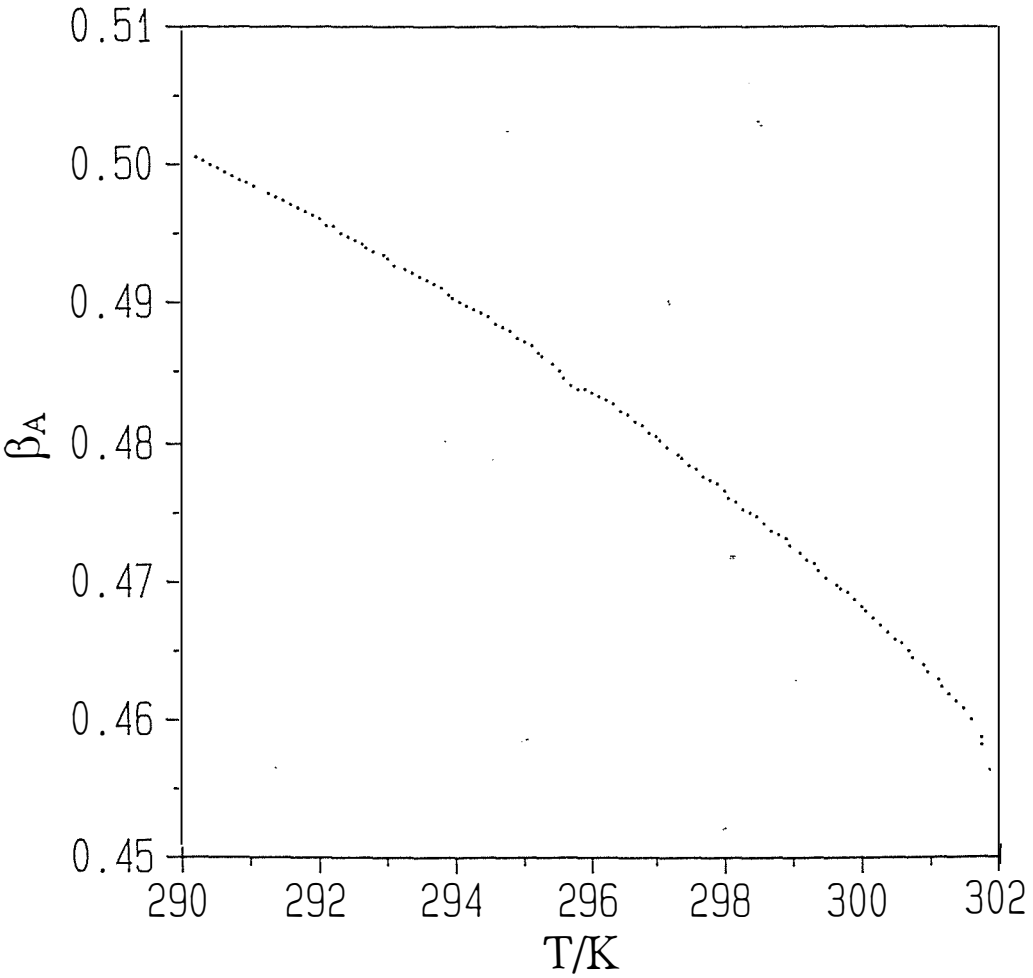

Figure 6.10 Plot of reduced ^2H quadrupole splittings versus reduced $S<P_2(\cos\alpha)>_s\beta$ values[3,6] for a $NH_4PFO/^2H_2O$ (w = 0.452) sample (see equation 6.6). The straight line has a slope of 1.0 and an intercept of 0 appropriate to a uniform distribution of ND_4^+ binding sites. The positive departure from equation 6.6 is due to preferential binding of ND_4^+ ions at sites with low surface curvature.

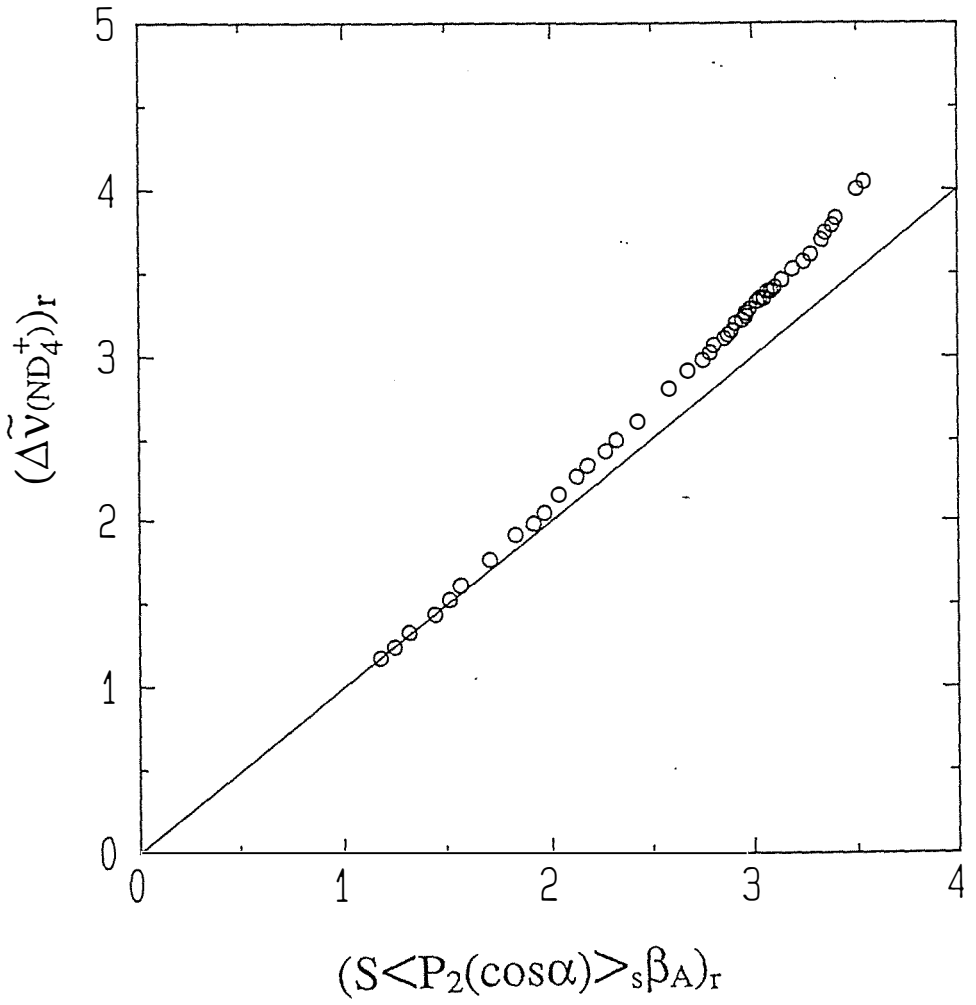

REFERENCES

[1]Boden N.; Corne S. A.; Jolley K. W., *J. Phys. Chem.* **1987**, *91* , 4092.

[2]Boden N.; Jolley K. W.; Smith M. H., *Liq. Cryst.* **1989**, *6* , 481.

[3]Boden N.; Clements J.; Jolley K.W.; Parker D.; Smith M. H., *J. Chem. Phys.* , In Press.

[4]Reeves L. W.; Tracey A.S., *J. Am. Chem. Soc.* **1974**, *96*, 365.

[5]McConnell H. M.; Thompson D. D., *J. Chem. Phys.* **1959**, *31* , 85.

[6]Parker D., Ph. D. Thesis, Leeds University, **1988**.

[7]Engström S.; Wennerström H., *J. Phys. Chem.* **1978**, *82* , 2711.

[8]Gunnarsson G.; Jönsson B.; Wennerström H., *J. Phys. Chem.* **1980**, *84* , 3114.

CHAPTER 7

THERMODYNAMICS OF MICELLIZATION

The lyotropic liquid crystal systems studied in this thesis are all micellar liquid crystals. To understand the differences in the behaviour of the CsPFO/^2H_2O and CsPFO/H_2O systems it should be instructive to consider the processes that govern the formation of the micelles themselves. Information about these processes can be obtained from studies of the thermodynamic of micellization.

There are many methods that can be used to measure the critical micelle concentration in surfactant solutions. The electrical conductivity used in this study was chosen for its convenience and ease of measurement.

7.1 DETERMINATION OF CRITICAL MICELLE CONCENTRATION

There are several treatments of the conductivity data that can be used to establish the location of the cmc. Figure 7.1a shows a plot of conductivity, κ, versus mole fraction of amphiphile, x, at 30 °C in both water and heavy water where it is clearly seen that the conductivity is linearly dependent on the concentration both below and above the cmc. This allows the cmc to be determined objectively from the intercept of the best fit straight lines of each data set (figure 7.1a). The cmc's obtained by this method are in good agreement with those obtained when the molar conductivity, Λ, is plotted against the square root of the concentration. The plot of Λ vs $\sqrt{m}$ at 30 °C for the water and heavy water is given in figure 7.1b. From the plot it can be seen that this treatment does not allow the cmc to be measured objectively since the point of intersection of the data from below and above the cmc is not so well defined. It is

Figure 7.1 (a) A plot of electrical conductivity, κ, versus mole fraction amphiphile, x, for solutions of CsPFO in H_2O (o) and ^2H_2O (•). The cmc is identified by the discontinuity in the concentration dependence of the conductivity.

(b) A plot of molar conductivity, Λ, versus the square root of the molality, $\sqrt{m}$, for CsPFO in H_2O (o) and in ^2H_2O (•). The cmc's are at molalities of 0.0269 mol kg^{-1} and 0.0272 mol kg^{-1} respectively.

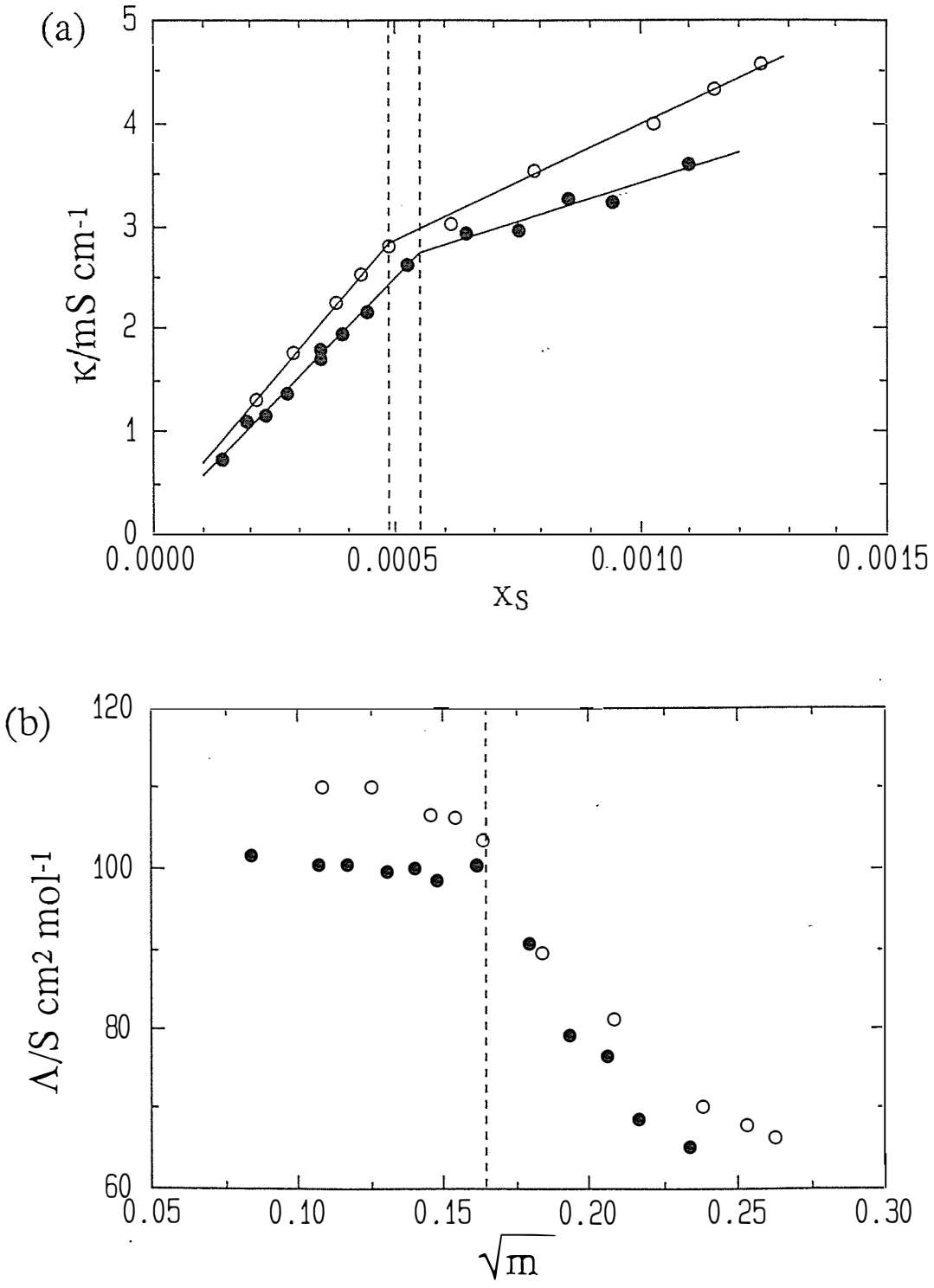

interesting to note that in studies on the NaPFO/water system[1], the two methods referred to above gave different values for the cmc's.

The cmc's obtained from the κ vs x method for the CsPFO/^2H_2O and CsPFO/H_2O systems are summarized in table 7.1. The temperature dependence of the cmc's for the two systems is graphically illustrated in figure 7.2.

Table 7.1 The cmc's of the CsPFO/^2H_2O and CsPFO/H_2O systems at various temperature.

T/°C	x cmc × 10^4	
	H_2O	D_2O
5	5.3	6.3
10	5.1	6.0
20	4.8	5.6
30	4.8	5.3
40	4.8	5.3
50	5.0	5.5
60	5.2	5.7
70	5.4	6.2
80	5.9	6.5
90	6.3	7.1

Figure 7.2 The temperature dependence of the critical micelle concentrations of solutions of CsPFO in H_2O (o) and in ^2H_2O (•).

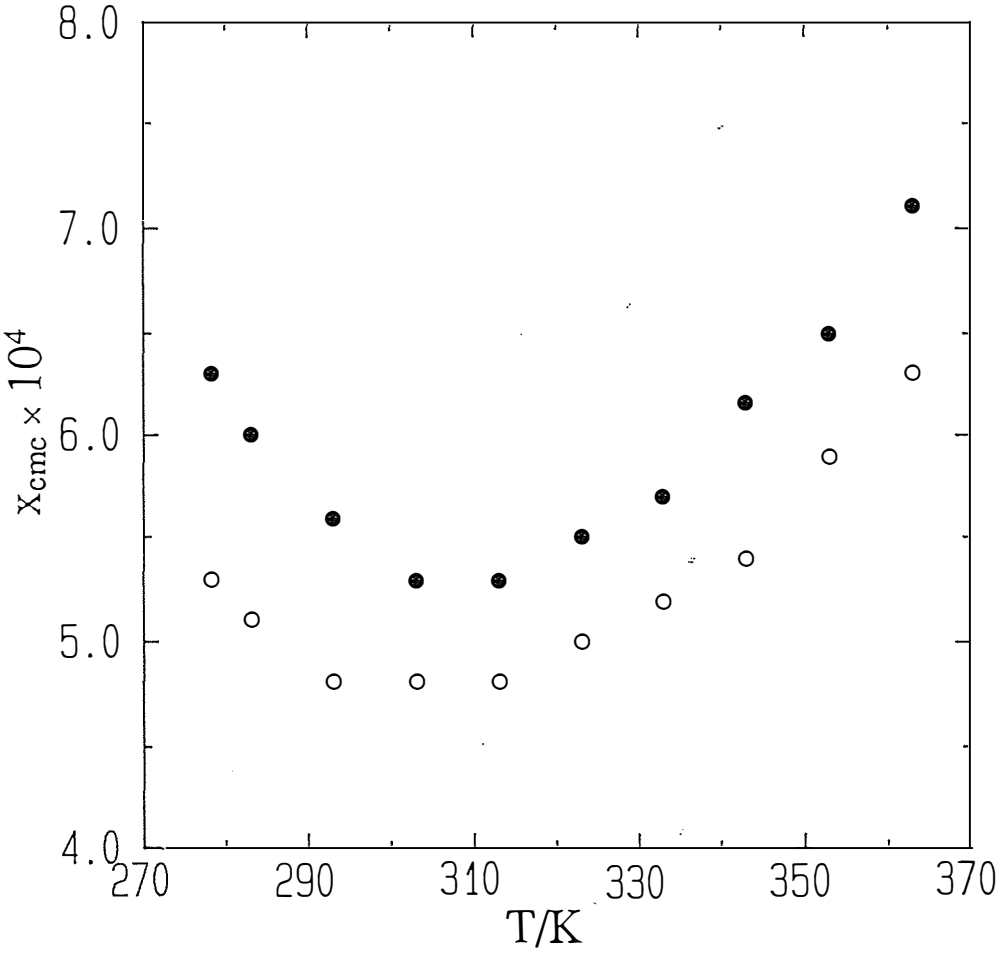

7.2 CALCULATION OF THERMODYNAMIC PARAMETERS.

The equilibrium between surfactant ion monomers (PFO^-), counter-ions (Cs^+) and monodisperse micelles (M) can be written,

$$nPFO^- + cCs^+ = M^{Z^-} \qquad [7.1]$$

where Z is the charge on the micelle and c is the number of counter-ions associated with the micelles (= n-Z). The equilibrium constant for the above process is

$$K = x_{M^{Z^-}}/((x^n_{PFO^-})(x^c_{Cs^+})) \qquad [7.2]$$

where x is the concentration expressed in terms of mole fraction. The standard free energy of micellization per mole of monomer is given by

$$\frac{\Delta G}{RT} = -\frac{1}{n}\ln x_{M^{z-}} + \ln x_{PFO^-} + (1-\frac{Z}{n})\ln x_{Cs^+} \qquad [7.3]$$

This equation can be rewritten in terms of x_{cmc} by assuming that only a small proportion of the surfactant is micellized at the cmc (≈2%)[1] where

$$\frac{\Delta G}{RT} = -\frac{1}{n}\ln 0.02\frac{x_{cmc}}{n} + \ln 0.98 x_{cmc} + (1-\alpha)\ln 0.98 x_{cmc} \qquad [7.4]$$

where α ($\equiv \frac{Z}{n}$) is the degree of dissociation of the counter-ions from the micelle *i.e.* α=1 for a totally ionized micelle. To determine ΔG from equation 7.4 we need knowledge of both n and α.

Small angle neutron scattering experiments[2] have measured the aggregation number at the cmc for the $NaPFO/H_2O$ system. The value of n for this system has been found to be 23 compared to the value of 15 estimated from ^{19}F NMR measurements[1]. These values are consistent with spherical or nearly spherical micelles. The calculated value for a spherical micelle[3] is 18. If the micelle is non-spherical then higher aggregation numbers are possible, as have been reported for the NH_4PFO/H_2O system[4] where n was found to have a value of 43 for a 0.12 mol dm^3 sample. The larger n, the

smaller the contribution from the micelle concentration term in equation 7.4. Taking the value of n as that for a spherical micelle (*i.e.* 18) enables the maximum contribution of the micelle concentration term to be calculated. For the CsPFO/H_2O system at 30 °C where $x_{cmc} = 4.8 \times 10^{-4}$ and α=0.34, the micellar contribution is calculated to be +0.80RT compared with the monomer and counter-ion contributions of -7.66RT and -5.05RT respectively. If the micelle concentration term is ignored therefore, the resulting value for ΔG will be at the most 6% too small. Because of this and because there is no reliable data for n for the dilute region of the CsPFO/H_2O system, the micelle concentration term has been dropped from equation 7.4 and the free energies of micelle formation have been calculated using the simplified expression

$$\frac{\Delta G}{RT} = (2-\alpha)\ln x_{cmc} \qquad [7.5]$$

To calculate the free energy of micellization we require values for α. There are two techniques that have been used to calculate α from conductivity measurements. Firstly there is the method used by Evans *et al.*[5,6] where $\alpha \equiv ((\partial\kappa/\partial m)_{m>cmc})/((\partial\kappa/\partial m)_{m<cmc})$ is the ratio of the slopes above and below the cmc. An alternative method is that applied by Mukerjee *et al.*[1,7] where α is calculated from $\left(\frac{\partial\kappa}{\partial c}\right)$ above the cmc and the molar conductivity, λ^+, of the Cs^+ ions at the cmc,

$$\frac{\partial\kappa}{\partial c} = \alpha(\lambda^+ + F\mu) \qquad [7.6]$$

where μ is the ionic mobility of the micelles and F is the Faraday constant. To obtain α it is necessary to make some assumptions concerning λ^+ and μ. The first step is to take 25 °C as our reference temperature and refer all other measurements back to this. The value of μ at 25 °C has been estimated to be 3.9×10^4 cm^2 V^{-1} s^{-1} for NaPFO micelles in water[7] and in the absence of any other information we assume the same value for our CsPFO micelles in water. Figure 7.3a shows plots of $\frac{\partial\kappa}{\partial c}$ vs T for the both systems. From these plots a value for $\frac{\partial\kappa}{\partial c}$ at the reference temperature can be interpolated. Figure 7.3b shows plots of the molar conductivities of the solutions at the

Figure 7.3 Temperature dependence of (a) $\frac{\partial \kappa}{\partial c}$ and (b) Λ_{cmc} for solutions of CsPFO in H_2O (o) and in ^2H_2O (•).

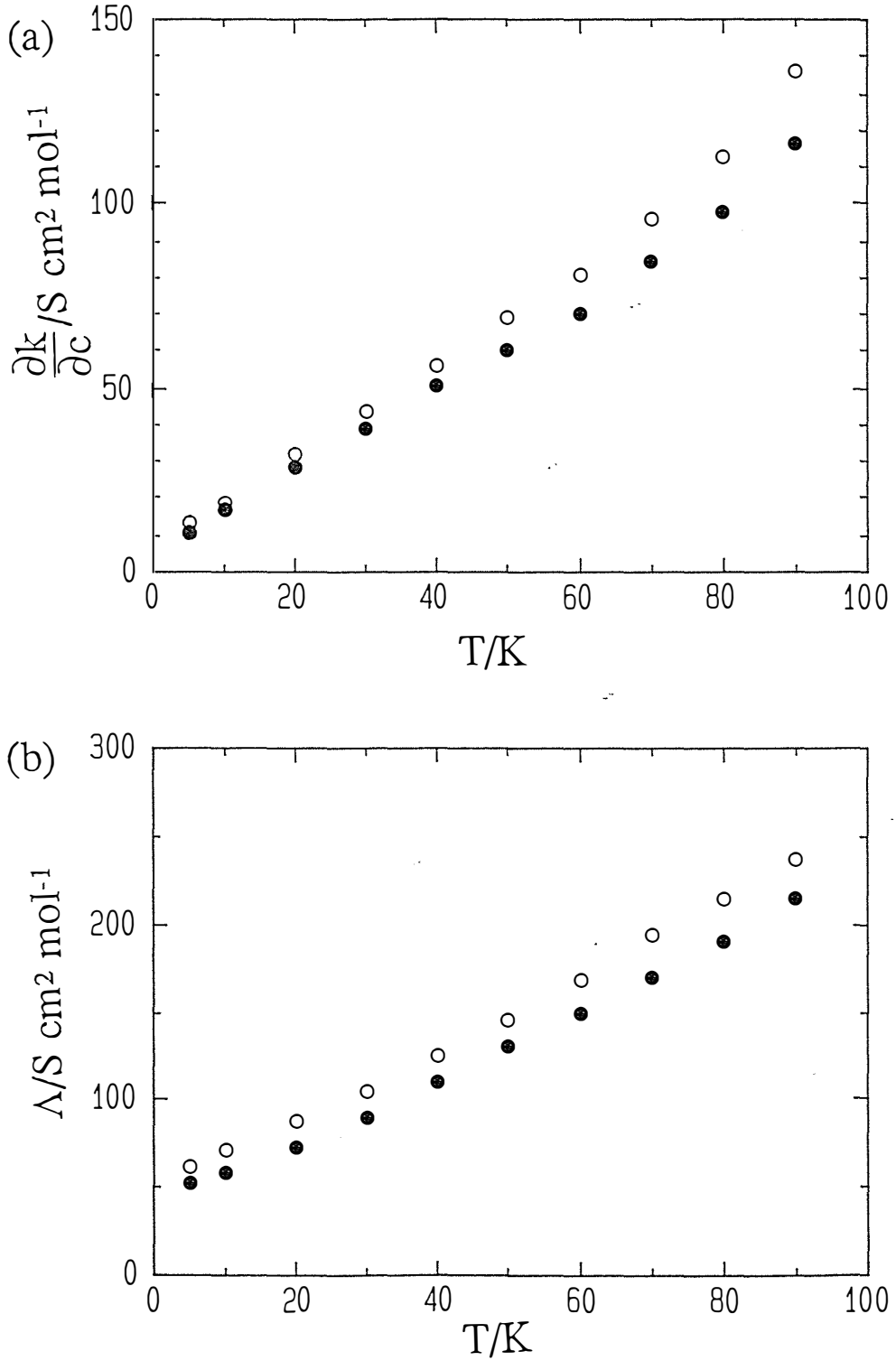

cmc, Λ_{cmc}, vs T for the water and heavy water systems from which Λ_{cmc} at 25 °C can be calculated. The data used in the construction of these figures is given in table 7.2. From values of Λ at the cmc we can calculate λ^+, the molar conductivity of the Cs^+ ions if the transference number t_+ is known, from

$$\lambda^+ = \Lambda t_+. \qquad [7.7]$$

The transference number was determined from $\lambda^\circ_{Cs^+} / \Lambda_{soln}$ at 25 °C and assumed to be the same at all temperatures. Taking $\lambda^\circ_{Cs^+}$ to be 77.2 S cm^2 mol^{-1} [8] gives a transference number of 0.8. At 25 °C the interpolated values of $\frac{\partial \kappa}{\partial c}$ and Λ_{cmc} are 37.9 S cm^2 mol^{-1} and 94 S cm^2 mol^{-1} respectively. Substituting into equation 7.6 gives a value of α at 25 °C of 0.34. Using this value as a reference point we can find α at any temperature by assuming that the change in μ is inversely proportional to the change in viscosity of the solvent and proportional to the change in charge density on the micelle as described by $\frac{\alpha_T}{\alpha_{25}}$. The slope $\frac{\partial \kappa}{\partial c}$ at any temperature can thus be written[1]

$$\frac{\partial \kappa}{\partial c} = \alpha_T \left[\lambda^+ + F\mu_{25} \left(\frac{\alpha_T}{\alpha_{25}} \times \frac{\eta_{25}}{\eta_T} \right) \right] \qquad [7.8]$$

All terms in the above equation are known apart from α_T. To obtain corresponding α values for the heavy water system a value for μ in the solvent must be known. In the absence of a literature value the ionic mobility of the micelles in heavy water was determined by making use of the Nernst-Einstein and Stokes-Einstein relationships

$$i.e.\ \mu(^2H_2O)_{25} = \mu(H_2O)_{25} \times \frac{\eta(^2H_2O)_{25}}{\eta(H_2O)_{25}} \qquad [7.9]$$

Literature values for the viscosities of water[9] and heavy water[10] were used. The values of α obtained from the two treatments are given in table 7.3 and the free energies of micellization are given in table 7.4.

Table 7.2 Conductivity data for water and heavy water systems.

T /°C	H_2O		^2H_2O	
	$\frac{\partial\kappa}{\partial c}$ /S cm^2 mol^{-1}	Λ_{cmc}/S cm^2 mol^{-1}	$\frac{\partial\kappa}{\partial c}$ /S cm^2 mol^{-1}	Λ_{cmc}/S cm^2 mol^{-1}
5	13.6	61	10	53
10	18.7	70	17	57
20	31.9	87	28	73
30	43.9	105	39	90
40	56.0	125	51	110
50	69.1	145	60	130
60	81.2	168	70	150
70	95.7	193	84	170
80	113	215	98	190
90	136	236	116	215

Table 7.3 α values for the CsPFO/H_2O and CsPFO/^2H_2O systems at the cmc's.

T/°C	Evans Treatment		Mukerjee Treatment	
	α H_2O	α ^2H_2O	α H_2O	α ^2H_2O
5	0.28	0.26	0.21	0.20
10	0.35	0.32	0.25	0.27
20	0.38	0.35	0.31	0.32
30	0.41	0.37	0.34	0.36
40	0.42	0.39	0.36	0.37
50	0.44	0.42	0.37	0.37
60	0.45	0.44	0.37	0.37
70	0.45	0.45	0.38	0.38
80	0.46	0.47	0.39	0.39
90	0.49	0.50	0.41	0.40

Table 7.4 The free energy of micellization calculated for the CsPFO/H_2O and CsPFO/^2H_2O systems using equation 7.5. The α values used were calculated from the best fit line to the data between 20 °C and 90 °C (see text).

T/°C	Evans Treatment		Mukerjee Treatment	
	ΔG/kJ mol^{-1} H_2O	ΔG/kJ mol^{-1} ^2H_2O	ΔG/kJ mol^{-1} H_2O	ΔG/kJ mol^{-1} ^2H_2O
5	-28.4	-28.6	-31.2	-30.7
10	-29.0	-29.2	-31.2	-30.2
20	-30.0	-30.1	-31.5	-30.7
30	-30.7	-31.0	-32.0	-31.2
40	-31.5	-31.6	-32.6	-32.0
50	-32.0	-32.0	-33.3	-32.9
60	-32.6	-32.4	-34.1	-33.7
70	-33.1	-32.6	-34.8	-34.2
80	-33.4	-32.8	-35.1	-34.7
90	-33.7	-32.9	-35.4	-35.0

The enthalpies of micelle formation can be calculated using the Gibbs-Helmholtz equation

$$\Delta H = -T^2 \frac{\partial\left(\frac{\Delta G}{T}\right)}{\partial T} \qquad [7.10]$$

Substituting for ΔG (equation 7.5) we obtain

$$\Delta H = -RT^2\left\{(2-\alpha)\left[\frac{\partial \ln x_{cmc}}{\partial T}\right]_p - \ln x_{cmc}\left[\frac{\partial \alpha}{\partial T}\right]_p\right\} \qquad [7.11]$$

The second term in the above equation has often been ignored in ΔH calculations, but it can have a profound effect as is illustrated by comparing the ΔH values calculated from the Evans and Mukerjee α values.

The temperature dependence of α from the Evans treatment is illustrated graphically for both systems in figure 7.4. There is a sharp decrease in α at low temperatures (<25 °C) which has not previously been reported. We can find no

Figure 7.4 Temperature dependence of the fraction of free ions, α, calculated from $(\partial\kappa/\partial m)_{m>cmc}/(\partial\kappa/\partial m)_{m<cmc}$ for solutions of CsPFO in H_2O (o) and in ^2H_2O (•).

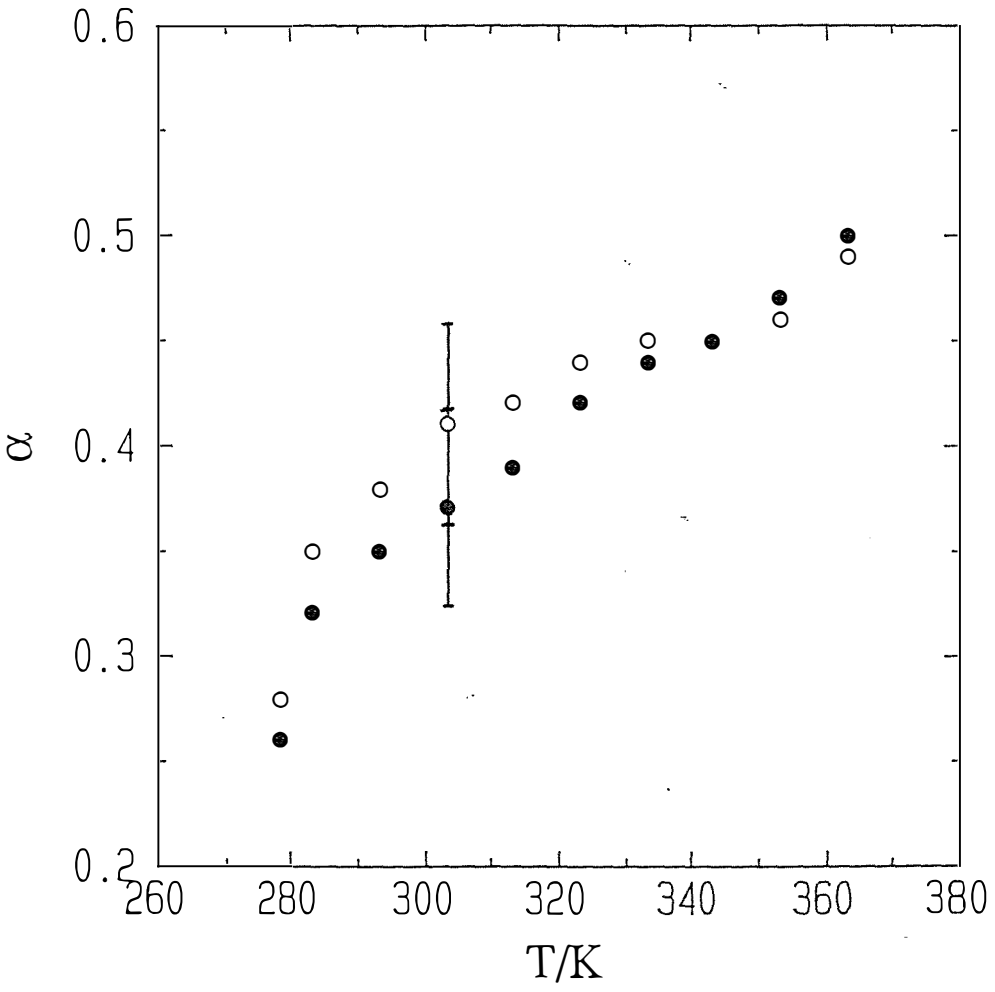

literature data for the variation of α at temperatures less than 25 °C. In all studies to date, which do not go to such low temperature as the present study[1,5,6], $\frac{\partial\alpha}{\partial T}$ has been found to be linear and the sharp decrease has not been observed. If it is real then there will be a large anomalous contribution to ΔH from the term which includes $\frac{\partial\alpha}{\partial T}$. We have therefore fitted only the data from 20 to 90 °C to obtain slopes $\frac{\partial\alpha}{\partial T}$ of 1.3×10^{-3} K^{-1} and 2.0×10^{-3} K^{-1} in water and heavy water respectively. The enthalpies and entropies of micelle formation calculated using α's derived from the Evans treatment are presented in table 7.5. and are plotted versus temperature in figure 7.5. The trends in the thermodynamic parameters for the two systems are best seen by reference to figure 7.5 where it can be seen that the ΔH and $T\Delta S$ curves are parallel to each other over the full temperature range. This is in conflict with our understanding of the water and heavy water structures. As the structural difference between the solvents breaks down at higher temperatures we would expect the entropy term to become less important and therefore the curves for the two solvents to come together. The reason the ΔH (and $\therefore$ ΔS) values do not converge at high temperatures is the higher $\frac{\partial\alpha}{\partial T}$ for the ^2H_2O data (equation 7.11). The problem with the Evans treatment is the precision in the measurement of α. The method involves taking the ratio of two slopes that already have a sizable error. If we considered the error bars in in figure 7.4 then we could say that there is no real difference in $\frac{\partial\alpha}{\partial T}$ between the two solvent systems. On taking an average value for the two systems the ΔH curves do converge at higher temperatures similar to those of the Mukerjee treatment which follows.

Figure 7.5 Temperature dependence of the thermodynamic parameters of micellization for solutions of CsPFO in H_2O (o) and in ^2H_2O (•), using "Evans Treatment" α values given in table 7.3.

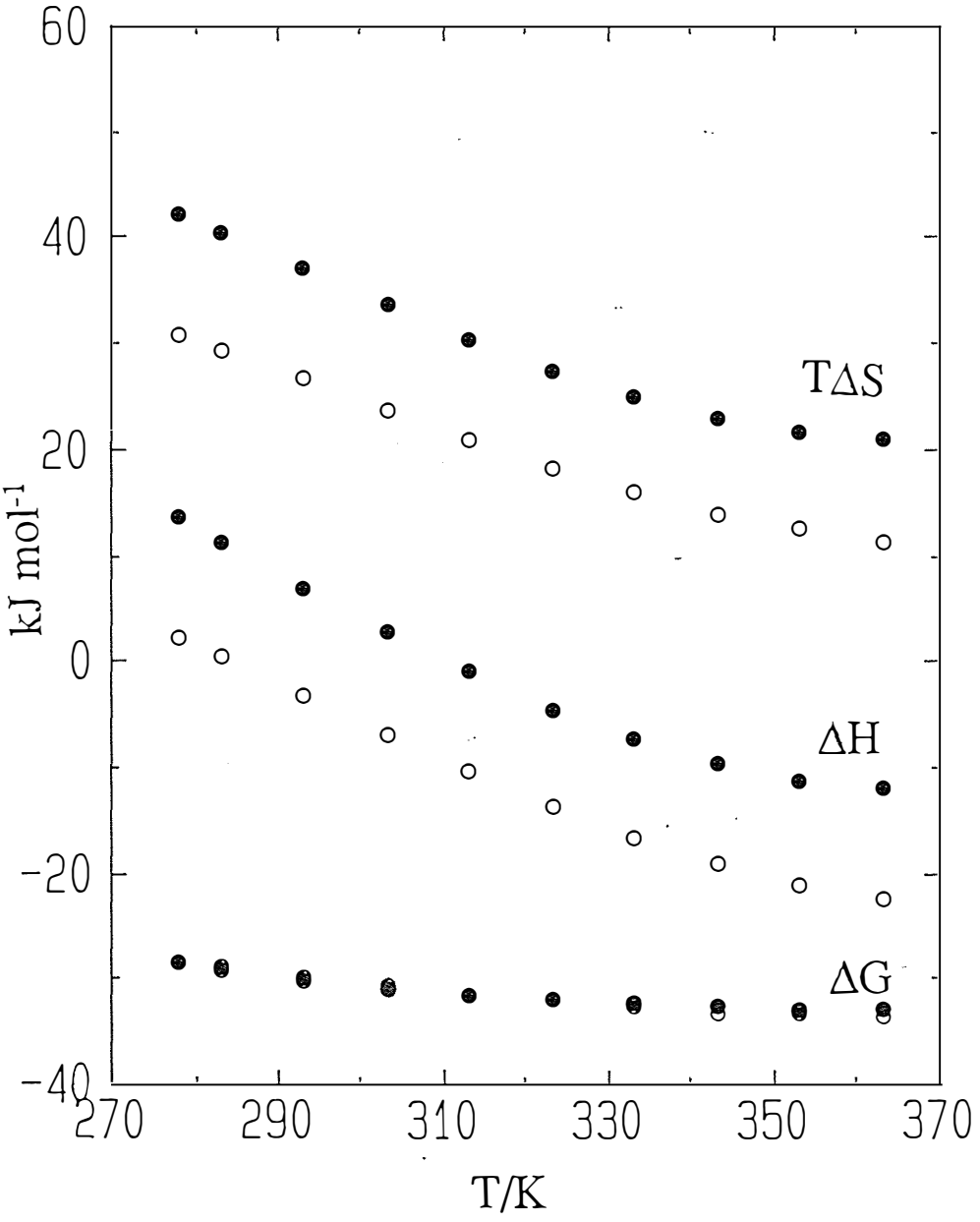

Table 7.5 Thermodynamic parameters derived from α's calculated by the Evans treatment.

T/°C	ΔH/kJ mol^{-1}		TΔS/kJ mol^{-1}		ΔS/J mol^{-1} K^{-1}	
	H_2O	^2H_2O	H_2O	^2H_2O	H_2O	^2H_2O
5	2.2	13.6	31	42	110	152
10	0.3	11.3	29	40	103	143
20	-3.4	7.0	27	37	91	126
30	-7.1	2.8	24	34	78	111
40	-10.5	-1.1	21	30	67	97
50	-13.7	-4.5	18	27	57	85
60	-16.6	-7.5	16	25	48	75
70	-19.1	-9.7	14	23	41	67
80	-21.0	-11.2	12	22	35	61
90	-22.5	-11.9	11	21	31	58

There is less systematic error in the Mukerjee treatment because α is calculated from only one slope *i.e.* $\frac{\partial \kappa}{\partial c}$ above the cmc. It can be seen from table 7.3 that there are no significant differences in α between the systems and therefore the same $\frac{\partial \alpha}{\partial T}$ (= 0.001 K^{-1}) was used in the calculation of the enthalpy of micellization for water and heavy water and the value at 5 °C and 10 °C were omitted for reasons already discussed. The temperature dependence of the enthalpies and entropies of micelle formation as obtained using the Mukerjee treatment are set out in table 7.6 and for illustrative purposes are plotted in figure 7.6. In subsequent discussion only the thermodynamic parameters obtained using the Mukerjee treatment will be considered.

Figure 7.6 Temperature dependence of the thermodynamic parameters of micellization for solutions of CsPFO in H_2O (o) and in ^2H_2O (•), using "Mukerjee Treatment" α values given in table 7.3.

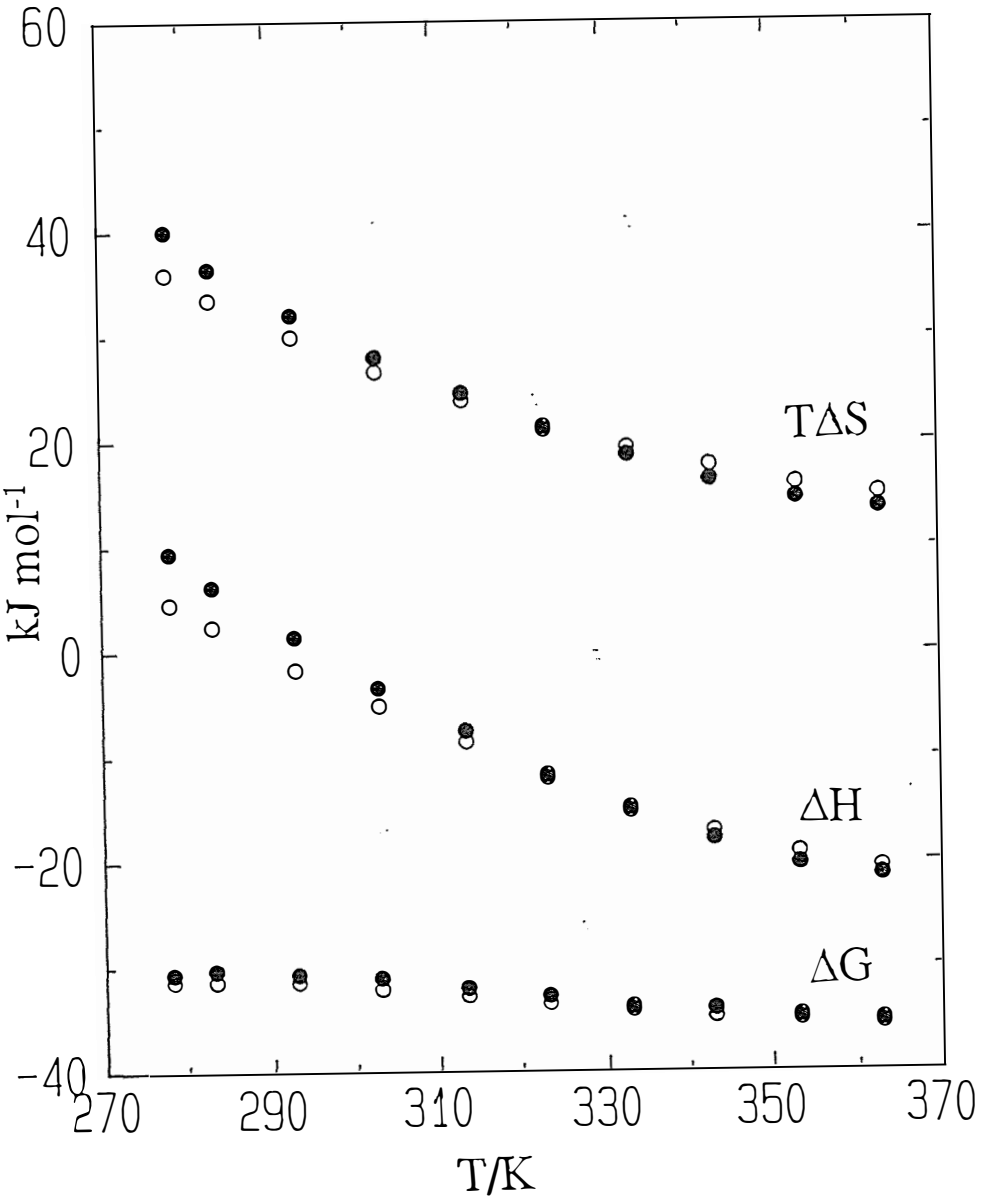

Table 7.6 Thermodynamic parameters derived from α's calculated by the Mukerjee treatment.

T/°C	ΔH/kJ mol^{-1}		TΔS/kJ mol^{-1}		ΔS/J mol^{-1} K^{-1}	
	H_2O	^2H_2O	H_2O	^2H_2O	H_2O	^2H_2O
5	4.5	9.4	36	40	128	144
10	2.4	6.4	34	37	119	129
20	-1.6	1.3	30	32	102	109
30	-5.3	-3.4	27	28	88	92
40	-8.7	-7.7	24	24	76	78
50	-11.9	-11.7	21	21	66	66
60	-14.9	-15.2	19	18	58	55
70	-17.3	-18.0	17	16	51	47
80	-19.2	-20.3	16	14	45	41
90	-20.6	-21.5	15	14	41	37

7.3 COMPARISON WITH PREVIOUS CMC STUDIES

In the following sections our results are compared with the results of other studies. Most of the work done on the cmc's of perfluorinated surfactants have been carried out in water so only the thermodynamic parameters determined for the CsPFO/H_2O system can be compared with literature studies.

7.3.1 Comparison of CMC and CMC versus Temperature Behaviour

The characteristic shape of a cmc versus temperature plot is a U-shaped curve. The CsPFO/H_2O system (figure 7.2) shows this behaviour which is similar to that of KPFO, NaPFO and sodium decyl sulphate systems presented by Mukerjee *et al.*[1] although the slopes $\frac{\partial \ln x_{cmc}}{\partial T}$ on either side of the minimum are not as large for the CsPFO system. The CsPFO micelles form at approximately the same concentrations as the KPFO micelles, which is lower than that for both sodium decyl sulphate and NaPFO. Studies on LiPFN and NaPFN by La Mesa and Sesta[11] indicate that the cmc's for these systems are considerably less than those of pentadecafluorooctanoate salts.

The effect of lengthening the hydrophobic tail is to reduce the cmc as shown in cmc measurements of a series of alkyltrimethylammonium bromides and on a series of alkyl sulphates[12]. The behaviour of the CsPFO cmc's is consistent with the studies in the literature.

Studies by Berr[12] and by Chang and Kaler[13] using hydrocarbon surfactants reported that the effect of substitution of heavy water for water as the solvent is to lower the cmc. This is opposite to the findings of the present study where it was found that the cmc's are lower in water (see figure 7.1 and table 7.1).

7.3.2 Comparison of Thermodynamic Parameters

7.3.2.1 Free Energy of Micelle Formation

The free energy of micelle formation tends to be fairly constant with changing temperature. For NaPFO[1] between 20 and 60 °C the value of ΔG decreases by 12% (-25.6 to -28.8 kJ mol^{-1}) and for KPFO[1] between 30 and 85 °C the ΔG values change by only 7% (-26.9 to -28.7 kJ mol^{-1}). For tetradecyltrimethylammonium bromide micelles[5] ($C_{14}TAB$) the free energy of micellization increases from -24.2 to -16.0 kJ mol^{-1} over a temperature range of 25 to 166 °C although over the temperature range covered in the present study the change in ΔG is small.

The variation of the free energy of micellization for the CsPFO/H_2O system is from -31.2 kJ mol^{-1} at 5 °C to -35.4 kJ mol^{-1} at 90 °C or approximately 12% and in line with the behaviour exhibited by the other fluorocarbon systems. The values for the ΔG of micellization are more negative than those for the KPFO system[1], even though the cmc values are similar, as a result of the smaller values of α for the CsPFO/H_2O system.

7.3.2.2 Enthalpy of Micelle Formation

Information on the enthalpies of micellization is not readily available but two studies have shown that ΔH decreases with an increase in temperature. For perfluorinated surfactants (the data for KPFO and NaPFO was similar so it was combined)[1] the enthalpies are positive at low temperatures and become negative at higher temperatures (9.2 kJ mol^{-1} at 25 °C to -18.4 kJ mol^{-1} at 62.5 °C). The reported ΔH values for the hydrocarbon surfactant $C_{14}TAB$ start negative and become even more negative[5]. The minima in the temperature dependence of the cmc correspond to the point at which $\Delta H = 0$ therefore this point is less than 25 °C for the $C_{14}TAB$ system.

The temperature dependence of ΔH for the CsPFO/H_2O system is similar to that of the fluorocarbon systems already reported. The ΔH values for our system start positive and become negative with increasing temperature. The more negative enthalpies of the hydrocarbon systems compared with the fluorocarbon systems are because hydrocarbon chains have more attraction for each other than fluorocarbon chains[14].

7.3.2.3 Entropy of Micelle Formation

The entropy of micellization is a decreasing function of the temperature. The entropy component of the free energy is more important at lower temperatures where the solvent has a higher degree of structure. For NaPFO and KPFO[1] ΔS goes from 119 J K^{-1} mol^{-1} at 25 °C to 46 J K^{-1} mol^{-1} at 55 °C. The entropy of micellization goes from a small positive to a large negative quantity in the $C_{14}TAB$ system.

CsPFO shows similar behaviour to the NaPFO and KPFO systems. The hydrophobic effect is much stronger for fluorocarbons than for hydrocarbons[1]. This is shown in the larger entropy increase as the fluorocarbon chain is removed from the solvent allowing an overall relaxation in the solvent structure (as witnessed by the relatively large volume changes at the cmc[1]).

7.4 THE ISOTOPE EFFECT ON MICELLIZATION

7.4.1 CsPFO in Water and Heavy Water

It has been extensively argued in the literature[1,2] that it is the hydrophobic effect that dominates the free energy of micellization of fluorocarbon surfactants. Evidence for this includes; higher interfacial tensions between fluorocarbons and water[14], higher volume changes on micellization[7], lower solubilities of fluorocarbons in water[15,16]. This is in contrast to hydrocarbon surfactants where there is a large enthalpy contribution to the free energy of micellization derived from interchain interactions in the micelle[5]. These interactions along with the interactions responsible for removing the chains from water produce the total hydrophobic contribution to ΔG[17]. The greater hydrophobicity of the fluorocarbon surfactants is exhibited in their lower cmc's than for a hydrocarbon surfactant with a corresponding chain length.

This leads to two expectations, firstly the hydrophobic effect will be greater in heavy water than water due an increase in the entropy component of the free energy and that the isotope effect will be more prominent in fluorocarbon systems where the hydrophobic interaction is more important.

Studies have been performed on the effect of substituting heavy water for water as the solvent for a series of hydrocarbon surfactants[12]. These were for a series alkyltrimethylammonium bromides (C_xTAB) and a series of sodium alkyl sulphates and in most cases at 25 °C the free energy of micellization was more negative for the ^2H_2O solutions, although the differences do not seem significant (with the possible exception of the $C_{16}TAB$ system). This is consistent with an increased entropy component for ^2H_2O which is intrinsically a more structured liquid than H_2O therefore the monomer will be at a higher free energy in ^2H_2O.

In contrast to the study by Berr[12] ΔG values of the CsPFO systems tend to be slightly less negative in heavy water. This is contrary to expectation and is quite possibly a consequence of the simplifications used in the theory and limitations in the accuracy with which α values can be measured. In calculating ΔG's the micelle concentration term was ignored which means that possible differences in n between the two systems are not being accounted for. The neglect of variations in n between the two solvent systems is justified in the isotope effect study on the C_xTAB system[12] where aggregation numbers are greater than 50. In our system however, the aggregation number is probably too small to allow us to omit the micellar concentration term from equation 7.4. If the aggregation number was 18 at the cmc for the CsPFO/H_2O system then the aggregation number in the CsPFO/^2H_2O system would only have to be 22 to remove the difference in the ΔG values between the systems. Of course an increase in the aggregation number requires non spherical micelles. At higher concentrations this has been shown to be the case[18] and so it is not unreasonable to expect a slight deviation from spherical micelles, which will then be able to accommodate greater numbers of amphiphile molecules. What is needed to solve this problem is a detailed small angle neutron scattering study on both systems. The other point that must be resolved is the variation of the bound ion fraction, β. We can find no evidence in our study that β is different in water and heavy water at a given temperature (or composition). It is reasonable to assume however that n and β are linked as was found in a study on the NaPFO/H_2O system[2], in which it was shown that above the cmc an increase in the aggregation number was paralleled by a decrease in the free fraction of ions, α (increase in β). If the micelles are larger in the CsPFO/^2H_2O system than in the CsPFO/H_2O system (which logically appears to be the case), then the value of α will be smaller which will lead to a higher negative ΔG of micelle formation. Further evidence that aggregation numbers and bound ion fractions, at least in concentrated solutions, are greater in heavy water, will be presented in chapter 8.

REFERENCES

[1]Mukerjee P.; Korematsu K.; Okawauchi M.; Sugihara G., *J. Phys. Chem.* **1985**, *89*, 5308.

[2]Berr S. S.; Jones R. R. M., *J. Phys. Chem.* **1989**, *93* , 2555.

[3]Boden N.; Clements J.; Jolley K.W.; Parker D.; Smith M. H., *J. Chem. Phys.* , In Press.

[4]Burkitt S. J.; Ottewill R. H.; Hayter J. B.; Ingram B. T., *Colloid Polymer Sci.* **1987**, *265* , 619.

[5]Evans D. F.; Wightman P. J., *J. Colloid Interface Sci.* **1982**, *86* , 515.

[6]Evans D. F.; Allen M.; Ninham B. W.; Fouda A., *J. Solution Chem.* **1984**, *13* , 87.

[7]Sugihara G.; Mukerjee P., *J. Phys. Chem.* **1981**, *85* , 1612.

[8]Robinson R. A.; Stokes R. H., *Electrolyte Solutions* **1968**, 2nd ed revised (Butterworths, London).

[9]Kaye G. W. C.; Laby T., *Tables of Physical and Chemical Constants* **1986**, 15th edition.

[10]Millero F. J.; Dexter R.; Hoff E., *Chem. Eng. Data* **1971**, *16* , 85.

[11]La Mesa C.; Sesta B., *J. Phys. Chem.* **1987**, *91* , 1450.

[12]Berr S. S., *J. Phys. Chem.* **1987**, *91* , 4760.

[13]Chang N. J.; Kaler E. W., *J. Phys. Chem.* **1985**, *89* , 2996.

[14]Mukerjee P.; Handa T., *J. Phys. Chem.* **1981**, *85* , 2298.

[15]Wen W. -Y.; Muccitelli J. A., *J. Solution Chem.* **1979**, *8* , 225.

[16]Wilhelm E.; Battino R.; Wilcock R. J., *Chem. Rev.* **1977**, *77* , 219.

[17]Hunter R. J., *Foundations of Colloid Science, Vol 1*, **1987**, (Oxford University Press, Oxford).

[18]Boden N.; Corne S A.; Holmes M. C.; Jackson P. H.; Parker D.; Jolley K. W., *J. Physique* **1986**, *47* , 2135.

CHAPTER 8

DISCUSSION

8.1 ISOTOPE EFFECTS ON THE CsPFO/WATER PHASE DIAGRAM

The phase diagrams of CsPFO in water and in heavy water differ in the temperatures of the phase transitions (see table 8.1) and in the location of the triple points (see table 8.2). When comparing phase transition temperatures between the two systems it is better to use volume fraction versus temperature space. This can be seen by considering the modified Maier-Saupe expression[1] for the nematic to isotropic transition temperature: $T_{NI} = (0.2202/k)\varepsilon_{mm}\phi/V_m$, where ε_{mm} is the strength of the anisotropic dispersive interaction between the micelles and V_m is the volume of a micelle. For a discoidal micelle it is plausible to expect that $\varepsilon_{mm} \propto \tilde{n}^2$ so that $T_{NI} \propto \tilde{n}\phi$. A comparison of the T_{NI} and T_{LN} phase transition temperatures versus volume fraction of surfactant is shown in figure 8.1. Both of these transition lines are at a higher temperature for a given volume fraction in the CsPFO/^2H_2O system (or at a higher volume fraction for a given temperature in the CsPFO/H_2O system). The separation between the T_{NI} curves for the two systems decreases with increasing temperature, from $\approx$ 3.8 K at $\phi = 0.118$ to $\approx$ 1.8 K at $\phi = 0.405$. The curves for T_{LN} exhibit a similar convergence at high temperatures. In addition, the width of the nematic phase is 4% ($\approx$ 240 mK) wider for the CsPFO/H_2O system over most of the composition range. The solubility curve is lower in the CsPFO/H_2O system as illustrated by the location of the Krafft points (280 K and 274 K for heavy water and water respectively) and the nematic phase is stable to higher temperatures in the ^2H_2O system as can be seen from a comparison of the $T_{P(I,N,L)}$ triple points (351.23 K and 342.72 K respectively).

Figure 8.1 The concentration dependence of the transition temperatures T_{NI} (circles) and T_{LN} (squares) in the CsPFO/H_2O (open symbols) and CsPFO/^2H_2O (closed symbols) systems.

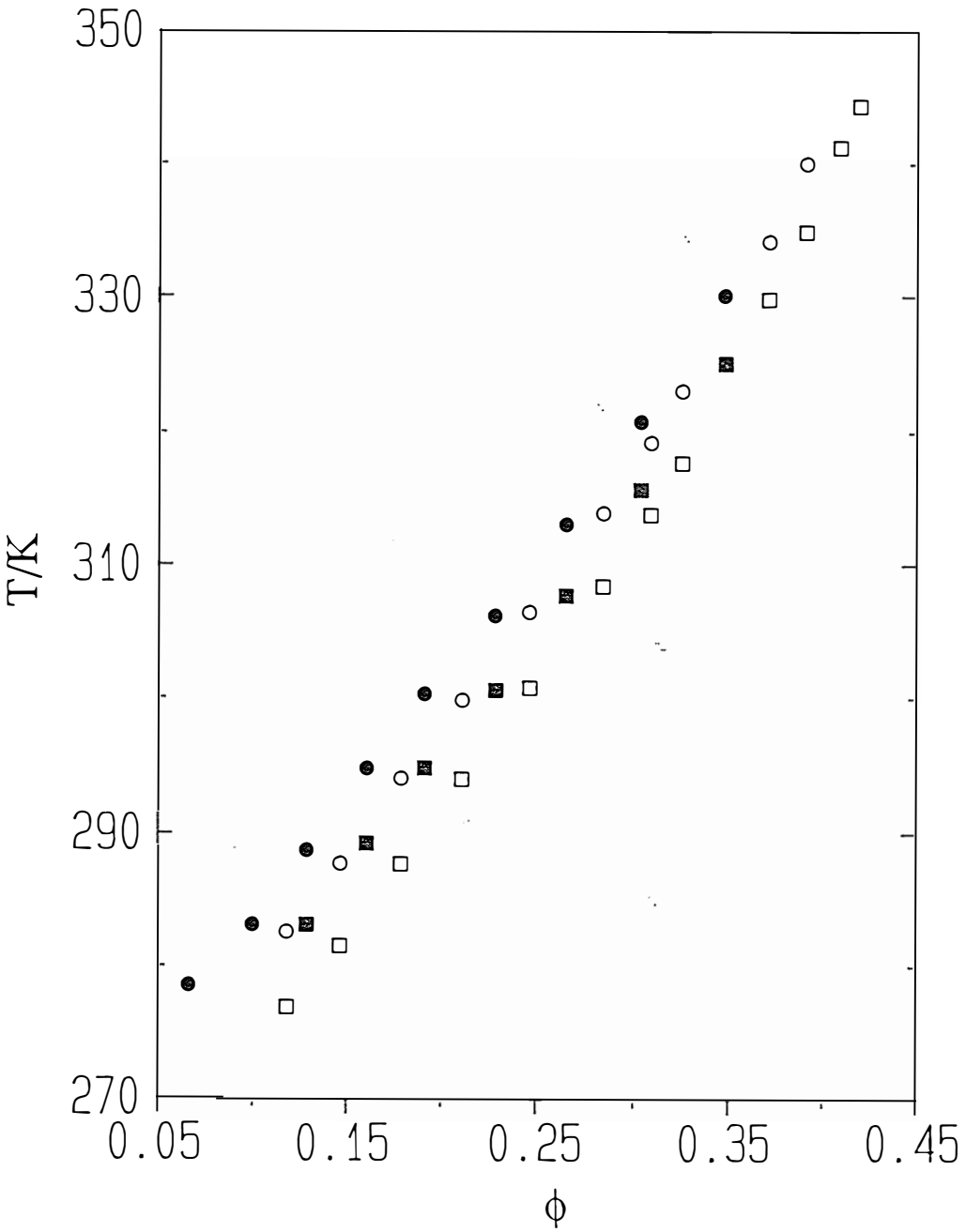

Table 8.1 The transition temperatures for the CsPFO/H_2O and CsPFO/^2H_2O system have been fitted to polynomials for ease of generating transition temperatures for any sample. The polynomial takes the form $a+bw+cw^2+dw^3$ with the valid concentration range falling within w_{max} and w_{min}.

CsPFO/H_2O

Transition	a	b	c	d	w_{min}	w_{max}
T_{IN}	229.96	333.04	-664.56	669.45	0.238	0.650
T_{NI}	238.52	263.08	-482.11	514.99	0.238	0.6325
T_{NL}	-101.89	2246.1	-4393.7	3087.7	0.450	0.6325
T_{LN}	202.13	465.40	-925.85	839.76	0.300	0.650
T_c	271.71	133.09	-648.22	1087.8	0.030	0.250
T_c	247.94	234.91	-524.63	395.84	0.250	0.875

CsPFO/^2H_2O

Transition	a	b	c	d	w_{min}	w_{max}
T_{IN}	234.36	355.40	-737.29	744.48	0.200	0.700
T_{NI}	237.32	328.85	-662.23	647.59	0.220	0.632
T_{NL}	104.21	1148.0	-2407.1	1912.9	0.430	0.632
T_{LN}	220.02	404.42	-822.52	790.17	0.300	0.700
T_c	281.17	281.17	-51.363	56.811	0.200	0.700

Table 8.2 The fixed points for the CsPFO/^2H_2O and CsPFO/H_2O systems.

CsPFO/^2H_2O

		T/K	w	ϕ	c/mol dm^{-3}	x
T_p(I,N,L)	isotropic	351.23	0.626	0.425	1.946	0.0578
	nematic		0.632	0.426	1.975	0.0592
	lamellar		0.648	0.443	2.054	0.0632
T_p(I,N,K)	isotropic	285.2	0.221	0.111	0.510	0.0103
	nematic		0.225	0.114	0.520	0.0105
T_p(HI,I,K)	isotropic	275.8	0.011	0.0049	0.0224	0.00041
C_{ep}	nematic =					
	lamellar	285.72	0.287	0.151	0.691	0.0145
K_p		280.0	0.014	0.0062	0.029	0.00052
T_f	heavy ice	276.95				
T_{cp}		304.80	0.43	0.25	1.14	0.027

CsPFO/H_2O

		T/K	w	ϕ	c/mol dm^{-3}	x
T_p(I,N,L)	isotropic	342.72	0.628	0.398	1.821	0.0527
	nematic		0.632	0.402	1.840	0.0536
	lamellar		0.644	0.414	1.897	0.0563
T_p(I,N,K)	isotropic	281.31	0.233	0.108	0.496	0.00992
	nematic		0.235	0.109	0.501	0.0100
T_p(Ice,I,K)	isotropic	272.0	0.009	0.0036	0.016	0.0003
C_{ep}	nematic =	281.7				
	lamellar		0.302	0.148	0.675	0.0141
K_p		274.0	0.016	0.0066	0.030	0.00054
T_f	ice	273.15				
T_{cp}		302.05	0.46	0.25	1.16	0.027

The convergence of the phase transition temperature curves at high temperature probably has its origin in the same effect that causes the curves for the enthalpies and entropies of micellization to converge *i.e.* a lessening of the role the hydrophobic effect plays in the two systems as the structural differences in the two solvents become less.

The higher transition temperatures for the CsPFO/^2H_2O system suggests larger micelles at a given volume fraction in the system.

In the absence of a direct method for monitoring the change in ñ with changing the solvent we can get some idea of the micelle size variation by comparing the ^{133}Cs quadrupole splittings at the transition temperatures. Figures 8.2a and 8.2b show the quadrupole splittings versus ϕ for both CsPFO systems at T_{NI} and T_{NL} respectively. Overall these plots indicate that the product $\beta_{Cs}S\langle P_2(\cos\alpha)\rangle_s$ is the same at the transition in ^2H_2O and H_2O for a given volume fraction (see equations 3.22 and 3.23). Assuming that the order parameter S is the same in the two systems at the phase transition temperatures, means that the micelles have the same size and shape. The implication of this is that at any given ϕ and temperature the micelles will be larger in heavy water. This finding is supported by a comparison of the ^{133}Cs quadrupole splittings and chemical shift anisotropies in the water and heavy water systems at a constant temperature (285 K *i.e* in the lamellar phase). With increasing concentration both the quadrupole splittings (figure 8.3a) and the chemical shift anisotropies (figure 8.3b) increase with the heavy water values being consistently greater. Thus at any given volume fraction the product $S\langle P_2(\cos\alpha)\rangle_s\beta_{Cs}$ is greater in ^2H_2O than in H_2O. Since the value of S varies little with temperature in the lamellar phase[2] then $\langle P_2(\cos\alpha)\rangle_s\beta_{Cs}$ is greater in the heavy water system. This probably implies that both quantities $\langle P_2(\cos\alpha)\rangle_s$ and β_{Cs} are bigger in the heavy water system, *i.e.* the larger micelle size is associated with an increase in the fraction of bound counter-ion[3]. This assertion is supported by a comparison of the isotope effects on the quadrupole splitting and chemical shift anisotropies with the isotope effect on the chemical shifts which was demonstrated in sections 4.4.2 and 4.4.3. The ratio of the CsPFO/^2H_2O quadrupole splittings to those in the CsPFO/H_2O system are exactly the same as the ratio of the anisotropies which indicates that the isotope effect is caused by changes in $\langle P_2(\cos\alpha)\rangle_s\beta_{Cs}$ only (see equations 3.22 and 3.26). The ratio varies from 1.12 at ϕ=0.25 to 1.09 at ϕ=0.325. The ratio of the CsPFO/^2H_2O chemical shifts to those of

Figure 8.2 ^{133}Cs quadrupole splittings as a function of volume fraction of surfactant at (a) T_{NI} and (b) T_{NL} for the CsPFO/H_2O (o) and CsPFO/^2H_2O (•) systems.

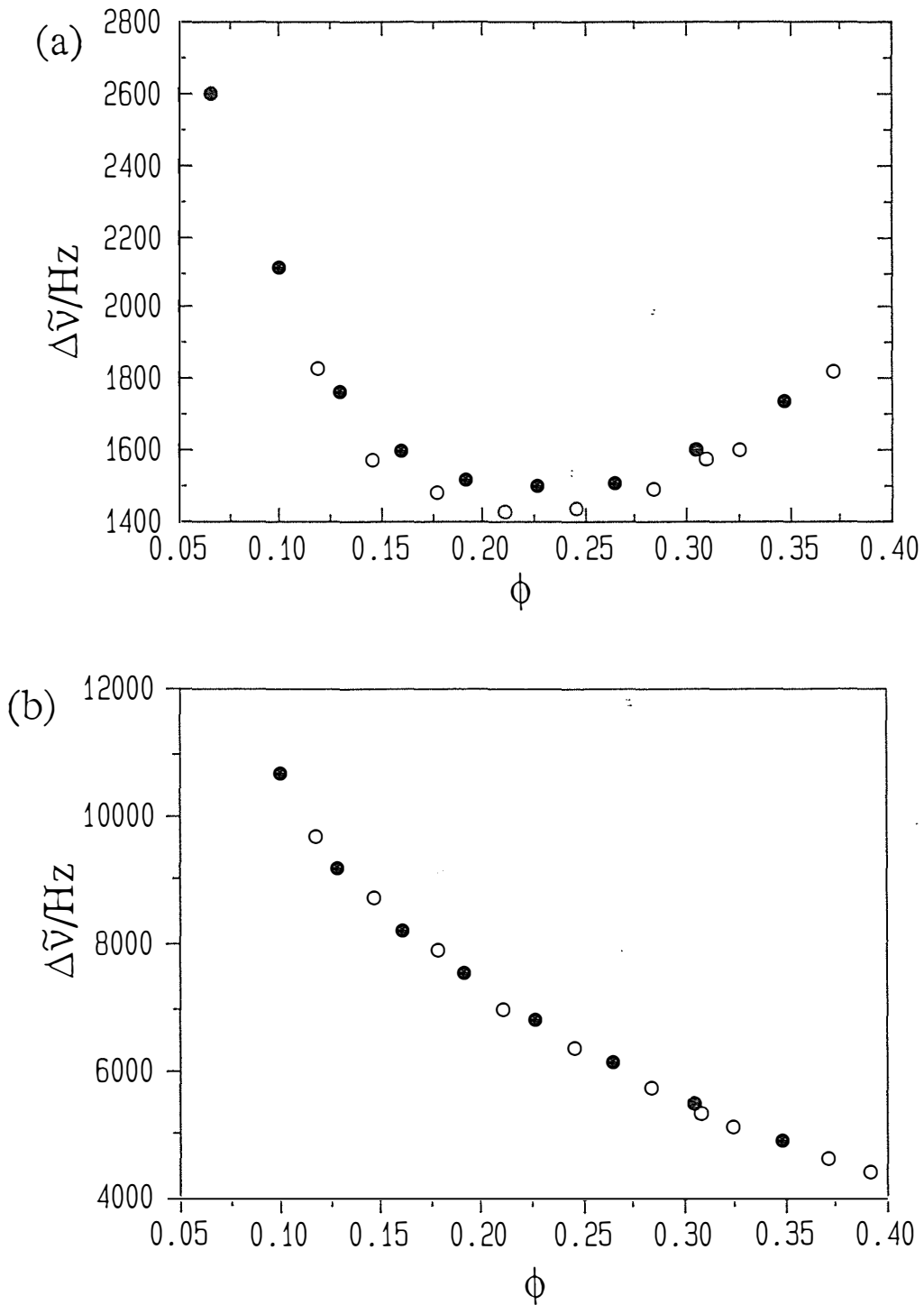

Figure 8.3 The concentration dependence of (a) the ^{133}Cs quadrupole splittings and (b) the chemical shift anisotropy in the lamellar phase (T = 285 K) of the CsPFO/H_2O (o) and CsPFO/^2H_2O (•) systems.

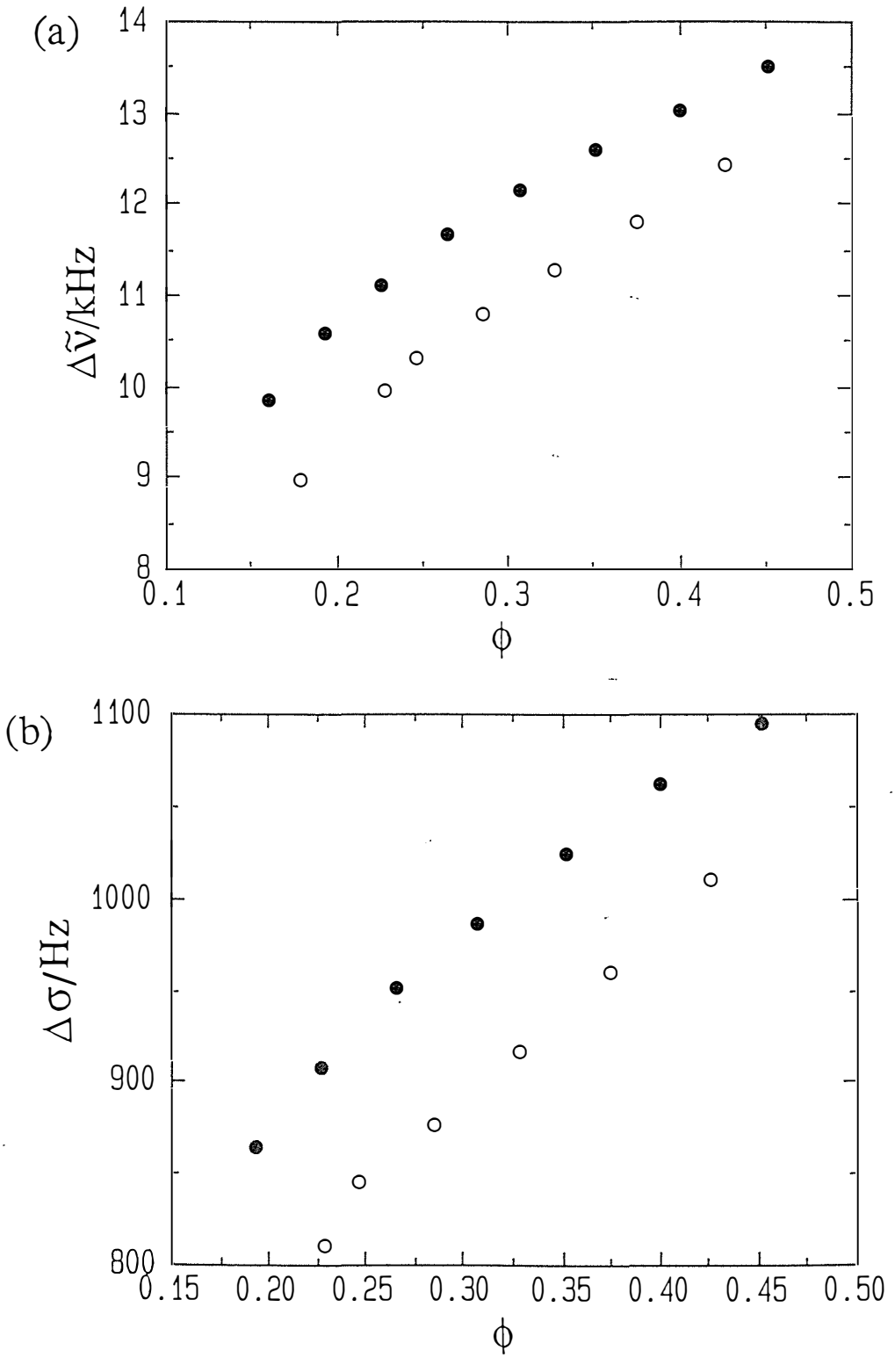

the CsPFO/H_2O system are the result of change in only β_{Cs} (see equation 3.27) between the systems. The ratio varies from 1.06 at ϕ=0.2 to 1.04 at ϕ=0.352. This difference in the ratios implies that an increase in β_{Cs} is accompanied by a corresponding increase in $\langle P_2(\cos\alpha)\rangle_s$, *i.e.* an increase in the micelle aggregation number.

Some idea of the change in the magnitude in ñ involved can be obtained from a consideration of CsPFO/^2H_2O and CsPFO/H_2O samples at a given volume fraction. The ratio of the quadrupole splittings and chemical shifts at the volume fraction of the CsPFO/^2H_2O w=0.55 sample (ϕ = 0.352) are 1.09 and 1.04 respectively.

$$i.e. \quad \frac{\langle P_2(\cos\alpha)\rangle_s \beta_{Cs} \text{ in } {}^2H_2O}{\langle P_2(\cos\alpha)\rangle_s \beta_{Cs} \text{ in } H_2O} = 1.09$$

and

$$\frac{\beta_{Cs} \text{ in } {}^2H_2O}{\beta_{Cs} \text{ in } H_2O} = 1.04$$

giving

$$\frac{\langle P_2(\cos\alpha)\rangle_s \text{ in } {}^2H_2O}{\langle P_2(\cos\alpha)\rangle_s \text{ in } H_2O} = 1.05. \qquad [8.1]$$

The aggregation number at 285 K for the CsPFO/^2H_2O w = 0.55 sample is 220[4]. To obtain the axial ratio of the oblate ellipsoidal micelle it is assumed that V_m=ñV_A where V_A is the volume of an amphiphile monomer (= 3.6×10^{-28} m^3) and that the length of the minor axis of the micelle is equivalent to the length of two PFO^- chains (2.2 nm)[2]. An ñ of 220 gives an axial ratio of 0.265 for the micelle, which corresponds to a $\langle P_2(\cos\alpha)\rangle_s$ value[1] of 0.703. From equation 8.1 we obtain a value for $\langle P_2(\cos\alpha)\rangle_s$ for a PFO^- micelle in water at a volume fraction of 0.352 of 0.669, which corresponds to an axial ratio of 0.289 and an aggregation number of 185. Substitution of heavy water by water at a constant amphiphile mole fraction of 0.352 thus results in a smaller micelle with a decrease in ñ of about 16%.

The small difference between the $\Delta\tilde{\nu}$ values at T_{NI} for $\phi < 0.3$ (figure 8.2a) shows that there is a small intrinsic isotope effect, over and above that associated with the change in $\tilde{n}$ and β_{Cs}, but not for T_{NL} (figure 8.2b). In H_2O at T_{NI}, either S, $\langle P_2(\cos\alpha)\rangle_s$ or β_{Cs}, or all of them, are smaller, *i.e.* the transition occurs at a higher temperature. Considering the expression for T_{NI}

$$T_{NI} = C\tilde{n}\phi \qquad [8.2]$$

where C incorporates all the constant terms and is proportional to ε_{mm}, the strength of the anisotropic interaction between the micelles, then if C were exactly the same for H_2O and ^2H_2O, we would expect $\tilde{n}$ and β_{Cs} to be identical too. The fact that this is not observed (*i.e.* different quadrupole splittings) means that C is a little larger for H_2O than for ^2H_2O. The larger C, the larger ε_{mm} and hence the transition would be at a higher temperature *i.e.* the greater strength of the anisotropic interaction for a given $\tilde{n}$, the higher the transition temperature. The origin of the higher value for C in water is not understood. It cannot be due simply to the dielectric constant differences between the two solvents since H_2O has a higher dielectric constant although the difference is only small[5]. It is more likely in these concentrated ionic solutions that it is the fraction of bound ions which is the major contribution to small variations in ε_{mm} (and C). If the bound ion fraction is greater then ε_{mm} will be smaller.

Further support for the micelles having approximately the same size and shape at the phase transition temperatures is provided by a comparison between the CsPFO/^2H_2O and the NH_4PFO/^2H_2O ^2H quadrupole splitting at T_{NI} and T_{LN} (figure 8.4). The magnitude of the ^2H quadrupole splittings depends on $\langle P_2(\cos\alpha)\rangle_s$ and $\frac{x_A}{x_W}$ (equation 3.20). The $\frac{x_A}{x_W}$ ratio between the NH_4PFO and CsPFO systems differs by only about 4% at any given volume fraction so by far the major contribution to the variation in the splittings with ϕ (assuming constant S for both systems at the phase transition temperatures) is the magnitude of $\langle P_2(\cos\alpha)\rangle_s$ *i.e.* the size of the micelle.

Figure 8.4 The concentration dependence of the ^2H quadrupole splittings at T_{NI} (circles) and T_{LN} (squares) for the $NH_4PFO/^2H_2O$ (open symbols) and $CsPFO/^2H_2O$ (closed symbols) systems.

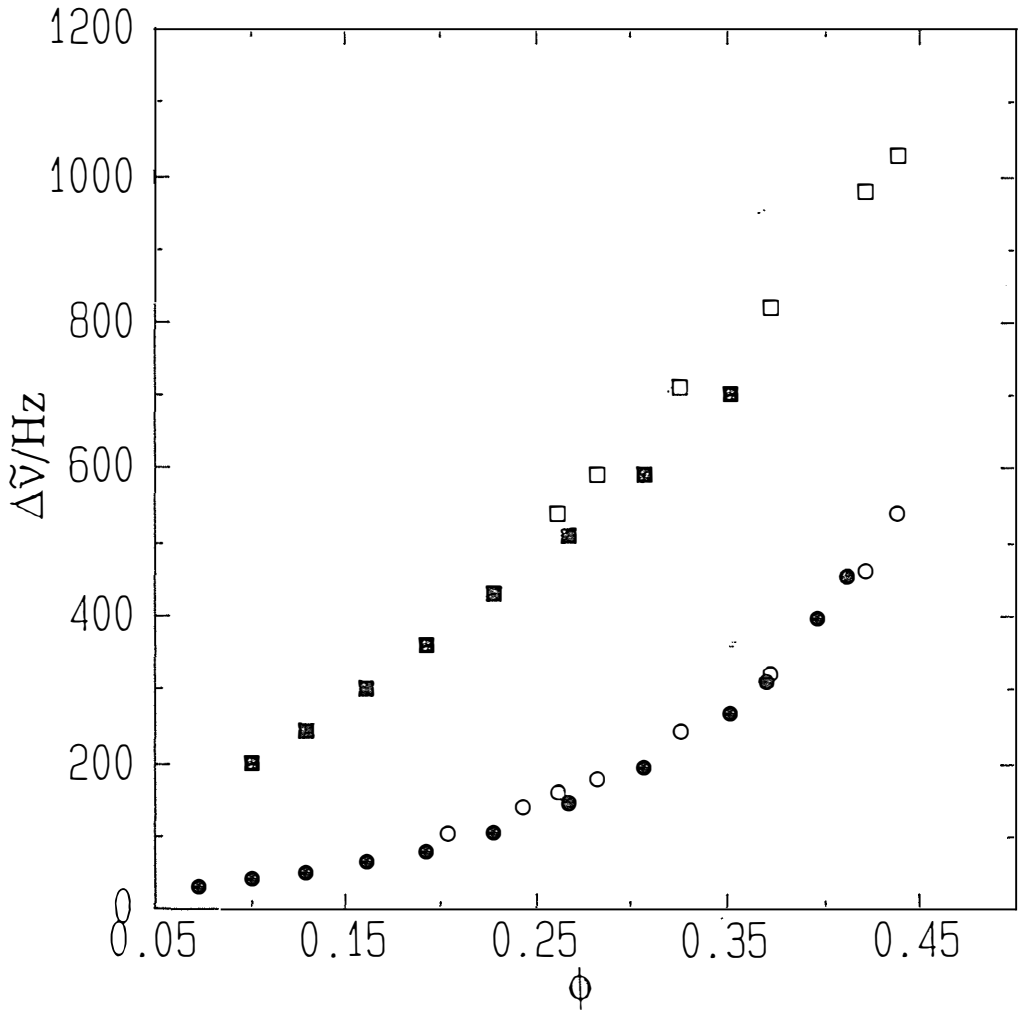

The agreement along the T_{NI} transition line is excellent and illustrates the role of the volume fraction and aggregation number in driving the phase transition. At a given volume fraction the phase transition occurs when the micelle reaches a certain size. This means that if equation 8.2 is correct the value of C is smaller in the NH_4PFO system.

The agreement between the quadrupole splittings at T_{LN} is not as good and it appears that the micelles are bigger in the NH_4PFO system although the difference is only small. The actual phase transition temperatures in the ammonium system are ≈23 K lower at any given volume fraction. This is because substituting NH_4^+ for Cs^+ makes the micelles smaller and so the transition temperature has to be lowered until the micelles reach the size and shape necessary for the transition to occur.

8.2 ISOTOPE EFFECTS ON THE NH_4PFO/WATER PHASE DIAGRAM

The isotope effect in the NH_4PFO system shows essentially the same behaviour as the CsPFO system in that the water phase transitions occur at lower temperatures than the transitions in a heavy water sample of the same volume fraction. The T_{NI} and T_{LN} phase transition curves converge at high temperatures as in the CsPFO systems. The volume fraction dependence of the phase transition temperatures are shown in figure 8.5. This indicates that the solvent isotope effect has the same origin in both systems. As the difference in the solvent structure between H_2O and ^2H_2O is reduced at higher temperature so is the difference in the size and shape of the aggregate in the respective solvents and thereby the difference in the phase transition temperatures. The fact that the isotope effect is the same in the two systems argues for an origin that is due to the enhanced hydrophobicity in ^2H_2O compared to H_2O. There will be two effects. Firstly aggregation will be promoted by lowering the free energy of transferring a surfactant molecule from solution to a micelle and secondly the interfacial tension at the micelle/solution interface will be raised. This will promote a reduction of the interfacial

Figure 8.5 The concentration dependence of the transition temperatures T_{NI} (circles) and T_{LN} (squares) for the NH_4PFO/H_2O (open symbols) and $NH_4PFO/^2H_2O$ (closed symbols) systems.

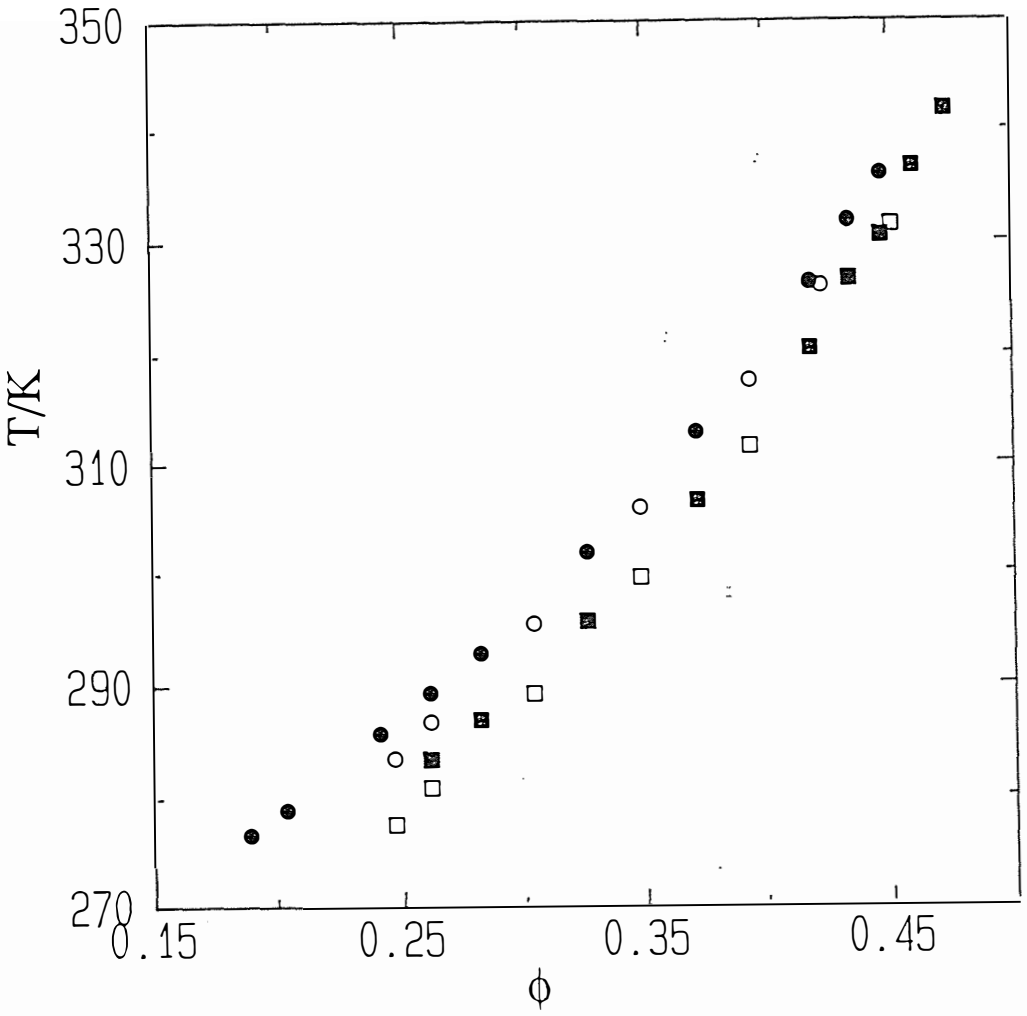

area per surfactant which will result in an increase in charge density. This term will promote ion condensation. Thus, the enhancement in ion binding will lead to a growth in micelles as seen in the phase behaviour. It also explains the higher cmc's for fluorocarbon surfactants.

8.3 INFLUENCE OF THE COUNTER-ION ON PHASE BEHAVIOUR

A comparison of the liquid crystal phase transition curves for the CsPFO/^2H_2O and NH_4PFO/^2H_2O systems is shown in ϕ versus T space in figure 8.6. It can be clearly seen that the effect of the counter-ion is simply to alter the temperature at which the transitions occur. The phase structure itself is not affected by substituting a Cs^+ for an NH_4^+ counter-ion. The reason for this has already been referred to, *i.e.* the effect of changing counter-ion is to alter the size and shape of the aggregate. Substituting NH_4^+ for Cs^+ gives rise to smaller micelles for a given volume fraction and therefore as a consequence lower phase transition temperatures.

The micelle size variation is probably a consequence of the distance of the cation charge layer from the plane of anionic charge. It has been shown in section 4.4.3 that for Cs^+, at least, the hydration sphere remains intact on binding to the micelles and for a comparison of ions it would seem reasonable to compare the distances between the centre of the ion and the centres of the nearest water molecules as shown in table 8.6.

Table 8.6 Ion to water distances in the inner hydration shell of the alkali metal ions[6].

ion	d/nm
Li^+	0.207
Na^+	0.237
K^+	0.273
NH_4^+	0.305
Cs^+	0.308

Figure 8.6 The concentration dependence of the transition temperatures T_{NI} (circles) and T_{LN} (squares) in the $NH_4PFO/^2H_2O$ (open symbols) and $CsPFO/^2H_2O$ (closed symbols) systems.

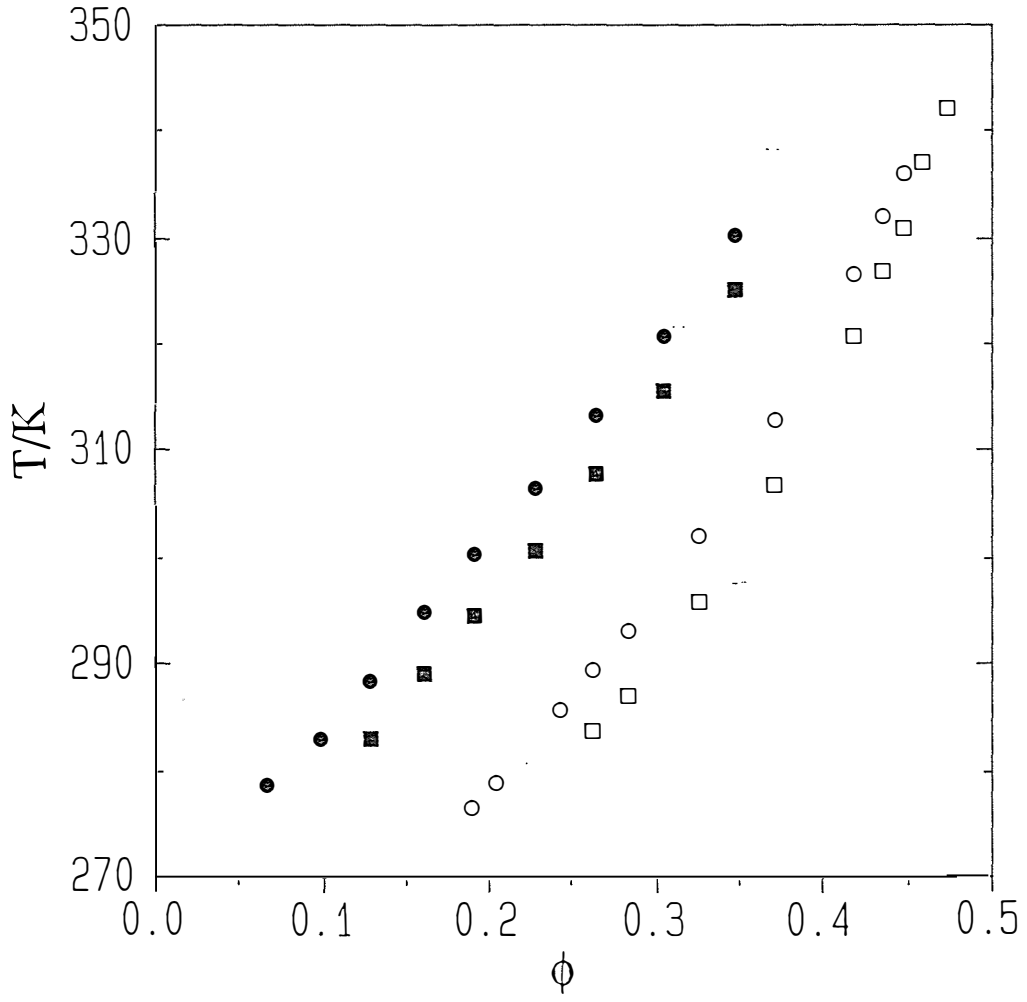

These distances will determine the distance of nearest approach of the oppositely charged ions, *i.e.* they will determine the distance of the cationic charge from the plane of anionic charge. The presence of oppositely charged species will offset the electrostatic repulsion between the surfactant head groups and cause a contraction of the surface. Unfortunately there is no value for the rubidium ion in table 8.6 but the hydrated ionic ratio of the two ions are similar[7] and it is reasonable to expect then to have similar ion-water distances too.

The RbPFO system suffers from the fact that the solubility curve is at much higher temperatures than it is for the NH_4PFO and CsPFO salts[8], but at a volume fraction of 0.325 T_{NI} has been measured to be 317.15 K which is in between that of the caesium and ammonium salts. If a full phase diagram were possible for this salt it would show exactly the same phase behaviour as NH_4PFO and CsPFO, the influence of the Rb^+ ion is to slightly modify the head group repulsions at the anionic charge layer. Both the NaPFO and KPFO are also quite insoluble and no micellar liquid crystal phases have been found. This is simply a result of the T_c curves being at too high a temperature for the formation of stable nematic phases. The lithium salt forms extensive lamellar phases[9] which is quite likely a consequence of it being able to get close to the layer of anionic charge thus promoting planar surfaces and classical lamellar phases. Loss of curvature in the micelle surface will lead to micellar growth and an increase in the surface charge density which will favour the binding of counter-ions at the surface, *i.e.* an increase in β is a consequence of the growth and associated change in charge density of the micelle[10]; it is not the cause of the growth, merely the effect. The effect of counter-ions on micelle size is probably not related to the hydration energies of the ions. Although the hydration energies of Cs^+, Rb^+ and NH_4^+ (-283, -308 and -329 kJ mol^{-1}) have the expected trend to account for the observation that the T_{NI}'s for the systems are $Cs^+ > Rb^+ > NH_4^+$, Li^+ has a much higher hydration energy (-531 kJ mol^{-1}) than any of these and it strongly promotes planar surfaces. If hydration energies were important

we would also expect hydrocarbon systems to exhibit phase behaviour that was strongly counter-ion dependent and this is not so.

8.4 THE STRENGTH OF THE ISOTROPIC TO NEMATIC TRANSITION

The quantity T_{IN} -T^* can be used as a measure of the strength of the nematic to isotropic transition. In a recent theoretical paper[11] an expression for T_{IN} -T^* was obtained in terms of the volume fraction of micelles and a quantity, λ, which described the 'strength' of the anisotropic steric interactions. This quantity is expressed as a function of the dimensions of the micelle. Thus T_{IN} -T^* is expressed simply as a function of micelle size and shape and the micelle volume fraction. This theory was successful in accounting for T_{IN} -T^* being much smaller in lyotropic liquid crystals than in thermotropic liquid crystals and also for its strong increase with ϕ. The only data that the theory was tested on was that for the CsPFO/H_2O system[12].

In the preceding discussion it was shown that for a given volume fraction the size and shape of the micelle at T_{NI} was the same for all systems studied *i.e.* the transition is determined by the physics of the system rather than the chemistry. The strength of the transition (T_{IN} -T^*) should also be determined by the physics of the system. In chapter 5, T_{IN} -T^* was measured as a function of concentration for the CsPFO/^2H_2O system only. However it was demonstrated that the quantity is directly proportional to T_{IN} -T_{NI} which could be used as an alternative and more sensitive measure of the transition strength.

Figure 8.7 shows the concentration dependence of T_{IN} -T_{NI} for all of the systems studied in this thesis. It is clear that all points, particularly for $\phi < 0.375$, lie on the same curve, an impressive demonstration that it is the physics which dominate the transition. The chemistry affects the size and shape of the aggregate, but at the phase transition

Figure 8.7 Concentration dependence of the width of the nematic/isotropic mixed phase region (T_{IN} - T_{NI}) in the CsPFO/H_2O (o), CsPFO/^2H_2O (•), $NH_4PFO/^2H_2O$ (■) and NH_4PFO/H_2O (□) systems.

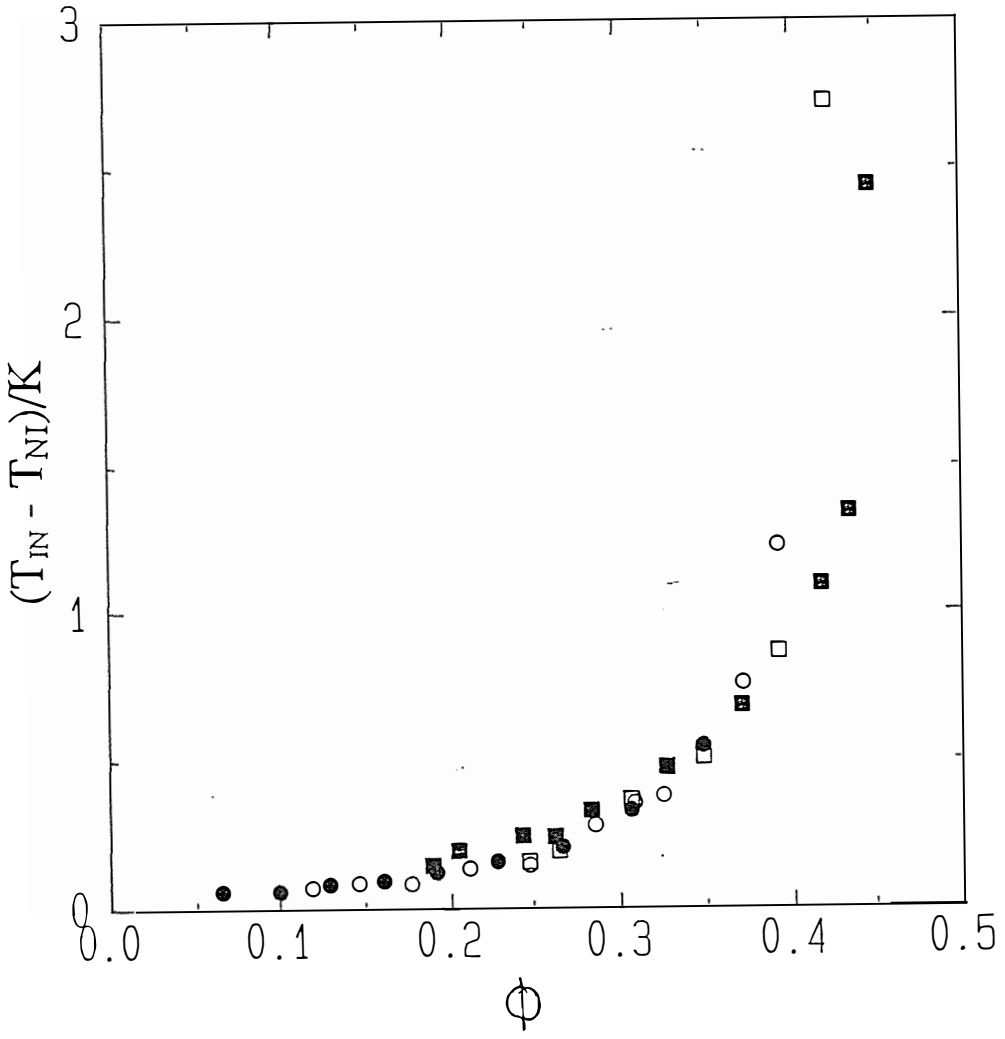

temperature the dominating driving force is simply the geometry of the micelles and the excluded volume.

8.5 CONCLUDING COMMENTS

There is a large amount of further work needed to be done on the perfluorinated surfactant solutions in order to understand the factors that control the stability of discrete discoidal micelles. It is important to identify the important molecular interactions that are responsible for the stability of the micelle. There are several possibilities The hydrophobic interaction between the fluorocarbon chains and water at the interface is one possibility. Evidence for this comes from the growth of the micelle on substituting ^2H_2O for H_2O and the decrease in size on raising the temperature. Chain-chain interactions are also important, since the micelle grows with increasing chain length. Counter-ion binding is also important; the phase diagram for the $NH_4PFO/^2H_2O$ system is almost identical to that for $CsPFO/^2H_2O$ in temperature/volume fraction space, except that the transition temperatures are $\approx$23 K lower. This is because substitution of NH_4^+ for Cs^+ makes the micelle smaller.

In order to explain the stability of discoidal micelles a quantitative assessment, experimental and theoretical, of the above interactions is essential. On the experimental front it is therefore necessary to produce high resolution phase diagrams of the various perfluorinated surfactant systems and examine closely the effects of change in the counter-ion, solvent, added electrolyte and fluorocarbon chain. These studies must be paralleled by structural studies on the size and shape of the aggregate and the order of the liquid crystalline mesophases.

It will also be important to address the question as to why micelles form lamellar phases as opposed to classical bilayers or as opposed to columnar phases.

REFERENCES

[1]Boden N.; Corne S. A.; Jolley K. W., *J. Phys. Chem.* **1987**, *91* , 4092.

[2]Boden N.; Corne S A.; Holmes M. C.; Jackson P. H.; Parker D.; Jolley K. W., *J. Physique* **1986**, *47* , 2135.

[3]Berr S. S.; Jones R. R. M., *J. Phys. Chem.* **1989**, *93* , 2555.

[4]Parker D., Ph. D. Thesis, Leeds University, **1988**.

[5]*CRC Handbook of Chemistry and Physics 52ed.* (The Chemical Rubber Co., Cleveland, Ohio; ed. Weast R. C.) **1971-72**, p E-49.

[6]Marcus Y., *J. Solution Chem.* **1983**, *12* , 271.

[7]Conway B. E., *Studies in Physical and Theoretical Chemistry 12; Ionic Hydration in Chemistry and Biophysics* , (Elselevier Scientific Publishing Company, Amsterdam) **1981**, p 73.

[8]Rosenblatt C., *J. Colloid. Interface. Sci.* **1989**, *131*, 236.

[9]Everiss E.; Tiddy G. J. T.; Wheeler B. A., *J. Chem. Soc. Faraday Trans. I* **1976**,*72* , 1747.

[10]Boden N.; Clements J.; Jolley K.W.; Parker D.; Smith M. H., *J. Chem. Phys.* , In Press.

[11]Kuzma M. R.; Gelbart W. M.; Chen Z-Y., *Phys. Rev. A* **1986**, *34* , 2531.

[12]Rosenblatt C.; Kumar S.; Litster J. D., *Phys. Rev. A* **1984**, *29* , 1010.

CsPFO/H_2O Sample Transition Temperatures

w	ϕ	T_{IN}	T_{NI}	T_{LN}	T_{NL}
0.251	0.118	282.68	282.61	276.85	
0.300	0.146	287.76	287.68	281.59	
0.352	0.178	293.98	293.89	287.70	
0.400	0.21	299.97	299.84	294.00	
0.450	0.246	306.64	306.49	300.76	
0.500	0.284	314.16	313.88	308.36	308.42
0.530	0.309	319.46	319.10	313.84	313.99
0.550	0.325	323.28	322.90	317.66	317.95
0.600	0.371	334.84	334.08	329.95	330.84
0.623	0.392	341.17	339.95	335.00	338.42
0.640	0.410	346.90		341.25	
0.650	0.420	350.72		344.50	

NH_4PFO/^2H_2O Sample Transition Temperatures

w	ϕ	T_{IN}	T_{NI}	T_{LN}	T_{NL}
0.283	0.189	276.69	276.54		
0.302	0.204	279.02	278.82		
0.351	0.242	285.96	285.72		
0.375	0.262	289.53	289.29	283.48	
0.400	0.283	293.38	293.05	287.05	
0.450	0.326	302.61	302.13	296.00	
0.501	0.371	313.58	312.90	306.63	306.72
0.551	0.418	327.60	326.51	320.64	322.07
0.569	0.435	333.34	332.00	326.70	329.08
0.582	0.448	338.58	336.14	330.81	333.79
0.595	0.460	343.53		337.00	
0.610	0.474	351.91		342.00	
0.646	0.510	370.02			

NH_4PFO/H_2O Sample Transition Temperatures

w	ϕ	T_{IN}	T_{NI}	T_{LN}	T_{NL}
0.3802	0.247	283.75	283.59		277.48
0.4005	0.263	287.08	286.88		280.96
0.4511	0.305	295.90	295.53		289.36
0.5020	0.349	306.42	305.91	299.80	299.72
0.5500	0.393	318.40	317.53	312.19	311.56
0.5806	0.422	328.90	326.18		
0.6122	0.452	337.60			331.80